ERREURS ANALOGIQUES DANS LES CAN A BANCS DE FILTRES HYBRIDES"Méthodes d'estimation et nouvelles structures"

Davud Asemani

University of ParisSud
Supelec

ANALOG NON-IDEALITIES IN HYBRID FILTER BANK ANALOG TO DIGITAL CONVERTERS "ESTIMATION METHODS AND NEW STRUCTURES"

A Thesis in
Department of Signal Processing and Electronic Systems
by
Davud Asemani

Submitted in Partial Fulfillment
of the Requirements
for the Degree of

Doctor of Philosophy

July 2007

Résumé

Les Convertisseurs Analogique-Numérique (CAN) à Bancs de Filtres Hybrides (BFH) sont de bons candidats pour répondre aux exigences des futurs systèmes de communication devant être versatile, intelligent et à large-bande. Cependant, les BFH montrent une grande sensibilité aux non-idéalités analogiques du banc d'analyse, de sorte que les CAN à BFH classiques ne seraient pas pratiquement utilisables à moins que ces erreurs ne soient corrigées. Les efforts, dans cette thèse, ont porté sur l'étude de ce problème afin de proposer des pistes de solutions. A cet égard, la conception des BFH est, d'abord, décrite sous la forme de matrice. Puis, en utilisant des circuits analogiques simplement réalisables ainsi que des filtres numériques à Réponse Impulsionnelle Finie (RIF), les BFH sont conçus pour la conversion A/N. Selon la simulation des CAN à BFH, nous montrons que la sensibilité de ceux-ci aux erreurs analogiques est très élevée puisque la matrice d'analyse associée est mal-conditionnée, surtout dans le cas où le suréchantillonnage est utilisé. Pour estimer numériquement les imperfections des circuits analogiques, nous proposons l'utilisation de méthodes d'estimation aveugle, basées sur des statistiques de seconde-ordre ou d'ordre supérieur. Cependant, ces techniques semblent ne pas être applicables aux BFH classiques en raison du sous-échantillonnage inclus à chaque branche du CAN à BFH. Ainsi, pour exploiter les techniques numériques pour la correction des imperfections analogiques des filtres d'analyse, nous proposons de nouvelles structures à Entrée-sortie Multiple (ESM). Dans ces structures, il n'existe plus aucune opération de sous-échantillonnage entre les entrée-sortie associées. Les simulations prouvent que les BFH à ESM (à sous-bande et à multiplexage temporel) mènent non seulement à une meilleure résolution mais aussi à une sensibilité moins élevée par rapport aux BFH classique. En conclusion, en utilisant les BFH à ESM, les méthodes aveugles telles que la déconvolution ou l'annulation du bruit peuvent être employées afin de réduire encore la sensibilité aux non-idéalités analogiques.

Les mots clés: *Bancs de filtres hybrides, convertisseur analogique-numérique, la radio logicielle, non-idéalités analogiques, les méthodes aveugles.*

Abstract

Hybrid Filter Bank (HFB) A/D converters are a good candidate for realizing the future versatile, intelligent and wide-band communication systems. However, the HFB structures exhibit a large sensitivity to the analog non-idealities of analysis part so that the classical HFB ADCs are not practically useful unless these errors are corrected. The efforts have been made in this thesis to more profoundly study this problem and to propose a group of possible solutions. Firstly, the design phase of related HFBs is described in the matrix form. Considering the simply realizable first- and second-order analog circuits as analysis filter bank and FIR digital synthesis filters, the HFB structures are designed for A/D conversion in this thesis. Simulating some exemplary HFB ADCs, it is shown that the sensitivity of HFB to analog errors is so large because the related analysis matrix is ill-conditioned, particularly in the case of oversampling process. Using Second-Order and Higher-Order Statistics, it is shown that the analog imperfections of analog circuits may digitally be estimated through the output samples. However, these techniques appear not to be applicable to the conventional HFB structure because of under-sampling process included at each branch of HFB-based ADC. Thus, for exploiting the digital techniques to estimate and then correct the analog imperfections of analysis filter bank, new Multiple-Input Multiple-Output (MIMO) HFB structures are proposed so that there exist no under-sampling operation anymore between the related input-output signals. The simulations show that the MIMO (TDM and subband) HFB architectures provide not only a better output resolution but a less sensitivity to the realization errors of analysis filter bank than the classical HFB. Finally, using the TDM and subband MIMO HFBs, it is proposed to use the blind methods such as blind deconvoluton or Automatic Noise Cancelation (ANC) for compensating and then reducing the sensitivity to the analog non-idealities.

Keywords: *Hybrid Filter Bank, parallel A/D conversion, Software-Defied Radio, analog non-idealities, blind techniques.*

Dedication

To Pegah,

> *An angel, robed in spotless white,*
> *bent down and kissed the sleeping night.*
> *Night woke to blush; the sprite was gone.*
> *Men saw the blush and called it Dawn.*

Acknowledgments

A teacher affects eternity; he can never tell where his influence stops.
H.B. Adams

I wish to express my deepest gratitude to my advisor, Prof. Jacques Oksman, for his guidance throughout my graduate studies at Supélec. His continuous support and his advises were invaluable to the preparation of the thesis. I would like to thank my thesis committee: Prof. Benabes, Prof. Duhamel, Prof. Hélard, and Prof. Pesquet. I am also grateful to Prof. Fleury, Dr Lelandais, and Dr Poulton for their support and constructive comments. During these three years, I have been honored to work and discuss with many colleagues and friends whose friendship has enriched my professional and personal life. I believe in you and trust you with my friendship: Prof. Djafari, Prof. Kielbasa, Dr Juillard, Dr Guessab, Dr Baili, Dr Najafi, Dr Pourmir, Dr Gauthier, Dr Benoit, Dr Gholami, Mohammad, Emilie, Alexia, Cécile, Sadjad, Ali, Françis, Luc, Sophie, Fabienne, Philippe, Rim, Julien, Rawad, Morgan, Eric, Sorore, Gilbert and Mr. Vuong.
This work has been completed with the permanent encouragement and support of my family. I wish to give my deepest gratitude to them. Many thanks also to Ahad, Mahvash and Pouya who supported me so much.

List of publications

- **Journal papers**

1. Asemani D., Oksman J.,*Time-Division Multiplexing architecture for HFB-based A/D converters*, under preparation for IEEE Trans. on Circuits and Systems, CAS-I.

2. Asemani D., Oksman J., Duhamel P.,*Subband architecture for HFB-based A/D converters*, under preparation for IEEE Selected Topics in Signal Processing, 2007.

- **Conference papers**

1. Asemani D., Oksman J.,*A wide-band A/D converter for the software defined radio systems*, IEEE Conference on Signal Processing for Communications (ICSPC), Dubai, UAE, Nov., 2007.

2. Asemani D., Oksman J.,*Sensitivity of time-division multiplexing parallel A/D converters to analog imperfections*, IEEE conference on Signal Processing Systems (SiPS), Shanghai, China, Oct., 2007.

3. Asemani D., Oksman J.,*Time-Division Multiplexing Architecture for Hybrid Filter Bank A/D converters*, IEEE MidWest Symposium on Circuits and Systems (MWSCAS), Montréal, Canada, Aug., 2007.

4. Asemani D., Oksman J.,*Performance of subband HFB-based A/D converters*, International Symposium on Signal Processing and its Applications (ISSPA), Sharjah, UAE, Feb., 2007.

5. Asemani D., Oksman J.,*Subband architecture for HFB-based A/D converters* , International Symposium on Communications and Information Technologies (ISCIT), Bangkok, Thailand, Oct., 2006.

6. Asemani D., Oksman J.,*Influences of oversampling and analog imperfections on Hybrid Filter Bank A/D converters* , IEEE MidWest Symposium on Circuits and Systems (MWSCAS), San Juan, Puerto Rico, Aug., 2006.

7. Asemani D., Oksman J., Poulton D.,*Digital estimation of analog imperfections using blind equalization* , IEEE European Signal Processing Conference (EUSIPCO), Florence, Italy, Sep., 2006.

8. Asemani D., Oksman J., Poulton D.,*Modeling the imperfections of analog circuits using Second-Order Statistics* , IEEE International Symposium on Communications, Control and Signal Processing (ISCCSP), Marrakesh, Morocco, March, 2006.

9. Asemani D., Oksman J.,*Two-stage synthesis filters for Hybrid Filter Banks A/D converters*, IEEE conference on Signal Processing Systems (SiPS), Athens, Greece, Nov., 2005.

Table of Contents

List of Figures

List of Tables

List of Symbols

$(.)^{\dagger}$	pseudo-inverse of the operand matrix
$(.)^{H}$	Transpose-conjugate of the operand
$(.)^{T}$	Transpose of the operand
$\|.\|$	L_2-norm of the operand
$\|.\|_F$	Frobenius norm of the operand
$\star$	Linear convolution operation
$\otimes$	Kronecker production
Re(.)	Real part of operand
Im(.)	Imaginary part of operand
$\mathbb{Z}$	Set of integers
$\mathcal{R}$	Set of real numbers
ω	Frequency related to the discrete-time Fourier transform
Ω	Frequency related to the continuous-time Fourier transform
M	Number of branches of HFB structures
T	Sampling period associated with the Nyquist rate
N	Number of frequency points used in the design of synthesis stage
$x(t)$	Input analog signal
$H_k(s)$	Transfer function of analog analysis filter at the k^{th} branch
$H_k(j\Omega)$	Frequency response of analog analysis filter at the k^{th} branch

$H_k^{'}(j\Omega)$	Frequency response of $H_k(j\Omega)$ considered in the interval $\left[\frac{-\pi}{T}, \frac{\pi}{T}\right]$
$\widetilde{H}_k(j\Omega)$	Periodic extension of $H_k^{'}(j\Omega)$ with the period $\frac{2\pi}{T}$
$h_k(t)$	Impulse response of $H_k(j\Omega)$
$h_k^{'}(t)$	Impulse response of $H_k^{'}(j\Omega)$
L	Number of coefficients of each FIR synthesis filter
n'	Discrete-time index associated with the sampling rate $\frac{1}{T}$
n_d	Delay length for designing the FIR synthesis filters (often equal to $\frac{L}{2}$)
$T_0(e^{j\omega})$	Distortion function of the classical HFB structure
$T_m(e^{j\omega})$	m^{th} aliasing term of the classical HFB structure ($1 \leq m \leq M-1$)

Abbreviations

$\Delta\Sigma$	Delta-Sigma, p. 27
ADC	Analog to Digital Converter, p. 26
ANC	Automatic Noise Canceling, p. 154
BIBO	Bounded-Input Bounded-Output, p. 133
BSS	Blind Source Separation, p. 155
CCD	Charge-Coupled Devices, p. 30
CMA	Constant Modulus Algorithm, p. 78
DAC	Digital to Analog Converter, p. 28
DTFT	Discrete-Time Fourier Transform, p. 112
FDMA	Frequency-Division Multiple Access, p. 120
FIR	Finite-Impulse Response, p. 32
FT	Fourier Transform, p. 178
GB	Guard Band, p. 123
GSM	Global System for Mobile communication, p. 137
HFB	Hybrid Filter Bank, p. 30
HOS	Higher-Order Statistics, p. 35
i.i.d.	independent and identically-distributed, p. 71
ICI	Inter-Channel Interference, p. 119
IIR	Infinite-Impulse Response, p. 32

ISI Inter-Symbol Interference, p. 189

LPE Linear Prediction Error , p. 174

LS Least Squares, p. 33

LTI Linear Time-Invariant, p. 30

MAI Multiple Access Interference, p. 196

MIMO Multiple-Input Multiple-Output, p. 89

ML Maximum Likelihood, p. 175

MODEM MODulator-DEModulator , p. 174

MSC Multistage Successive Cancelation , p. 198

NDE Non-Destructive Evaluation , p. 174

OSR OverSampling Ratio, p. 28

pdf probability density function, p. 175

PF Post-Filtering, p. 127

PR Perfect Reconstruction, p. 32

QMF Quadrature Mirror Filters, p. 30

RC Resistor-Capacitor, p. 39

RLC Resistor-Inductor-Capacitor, p. 39

SC Switched-Capacitor, p. 31

SDR Software-Defined Radio, p. 28

SEA Super-Exponential Algorithm, p. 69

SIMO Single-Input Multiple-Output, p. 130

SNR Signal to Noise Ratio, p. 26

SOCS Second-Order Cyclostationary Statistics, p. 175

SOS Second-Order Statistics, p. 35

SVD Singular Value Decomposition, p. 94

TDM Time-Division Multiplexing, p. 130

TDMA Time-Division Multiple Access, p. 138

TLS Total Least Squares, p. 39

Chapter 1

Résumé de la thèse en français

La vérité vaut bien qu'on passe quelques années sans la trouver.
- Renard

1.1 Sensibilité des convertisseurs à BFH à multiplexage temporel par rapport aux erreurs analogiques

Ce chapitre est basé sur les articles suivantes:

- Asemani Davud, Oksman Jacques, Sensitivity of time-division multiplexing parallel A/D converters to analog imperfections ", IEEE workshop on signal Processing Systems (SiPS), Shanghai, Chine, 2007.
- Asemani Davud, Oksman Jacques, " A wide-band A/D converter for the Software-Defined Radio systems", IEEE International Conference on Signal Processing and Communications (ICSPS), Dubai, UAE, 2007.

1.1.1 Introduction

Le défi important dans la conversion Analogique/Numérique (A/N) et Numérique/ Analogique (N/A) est d'atteindre simultanément une grande vitesse ainsi qu'une haute résolution. Les convertisseurs sigma-delta ($\Sigma\Delta$) sont capables de fournir la

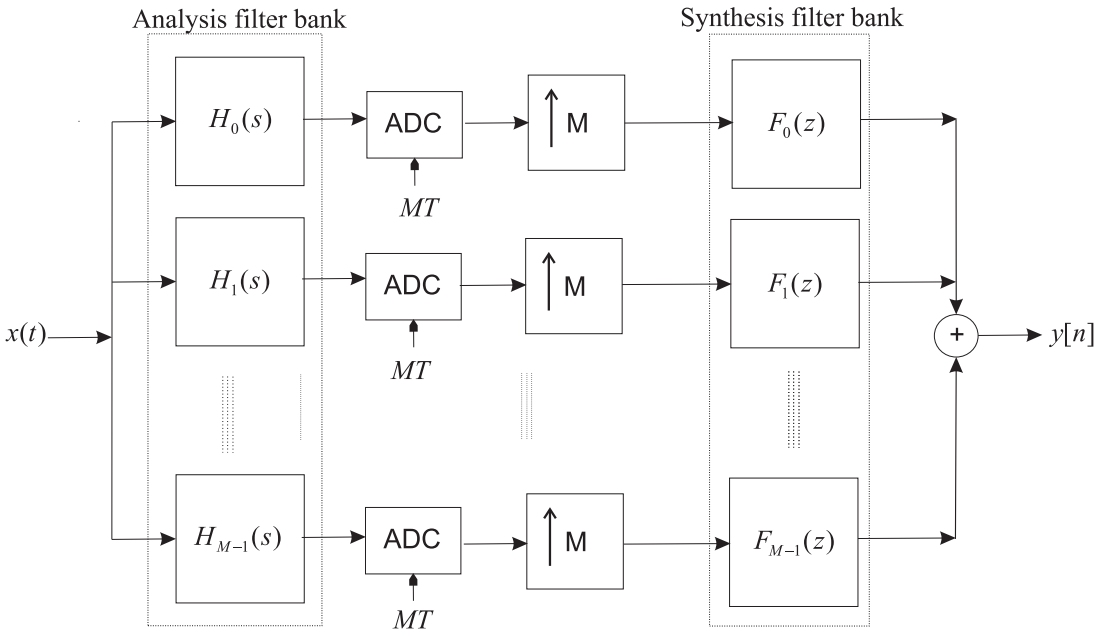

Figure 1.1. L'architecture classique de BFH à temps continu pour la conversion A/N parallèle.

meilleure résolution, mais sont néanmoins limités quant à la largeur de la bande de conversion [1]. La demande en convertisseurs A/N ou N/A ayant des vitesses plus élevées a considérablement augmenté car ils serviraient à réaliser les nouveaux systèmes de communication tels que la radio logicielle qui seraient à l'origine d'une nouvelle industrie sur une plus grande échelle encore que l'industrie de l'ordinateur personnel [2]. La radio logicielle se caractériserait par une plus grande versatilité et intelligence. En mettant des Convertisseurs A/N (CAN) à haute précision en parallèle, on pourrait réaliser un CAN à large bande. Dans ce sens, on a déjà proposé les structures à l'entrelacement temporel et celles des Bancs des Filtres Hybrides (BFH) à temps discret. Elles rencontrent néanmoins respectivement les problèmes suivants : une haute sensibilité à la disparité des convertisseurs et la limitation en vitesse due aux limites du circuit [3]. On a proposé la structure de BFH à temps continu employant des filtres d'analyse analogiques pour résoudre les problèmes des structures précédemment mentionnées. La figure 1.1 représente la structure classique de BFH à temps continu employée à la conversion A/N où M et T sont associées au nombre de branches et à la période de Nyquist de l'entrée $x(t)$ [4].

Dans cette structure parallèle, M convertisseurs A/N sont maintenant utilisés qui fonctionnent tous parallèlement à une fréquence qui est M fois moins élevée que la fréquence de Nyquist. Supposons que le spectre de l'entrée d'origine $x(t)$ est limité à la fréquence maximale $\pm\frac{1}{T}$. A la sortie des BFH, apparaissent des interférences appelées aliasing qui restreint la résolution finale comme le bruit de quantification. Les convertisseurs A/N en structure BFH ont une bonne performance en terme d'aliasings même en utilisant des filtres analogiques simples tels que ceux de premier et second ordre si un petit rapport du sur-échantillonnage est considéré. Cependant, la performance se dégrade considérablement en prenant en compte même de petites erreurs dans les filtres d'analyse [5]. Il est alors nécessaire d'une façon ou d'une autre d'atténuer ou compenser la sensibilité aux imperfections des filtres analogiques pour rendre pratiquement utile ces CAN parallèles. Des techniques numériques ont été proposées pour surmonter ce problème de la sensibilité élevée aux erreurs de réalisation chez les CAN en structure BFH. Néanmoins, les méthodes proposées sont limitées à certaines erreurs ou situations [6]. Pinheiro et al. ont essayé d'optimiser la conception des structures de BFH en termes d'imperfections analogiques [7], mais leur solution ne propose pas une technique de compensation. Ils ont juste mis en place un critère correspondant à un compromis entre la distorsion et les aliasings qui mène à une amélioration de moins de 5 dB dans le Rapport Signal sur Bruit (RSB). En outre, cette amélioration a été constatée pour la structure classique de BFH sans effectuer de sur-échantillonnage. Quand le sur-échantillonnage n'est pas employé, la structure de BFH est relativement robuste contre les imperfections analogiques des filtres d'analyse [5], mais la performance de celle-ci n'est pas acceptable pour les applications pratiques à moins qu'un petit rapport du sur-échantillonnage soit considéré. Des techniques aveugles tels que la déconvolution pourraient être utilisées afin d'améliorer la sensibilité des structures de BFH aux imperfections analogiques si ces structures représentaient un Système Linéaire Invariant (SLI) dans le temps. Cependant, l'architecture classique de BFH est associée à une relation entrée-sortie variante dans le temps en raison du processus de décimation qui s'effectue implicitement au cours de l'échantillonnage en cadence $\frac{1}{MT}$. Par conséquent, il n'est pas possible d'appliquer directement une technique aveugle notamment la décorrélation au CAN à structure BFH. On a récemment proposé une nouvelle structure de BFH nommée ar-

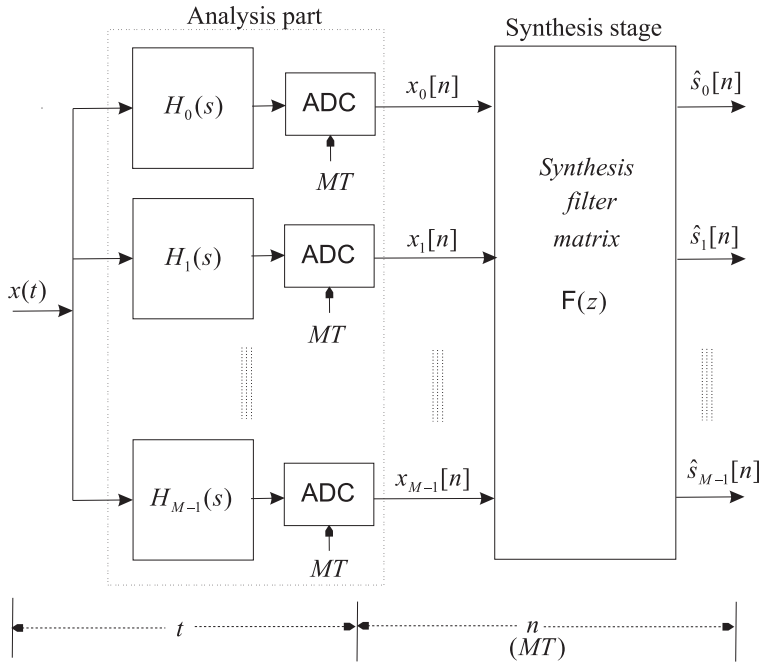

Figure 1.2. . L'architecture de multiplexage temporel pour la conversion A/N en BFH où sont estimées les composants MRT d'entrée à la sortie.

chitecture de Multiplexage par Répartition dans le Temps (MRT) dont la relation entrée-sortie est invariante dans le temps (cf. le chapitre 5). Cette structure MRT de BFH est représentée dans la figure 1.2. On peut voir qu'une matrice $F(z)$ des M^2 filtres numériques est considérée dans l'étape de synthèse pour une structure BFH de M branches, à la place de M filtres exigés pour celle de BFH classique (voir figures 1.2 et 1.1). Dans l'architecture MRT de BFH, on construit le vecteur d'entrée $\mathbf{s}[n]$ avec les M échantillons consécutifs de l'entrée d'origine (en cadence Nyquist):

$$\mathbf{s}[n] = \begin{bmatrix} s_0[n] \\ s_1[n] \\ \vdots \\ s_{M-1}[n] \end{bmatrix} = \begin{bmatrix} x(n'T) \\ x((n'-1)T) \\ \vdots \\ x((n'-(M-1))T) \end{bmatrix}_{n'=nM} \tag{1.1}$$

n' et n représentent respectivement les indices temporelles associés aux périodes T et MT. Donc, les BFH à structure MRT cherchent à estimer le vecteur d'entrée à sa sortie. Contrairement à l'architecture classique, une technique aveugle tel que la décorrélation pourrait être appliquée à l'architecture MRT de BFH afin

de corriger les imperfections analogiques. D'ailleurs, les simulations spectrales ont montré que la structure aboutit à une beaucoup plus grande performance que celle de la structure classique en l'absence des erreurs analogiques (cf. le chapitre 5). Dans cette partie, des BFH à structure MRT sont simulés dans le domaine temporel pour démontrer dans un premier temps la validité du modèle proposé en terme de résolution de la sortie. Et puis, la performance de celui-ci est également étudiée en présence des erreurs de réalisation et comparée avec celle des BFH classique. L'organisation de cette partie est résumée ci-après. Tout d'abord, les BFH à structure MRT sont brièvement présentés et les équations de la Parfaite Reconstruction (PR) sont introduites dans le paragraphe suivant. Puis, les simulations dans le domaine temporel sont réalisées pour udes BFH à 8 branches. La résolution et la sensibilité aux imperfections analogiques des filtres d'analyse sont représentées et comparées pour l'architecture MRT et classique dans le paragraphe 1.1.3. Enfin, les résultats des simulations et l'interprétation sont résumés dans le paragraphe de conclusion 1.1.4.

1.1.2 Le BFH à structure MRT

1.1.2.1 Le modèle à entrées et sorties multiples

Dans le paragraphe précédent, on a mentionné que l'architecture MRT fournit une structure à entrées et sorties multiples pour les BFH. Pour mieux comprendre les BFH à structure MRT, un modèle à entrées et sorties multiples est représenté pour le CAN à structure MRT dans la figure **??**. Dans ce modèle, le bruit de quantification est négligé. Le vecteur d'entrée $\mathbf{s}[n]$ peut facilement être identifié dans ce modèle (voir le chapitre 5). Pour la simplicité, l'entrée d'origine $x(t)$ est remplacée par $x[n']$ qui représente l'entrée échantillonnée à la fréquence de Nyquist $\frac{1}{T}$ ($x[n'] = x(n'T)$). Celui-ci est le signal estimé à la sortie. Comme on montre dans ce modèle à entrées et sorties multiples, l'opération de décimation n'existe plus entre la nouvelle entrée $\mathbf{s}[n]$ et sortie $\hat{\mathbf{s}}[n]$. Donc, la relation entrée-sortie correspondra à un SLI. La matrice (virtuelle) $\mathbf{H}(z)$ des filtres d'analyse utilisée dans le modèle est constituée de M^2 filtres numériques. Chaque élément $H_{kr}(z)$

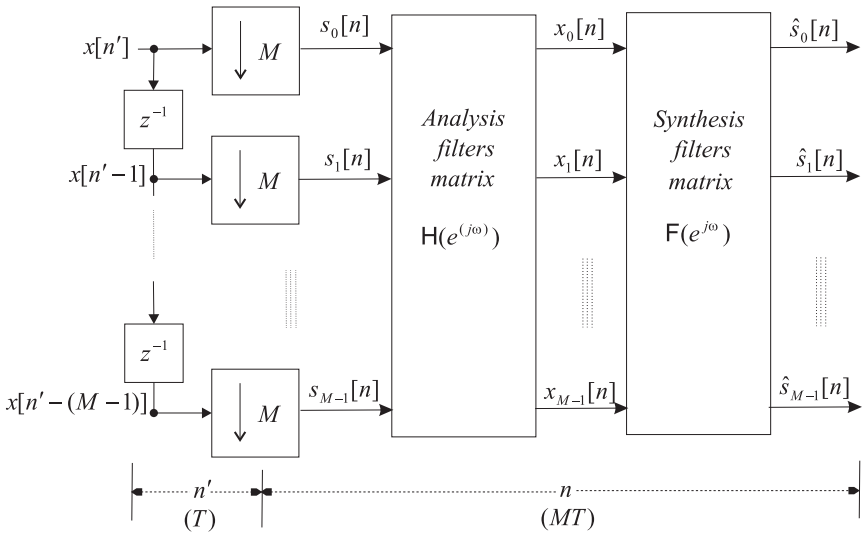

Figure 1.3. Le modèle à entrées et sorties multiples du CAN consistant en un BFH à structure MRT où n' et n représentent respectivement les indices temporels associés aux périodes T et MT.

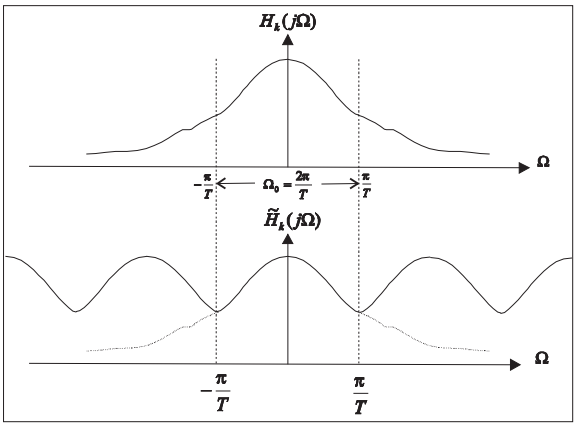

Figure 1.4. Le filtre analogique (en haut) et celui qui a subit une extension périodique de la fréquence $\frac{1}{T}$.

peut être obtenu à partir du filtre analogique $H_k(s)$ de la $k$ème branche:

$$H_{kr}(e^{j\omega}) = \frac{1}{M} e^{j\frac{\omega}{M}r} \sum_{m=0}^{M-1} e^{-j\frac{2\pi}{M}rm} \widetilde{H}_k(j\frac{\omega}{M} - j\frac{2\pi}{M}m) \tag{1.2}$$

$\widetilde{H}_k(j\Omega)$ représente l'extension périodique du filtre analogique $H_k(j\Omega)$ comme illustré par la figure 1.4. Les variables Ω et ω représentent respectivement les fréquences liées au signal analogique et discret dans le temps. On a démontré

que chaque élément de la matrice $\mathbf{H}(z)$ représente un filtre causal et stable si et seulement si les filtres analogiques d'analyse sont tous causaux et stables (cf. le chapitre 5). Dans l'architecture MRT (la figure 1.2), on reconstruit l'entrée d'origine à partir des M signaux $x_0[n]$, $x_1[n]$,, et $x_{M-1}[n]$ (les sorties de la pièce d'analyse) seuls. D'après le modèle MRT (la figure 1.3), les sorties de l'étape d'analyse ($x_0[n]$, $x_1[n]$,, et $x_{M-1}[n]$) peuvent être décrites en termes du vecteur d'entrée $\mathbf{s}[n]$ dans le domaine de fréquence comme:

$$\mathbf{X}(e^{j\omega}) = \mathbf{H}(e^{j\omega})\mathbf{S}(e^{j\omega}) \tag{1.3}$$

Une relation de SLI peut apparemment se percevoir dans cette équation entre $\mathbf{X}(e^{j\omega})$ et $\mathbf{S}(e^{j\omega})$. Pour estimer et reconstruire les signaux $\mathbf{S}(e^{j\omega})$, on peut évaluer une matrice $\mathbf{F}(e^{j\omega})$ comprenant M filtres numériques de synthèse. En conséquent, le vecteur de sortie s'obtient par la relation suivante :

$$\widehat{\mathbf{S}}(e^{j\omega}) = \mathbf{F}(e^{j\omega})\mathbf{X}(e^{j\omega}) = \mathbf{F}(e^{j\omega})\mathbf{H}(e^{j\omega})\mathbf{S}(e^{j\omega}) \tag{1.4}$$

1.1.2.2 La conception de la matrice des filtres de synthèse

Le CAN d'architecture BFH à structure MRT est considéré (la figure 1.2). Dans le paragraphe précédent, on a expliqué que les M échantillons successifs de l'entrée d'origine sont considérés comme le nouveau vecteur d'entrée qui sera estimé à la sortie des BFH à structure MRT. Si une des matrices de filtres d'analyse ou ceux de synthèse est connue à priori, l'autre peut être calculée. Dans la pratique, il est préférable de supposer les filtres analogiques (banc d'analyse) a priori connus à cause des contraintes des circuits analogiques. Ainsi, on désire concevoir les filtres de synthèse (numériques) en supposant a priori M circuits analogiques comme étant les filtres d'analyse. Pour obtenir commodément la matrice des filtres de synthèse, le bruit de quantification des convertisseurs A/N de toutes les branches est de nouveau négligé. En employant le modèle du CAN à structure MRT (la figure 1.3), les équations de RP seront :

$$\mathbf{F}(e^{j\omega}).\mathbf{H}(e^{j\omega}) = \mathbf{I}.e^{-j\omega n_d} \tag{1.5}$$

où **I** représente la matrice identité de dimension $M \times M$ et n_d représente un retard quelconque. Le retard est ajouté pour maintenir la causalité. En employant la méthode d'optimisation des Moindres Carrées (MC), l'équation 1.11 mène à la solution suivante pour chaque fréquence donnée:

$$\mathbf{F}(e^{j\omega}) = e^{-j\omega n_d}\mathbf{H}^{-1}(e^{j\omega}) \tag{1.6}$$

où l'existence de la matrice inverse $\mathbf{H}^{-1}(e^{j\omega})$ est implicitement supposée (le choix des filtres d'analyse est fait de telle façon que la matrice d'analyse soit non-singulière). Cette relation peut être établie pour les N fréquences quelconques (pour garder l'interpolation appropriée). Ainsi, la réponse en fréquence de chaque filtre de synthèse peut être obtenue à partir de l'équation 1.6. Un filtre à Réponse Impulsionnelle Finie (RIF) peut être employé pour estimer chaque élément de la matrice des filtres de synthèse. En utilisant des estimations à RIF des filtres de synthèse, des termes de distorsion et des interférences apparaissent à la sortie. Alors, tout signal de sortie peut être exprimé en termes de fonctions de distorsion et d'interférences. Celles-ci peuvent s'appeler les Interférences Inter-Canaux (IIC). Les IIC sont équivalentes aux termes d'aliasing de l'architecture classique. Supposons des filtres de synthèse à RIF, la matrice est définie comme suivant:

$$\mathbf{T}(e^{j\omega}) = \mathbf{F}(e^{j\omega})\mathbf{H}(e^{j\omega})$$

Où $\mathbf{T}(e^{j\omega})$ est une matrice contenant la fonction de la distorsion et celles des IIC. En intégrant avec équation 1.4, tout signal de sortie $\widehat{s}_k[n]$ peut être décomposé dans le domaine de fréquence comme:

$$\hat{S}_k(e^{j\omega}) = \underbrace{T_{kk}(e^{j\omega})S_k(e^{j\omega})}_{distorsion} + \underbrace{\sum_{m=0,m\neq k}^{M-1} T_{km}(e^{j\omega})S_m(e^{j\omega})}_{IIC} \tag{1.7}$$

L'élément diagonal $T_{kk}(e^{j\omega})$ de la ligne k de la $\mathbf{T}(e^{j\omega})$ décrit la fonction de distorsion du $k$ème composant du MRT. Les autres M-1 éléments de cette ligne représentent les IIC présentes dans la sortie $\widehat{s}_k[n]$. $e^{-j\omega n_d}$ est la valeur idéale pour la fonction de distorsion et les éléments IIC sont idéalement nuls.

1.1.3 Simulations d'un CAN à structure MRT et à huit branches

1.1.3.1 Conception dans le domaine temporel

En utilisant l'environnement MATLAB/Simulink, un CAN à structure MRT et à huit branches est simulé dans le domaine temporel. Un banc de filtres d'analyse simplement réalisables comprenant un circuit RC (Résistance-Capacité) et sept circuits RCI (Résistance-Capacité-Inductance) est utilisé. Le filtre RC fonctionne en tant que filtre passe-bas. Les sorties suivent bien les signaux d'entrée avec un retard Mn_dT. On rappelle que le retard temporel de l'architecture classique est n_dT (ou bien M fois moins élevé que celui de l'architecture MRT) bien que les deux architecture suppose le même retard discret n_d. En effet, dans l'architecture MRT on ne fait pas un élevage de fréquence à l'opposé du cas classique (voir les figures 1.1 et 1.2). Des filtres RIF ayant 64 coefficients ont été utilisés comme banc des filtres de synthèse. Pour obtenir un niveau des IIC qui serait pratiquement acceptable, on a proposé qu'une petite partie du spectre de chaque composante MRT soit réservée comme Bande de Garde (BG) (cf. le chapitre 5). D'une manière équivalente, une partie du spectre n'est pas occupé par le signal d'entrée dans le cas d'architecture classique ce qui implique un sur-échantillonnage. Le rapport de BG représente le pourcentage de chaque sous-signal de MRT consacré à la BG. Le rapport de sur-échantillonnage correspond au pourcentage de la fréquence de Nyquist $\frac{1}{T}$ qui n'est pas employé par le signal d'entrée. On utilise ici le rapport de sur-échantillonnage optimal 7% constaté dans [5]. De la même manière, on a utilisé un rapport de BG 7% pour l'architecture MRT. La figure 1.5 montre le spectre d'erreur quand un signal sinusoïdal à la fréquence $\omega_0 = 0,5\frac{\pi}{8T}$ est présenté à l'entrée des deux structures. Pour cette entrée sinusoïdale, aucun signal n'apparat aux bandes de garde des huit composants de MRT. Remettant en série les composante parallèles de MRT (les sorties), l'entrée d'origine $x[n']$ est simplement reconstruite. La figure 1.5 montre clairement que l'on a une meilleure performance pour l'architecture MRT par rapport à classique supposant une entrée sinusoïdale. Un signal aussi important apparat dans les bandes de sur-échantillonnage dans le cas classique. Donc, une étape Post-Filtrage (PF) serait incontournable pour enlever le signal d'erreur apparaissant en bande de sur-échantillonnage. Par contre, le bruit dans

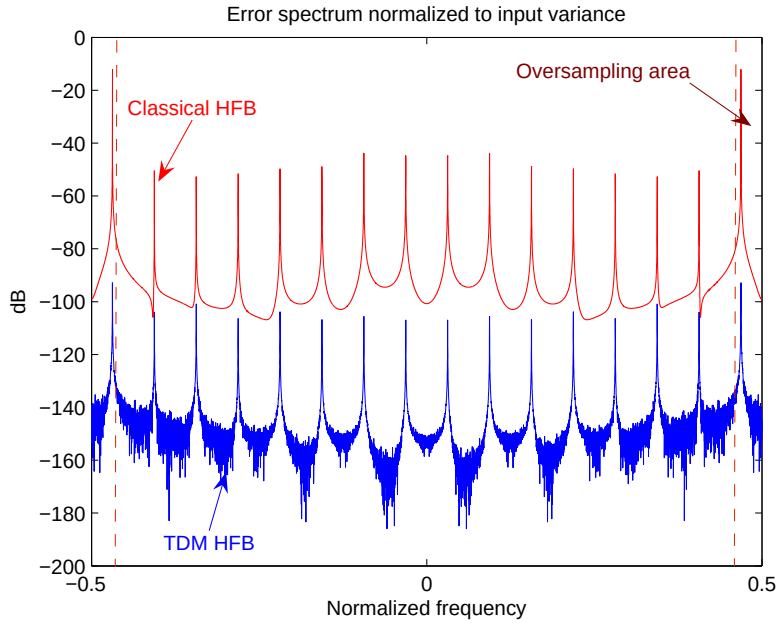

Figure 1.5. Le spectre d'erreur associé à l'architecture MRT (en bleu) et classique (en rouge) pour une entrée sinusoïdale.

les BG de l'architecture MRT ne s'amplifie pas. Par exemple, le Rapport de Signal à Bruit (RSB) de la sortie est presque 49 dB dans le cas classique lorsqu'un PF n'est pas utilisé. Mais, le RSB s'améliore au 73 dB quand on élimine la bande de sur-échantillonnage (autrement dit faire le PF). Le PF n'est pas nécessaire pour le cas MRT puisque l'erreur ne s'intensifie pas dans ses BG pour ce signal sinusoïdal. Le RSB de l'architecture MRT est 123dB qui représente une grande supériorité de 50 dB par rapport au cas classique. La figure 1.6 représente une comparaison entre l'architecture MRT et classique pour un signal chirp en entrée. Le chirp d'entrée balaye le spectre entre les fréquences zéro et $(1-\alpha)\frac{\pi}{T}$ où α représente le rapport de sur-échantillonnage de 7%. Ni les BG, ni la bande de sur-échantillonnage n'ont été filtrées dans cette figure. En négligeant les BG et la bande de sur-échantillonnage, les architectures MRT et classique sont respectivement associées aux RSB 91 dB et 63 dB. Etant donné que la sortie du CAN à structure classique a été post-filtrée pour éliminer la bande de sur-échantillonnage, la sortie de chaque branche du CAN à structure MRT est également post-filtré avec le même filtre. L'architecture MRT a besoin de traiter M filtrage numériques correspondant aux M sorties. Les simulations dans le domaine temporel montrent que l'architecture MRT peut mener à

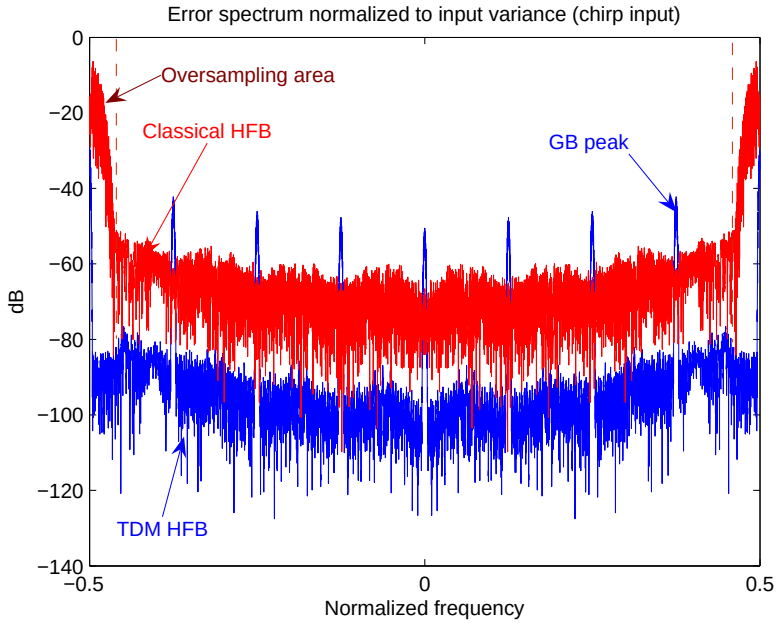

Figure 1.6. Le spectre d'erreur associé à l'architecture MRT (en bleu) et classique (en rouge) pour une entrée du chirp.

une meilleure performance que celle classique en l'absence d'erreurs de réalisations en ce qui concerne les interférences IIC (l'aliasing dans le cas classique).

1.1.3.2 Sensibilité aux imperfections analogiques

Pour étudier la sensibilité aux erreurs de réalisation, les structures classiques et MRT sont simulées en présence des imperfections analogiques. Les architectures de CAN à huit branches sont ici considérées comme dans le paragraphe précédent. Pour observer les effets des imperfections analogiques, tous les éléments électroniques (R, C et I) des filtres d'analyse sont supposés ayant un profil gaussien. L'écart type empirique de la distribution gaussienne est utilisé pour représenter les imperfections analogiques (STD). Les simulations sont répétées pour 1000 épreuves pour chaque valeur des erreurs de réalisation. La résolution de sortie des deux structures MRT et classique est prise comme référence pour faire la comparaison entre leurs performances. Dans un premier temps, on suppose que l'entrée est un signal sinusoïdal de fréquence $\omega_0 = 0,5\frac{\pi}{8T}$. La figure 1.7 montre la résolution de sortie (en bit) pour les deux architectures MRT et classique versus les erreurs

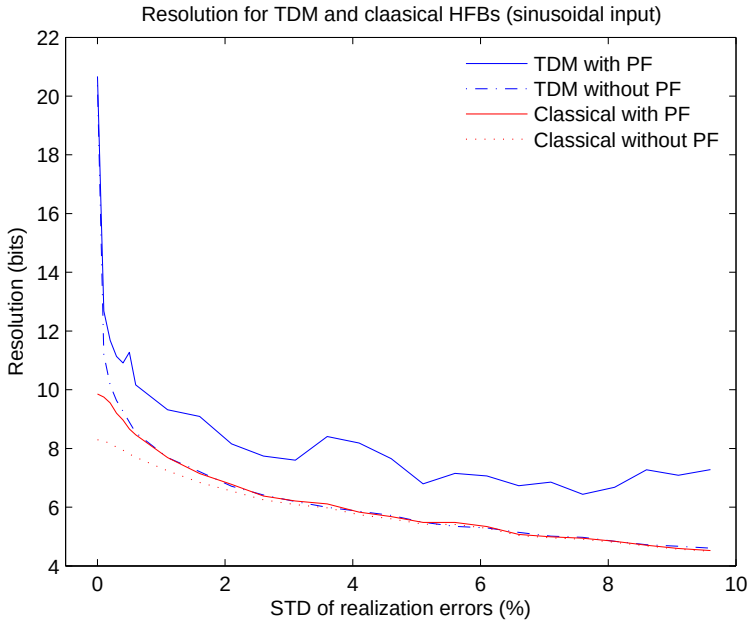

Figure 1.7. La résolution de sortie des architectures classiques (en rouge) et MRT (en bleu) versus l'écart type de la distribution des erreurs. Un signal sinusoïdal est appliqué à l'entrée

de réalisation (l'écart type de la distribution des erreurs). Si le PF est appliqué pour éliminer la bande de sur-échantillonnage et les BG associées respectivement aux cas classique et MRT, l'architecture de MRT présente une performance de 3 bits meilleure que celle lié au cas classique en présence des erreurs de réalisation. Cela signifie que l'architecture MRT est moins sensible que la classique aux erreurs de réalisation dans le cas de l'entrée sinusoïdale. Autrement dit, le RSB de l'architecture classique s'améliore de 20 dB en utilisant la structure MRT. Si les régions spectrales des BG ne sont pas filtrées pour le MRT, il mène à la même résolution que le CAN à structure classique après avoir filtré la bande de sur-échantillonnage. Ceci prouve que l'architecture de MRT peut fournir dans le plus mauvais des cas (c'est-à-dire sans PF) la même performance que celle du cas classique. Pour avoir une comparaison sur le spectre entier, un chirp balayant l'intervalle spectral entre 0 et $(1-\alpha)\frac{\pi}{T}$ est appliqué comme entrée. Le rapport de sur-échantillonnage α est supposé valoir 7%. Un procédé similaire au cas de l'entrée sinusoïdale est appliqué pour obtenir la sensibilité aux erreurs de réalisation. La figure 1.8 illustre la résolution de sortie associée au cas classique et MRT versus

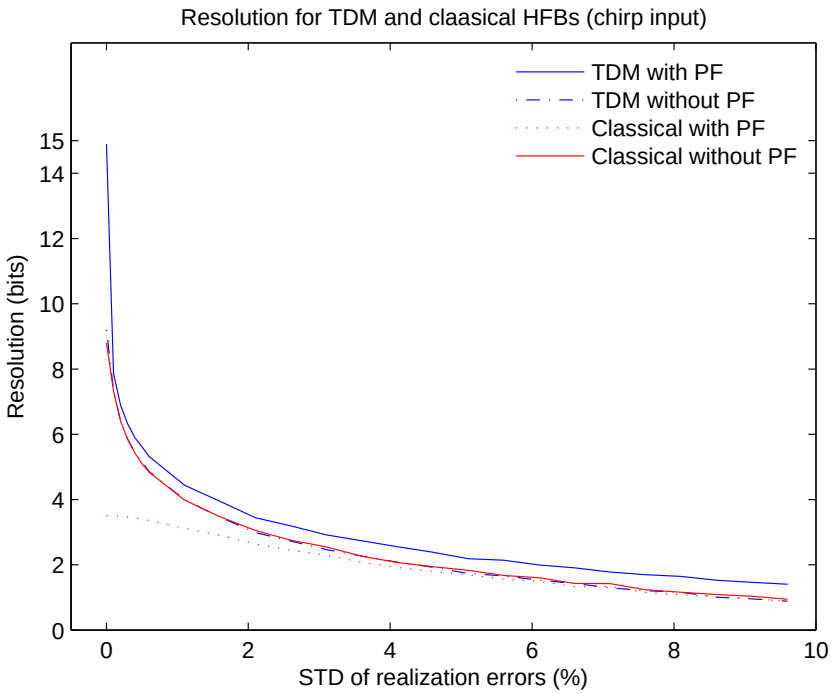

Figure 1.8. La résolution sortie des architectures classiques (en rouge) et MRT (en bleu) versus l'écart type de la distribution des erreurs. Un signal chirp est appliqué à l'entrée

les erreurs de réalisation. Pour le signal d'entrée chirp, l'architecture de MRT montre une performance meilleure d'environ 1 bit en présence des imperfections analogiques par rapport au cas classique. On rappelle que la performance du MRT est bien meilleure que dans le cas d'absence des erreurs de réalisation (voir la figure 1.8 pour les erreurs égales à zéro). Un autre résultat intéressant peut être déduit de ces deux simulations. Selon les figures 1.7 et 1.8, le MRT peut fournir une performance approximativement égale au classique même si aucun PF n'est considéré pour éliminer les BG. Cependant, si la bande de sur-échantillonnage n'est pas filtrée pour le CAN classique, la performance se dégrade beaucoup.

1.1.4 Conclusion

Les simulations du CAN à structure MRT dans le domaine temporel ont montrées que les équations mathématiques proposées pour l'architecture MRT sont pratiquement valides puisque le signal d'origine est précisément estimé à la sortie. On

a également montré que l'architecture MRT a une meilleure performance que le cas classique en termes de résolution de la sortie en l'absence des erreurs de la réalisation (environ 10 et 6 bits pour les entrées sinusoïdales et chirp respectivement). En présence des erreurs de réalisation, l'architecture MRT mène aussi à une plus grande résolution (3 bits et 1 bit) que l'architecture classique (pour les entrées sinusoïdales et chirp respectivement). Le PF semble être toujours nécessaire pour le BFH classique afin d'éliminer le signal du bruit apparaissant sur le sous-spectre de sur-échantillonnage. Bien que le CAN à structure MRT ait besoin de M^2 filtres numériques de synthèse par rapport à M filtres pour le cas classique, la complexité de calcul pour chaque échantillon de sortie est la même pour les deux structures parce que le MRT fournit M échantillons de sortie à chaque top d'horloge. En conclusion, un SLI régit la relation entre les entrées et sorties du CAN à structure MRT à l'opposé du cas classique où celle-ci ne représente pas un SLI. Ainsi, une méthode aveugle telle que la déconvolution peut être appliquée seulement à l'architecture de MRT pour corriger d'une manière adaptative les erreurs de réalisation. Cela n'est pas possible pour les systèmes variables dans le temps tel que le CAN à structure classique.

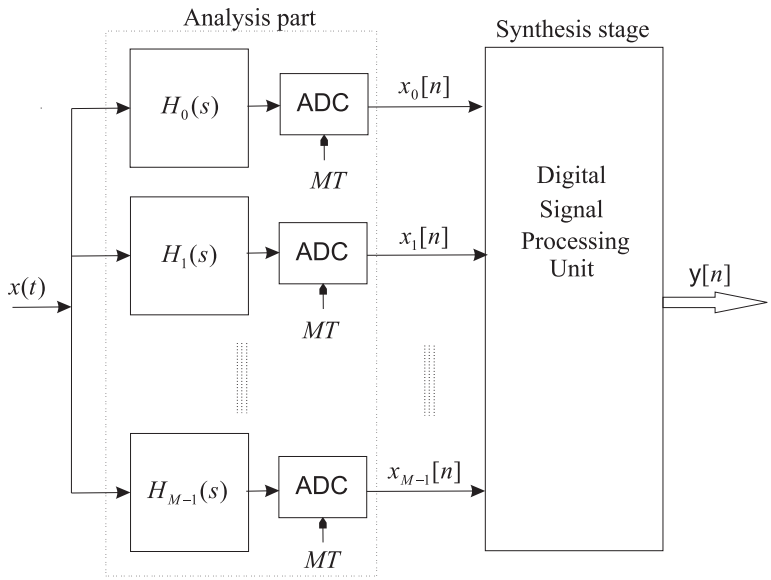

Figure 1.9. Le schéma général d'un CAN à BFH. La sortie y[n] représente soit une séquence soit un vecteur de signaux associés respectivement à l'architecture classique et à entré-sortie multiple.

1.2 Un convertisseur A/N à large-bande pour la radio logicielle

1.2.1 Introduction

Les CAN actuels ne peuvent pas encore remplir les conditions requieses pour le récepteur à large bande pour la radio logicielle. Un des principes de la radio logicielle est la compatibilité entre les diverses protocoles de communication sans fil [8]. Le récepteur et l'émetteur de la radio logicielle seraient ouverts à une plus grande largeur du spectre de telle manière que les filtres et le système qui distribue entre différrents canaux (channelizer) conventionnellement analogiques puissent être substitués par des traitements numériques. Par conséquent, le cot global du récepteur serait constant et indépendant du nombre de canaux [8]. Pour éviter les inconvénients des bancs de filtres en temps discret et ses difficultés de réalisation, il est proposé d'utiliser des filtres analogiques dans les BFH. La figure 1.9 illustre l'architecture générale d'un CAN à BFH. M filtres numériques construisent l'étape de synthèse dans l'architecture classique (la figure 1.10) [9, 10]. On a proposé les architectures à MRT et à sous-bande (la figure 1.11) de sorte qu'un système SLI

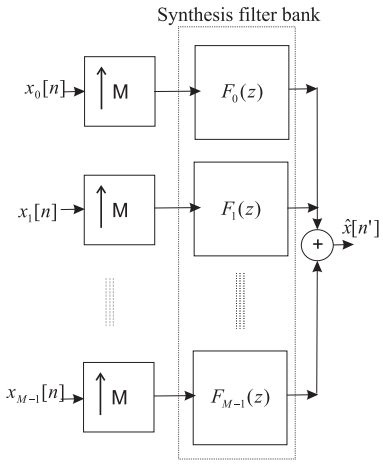

Figure 1.10. L'étape de synthèse des BFH à l'architecture classique

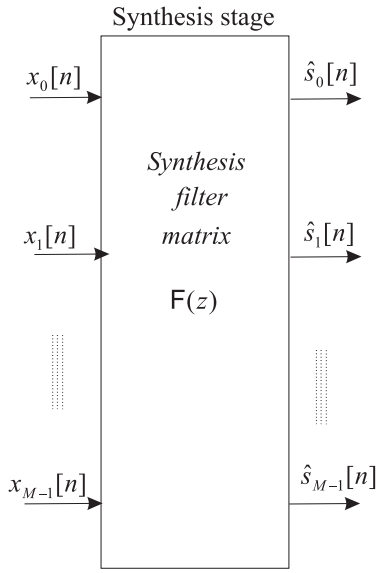

Figure 1.11. L'étape de synthèse des BFH à entrée-sortie multiple.

représenterait la relation entrée-sortie tandis que celle des BFH classique est non-SLI (cf. le chapitre 5). Les BFH à entrée-sortie multiple sont non seulement moins sensible aux erreurs analogiques, mais également compatible avec des techniques numériques telles que la deconvolution aveugle afin de compenser les erreurs. Une comparaison complète entre l'architecture classique et à entrée-sortie multiple est présentée en utilisant des simulations temporelles dans cette partie. Le prochain paragraphe présente les deux groupes d'architectures des BFH en résumé. Aussi, la conception des filtres de synthèse est décrite pour les BFH différents. Dans

le paragraphe 1.2.4, toutes les architectures des BFH sont simulées et comparées l'une à l'autre. Enfin, les résultats sont résumés en conclusion.

1.2.2 La reconstruction parfaite

1.2.2.1 Les BFH à architecture classique

Le CAN à BFH classique est montré dans les figures 1.9 et 1.10. En négligeant le bruit de quantification lié aux convertisseurs A/N à chaque branche, la description spectrale $\widehat{X}(e^{j\omega})$ de la sortie $\hat{x}[n']$ serait comme il suit [11]:

$$\widehat{X}(e^{j\omega}) = \underbrace{\widetilde{X}(j\Omega)\cdot T_{\circ}(e^{j\omega})}_{\text{terme de distortion}}\Big|_{\Omega=\frac{\omega}{T}} + \underbrace{\sum_{m=1}^{M-1}\widetilde{X}(j\Omega)\cdot T_m(e^{j\omega})}_{\text{termes d'aliasing}}\Big|_{\Omega=\frac{\omega}{T}-\frac{2\pi}{MT}m}$$

où $\widetilde{X}(j\Omega)$ représente l'extension périodique de l'entrée considérant l'intervalle spectral $[\frac{-\pi}{T}, \frac{\pi}{T}]$ (avec la période $\frac{2\pi}{T}$). La distorsion et les termes d'aliasings (m=1,$\cdots$, M-1) sont :

$$\begin{cases} T_{\circ}(e^{j\omega}) = \frac{1}{MT}\sum_{k=0}^{M-1} F_k(e^{j\omega})\cdot\widetilde{H}_k(j\frac{\omega}{T}) \\ \\ T_m(e^{j\omega}) = \frac{1}{MT}\sum_{k=0}^{M-1} F_k(e^{j\omega})\cdot\widetilde{H}_k(j\frac{\omega}{T} - j\frac{2\pi}{MT}m) \end{cases} \tag{1.8}$$

où $\widetilde{H}_k(j\Omega)$ est obtenu par prolongement périodique du filtre analogique d'analyse $H_k(j\Omega)$ avec la période $\frac{2\pi}{T}$ de la même manière que $\widetilde{X}(j\Omega)$. La reconstruction parfaite (RP) est accomplie quand la sortie et les échantillons d'entrée sont les mêmes sauf un possible retard. C'est à dire, les conditions de RP peuvent être interprétées comme il suit:

$$\begin{cases} T_{\circ}(e^{j\omega}) = e^{-j\omega n_d} \\ \\ T_m(e^{j\omega}) = 0 \qquad m = 1,\ldots,M-1 \end{cases} \tag{1.9}$$

1.2.2.2 L'Architecture à multiple entrée-sortie

Dans l'architecture sous-bande ou MRT (voir la figure 1.11), on cherche à parfaitement reconstruire un vecteur d'entrée $\mathbf{s}[n]$. Pour obtenir la matrice de filtres de synthèse, les M filtres analogiques d'analyse sont substitués par une matrice $\mathbf{H}(z)$ de filtres numériques de la dimension $M \times M$. Chaque élément $H_{kl}(e^{j\omega})$ de $\mathbf{H}(e^{j\omega})$ représente un filtre numérique qui pourrait être obtenu à partir du filtre analogique $H_k(j\Omega)$ selon le type de la structure à multiple entrée-sortie. Dans les cas sous-bande et à MRT, la réponse fréquentielle $\widehat{\mathbf{S}}(e^{j\omega})$ du vecteur $\widehat{\mathbf{s}}[n]$ de sorties peut être décrite en termes de vecteur $\mathbf{S}(e^{j\omega})$ d'entrée:

$$\widehat{\mathbf{S}}(e^{j\omega}) = \mathbf{T}(e^{j\omega})\mathbf{S}(e^{j\omega}) = \mathbf{F}(e^{j\omega})\mathbf{H}(e^{j\omega})\mathbf{S}(e^{j\omega}) \tag{1.10}$$

Où $\mathbf{T}(e^{j\omega})$ est une matrice contenant la distorsion et les interférences Inter-Canaux (IIC). Il suppose que la valeur estimée $\widehat{s}_k[n]$ de $k^{\text{ième}}$ élément $s_k[n]$ du vecteur d'entrée peut être développée en fréquence comme suivant :

$$\widehat{S}_k(e^{j\omega}) = \underbrace{T_{kk}(e^{j\omega})S_k(e^{j\omega})}_{\text{distorsion}} + \underbrace{\sum_{m=0,m\neq k}^{M-1} T_{km}(e^{j\omega})S_m(e^{j\omega})}_{\text{IIC}}$$

Le $k^{\text{ième}}$ élément diagonal $T_{kk}(e^{j\omega})$ de $\mathbf{T}(e^{j\omega})$ représente la distorsion liée à l'entrée $s_k[n]$. Les autres M-1 éléments de la $k^{\text{ième}}$ ligne de $\mathbf{T}(e^{j\omega})$ représentent les interférences IIC. Les IIC sont idéalement nuls. Puis, les équations de RP à chaque fréquence ω seront:

$$\mathbf{F}(e^{j\omega}).\mathbf{H}(e^{j\omega}) = \mathbf{I}.e^{-j\omega n_d} \tag{1.11}$$

Où $\mathbf{I}$ représente la matrice identité ($M \times M$) et n_d est un retard quelconque. n_d est considéré pour remplir la condition de causalité et est souvent remplacé par la moitié de la longueur L du filtre de synthèse. La matrice s'obtient pour les architectures à sous-bande et à MRT de la manière suivante.

• L'architecture à sous-bande

Pour obtenir la $k^{\text{ième}}$ ligne de la matrice $\mathbf{H}(e^{j\omega})$, le filtre analogique $H_k(j\Omega)$ est premièrement étudié dans l'intervalle $[\frac{-\pi}{T}, \frac{\pi}{T}]$. Puis, $H_{k0}(e^{j\omega})$, $H_{k1}(e^{j\omega})$, ..., et $H_{k(M-1)}(e^{j\omega})$ sont extraits de la même manière que les composants d'entrée

sous-bande sont obtenus à partir du signal d'origine.

• **L'architecture à MRT**

Dans le cas de MRT, l'extraction de $\mathbf{H}(e^{j\omega})$ peut être faite comme si les réponse impulsionnelles des filtres d'analyse étaient échantillonnées. Chaque élément $H_{kl}(e^{j\omega})$ de $\mathbf{H}(e^{j\omega})$ peut être obtenu à partir du filtre analogique $H_k(j\Omega)$ d'analyse dans le domaine fréquentielle paritr des quations prsentes au chapitre 5.

1.2.3 Conception d'étape de synthèse

En utilisant les équations de RP, un CNA à BFH peut être conçu à condition qu'un des bancs de filtres de synthèse ou d'analyse soit à priori connu. Selon les contraintes des circuits analogiques, on préfère, en pratique, concevoir les filtres numériques de synthèse en fixant un ensemble de circuits analogiques comme filtres d'analyse. La réponse en fréquence des filtres de synthèse peut être obtenue à chaque fréquence ω en utilisant les équations de RP connaissant les filtres d'analyse. Les filtres à Réponse Impulsionnelle Finie (RIF) sont choisis pour réaliser le banc de filtres de synthèse grâce à leur commodité ainsi que leur simplicité. En utilisant des filtres RIF, les équations seraient linéaires en termes de coefficients inconnus de filtres de synthèse. Puis, la réponse fréquentielle des filtres de synthèse peut être estimée par les filtres numériques à RIF. Le nombre L de coefficients de chaque filtre de synthèse joue un rôle important en déterminant la distorsion et les interférences d'aliasings (ou IIC dans le cas à entrée-sortie multiple). Dans la pratique, les équations de RP sont incompatibles aux fréquences près des bords spectraux ($\pm\frac{\pi}{T}$). Pour obtenir une résolution appropriée à la sortie des BFH à l'aide des filtres de synthèse à RIF, ces fréquences devraient être négligées. À cette fin, l'entrée analogique $x(t)$ est supposée d'occuper juste l'intervalle $[-(1-\alpha)\frac{\pi}{T}, (1-\alpha)\frac{\pi}{T}]$ dans le cas classique où α représente le rapport de sur-échantillonnage. On a constaté que le rapport optimal de sur-échantillonnage pour des BFH à huit branches est à peu près de 7%. De même, une partie spectrale de chaque composant d'entrée dans le cas à entrée-sortie multiple doit être désigné comme bande de garde (BG). Dans le cas des BFH à sous-bande, le BG couvre des basses ainsi que des hautes fréquences de chaque composant de sous-bande. Cependant, il suffit que le BG des BFH à MRT couvre des basses ou des hautes fréquences du spectre de chaque

composant MRT selon un nombre M pair ou impair de branches respectivement.

1.2.4 Évaluation des BFH à structures différentes

En utilisant une classe simple des circuits analogiques pour le banc de filtres d'analyse et en négligeant le bruit de quantification, un convertisseur A/N à BFH à huit branches est conçu et simulé dans ce paragraphe. On suppose que le banc de filtres d'analyse se compose de circuits du second-ordre (RLC) sauf un qui est constitué d'un circuit de premier-ordre (RC) en tant que filtre passe-bas. Tous les circuits de second-ordre ont une bande passante constante. Le banc de filtres de synthèse est composés par des filtres numériques à RIF comportant chacun 64 coefficients. Les résultats sont discutés et comparés pour les architectures classiques, à sous-bande et à MRT en termes de différents paramètres tels que la résolution de la sortie et la sensibilité aux erreurs analogiques.

• **Sensibilité aux erreurs analogiques**

Les tableaux 1.1 et 1.2 montrent la résolution de sortie pour les différentes architectures en appliquant les signaux sinusoïdaux et chirp en tant qu'entrée. Ils démontrent que la résolution de sortie est beaucoup plus élevée pour l'architecture à MRT et sous-bande que celle classique en l'absence des erreurs de réalisation de banc d'analyse. En présence des imperfections analogiques, la résolution de sortie réduit rapidement. En présence d'erreurs de réalisation, la résolution de sortie des BFH à MRT et sous-bande reste néanmoins approximativement 2 et 1 bit respectivement supérieure à celle des BFH classiques. Par conséquent, les architectures à entrée-sortie multiple montrent moins de sensibilité aux imperfections analogiques que les BFH classiques. Pour mieux évaluer la performance de différentes architectures, le signal d'erreur en sortie de chaque structure est comparé à celui du cas classique (la figure 1.12). Tous les composants de sortie des BFH à sous-bande sont nuls sauf la première sous-bande dans laquelle se trouve le signal sinusoïdal d'origine. Le signal d'erreur des BFH classiques est clairement plus grand que celui lié au cas à sous-bande et à MRT pour cette entrée sinusoïdale.

• **Emploi des techniques aveugles pour corriger les erreurs**

Les structures à MRT et à sous-bande sont associées à un SLI pour la relation entrée-sortie contrairement au cas classique. Les méthodes telles que l'annulation

Table 1.1. La résolution (en bit) de la sortie pour les différentes architectures des BFH en présence des erreurs analogiques et en supposant une entrée sinusoïdale.

Output resolution (in bits) for a sinusoidal input			
Realization errors (%)	The type of 8-branch HFB Architecture		
	Classical	Subband	TDM
0%	9.9	10.5	21
1%	8	10	9.8
5%	5.8	7	8

Table 1.2. La résolution (en bit) de la sortie des BFH à différentes architectures en présence des erreurs analogiques du banc de filtres d'analyse et en supposant un signal d'origine chirp.

Output resolution (in bits) for a chirp input			
Realization errors (%)	The type of 8-branch HFB Architecture		
	Classical	Subband	TDM
0%	9.6	10.1	17
1%	7.2	8.0	8.6
5%	5.3	6.1	6.6

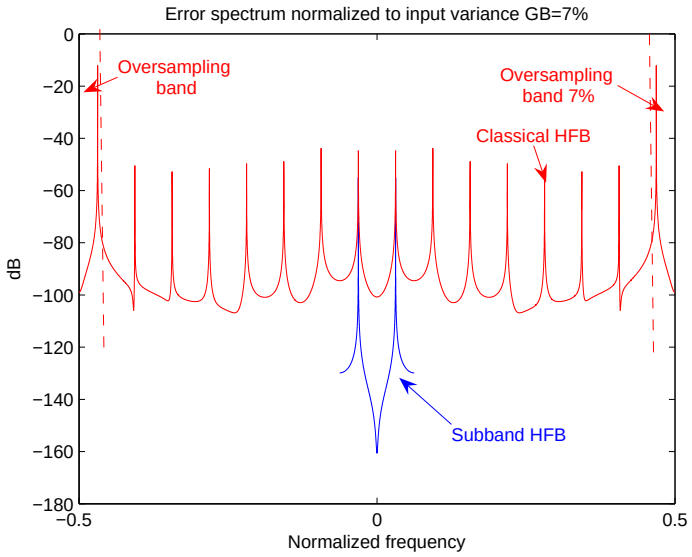

Figure 1.12. Le spectre du signal d'erreur pour l'architecture classique (en rouge) et à sous-bande (en bleu) en supposant un signal d'origine sinusoïdal en fonction de fréquence normalisée.

du bruit peuvent être appliquées à la structure à MRT ainsi qu'à celle à sous-bande afin de corriger les erreurs analogiques. Cependant, la technique de déconvolution aveugle est seulement applicable dans le cas à MRT. La structure à sous-bande ne peut pas exploiter les méthodes aveugles telles que la déconvolution. En fait, celle-ci est valable pour une entrée blanche à profil non-gaussien. En considérant la structure à sous-bande, cela est équivalent à la blancheur à la fois dans le temps et dans la fréquence. Par contre, un signal blanc dans le temps ainsi que dans la fréquence est forcément gaussien. Alors, on ne pourrait pas remplir les conditions d'une méthode aveugle pour la structure à sous-bande.

• **Complexité de l'étape de synthèse**

L'étape de synthèse se compose de M filtres numériques dans le cas des BFH classiques. Néanmoins, on a besoin d'une matrice de filtres numériques (comportant M^2 filtres) pour réaliser l'étape de synthèse des BFH à MRT ainsi qu'à sous-bande. Chaque filtre RIF comportant L coefficients effectue L multiplications afin de calculer sa sortie. Donc, l'étape de synthèse fera respectivement ML et M^2L multiplications dans les cas classique et à entrée-sortie multiple durant chaque cycle de calcul. D'autre part, une structure à entrée-sortie multiple fournit M échantillon en tant que sorties à chaque cycle de calcul à l'inverse d'un seul pour des BFH classique. Alors, le nombre de multiplications par rapport à chaque échantillon de sortie sera le même pour les deux groupes de BFH (L multiplication par chaque échantillon de sortie). En outre, les BFH à entrée-sortie multiple n'ont pas besoin des blocs de Zero-padding (étalement des zéros) qui sont utilisés pour l'architecture classique. En phase de conception, une différence encore importante existe. En supposant N points de fréquence en phase de conception de l'étape de synthèse, les BFH classiques sont associés à une matrice d'analyse de la dimension $MN \times MN$. Par contre, les structures à entrée-sortie multiple correspondent à de petites matrices d'analyse de la dimension $M \times M$ à chaque point de fréquence. Il est évident que l'on a besoin d'un beaucoup plus grand nombre de calcul pour obtenir l'inverse de la matrice de dimension $MN \times MN$ que celle des matrices de dimension $M \times M$. Ainsi, les BFH classiques dispose d'une phase de conception beaucoup plus complexe que celle de la structure à entrée-sortie multiple. Cette différence serait très importante si un algorithme adaptatif était employé afin de corriger les erreurs analogiques

1.2.5 Conclusion

Les différentes architectures des BFH pour réaliser des CAN en parallèle sont démontrées comme étant de bons candidats pour réaliser le concept de la radio logicielle. Deux architectures à entrée-sortie multiple nommée sous-bande et MRT sont présentées et les équations de RP sont décrites ainsi que la méthode de conception associée. Les BFH classiques, à sous-bande et MRT sont dans le domaine temporel. Les architectures à entrée-sortie multiple paraissent moins sensibles aux erreurs analogiques en terme de résolution de la sortie que celle classique. En outre, les deux groupes de BFH ont la même complexité de calcul. Enfin, les architectures à entrée-sortie multiple peuvent être corrigées en ce qui concerne les erreurs analogiques en utilisant la méthode d'annulation du bruit contrairement au cas classique. Par contre, les méthodes aveugles telles que la déconvolution n'est applicable qu'à la structure à MRT.

Chapter 2

Introduction

Minds are like parachutes. They only function when they are open.
- J. Dewar

The relation between an analog signal and its sampled form has been studied in the first half of twentieth century [12, 13]. The Analog to Digital (A/D) as well as Digital to Analog (D/A) converters are often one of the most critical components in the applications such as the storage of real time signals, radar signal processing systems, digital time-base correction and digital enhancement of images[4]. The rate and precision of conversion are two important factors in the design and use of A/D or D/A converters. The conversion rate is associated with the sampling clock and represents the speed of circuit. The precision of conversion is measured in bits or by Signal to quantization Noise Ratio (SNR) at the output. Figure 2.1 illustrates the actual different types of A/D converters [14]. The important challenge in A/D and D/A conversion is to achieve both of high-speed and high-resolution conversion at the same time, particularly for the communications systems. This feature is vital in some equipments and applications such as radar receivers, network analyzers, test equipments like oscilloscopes, modems and medical imaging systems[9]. The resolution, and thus the dynamic range of a Nyquist rate A/D converter (one output sample per each period of Nyquist rate) is limited by the component matching or offset spread at its front-end. The flash (or all parallel) A/D Converters (ADCs) represent the most commonly used architecture for high speed A/D conversion. In this case, the conversion rate is fundamentally limited

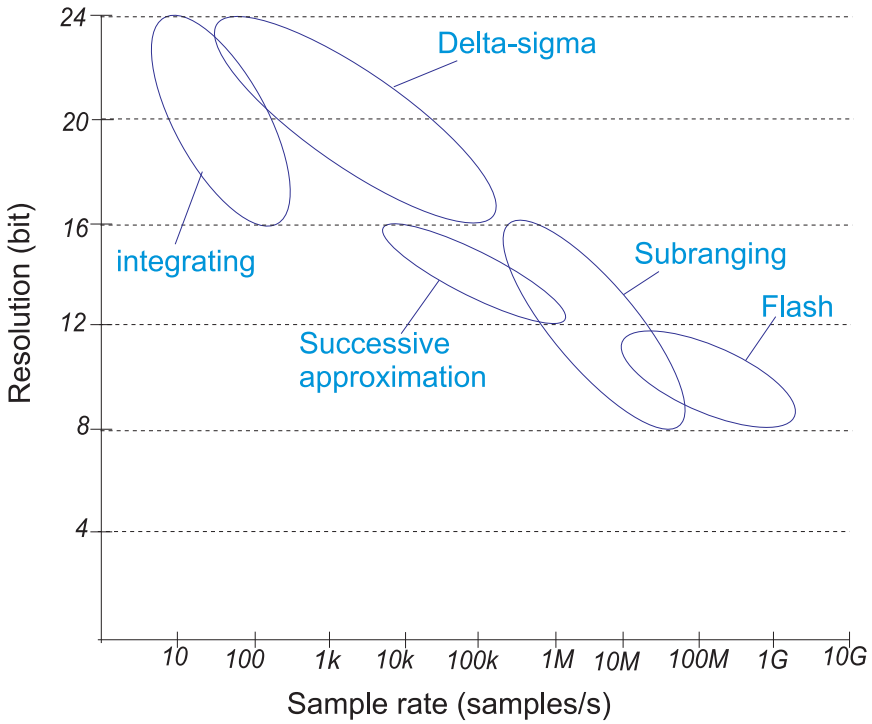

Figure 2.1. Different types of A/D converter in terms of resolution (in bits) versus the sampling rate (in samples per second) extracted from [14].

by the decision time for the latches comparing the input with the threshold levels [15]. However, the complexity of flash ADC circuit grows exponentially with the number of bits of the resolution. Accordingly, the flash converters are practically designed with about 10 bits in a single chip (see figure 2.1). Flash monolithic A/D converters are not available at a sufficiently low cost or price for commercial applications. Flash converters require a large die size and/or fairly exotic fabrication processes so that the relevant integrated circuits have remained too expensive for many applications such as television receivers. In addition, it is exceedingly difficult to integrate analog part with a VLSI digital signal processor for Flash A/D or D/A conversion technique because of the large ADC die size and for process bandwidth requirements.

Considering figure 2.1, oversampling A/D converters called delta-sigma ($\Delta\Sigma$) converters exist on the extreme of resolution. Over the last few years, the low cost and availability of quality $\Delta\Sigma$ devices have had a considerable impact on the hi-fidelity and voice-band audio. $\Delta\Sigma$ ADC can now provide almost 24 bits of reso-

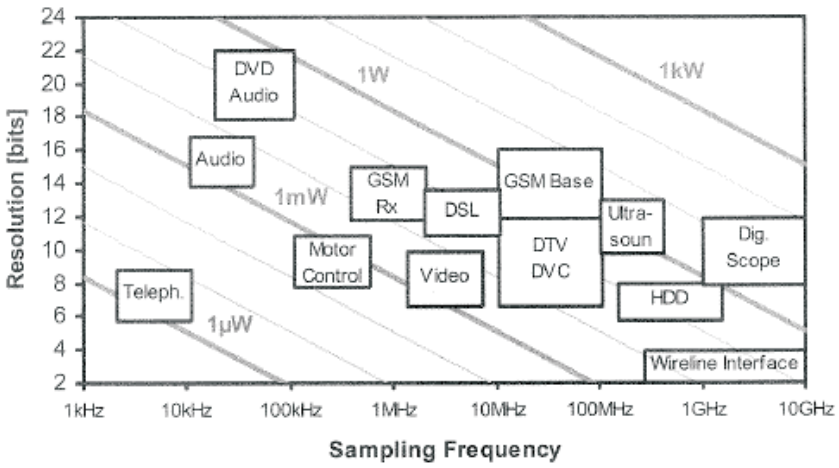

Figure 2.2. ADC applications in the speed/resolution space considering the equi-power contours extracted from [18].

lution for low frequency (about 100Hz) biomedical applications and easily produce the accuracy level of 20 bits for hi-fidelity audio systems [16]. However, a large OverSampling Ratio (OSR) is necessary to provide the high precision conversion. The total sampling rate is very limited because of the large OSR and practical constraints of electronic circuits [17]. The choice of an ADC or DAC (Digital to Analog Converter) for a specific application depends also on the other parameters such as power dissipation. In many cases, the throughput of ADCs is set by the allowable power dissipation [18]. Figure 2.2 shows several ADC applications in the speed/resolution space with contours of equal power consumption.

The demand for A/D or D/A converters with higher speeds has dramatically increased for realizing the new communications concepts such as Software-Defined Radio (SDR) approach [19, 20]. Nowadays, the performance of ADCs cannot still fulfill the requirements of the wide-band receiver of SDR approach. The available silicon technologies do not provide the performance required and the current converters are far from meeting them [21]. The primary target of SDR is to be compatible with various wireless communication protocols [8]. Stimulated by the need for a global communication network, SDR will form a new industry on an even larger scale than the personal computer industry [22, 2]. Figure 2.3 shows the general idea of software radio [23]. The receiver and transmitter of SDR are open to a wider segment of spectrum so that the conventional analog

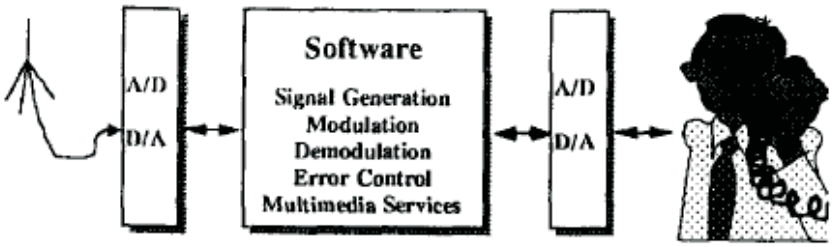

Figure 2.3. General idea of software-defined radio systems. The wide-band ADC and DAC are necessary for digitally realizing the conventionally analog parts such as modulator/demodulator and channelizer extracted from [26].

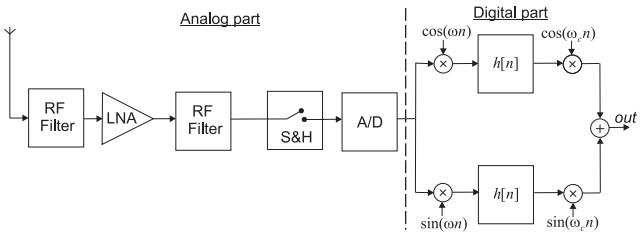

Figure 2.4. Example of a receiver topology [27].

sharp filters and channelizer are substituted by digital filtering [24, 25]. Then, the cost of receiver is independent of the channel number [8]. Moreover, for some years, the tendency is to place the ADC nearest the antenna. This implies that the converter processes wide-band signal and delivers a digital signal with a large resolution [27]. An exemplary architecture for this kind of receivers is shown in figure 2.4. Considering the large demands for higher sampling rates as well as the practical constraints of common A/D converters, the use of A/D converters in parallel has been attractive for four decades. In 1980, Black and Hodges proposed a new technique of high-speed A/D conversion which is realized through an array of time-interleaved parallel converters [28, 29]. This approach is able to provide a high sampling rate, a considerable reduction in die size consumption and power dissipation as well as it includes the on-chip compatibility with dense digital signal processors. Hewlett-Packard presented an 8 Gs/sec, 8 bit time-interleaved ADC with a signal bandwidth of nearly 2 GHz [4]. Timing errors, harmonic distortions and nonlinearities due to the mismatch between individual A/D converters, clock jitters of two rank sampling and uncontrolled quantization noise are the great problems of this technique [9, 30].

Generalized sampling theorem has been another inspiration for offering new parallel A/D converters. As a simple form of generalized sampling theorem, Shannon in his classic paper had even announced that a low-pass signal may be reconstructed if the samples of signal and its derivatives are available at a lower rate as follows [12]:

> *One can further show that the value of the function and its derivative at every other sample point are sufficient. The value and first and second derivatives at every third sample point give a different set of parameters which uniquely determine the function.*

An early result along these lines was given by Fogel, namely, that sampling a low-pass band-limited ($|\Omega| \leq \sigma$) signal and its first $(m-1)$ derivatives, each at a rate of $\frac{2\sigma}{m}$, suffices for a complete reconstruction of the analog signal [31]. Considering these simple extensions of sampling theory, Papoulis proposed the generalized sampling theorem showing that the complete reconstruction may be possible if any $(m-1)$ Linear Time-Invariant (LTI) filtered forms of input signal are available [32]. Based upon generalized sampling theorem which was offered by Papoulis and later discussed and extended by the others [33], multirate filter banks were proposed as a special extension of time-interleaving technique for A/D and D/A conversion [34, 35, 36]. Petraglia and Mitra offered a high-speed A/D conversion technique employing Quadrature Mirror Filter (QMF) banks [37]. Figure 2.5 illustrates this structure [38]. It includes two filter banks. The first one called analysis filter bank is a discrete-time filter bank and the other one consisting of digital filters is called synthesis filter bank. This idea has then been followed and studied by the others [39, 9, 10]. The discrete-time Hybrid Filter Bank (HFB) architecture overcomes the problems of extremely high sensitivity to the mismatch of converters and timing errors from which time interleaving structure suffers much [3]. The filters employed in the HFB architecture isolate the converters of each branch and attenuate the aliasing errors caused by gain and phase mismatches existing between every pair of channels. The analysis filters of discrete-time type used in this structure are commonly realized by Charge Coupled Devices (CCD). CCD architecture is well suited for low power and monolithic purposes but it is nevertheless limited to the moderate speeds (tens of MHz) and it would no longer be low power for high resolution applications [4]. Anyway, it is necessary to have

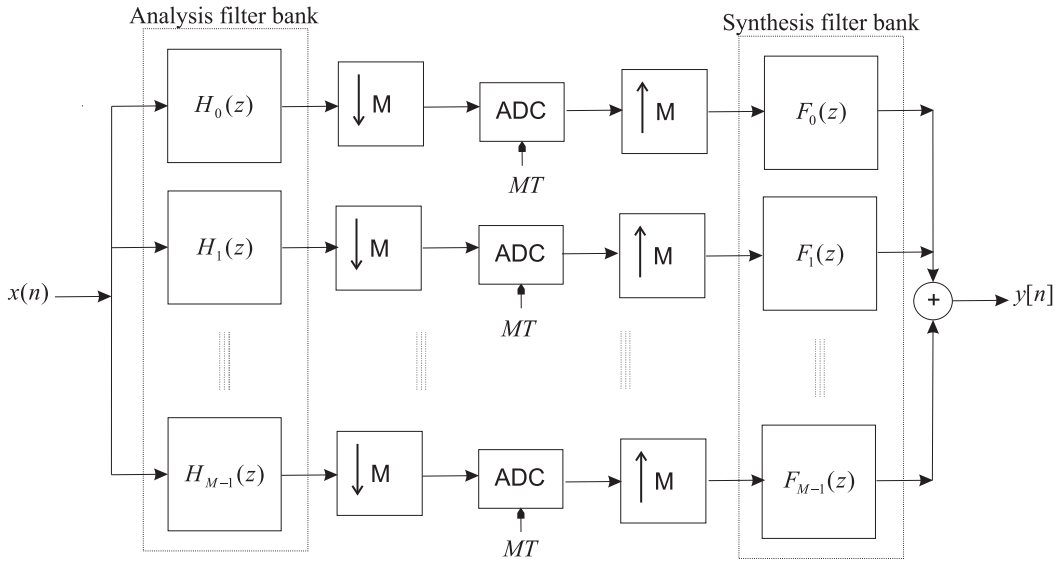

Figure 2.5. Parallel A/D converter using discrete-time parallel structure. Analysis filter bank includes Switched-Capacitor (SC) circuits.

a very fast and very high-precision sampler for input stage of discrete-time HFB A/D converters. Furthermore, Switched-Capacitors (SC) circuits employed in the input stage have to function at the same frequency that sampler operates. Noises generated by operational amplifiers and switches, limited gain-bandwidth product of operational amplifiers and limited capacitor ratio accuracy are the non-ideal effects of SC analysis filters representing the main sources of errors [19, 40].
Considering these disadvantages of discrete-time filter bank and its realization difficulties in A/D or D/A conversion, analog filter banks have been offered to operate instead of discrete-time analysis filter bank. Figures 2.6 and 2.7 show these continuous-time HFB structure for A/D and D/A converters respectively.

This idea was firstly presented and dealt with by Brown [34]. The technique was later discussed and developed by Velazquez [41, 42], Oliaei [43] and Lowenborg [44, 45, 46]. A frequency analysis of continuous-time HFB-based A/D converters has been proposed in [47]. In this frequency analysis, the distortion and interference (aliasing) terms are represented in terms of $2M-1$ expressions of analysis/synthesis filters for an HFB having M branches. Anyway, it may be interpreted using only M terms considering periodic extensions of analysis filters as in appendix A [11]. The approximations of standard filters Butterworth, Tcheby-

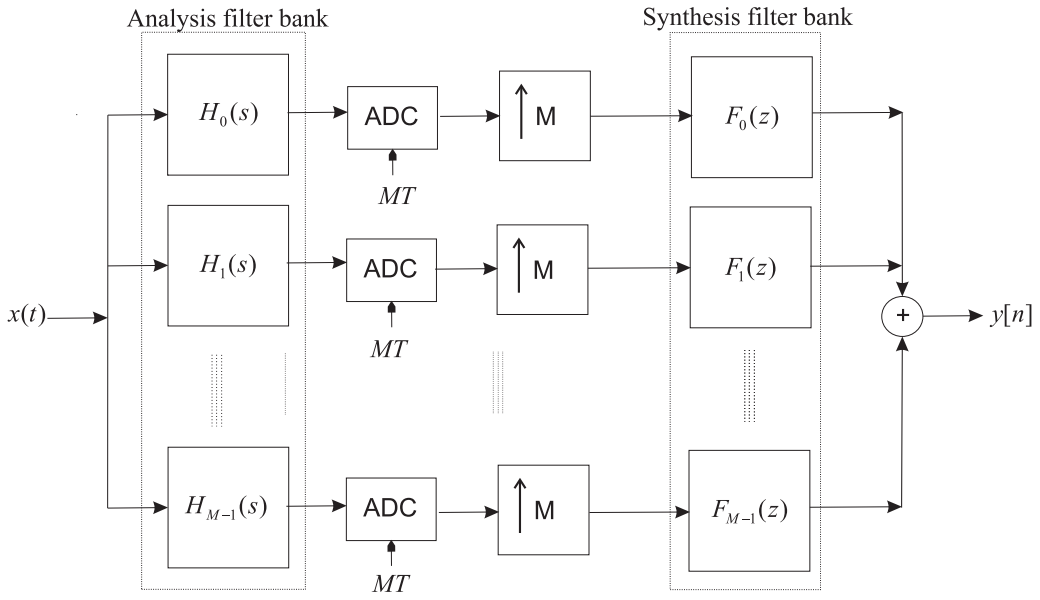

Figure 2.6. The structure of continuous-time HFB-based A/D converter.

chev and Cauer have been tried as the analog analysis filters [44, 48]. On the other hand, the feasibility of analog filters is very important in the design of HFB structures, particularly considering the constraints of electronic circuits at high frequencies. The simply realizable first- and second-order circuits including RC and RLC circuits may be a good candidate for this purpose [49, 50]. Infinite-Impulse Response (IIR) digital filters have been tried in the synthesis stage as well as Finite-Impulse Response (FIR) ones for two-channel [51, 52] and eight-channel HFB structures [53]. A slight improvement in the performance of HFB ADC has been reported for IIR synthesis filters but the instability problem remains unsolved in this case. Moreover, FIR synthesis filters maintain a linear relationship in terms of the coefficients of synthesis filters which may be useful for the compensation purposes (refer to chapter 5).

In the case of first- and second-order analysis filters, the performance of HFB structures in terms of aliasing interference is not so acceptable unless an oversampling ratio is used [54]. An oversampling ratio of 7% provides an obvious improvement for an eight-channel HFB structure as shown in the section 3.2.4 [54]. The Perfect Reconstruction (PR) equations are generally used for designing the FIR synthesis filters assuming the fixed analog analysis circuits [55, 56]. However, other criteria

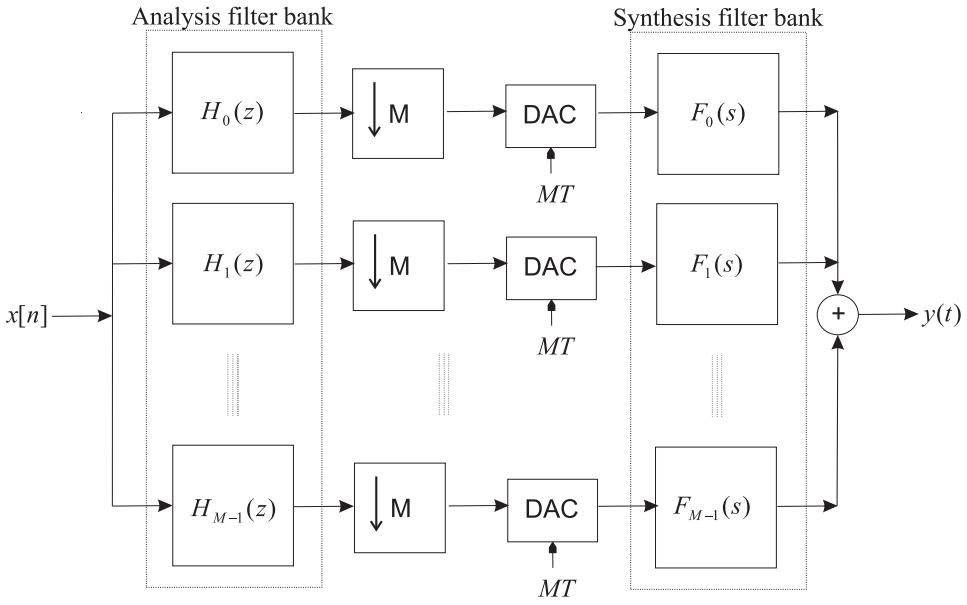

Figure 2.7. The architecture of continuous-time HFB-based D/A converter.

in terms of distortion and interference (aliasing) functions have been tried [57, 58]. Shu et al. have proposed a criterion based on H_∞ to which an optimization algorithm such as Least Squares (LS) may be applied for obtaining the synthesis filters [59, 60]. The proposed Minmax algorithm leads to an optimization criterion representing the sum of distortion and aliasing absolute values except a weighting factor influencing the distortion term [59]. Although, H_∞ optimization does not provide a large improvement but Shu et al. offer a model of HFB fully described in discrete-time domain neglecting the quantization process [59]. This model may be interesting considering chapter 5 where a discrete-time model is obtained from another point of view. The quantization noise has often been neglected for concentrating on the aliasing interferences in the mentioned works. However, the quantization and word-length effects have been studied in the HFB structures as well [61]. Assuming a high-resolution A/D converter at each branch of HFB ADC, it is possible to neglect quantization noise for studying the aliasing interferences which would be the dominant limit of output resolution in this case. This assumption is correct as long as the resolution of each branch ADC is sufficiently large compared to the resolution associated with the aliasing interference terms (because aliasing interferences may be considered like the quantization noise as an additive

noise which restricts the output resolution [62].
The real challenge in the implementation of HFB-based A/D converters is nevertheless its high sensitivity to the realization errors [63]. In fact, a very small deviation in the parameters of analysis filter bank results in a large degradation of performance so that the respective HFB ADC would no longer be useful [64]. The realization errors of analog analysis filters are rarely avoidable. The errors are associated with either the time-varying sources such as temperature drifts or the fixed unknown origins like analog imperfections of fabrication phase. Analog methods for decreasing the realization errors such as laser trimming and compensated circuit design are so expensive. On the other hand, these techniques are not at times applicable for example in the HFB case (see section 3.3.1). Moreover, the HFB-based A/D converters are so sensitive to the realization errors that a small deviation 0.5% from nominal values leads to a large degradation of performance as it is shown in section 3.3.2.1 [5]. The performance in the presence of even small realization errors degrades so that the HFB ADC will be useless unless a compensation technique is considered [5]. Digital techniques have been considered for overcoming the problem of high sensitivity to the realization errors recently [65, 6]. However, the proposed methods are often so limited to some types of errors [6, 9] or to a very specific case [66, 67]. Considering the realization errors in a general case, Pinheiro et al. tried to optimize the design of HFB structures in terms of realization errors [7]. However, the proposed solution is not a compensation technique. They have just proposed a weighted criterion of distortion and aliasing terms which only leads to less than five dB of improvement. This improvement is considered for the classical HFB-based ADC without any oversampling. When no oversampling is used, the HFB structure is less sensitive to the realization errors, but the related performance is not acceptable for practical applications as shown in section 3.2.4. In fact, it is necessary to look for a mechanism of compensation being capable of eliminating the effects of realization errors as much as possible. This method would be an adaptive algorithm to cope with the time-varying errors such as temperature drifts as well.
This thesis is an attempt to define digital methods aiming at firstly estimating, then compensating analog non-idealities in the electronic circuits particularly in some special case of ADCs, namely HFB-based structures which are supposed to be

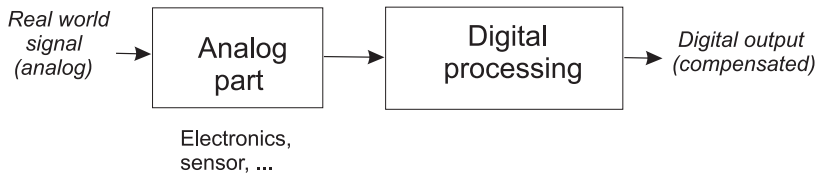

Figure 2.8. General diagram for digitally estimating and compensating the analog non-idealities of a system.

a very promising way for future, wide-band, versatile applications. This work takes place in the more general context of trying to use the power of digital methods in order to correct the compulsory analog part of general systems (see figure 2.8). This problem is linked with some kind of *blind* estimation since neither errors (system) nor input signal are known. The main objective of this thesis is firstly to study the effects of realization errors on HFB-based A/D converters to highlight the origins of sensitivity to realization errors. Then, the capability of compensation for these structures is discussed and reviewed so that new HFB architecture may be obtained in which the realization errors can be compensated.

The organization of this thesis may briefly be described as following. In the next chapter 3, HFB-based A/D converters are reviewed and their performance is studied in terms of oversampling procedure and realization errors. Considering different optimization techniques, the sensitivity to realization errors is discussed as well as the important factors contributing in the sensitivity. Chapter 4 deals with the blind equalization techniques. To digitally compensate the realization errors of analog circuits, Second-Order Statistics (SOS) may be used as well as Higher-Order Statistics (HOS). A survey on the blind estimation methods is provided, and both SOS and HOS are explored for applying to the analog circuits. It is also shown that the proposed blind methods in this chapter face with some problems for applying to the HFB-based A/D converters. In chapter 5, the possibility for compensating the realization errors of HFB structures is firstly discussed. Then, some new structures of HFB-based A/D converters are proposed. The proposed Multiple-Input Multiple-Output (MIMO) models of HFB structures are shown to be digitally compensable. The performance and sensitivity of new MIMO HFB structures are simulated and described as well. Finally, the chapter 6 of conclusion provides a short review on the results of the preceding chapters. Besides, the

possible architectures of HFB-based A/D converters are offered so that a compensation method is integrated. The perspectives and feasibility of new structures are discussed as well.

Chapter 3

Classical Hybrid Filter Bank A/D converters

Doubt is not a pleasant condition, but certainty is absurd.
- Voltaire

3.1 Introduction

Sampling rate and digital precision (in terms of resolution) are two important issues in dealing with A/D or D/A converters. Wide-band A/D or D/A converters are very wanted in new domains of telecommunications such as the software-defined radio approach [4]. Continuous-time Hybrid Filter Bank (HFB) structure has been regarded as a suitable candidate for that and has been studied for two decades [34]. HFB structures may be used to practically implement parallel A/D or D/A conversion [4]. Figures 2.6 and 2.7 show the (continuous-time) HFB structure for A/D and D/A conversion respectively. This chapter focuses on the classical architecture of maximally-decimated HFB-based A/D converters. According to the figure 2.6, an HFB-based A/D converter uses M A/D converters sampling at the rate of $\frac{1}{MT}$ which is M times less than the Nyquist rate $\frac{1}{T}$ associated with the analog input $x(t)$. The analog input signal $x(t)$ is supposed to be limited to the frequency band of $[\frac{-\pi}{T}, \frac{\pi}{T}]$. An HFB-based A/D converter consists of analysis and synthesis filter banks. In the continuous-time HFB case, the analysis and synthesis

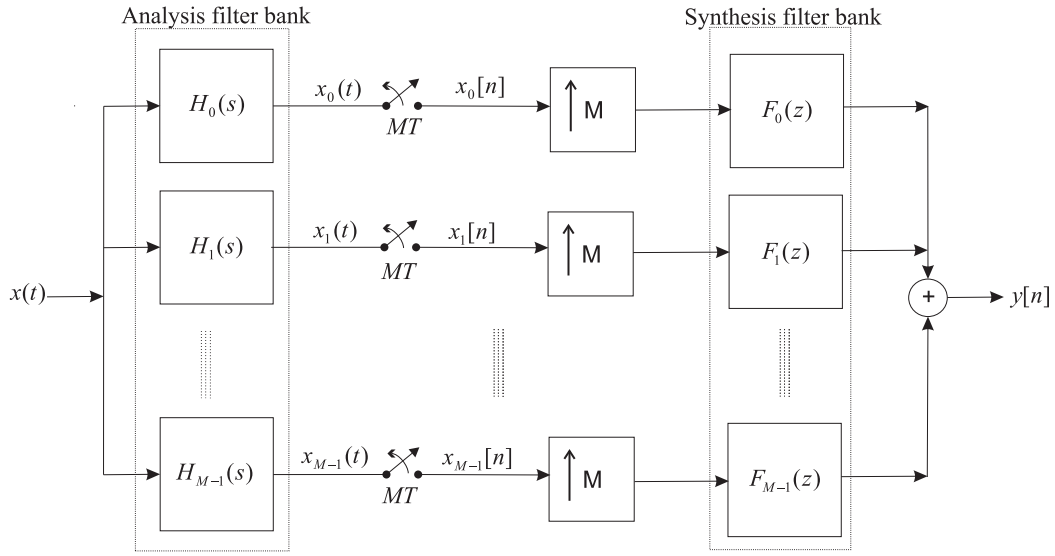

Figure 3.1. Simplified HFB-based A/D converter considering the maximally-decimated architecture. Neglecting the quantization process, each A/D converter has been substituted by a simple sampler.

filter banks contain M analog and digital filters respectively. The digital output of classical HFB-based A/D converter is subject to the frequency distortion and interferences [4]. The interferences called aliasing terms are originated from the spectral overlapping at each branch of HFB structure. Spectral overlapping is due to the undersampling process present at each branch. Digital synthesis filters try to eliminate these spectral overlapping terms. Nevertheless, practical digital synthesis filters are unable to completely suppress the aliasing terms appearing at the output of HFB structure because the frequency responses of ideal synthesis filters cannot be realized. It is due to the non-ideal aspects such as the limited capacity of Finite-Impulse Response (FIR) synthesis filters. Besides, interferences may be intensified because of practical constraints such as the analog imperfections of analysis filter bank. The reconstructed signal may have some distortions in addition to the additive aliasing terms as well. The distortion effects may often be compensated whilst, aliasing terms cannot be avoided. Aliasing terms are generally the dominant restricting source of resolution in the realization of HFB-based A/D converters [62].

To better pursue the aliasing and distortion effects, the quantizer parts of conversion are ignored throughout this report unless the opposite is indicated [62, 14].

Thus, neglecting quantizer parts, the A/D converter of each branch may be substituted with an ideal sampler. Figure 3.1 represents the classical HFB architecture for A/D conversion neglecting quantization process [4, 9].

The aliasing terms are the main restricting factors of output resolution in the HFB configuration. Lowenborg et al. proposed a general formulation to describe the aliasing and distortion functions associated with an HFB structure [62, 45, 44]. Using these equations, there are two possible methods for designing HFB structures. As the first method, it is theoretically possible to design analysis analog filters on the base of presumed synthesis digital filters. Secondly, it is also possible to design synthesis digital filters on the basis of a presumed set of analysis analog circuits. The second method is practically preferred since it may deal with the realizable analog circuits [55, 68]. Considering simple FIR digital filters at the synthesis stage along with first- and second-order electronic circuits (RC and RLC filters) in the analysis filter bank, Petrescu et al. minimize the aliasing terms in order to obtain the FIR synthesis filters [54]. They have proposed to use a small oversampling ratio to handle the associated aliasing problems. An 8-channel HFB structure is considered with the Least Squares (LS) technique for designing the FIR synthesis filters. It is based on a fixed presumed analysis filter bank (one RC circuit as low-pass filter along with seven RLC circuits as band-pass filters with equal passing bands). Using a small oversampling ratio, HFB-based A/D converters have shown a large reduction in the aliasing levels [54]. However, a high sensitivity to the analog imperfections of analysis filters have been reported in this case as shown in the section 3.3 [5].

In this chapter, design of synthesis filters is reviewed for the HFB-based A/D converters. To have a better view on the reconstruction constraints, the Perfect Reconstruction (PR) equations are demonstrated in the matrix form as well as the relationships associated with the design of HFB filter banks. The HFB-based A/D converters are discussed in terms of different values of oversampling ratio and the optimal oversampling ratio is obtained in the section 3.2. Then, section 3.3 provides a survey on the sensitivity to the analog imperfections in the HFB structures. The Total Least Squares (TLS) optimization method is described and applied to HFB structures in order to possibly reduce the sensitivity to analog imperfections in 3.3.2.2. Finally, the feasibility of HFB-based A/D converters is discussed and it

is demonstrated that a compensation technique is necessary for using the classical HFB structures in the conclusion section 3.4.

3.2 Designing HFB A/D converters

3.2.1 Perfect reconstruction equations

Considering the classical architecture of HFB-based A/D converters (figure 3.1), the synthesis filters ($F_i(z),\ i = 0, \cdots, M-1$) are designed so that the contribution of aliasing terms in the output is eliminated or minimized. The mutual information between the branches of HFB is exploited in the synthesis filter bank. Considering the problems of practical realization, analysis filters are assumed to be chosen and fixed firstly (refer to 3.1). Realization of HFB A/D converter is feasible if and only if the presumed analysis filters hold some conditions [33, 34]. This condition implies the existence of a unique series of synthesis filters (at least in the frequency domain) which ideally reconstructs the original analog signal without any aliasing or distortion [33, 34]. This condition supposes some constraints on the analysis filters (orthogonality of the respective analysis matrix explained in section 3.2.2). However, the approximation of respective ideal synthesis filters using real FIR sequences fails to completely eliminate the aliasing terms. A wide-band HFB-based A/D converter is achievable if the ensemble of the analysis/synthesis filters are obtained from the practical viewpoint so that the aliasing terms tend to zero or remain in an acceptable range.

Considering the appendix A, the frequency representation $Y(e^{j\omega})$ of the output $y[n]$ may be described in terms of the analysis and synthesis filters and input signal. For convenience, an intermediate variables $H_k^{'}(j\Omega)$ is defined as follows (for more details refer to the appendix A). $H_k^{'}(j\Omega)$ represents an analog filter as following:

$$H_k^{'}(j\Omega) = \begin{cases} H_k(j\Omega) & \Omega \in [-\frac{\pi}{T}, +\frac{\pi}{T}) \\ \\ 0 & \text{elsewhere} \end{cases}$$

where $H_k(j\Omega)$ is the k^{th} analog analysis filter. $\widetilde{X}(j\Omega)$ and $\widetilde{H}_k(j\Omega)$ are defined as the periodic extensions of $X(j\Omega)$ and $H_k^{'}(j\Omega)$ respectively with the period $\Omega_\circ = \frac{2\pi}{T}$

(refer to the appendix A). In fact, $\widetilde{H}_k(j\Omega)$ is achieved from periodically extending the k^{th} analog analysis filter (with the period $\frac{2\pi}{T}$ where T represents the Nyquist period) limited already to the band $[-\frac{\pi}{T}, +\frac{\pi}{T}]$. Using these terms and considering figure 3.1, the output of classical HFB-based A/D converter may be described as follows (see appendix A):

$$Y(e^{j\omega}) = \frac{1}{MT}\sum_{m=0}^{M-1}\widetilde{X}(j\frac{\omega}{T} - j\frac{2\pi}{MT}m)\sum_{k=0}^{M-1}\widetilde{H}_k(j\frac{\omega}{T} - j\frac{2\pi}{MT}m)\cdot F_k(e^{j\omega}) \qquad (3.1)$$

where ω represents the frequency associated with Discrete-Time Fourier Transform (DTFT) [69]. $F_k(e^{j\omega})$ stands for the k^{th} synthesis filter. Considering the above relationship (3.1), $T_k(e^{j\omega})$ for $0 \leq k \leq M-1$ is defined as following:

$$\begin{cases} T_0(e^{j\omega}) = \frac{1}{M}\sum_{k=0}^{M-1} F_k(e^{j\omega})\cdot\widetilde{H}_k(j\frac{\omega}{T}) \\ \\ T_m(e^{j\omega}) = \frac{1}{M}\sum_{k=0}^{M-1} F_k(e^{j\omega})\cdot\widetilde{H}_k(j\frac{\omega}{T} - j\frac{2\pi}{MT}m) \qquad m=1,\ldots,M\text{-}1 \end{cases} \qquad (3.2)$$

where $T_0(e^{j\omega})$ is the distortion function and $\{T_m(e^{j\omega}),\ m = 1, 2, \cdots, M-1\}$ represent $(M-1)$ aliasing functions. Perfect Reconstruction (PR) of analog input would be possible under some criteria. PR conditions would be useful for designing one of the analysis or synthesis filter bank while the other one is already known. To maintain PR conditions, the following set of equations are sufficient:

$$\begin{cases} T_0(e^{j\omega}) = e^{-j\omega n_d} \\ \\ T_m(e^{j\omega}) = 0 \qquad m=1,\ldots,M\text{-}1 \end{cases} \qquad (3.3)$$

n_d stands for an arbitrary integer (or a real number in global view). The delay term $e^{-j\omega n_d}$ has been considered instead of ideal distortion term (unity) to maintain the causality condition. It has been proposed to use the half length of FIR synthesis filters [70]. This value will be used throughout the simulations.

3.2.2 Designing filter banks of HFB-based A/D converter

To follow conveniently the design phase, it is better to summarize the previous relationships in a matrix-vectorial format. Accordingly, above-mentioned distortion-aliasing expressions may be described at each frequency ω as follows:

$$T(e^{j\omega}) = \frac{1}{M} H(j\frac{\omega}{T}) F(e^{j\omega}) \tag{3.4}$$

where the associated vectors are considered as follows:

$$T(e^{j\omega}) = \begin{bmatrix} T_0(e^{j\omega}) \\ T_1(e^{j\omega}) \\ \\ \vdots \\ \\ T_{M-1}(e^{j\omega}) \end{bmatrix}_{M\times 1} \qquad F(e^{j\omega}) = \begin{bmatrix} F_0(e^{j\omega}) \\ F_1(e^{j\omega}) \\ \\ \vdots \\ \\ F_{M-1}(e^{j\omega}) \end{bmatrix}_{M\times 1}$$

and $H(j\frac{\omega}{T})$ at the frequency ω is:

$$H(j\frac{\omega}{T}) = \begin{bmatrix} \widetilde{H}_0(j\frac{\omega}{T}) & \cdots & \widetilde{H}_{M-1}(j\frac{\omega}{T}) \\ \widetilde{H}_0(j\frac{\omega}{T} - j\frac{2\pi}{MT}) & \cdots & \widetilde{H}_{M-1}(j\frac{\omega}{T} - j\frac{2\pi}{MT}) \\ \\ \vdots & \vdots & \vdots \\ \\ \widetilde{H}_0(j\frac{\omega}{T} - j\frac{2\pi}{MT}(M-1)) & \cdots & \widetilde{H}_{M-1}(j\frac{\omega}{T} - j\frac{2\pi}{MT}(M-1)) \end{bmatrix}_{M\times M}$$

The M equations included in (3.4) correspond to a frequency point ω. To approximate the unknown filter bank, these equations may be considered in N ($N \gg M$) frequencies. N frequency points should be spread out throughout the band of interest (here $\left[\frac{-\pi}{T}, \frac{\pi}{T}\right]$) so that the approximation of unknown filter bank may be suitable. These frequencies are chosen equally spaced throughout this thesis. Now, assuming N frequency points $\{\omega_i,\ i = 1, 2, \cdots, N\}$, the equality (3.4) may be generalized in the matrix form as follows:

$$\mathbf{T} = \frac{1}{M}\mathbf{HF} \tag{3.5}$$

where the new parameters shown in bold are described as following:

$$\mathbf{T} = \begin{bmatrix} T(e^{j\omega_1}) \\ T(e^{j\omega_2}) \\ \\ \vdots \\ \\ T(e^{j\omega_N}) \end{bmatrix}_{MN\times 1} \qquad \mathbf{F} = \begin{bmatrix} F(e^{j\omega_1}) \\ F(e^{j\omega_2}) \\ \\ \vdots \\ \\ F(e^{j\omega_N}) \end{bmatrix}_{MN\times 1}$$

and the analysis filters matrix $\mathbf{H}$ is:

$$\mathbf{H} = \begin{bmatrix} H(j\frac{\omega_1}{T}) & & & \\ & H(j\frac{\omega_2}{T}) & \mathbf{0} & \\ & \mathbf{0} & \ddots & \\ & & & H(j\frac{\omega_N}{T}) \end{bmatrix}_{MN\times MN}$$

Considering the relationship (3.5) and PR conditions, the analysis filters matrix $\mathbf{H}$ is evidently required to be non-singular (a matrix with non-zero determinant). Otherwise, the respective architecture of parallel conversion is no longer useful because it would be impossible to reconstruct the analog input through the outputs of HFB branches. In other words, the equations (3.3) and (3.5) would not lead to a solution. This condition (non-singularity of $\mathbf{H}$) is implicitly supposed to be maintained throughout this thesis. Therefore, using (3.5), the aliasing and distortion terms can be extracted for N frequency points. To have the perfect reconstruction, it is required that the aliasing terms are all null. The distortion function in this case has to be equal to unity, but to have the capability of realizable causal synthesis filters, a delay term is generally considered. In other words, the output $y[n]$ of the mentioned HFB A/D converter will provide the exact samples of a shifted version $x(t - n_dT)$ of the analog input $x(t)$ with the sampling rate of $\frac{1}{T}$ provided that the PR conditions are held (noting that the sampling rate used at each branch of HFB architecture is $\frac{1}{MT}$ or M times less than the global Nyquist rate of $\frac{1}{T}$). Supposing the delay length n_d, the equations associated to the PR

conditions will then be as following:

$$\mathbf{HF} = \mathbf{B} \tag{3.6}$$

where the new constant vector $\mathbf{B}$ is defined as follows:

$$\mathbf{B} = \begin{bmatrix} B(e^{j\omega_1}) \\ B(e^{j\omega_2}) \\ \\ \vdots \\ \\ B(e^{j\omega_N}) \end{bmatrix}_{MN\times 1} \quad \text{that} \quad B(e^{j\omega_i}) = \begin{bmatrix} Me^{-j\omega_i n_d} \\ 0 \\ \\ \vdots \\ \\ 0 \end{bmatrix}_{M\times 1} \qquad i \in \{1, 2, \cdots, N\}$$

Invoking the prerequisite implicit condition for the PR equations (it means that $\mathbf{H}$ is a non-singular matrix), the matrix equation (3.6) may be solved. Then, it leads to a special frequency response for the synthesis filters represented by $\mathbf{F}_\circ$ if the analysis filters are known a priori. The vector of synthesis filters $\mathbf{F}_\circ$ is interpreted as the ideal synthesis filters (of course defined at only N frequency points) since the perfect reconstruction may be accomplished if $\mathbf{F}_\circ$ is used as the synthesis filters.
Assuming a known analysis filter bank, the problem is to design the respective suitable digital synthesis filters. FIR filters are conveniently-realizable and need only a limited resource of memory and processing. Using FIR filters, the equations would be linear in terms of the unknown coefficients of synthesis filters as well. Considering IIR digital filters, the problem will be no longer linear [71].
A series of FIR filters are considered as the synthesis filters. They are assumed to have L coefficients. The impulse responses of synthesis filters are then regarded as the sequences $\{f_k[n], k = 0, 1, \cdots, M-1\}$. $f_k[n]$ is zero except for the range $0 \leq n \leq L-1$. Thus, $f_k[n]$ is a real vector as following:

$$f_k = \begin{bmatrix} f_k[0] \\ f_k[1] \\ \\ \vdots \\ \\ f_k[L-1] \end{bmatrix}_{L\times 1} \qquad \text{that} \quad k \in \{0, 1, \ldots, M-1\}$$

To obtain the synthesis filters, the equation (3.6) should be described in terms of the vectors $\{f_k[n], k = 0, 1, \cdots, M-1\}$. $\mathbf{F}(e^{j\omega})$ used in (3.4) may be related to the impulse responses $\{f_k[n], k = 0, 1, \cdots, M-1\}$ through the matrix $\mathbf{A}$ of Fourier transform as following:

$$\mathbf{A}.\mathbf{f} = \mathbf{F} \tag{3.7}$$

where $\mathbf{f}$ is the overall vector of FIR synthesis filters as follows:

$$\mathbf{f} = \begin{bmatrix} f_0 \\ f_1 \\ \\ \vdots \\ \\ f_{M-1} \end{bmatrix}_{ML\times 1}$$

Considering the vector $\mathbf{F}$ used in (3.6), the matrix $\mathbf{A}$ of Fourier transform is:

$$\mathbf{A} = \begin{bmatrix} A(e^{j\omega_1}) \\ A(e^{j\omega_2}) \\ \\ \vdots \\ \\ A(e^{j\omega_N}) \end{bmatrix}_{MN\times ML}$$

that $A(e^{j\omega_i})$ is itself another matrix described as:

$$A(e^{j\omega_i}) = \begin{bmatrix} a^T(e^{j\omega_i}) & & \\ & \ddots & \\ \mathbf{0} & & \mathbf{0} \\ & & a^T(e^{j\omega_i}) \end{bmatrix}_{M\times ML} = \mathbf{I}_M \otimes a^T(e^{j\omega_i})$$

where $\mathbf{I}_M$ is the identity matrix $(M \times M)$ and $\otimes$ stands for the Kronecker production. The vector of $a^T(e^{j\omega_i})$ is described as following:

$$a^T(e^{j\omega_i}) = \begin{bmatrix} 1 & , & e^{-j\omega_i} & , \cdots , & e^{-j\omega_i(L-1)} \end{bmatrix}_{1\times L}$$

Finally, according to the preceding explanations, the impulse response $\mathbf{f}$ of synthesis filters may contribute in the relationship as follows:

$$\mathbf{HF} = \mathbf{B} \qquad\qquad \mathbf{Af} = \mathbf{F} \tag{3.8}$$

The first matrix equation in (3.8) (associated with (3.6)) consists of a square matrix $\mathbf{H}$ which should be non-singular. Otherwise, the relative HFB architecture would be unable to reconstruct the original signal as discussed earlier. Therefore, it yields a unique solution. The non-ideality emerges as soon as the second matrix equation in (3.8) (associated with the FIR approximation) is considered. The matrix $\mathbf{A}$ is not square $(MN \times ML)$. It is necessarily a tall matrix$(N > L)$ to provide an acceptable interpolation. Then, the solution is not unique and can only approximate the associated equations. The problem of designing HFB structure using FIR filters for the synthesis stage is effectively only a problem of digital filter design (FIR filters) which are required to fit a prescribed form. The desired vector $\mathbf{f}$ is real to provide real outputs. To better analyze and follow the result, the right equation in (3.8) may be described through the real vectors as following:

$$\mathbb{A}\mathbf{f} = \mathbb{F} \tag{3.9}$$

where $\mathbb{A}$ and $\mathbb{F}$ are:

$$\mathbb{A} = \begin{bmatrix} \mathrm{Re}(\mathbf{A}) \\ \\ \mathrm{Im}(\mathbf{A}) \end{bmatrix}_{2MN \times ML} \qquad \mathbb{F} = \begin{bmatrix} \mathrm{Re}(\mathbf{F}) \\ \\ \mathrm{Im}(\mathbf{F}) \end{bmatrix}_{2MN \times 1}$$

Re and Im stand for the real and imaginary parts respectively. It can be also applied to the left equation in (3.8) as follows:

$$\mathbb{H}.\mathbb{F} = \mathbb{B} \tag{3.10}$$

where the new matrix $\mathbb{H}$ and vector $\mathbb{B}$ are defined as:

$$\mathbb{H} = \begin{bmatrix} \mathrm{Re}(\mathbf{H}) & -\mathrm{Im}(\mathbf{H}) \\ \\ \mathrm{Im}(\mathbf{H}) & \mathrm{Re}(\mathbf{H}) \end{bmatrix}_{2MN \times 2MN} \qquad \mathbb{B} = \begin{bmatrix} \mathrm{Re}(\mathbf{B}) \\ \\ \mathrm{Im}(\mathbf{B}) \end{bmatrix}_{2MN \times 1}$$

3.2.3 A simply-realizable class of HFB-based A/D converters

Using a simply-realizable class of analog filters for the analysis filter bank, a group of HFB-based A/D converters is designed and simulated in this section. It is supposed that the analysis filter bank is composed of the second-order RLC circuits except one first-order RC circuit as low-pass filter. All the second-order RLC circuits are supposed to have a constant passing band ($\frac{\pi}{MT}$) as described in [50, 49]. For example, figure 3.2 shows the frequency responses of the mentioned analysis filters for an eight-branch HFB structure. Regarding the most straight way, it is possible to solve the respective series of the equations (3.9) and (3.10) to find the coefficients of the FIR synthesis filters. This may be established through two following methods:

- **Local optimization:** Two matrix equations (3.9) and (3.10) may be separately solved (or locally optimized). Regarding to this method, (3.10) is solved firstly considering N arbitrary frequency points ($N >> L$). Invoking

the non-singularity of the analysis matrix $\mathbb{H}$, the solution $\mathbb{F}_\circ$ is:

$$\mathbb{F}_\circ = \mathbb{H}^{-1}.\mathbb{B} \tag{3.11}$$

$\mathbb{F}_\circ$ is called the ideal synthesis filters. Secondly, $\mathbb{F}_\circ$ is substituted in the equation (3.9). Using the Least Squares (LS) optimization method, the approximated FIR synthesis filters $\mathbf{f}_\circ$ may be obtained. Thus, the impulse response of FIR synthesis filters is:

$$\mathbf{f}_\circ = \mathbb{A}^\dagger \mathbb{F}_\circ = (\mathbb{A}^T \mathbb{A})^{-1} \mathbb{A}^T \mathbb{F}_\circ \tag{3.12}$$

where $(.)^\dagger$ represents the pseudo-inverse of operand matrix. According to the LS algorithm, the solution is achieved from minimizing a criterion as follows:

$$\mathbf{f}_\circ = \arg \min_{\mathbf{f}} \|\mathbb{A}\mathbf{f} - \mathbb{F}_\circ\| = \arg \min_{\mathbf{f}} \sum_{k=0}^{M-1} \|\mathcal{TF}(f_k[n]) - \mathbf{F}_\circ{}^{(k)}\| \tag{3.13}$$

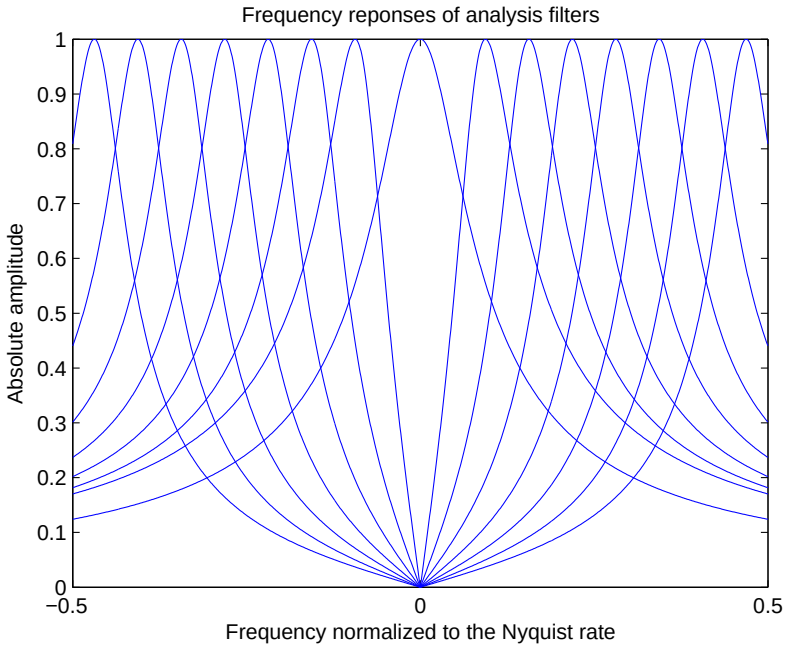

Figure 3.2. Absolute value of frequency responses of the analysis filters versus normalized frequency for an exemplary eight-branch HFB. The analysis filter bank consists of second-order RLC circuits except a first-order RC circuit as low-pass filter.

where $\mathcal{TF}(f_k[n])$ is the discrete-time Fourier transform of the FIR filter $f_k[n]$ and $\mathbf{F}_\circ{}^{(k)}$ represents the ideal frequency response of the k^{th} FIR synthesis filter. Each of M FIR synthesis filters has its distinct coefficients, then the above equality may be described as:

$$\min \sum_{k=0}^{M-1} \|\mathcal{TF}(f_k[n]) - \mathbf{F}_\circ{}^{(k)}\| = \sum_{k=0}^{M-1} \min \|\mathcal{TF}(f_k[n]) - \mathbf{F}_\circ{}^{(k)}\| \quad (3.14)$$

The relation (3.14) reveals that the solution is obtained as if the FIR synthesis filter of each branch is independently estimated through applying the LS technique.

- **Global optimization:** Another option is to integrate the equations (3.9) and (3.10) and to solve them simultaneously as following:

$$(\mathbb{H}.\mathbb{A})\mathbf{f} = \mathbb{B} \quad (3.15)$$

where the real vector of $\mathbf{f}$ represents the impulse response of FIR synthesis filters. Applying the LS technique to (3.15), it yields:

$$\mathbf{f}_\circ = (\mathbb{H}\mathbb{A})^\dagger \mathbb{B} = [(\mathbb{H}\mathbb{A})^T(\mathbb{H}\mathbb{A})]^{-1}(\mathbb{H}\mathbb{A})^T\mathbb{B} \quad (3.16)$$

According to the LS technique, $\mathbf{f}_\circ$ is equivalently achieved when undermentioned criterion is minimized:

$$\begin{aligned} \mathbf{f}_\circ &= \arg \min_{\mathbf{f}} \|(\mathbb{H}\mathbb{A})\mathbf{f} - \mathbb{B}\| \\ &= \arg \min_{\mathbf{f}} \|\mathbb{H}[\mathbb{A}\mathbf{f} - \mathbb{H}^{-1}\mathbb{B}]\| \\ &= \arg \min_{\mathbf{f}} \|\mathbb{H}[\mathbb{A}\mathbf{f} - \mathbb{F}_\circ]\| \end{aligned}$$

where the non-singularity of $\mathbb{H}$ has implicity been used to guarantee the existence of its inverse matrix. The analog analysis filters used in the simulation are approximately orthogonal (due to the distinct passing bands). This results in a quasi unitary analysis filter matrix ($\mathbb{H}^H\mathbb{H} \cong \mathbf{I}$). Accordingly, both local and global optimizations lead to the same solution. The simulations confirm this property as well.

According to the matrix analysis theory, following relationship may be considered [71]:

$$\sigma_m.\|\Delta\mathbb{F}\| \leq \|\mathbb{H}[\mathbb{A}\mathbf{f}_\circ - \mathbb{F}_\circ]\| \leq \sigma_1.\|\Delta\mathbb{F}\| \tag{3.17}$$

where

$$\Delta\mathbb{F} = \mathbb{A}\mathbf{f}_\circ - \mathbb{F}_\circ$$

$\Delta\mathbb{F}$ represents the deviation from the ideal synthesis filter ($\mathbb{F}_\circ$). σ_1 and σ_m are the largest and the least singular values (the first and the last or $2MN^{th}$ singular values) associated with the analysis matrix $\mathbb{H}$. Meanwhile, the minimum occurs when the real vector $[\mathbb{A}\mathbf{f} - \mathbb{F}_\circ]$ is parallel to the one of Singular Value Decomposition (SVD) vectors of $\mathbb{H}$ which is associated with the least singular value σ_m. This remark will be used in the analysis of sensitivity (section 3.3). According to the preceding discussions, both local and global optimization methods lead to the same synthesis filters for classical HFB structure. The equality of these methods originates from the choice of analysis filters which provides a unitary analysis matrix $\mathbb{H}$. It is important to remind that the local and global optimization methods do not lead to the same solution in the oversampling case (subsection 3.2.4).
Figure 3.3 shows the impulse response of the synthesis filters obtained for a two-channel HFB structure ($M = 2$) assuming the length of 64 coefficients for the FIR synthesis filters. Figure 3.4 illustrates the respective distortion and aliasing functions in dB versus normalized frequencies. If the number of coefficients of the FIR synthesis filters is chosen larger than 64, there will be no considerable reduction in the aliasing terms, but the fluctuations increase. Besides, using the larger values of delay n_d ($n_d > 32$), the fluctuations of the aliasing terms reduce. The aliasing and distortion functions for the same two-channel HFB considering $n_d = 42$ is shown in figure 3.5. It is seen that the fluctuations have decreased so much. The average interference (aliasing terms) nevertheless rises slightly. It is necessary to mention that if we change either the delay length or the number of coefficients of the FIR synthesis filters, there will be no important effect on the maximum value of the aliasing term. The maximum aliasing appears approximately robust and constant.
This trial has been repeated for a structure including 8 branches. Analysis filter bank includes an RC low-pass filter at first branch but second-order RLC circuits are used for the other seven branches (figure 3.2). The analysis filters are designed

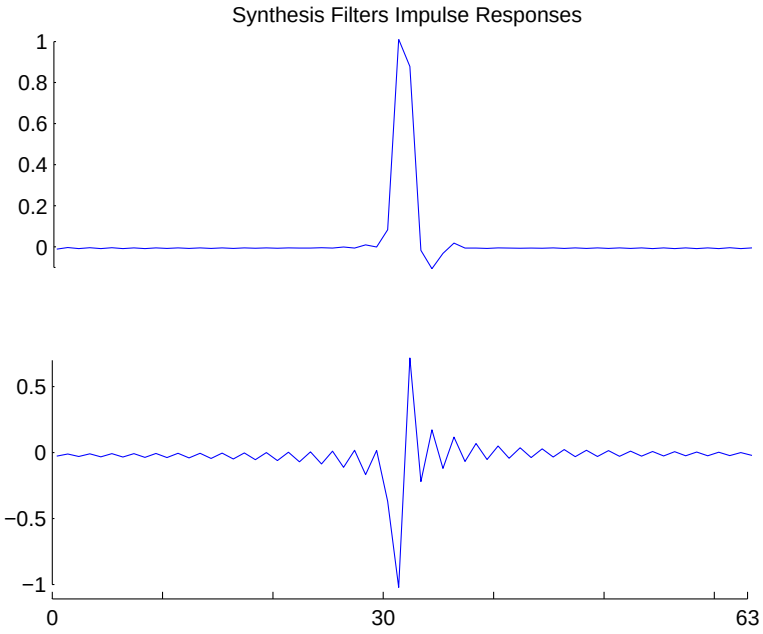

Figure 3.3. Impulse response of the synthesis filters for a two-channel HFB structure. The analysis filter bank includes an RC and an RLC circuit. FIR filters have 64 coefficients and n_d is 32.

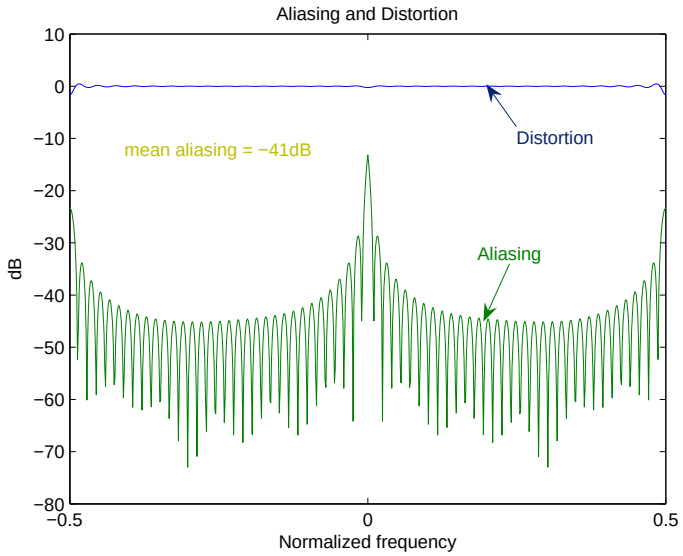

Figure 3.4. Distortion and aliasing terms (in dB) for a two-channel HFB structure. The analysis filter bank includes an RC and an RLC circuit. FIR synthesis filters have 64 coefficients and n_d is supposed to be 32.

with a constant passing band of $\frac{\pi}{8T}$. Synthesis filters are supposed to be FIR digital filters with 64 coefficients. Figure 3.6 illustrates the respective aliasing and

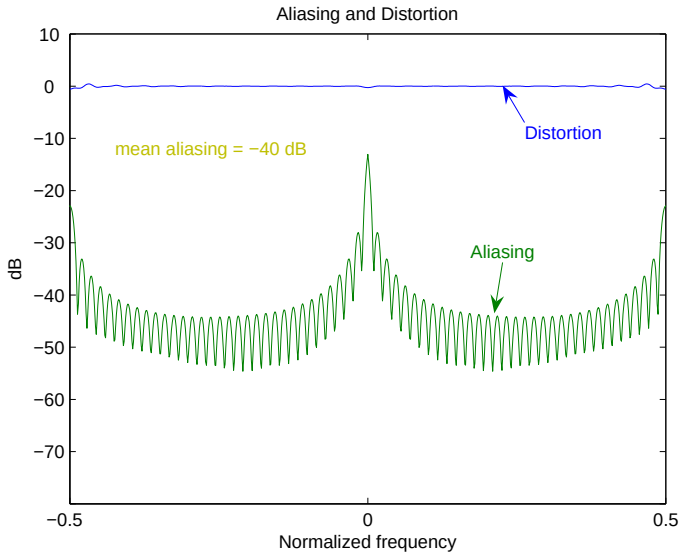

Figure 3.5. Distortion and aliasing terms (in dB) for a two-channel HFB structure. The analysis filter bank includes an RC and an RLC circuit. FIR synthesis filters consist of 64 coefficients and n_d is 42.

distortion functions (in dB) versus normalized frequencies.

When the FIR synthesis filters consist of larger number of coefficients, no important change is seen in the performance except a little improvement in aliasing like to the two-branch case. For example, using 128 coefficients for each FIR filter, the new average of aliasing terms is equal to $-53dB$ which is $7dB$ better than the one achieved for the case of 64 coefficients. If synthesis stage is realized with even longer FIR filters, the fluctuations of the aliasing terms will increase. It may reveal the happening of an over-fitting. Supposing a delay length of $n_d = 42$ and with the same FIR synthesis filters, the fluctuations of aliasing terms disappear approximately but the mean value increases slightly. The maximum value of aliasing terms is again robust and unchanging versus the modification of synthesis filters. Considering the shape of the impulse responses (for example figure 3.3), there is a similarity between the FIR synthesis filters and the orthogonal basis of the wavelet structure [72]. The analysis filters that we have used (the RC and RLC resonator circuits) are quasi-orthogonal since their passing bands do not overlap. Thus, it has led to a quasi-orthogonality of synthesis filters.

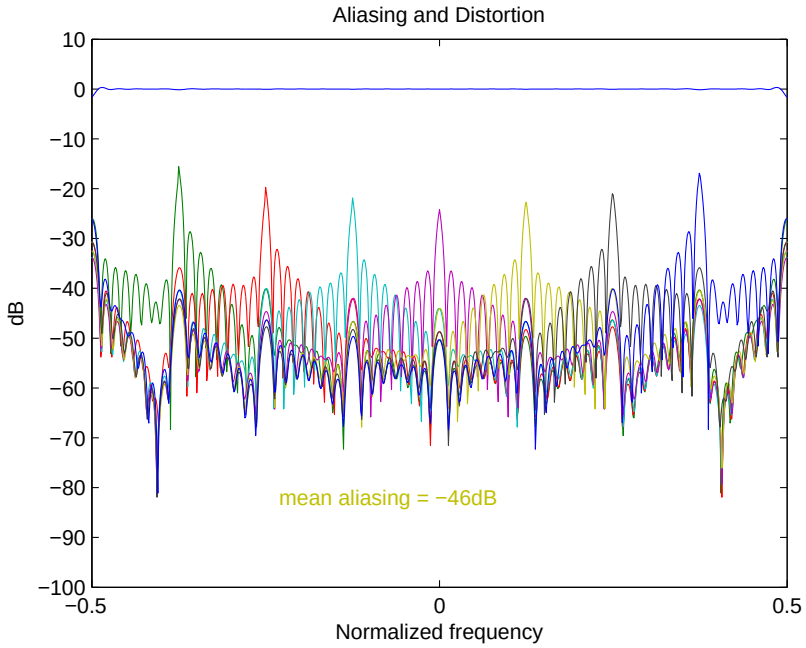

Figure 3.6. Distortion and aliasing terms (in dB) for an eight-channel HFB structure. One RC and seven RLC circuits construct the analysis filter bank. Synthesis filter bank uses FIR synthesis filters with 64 coefficients.

3.2.4 Oversampling method

The aliasing terms may be considered as an additive noise source which restricts the output resolution of HFB A/D converters as well as the quantification noise. The performance of HFB A/D converters in terms of aliasing terms is not so acceptable using typical FIR synthesis filters (subsection 3.2.3). Then, it is necessary to somehow improve the performance.

Invoking (3.8) and the aliasing curves in figures 3.4 and 3.6, it is observed that the aliasing terms deteriorate around the particular frequency points. These frequencies are all an integer multiple of $\frac{2\pi}{M}$ ($k\frac{2\pi}{M}$, $0 \leq k \leq M-1$). There is an incompatibility in PR equations around these frequencies. It corresponds to the frequency points situated at the borders of the band (around $\pm\frac{\pi}{T}$). To mitigate the effects of this fracture points, it is offered not to consider the frequency borders [54]. It would be equivalent to use a small oversampling ratio so that the equations representing the border frequencies are eliminated (i.e. the analysis filters are supposed to be null near the frequency borders $\pm\frac{\pi}{T}$) [54].

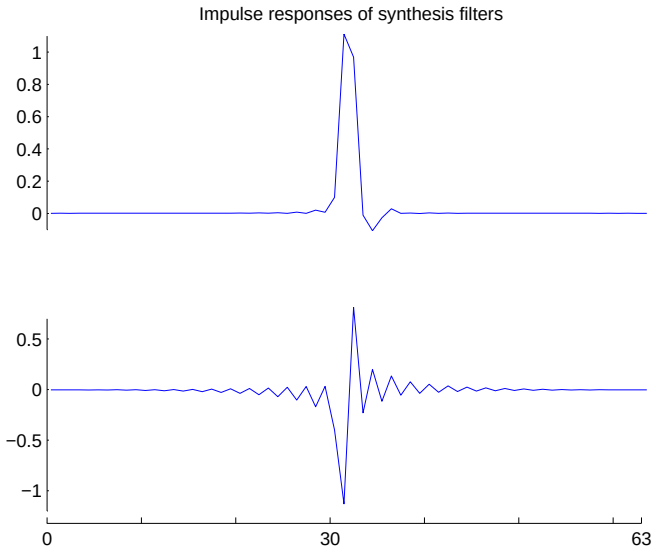

Figure 3.7. Impulse response of the synthesis filters for a two-channel HFB structure supposing an oversampling ratio of 7%. The analysis filter bank consists of an RC first-order and an RLC second-order circuit.

Using a small oversampling ratio, the preceding relationships (3.9) and (3.10) are still valid but the rows associated with the frequencies $|\Omega| > \frac{\pi}{T}(1-\alpha)$ are eliminated. α represents the oversampling ratio. This elimination originates from the oversampling process according to which the input spectrum is supposed to be $[-\frac{\pi}{T}(1-\alpha), +\frac{\pi}{T}(1-\alpha)]$. Then, the output of analysis filters would be zero in the frequency domain for the frequencies $|\Omega| \geq \frac{\pi}{T}(1-\alpha)$. In other words, there have already (without oversampling) been M equations associated with each frequency ω according to (3.3) and (3.4). Invoking the oversampling process, one of these M equations may be omitted depending on the frequency (see (3.4)). Thus, there would exist $(M-1)$ equations associated with M unknown values ($F(e^{j\omega})$ in (3.4)) in this case (of course at some frequencies). It is evident that its solution is not unique at the mentioned frequency. Considering N above-mentioned frequency points, $\mathbb{H}'$ and $\mathbb{B}'$ substitute $\mathbb{H}$ and $\mathbb{B}$ respectively in **??**Ch:2-eq10) and (3.10). Therefore, the matrix $\mathbb{H}'$ is no longer square (some rows of $\mathbb{H}$ have been omitted).

The local and global optimizations do not lead to the same solution in this case. Applying the global optimization method, the following solution is achieved:

$$\mathbf{f}_\circ = (\mathbb{H}'\mathbb{A}')^\dagger \mathbb{B}' = [(\mathbb{H}'\mathbb{A}')^T(\mathbb{H}'\mathbb{A}')]^{-1}(\mathbb{H}'\mathbb{A}')^T\mathbb{B}' \tag{3.18}$$

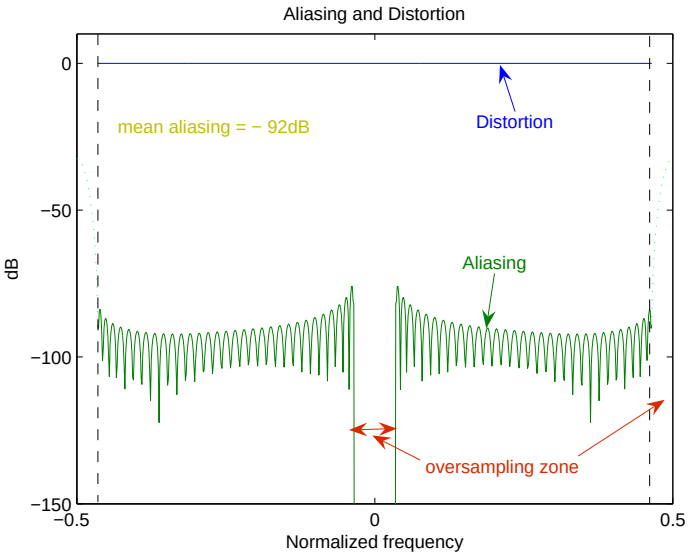

Figure 3.8. Distortion and aliasing terms (in dB) for a two-channel HFB structure. The analysis filter bank includes an RC and an RLC circuits. FIR synthesis filters having 64 coefficients and an oversampling ratio of 7% are used.

It is associated with the minimization of following criterion:

$$\mathbf{f}_{\circ} = \arg \min_{\mathbf{f}} \|(\mathbb{H}^{'}\mathbb{A}^{'})\mathbf{f} - \mathbb{B}^{'}\| \tag{3.19}$$

In this case, the M FIR synthesis filters are obtained simultaneously and the new analysis matrix $\mathbb{H}^{'}$ establishes a relationship between the absolute errors corresponding to the synthesis filters. Then, there is no unique (ideal) synthesis filter bank which may result in the ideal conditions (aliasing equal to zero). The global optimization method provides a much better performance than the latter (local optimization) since it performs the optimization of M synthesis filters at the same time. It has been approved by simulations. To have a better approximation and to more exploit the mutual information between different branches, the global optimization method is utilized for solving the equations through LS technique. Figure 3.7 demonstrates the impulse responses of synthesis filters for a two-branch HFB structure considering an oversampling ratio of 7%. The respective aliasing and distortion terms are illustrated in figure 3.8.

In fact, the oversampling technique eliminates the frequency points where the equations are very difficult to be held. Comparing this result with the counterpart of preceding subsection 3.2.3 , one can discover that the impulse responses of the synthesis filters are the same except at the beginning and ending. In other words,

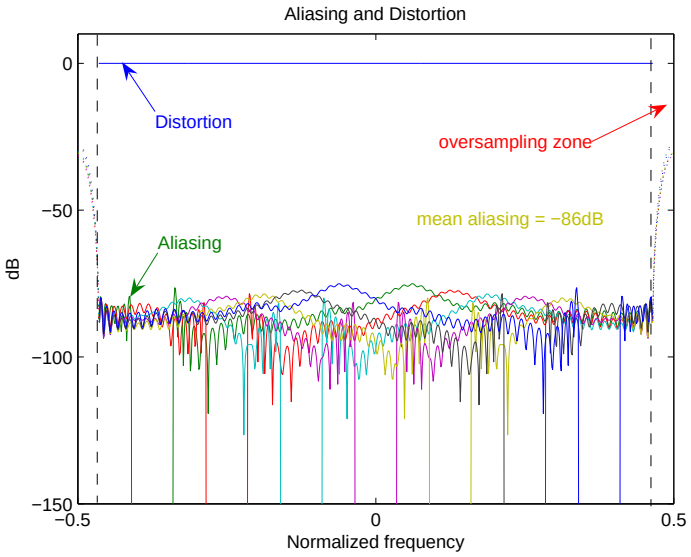

Figure 3.9. Distortion and aliasing terms (in dB) for an eight-channel HFB structure. FIR synthesis filters have 64 coefficients and oversampling ratio is 7%. The analysis filter bank includes an RC and seven RLC circuits.

the little fluctuations at the beginning and ending borders have been omitted (compare figures 3.3 and 3.7). This trial has been repeated for a structure including 8 branches. The analysis filter bank is the same one used in the previous subsection 3.2.3. FIR synthesis filters have been considered with 64 coefficients. The oversampling ratio is 7%. Figure 3.9 shows the aliasing and distortion functions in this case. To better show the effect of oversampling process, the first aliasing term has been illustrated for the oversampling ratios of 7% and 0 in figure 3.10. It is seen that the performance is apparently improved. When the oversampling ratio increases, the aliasing terms decrease. The distortion function is nevertheless maintained at the unity. However, the aliasing terms do not decrease anymore when the oversampling ratio approaches $\frac{1}{M}$. Figure 3.11 illustrates the average aliasing term versus oversampling ratio for an eight-channel HFB structure. It is seen in figure 3.11 that there is no decrease in the average aliasing for the oversampling ratios larger than 8%. It is necessary to mention that the oversampling ratio may not exceed $\frac{1}{M}$. Otherwise, there exist no longer a maximally-decimated structure.

Using the oversampling process, the analysis matrix $\mathbb{H}'$ tends toward rank deficiency. In fact, larger the oversampling ratio is chosen, more the matrix of analysis filters is ill-conditioned. Figure 3.12 shows the condition number related to the

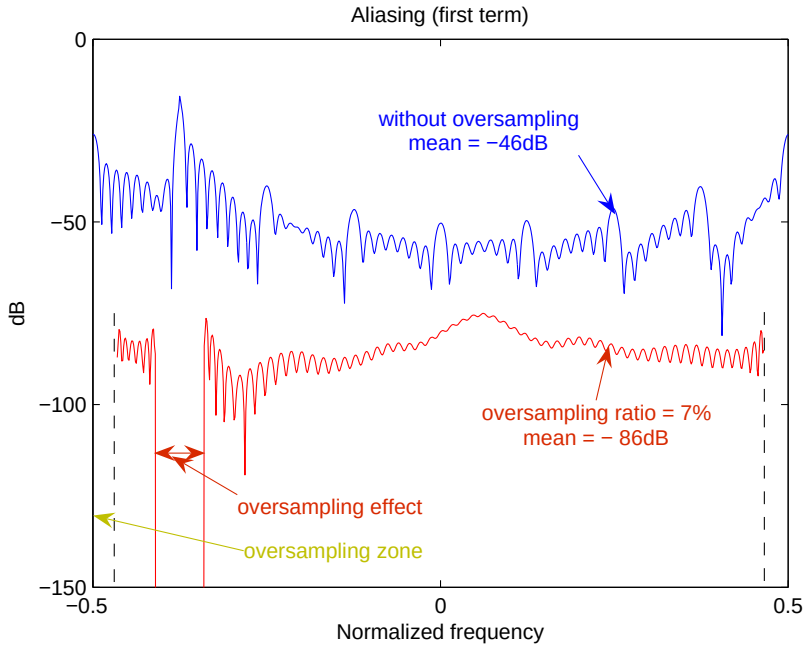

Figure 3.10. First aliasing terms (in dB) of an eight-channel HFB structure for the oversampling ratios of 7% and 0%. The FIR synthesis filters have 64 coefficients and the analysis filter bank includes an RC and seven RLC circuits.

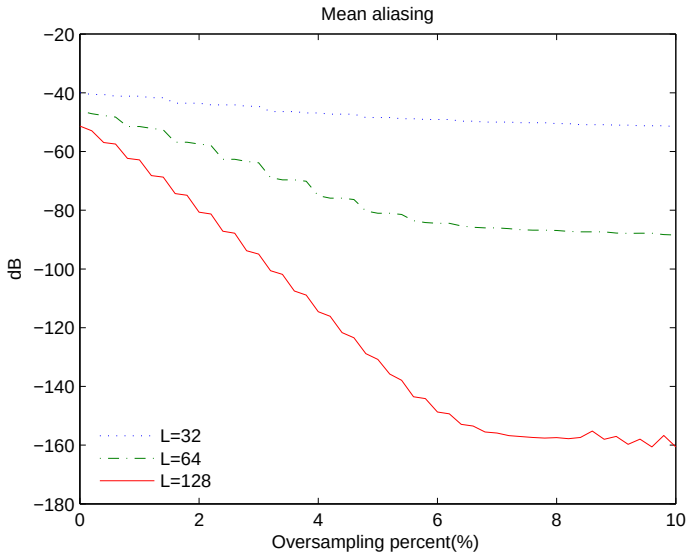

Figure 3.11. Aliasing term (in dB) for an eight-channel HFB structure versus oversampling ratio (%). L represents the length of FIR synthesis filters. The analysis filter bank includes an RC and seven RLC circuits.

coefficient matrix ($\mathbb{H}'\mathbb{A}'$) versus oversampling ratio. At the limit, when the oversampling ratio approaches the ratio of $\frac{1}{M}$, this matrix will be more ill-conditioned

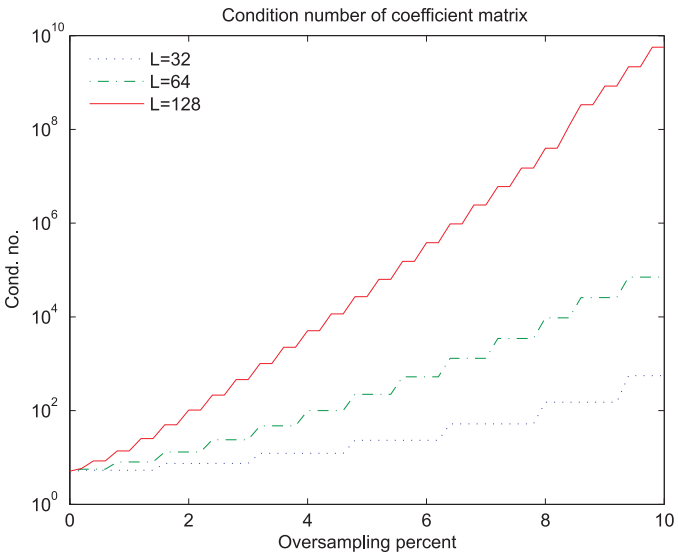

Figure 3.12. Condition number of coefficient matrix versus the oversampling ratio for an eight-channel HFB A/D converter.

(larger condition number) and the prediction (or interpolation) properties of the solution reduces.

3.3 Sensitivity to realization errors

3.3.1 Analog imperfections of HFB structure

According to the previous section, HFB-based A/D conversion provides an acceptable aliasing level if the oversampling process is considered. Supposing the oversampling ratio 7%, the level of aliasing mean decreases to $-86dB$ for the FIR synthesis filters consisting of 64 coefficients. However, the analog imperfections which are always present during the fabrication procedure of the electronic components, have not been considered. HFB structures have exhibited a large sensitivity to these imperfections [64, 5]. The performance of the proposed architectures in presence of analog imperfections deteriorates so that they may be no longer useful [5]. On the other hand, electronic components are always subject to realization errors. The realization errors are mostly originated from the non-ideal phenomena due to fabrication [73]. Meanwhile, there are some time-dependent variations in the parameters of analog circuits as well. These analog imperfections may be associated with aging and ambience factors such as temperature drifts. The

analog imperfections are always unknown. For being capable to handle the analog imperfections in HFB structures, it is necessary to initially know and study the sensitivity of optimization methods exactly. Appendix B provides a brief survey on the sensitivity analysis of optimization methods. It would be useful to analyze the sources from which the high sensitivity of HFB structures to analog imperfection is originated. This will enable us to include the associated results at the optimization as well as at the search for new structures. The analysis of optimization methods presented in appendix B assumes a condition according to which the rank of coefficient matrix remains unchanged. In terms of HFB structure, it means that the analog imperfections do not change the rank number of analysis matrix. This condition is always held through the HFB structures. Otherwise, the HFB structure will not respect the reconstruction prerequisite condition (non-singularity of analysis matrix).

3.3.2 Performance of HFB A/D converters versus realization errors

3.3.2.1 Classical HFB structure in presence of realization errors

The effects of analog imperfections on the performance of HFB-based A/D converters are studied in this section. For simulation purpose, an 8-channel HFB-based A/D converter has been used. This is the same HFB structure that was considered in the section 3.2.3. The effects of oversampling process on the performance of HFB structures are also studied in the presence of analog imperfections. The classical HFB architecture for A/D conversion (figure 3.1) is here considered. In practice, only the design (or nominal) values of parameters are known for the analysis filters. The real parameters of analysis filter bank have generally some deviations from the nominal values. The synthesis filter bank is designed according to the nominal parameters instead of the real ones. So, the designed synthesis filter bank is not optimal for the real analysis filter bank. To measure the sensitivity $S_{\mathbf{f}}$ of HFB structure to realization errors, the relative deviation of synthesis filter bank is defined as follows (refer to appendix B):

$$S_{\mathbf{f}} = \frac{\|\mathbf{f} - \mathbf{f}_\circ\|}{\|\mathbf{f}_\circ\|} \tag{3.20}$$

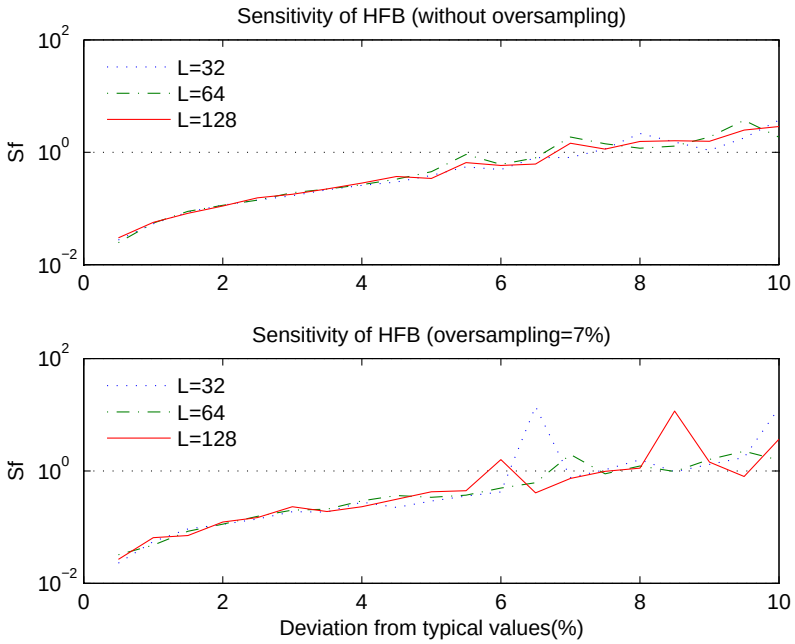

Figure 3.13. Sensitivity $S_{\mathbf{f}}$ (logarithmic) versus the deviation from typical values (%) for the case of no oversampling (above) and with oversampling 7% (below). The curves are related to the classical HFB structure. L represents the length of FIR synthesis filters.

where $\mathbf{f}_\circ$ and $\mathbf{f}$ are the impulse responses of synthesis filter bank considering no realization error and practical (with realization errors) cases respectively. This measure would be almost independent from the length of FIR synthesis filters because of relativity [74]. The electronic elements (R, C and L) of analysis filter bank are assumed to include Gaussian random deviations from their nominal values. In this section, the standard deviation of the error distribution is used as the parameter of deviation from typical (or design) values. Using an 8-branch HFB structure, the simulations have been performed for 1000 trials of the Gaussian realization errors. The performance is studied in terms of the different deviations from typical values. Figure 3.13 demonstrates $S_{\mathbf{f}}$ versus the deviation from typical values for the classical HFB structure in the logarithmic scale. In both cases of oversampling ratios 0 and 7%, the sensitivity increases about linearly versus the deviation ratios of electronic elements (in logarithmic scale). Figure 3.14 shows the mean and maximum aliasing versus the deviations from typical values without oversampling process. Figure 3.15 shows the same when the oversampling ratio

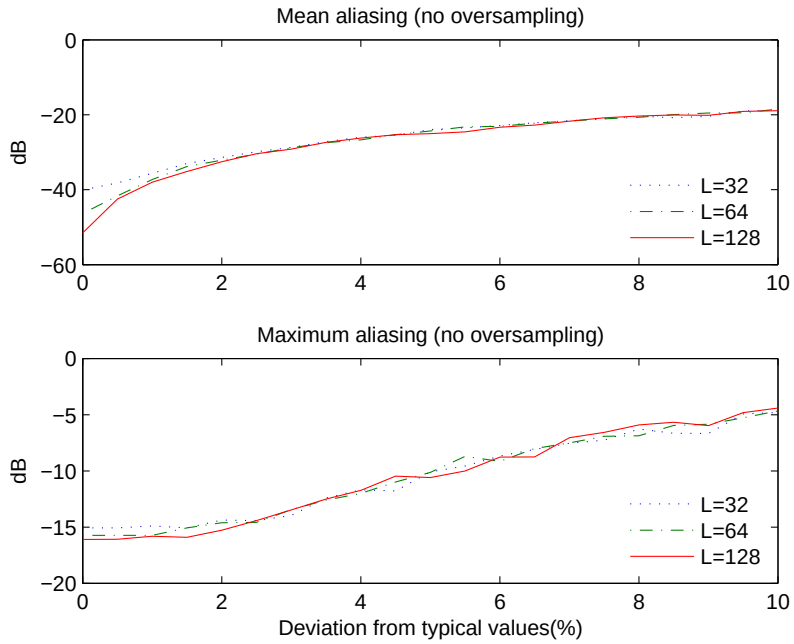

Figure 3.14. Mean (above) and maximum (below) aliasing functions in dB versus the deviation from typical values (%). The curves belong to the classical HFB structure. In this case, no oversampling has been used. L represents the number of coefficients used for FIR synthesis filters.

is equal to 7%. Comparing the figures 3.14 and 3.15, it may easily be seen that the performance of HFB-based ADC degrades rapidly in the presence of realization errors. Though, oversampling process provides a lower aliasing level for the HFB-based A/D converters (refer to subsection 3.2.4), but it causes an increase in the sensitivity to realization errors. In fact, the oversampling process eliminates the equations that are not compatible in the optimization procedure. Considering these equations, aliasing terms are large. However, the oversampling process increases the condition number associated with the analysis matrix (figure 3.12). The design of synthesis filters of HFB structures is a non-zero-residual problem when FIR filters are used. Accordingly, the sensitivity would be proportional to the square of condition number associated with analysis matrix in this case (refer to the appendix B). Then, oversampling process deteriorates intensely the sensitivity of HFB structure to realization errors. In other words, oversampling process improves the performance of HFB structure at the expense of sensitivity increase.

Although, the sensitivity of HFB structure to analog imperfections is less when

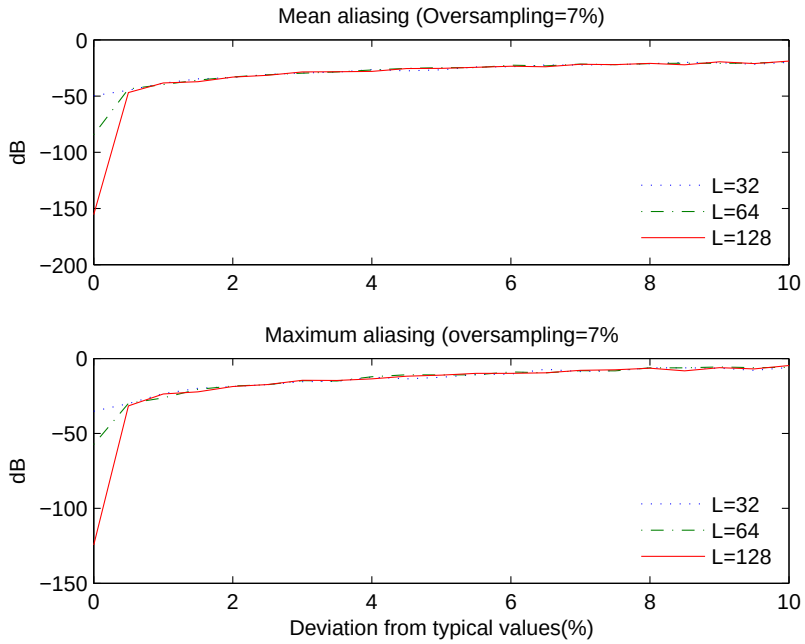

Figure 3.15. Mean (above) and maximum (below) aliasing functions in dB versus the deviation from typical values (%). The curves belong to the classical HFB structure and the oversampling ratio 7% has been used. L shows the length of FIR synthesis filters.

the oversampling process is not used, but the performance of HFB is not acceptable for A/D conversion purposes. It may be seen that the aliasing terms dominate the output of HFB A/D converter when the electronic circuits of the analysis filter bank are subject to the deviations even about 1% from typical values (figure 3.15).

3.3.2.2 Using total least squares method

To reduce the large sensitivity of HFB to the realization errors, HFB structure may be designed according to another optimization method instead of LS one. Total Least-Squares (TLS) or errors in variables optimization method is a candidate for decreasing the sensitivity to the deviations of coefficient matrix (refer to the appendix C) [75, 76]. TLS is an alternative to the Least-Squares (LS) method and uses the fact that the errors can exist both in the focusing allocation matrix and the estimated location matrix at the frequency bin for array processing [77]. TLS may be used for the localization of wide-band signals in array processing. TLS can then be used for designing the synthesis filters of classical HFB instead of LS

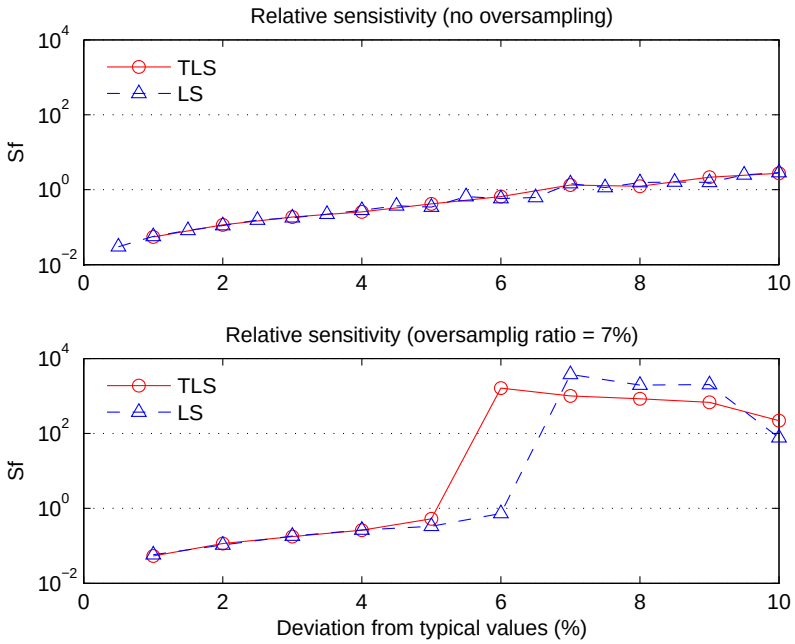

Figure 3.16. Sensitivity $S_{\mathbf{f}}$ (logarithmic) versus the deviation from typical values (%) in the case of no oversampling (above) and with oversampling 7% (below) using TLS and LS optimization methods. The synthesis filters have 128 coefficients.

optimization technique. To apply the TLS method as explained in appendix C, it is possible to imagine the data matrix Λ and measurement vector $\mathbf{b}$ in terms of HFB formulations (sections 3.2 and 3.3.1) as following:

$$\Lambda = \mathbb{H}.\mathbb{A} \qquad \text{and} \qquad \mathbf{b} = \mathbb{B} \tag{3.21}$$

In the HFB case, the analog imperfections appear only in the matrix $\mathbb{H}$ (and then in Λ) and there is no perturbation on the fixed vector $\mathbb{B}$ (or equivalently in measurement vector $\mathbf{b}$). An eight-channel HFB structure is considered with the same parameters used already for the LS optimization method.
The sensitivity to analog imperfections associated with the TLS and LS optimization methods is shown in figure 3.16 for comparison. The performances are approximately equal and the TLS optimization technique shows no improvement in the performance. Figure 3.17 shows the aliasing terms related to TLS and LS optimization methods considering oversampling ratios 0 and 7%. Aliasing terms do not reduce for TLS case. In fact, TLS is anticipated to improve the performance

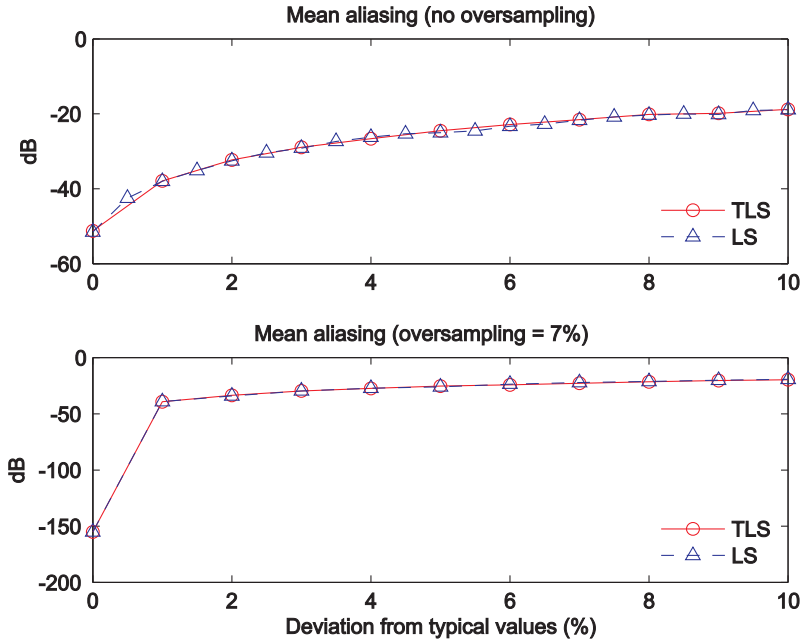

Figure 3.17. Mean aliasing functions in dB versus the deviation from typical values (%) for TLS and LS optimization methods considering no oversampling (above) and the oversampling ratio 7% (below). FIR synthesis filters have 128 coefficients.

for zero-residual problems [74, 78]. The design of synthesis filter bank of HFB is not a zero-residual problem because there is no FIR synthesis filter bank leading to a null aliasing (refer to subsection 3.2). Therefore, the TLS optimization method does not lead to a lower sensitivity to analog imperfections (figures 3.16 and 3.17).

3.4 Summary and discussion

The performance of conventional HFB-based A/D converters has been studied neglecting the quantization noise in this chapter. Using FIR synthesis filters, the aliasing terms are very large so that HFB structures do not appear useful for A/D conversion. Applying a small oversampling ratio, HFB structures show a good performance in terms of aliasing and distortion terms. There is always an optimal oversampling ratio depending on the number of branches and analysis filter bank. The optimal value for an eight-channel HFB using first- and second-order analysis

filters is about 7% (see figure 3.11).
However, HFB structures appear to be very sensitive to the analog imperfections so that the output resolution is not acceptable for even 1% of realization errors. Though, the oversampling process decreases the aliasing terms of HFB structures, but leads to a large increase in the relative sensitivity to analog imperfections. The sensitivity of HFB structures is proportional to the squared condition number associated with the coefficient matrix. The oversampling process increases the condition number which leads to a larger sensitivity to realization errors. TLS optimization technique is a candidate for reducing the sensitivity of LS solution for zero-residual problems. Using TLS technique, no improvement is obtained in the sensitivity of HFB structures because the design of FIR synthesis filters of HFB structures is a non-zero-residual problem. Therefore, the classical HFB architecture with practical FIR synthesis filters is not useful for implementing the real A/D converters unless a compensation technique is incorporated to reduce the effects of analog imperfections. For practically using HFB-based A/D converters, a mechanism is required either to decrease the aliasing terms or to provide a robustness in reference to the realization errors simultaneously. Two strategies may be useful for this purpose. New HFB architectures can be obtained so that the related sensitivity decreases as the first solution. Secondly, the sensitivity of HFB structures to analog imperfections may be handled by compensating the imperfections of analysis filter bank. To compensate the errors, analog imperfections have to be estimated. Next chapter will deal with these techniques as the estimation method. New HFB architectures are proposed to overcome the problem of analog imperfections in HFB-based A/D converters in the chapter 5 as well.

Chapter 4

Blind estimation of realization errors in analog circuits

We think in generalities, but we live in details.
- Whitehead

4.1 Introduction

Despite the fast development of the digital technology and the signal processing methods, it is still at times required to use the analog circuits either through an analog system or along with a digital part at the mixed analog/digital circuits. Both the discrete and integrated electronic components of analog circuits are always subject to random deviation from the nominal values [73, 79]. Therefore, the analog electronic circuits associated with LTI systems are characterized by the transfer functions which include uncertainties. The coefficients of numerator and denominator of these transfer functions may be considered as random numbers. The average values of the coefficients represent the typical or nominal values. The difference between the typical and real values called the deviations from typical values is unknown. The realization errors associated with the fabrication process can be considered as time-independent factors. However, the analog imperfections include some time-varying contributions related to the phenomena such as the operative temperature. To lessen the fabrication imperfections of analog circuits,

some possibilities exist such as laser trimming in the case of integrated circuits at the production phase. The laser trimming is generally too expensive [80]. Moreover, the time-varying imperfections cannot be compensated during the fabrication phase. Accordingly, digital compensation may be considered as a suitable solution particularly when the mixed analog-digital circuits are dealt with.

Analog imperfections degrade the performance of analog circuits. This deterioration is sometimes so large that the related circuits are no longer useful. For example, delta-sigma A/D converters exhibit a high sensitivity to the nonlinearity of their internal multi-bit D/A converters [1]. The cascade architecture (MASH) has been proposed to handle this high sensitivity and the instability from which the delta-sigma modulators suffer. In return, a large sensitivity to analog circuit imperfections emerge when MASH is used [1]. In Switched-Capacitor (SC) circuits, these imperfections are mostly related to finite op-amp gains, capacitor ratio errors and settling times [81]. HFB-based A/D converters are much sensitive to the analog imperfections as shown in the previous chapter. To overcome the analog imperfections in wide-band HFB-based A/D converters, Velazquez proposed a digital calibration method [9]. The calibration was established in the whole spectrum but the adaptive compensation of proposed comb filter was classified according to the different origins of the imperfections. Petrescu has also proposed a digital calibration technique using a known analog input for calibrating the design phase [50]. This algorithm necessitates to accommodate a calibration process circuit in the system. To correct the realization errors of analysis filter bank, the unknown (or main) input is disconnected and an internal calibration signal is applied to the converter. This calibration circuit would occupy an important part of die size. Besides, it requires to generate a wide band analog input which covers the whole frequency band of interest.

Till now, most of proposed digital compensation techniques deal with specific imperfections (for example only with capacitor ratio or with finite op-amp gain error). Accordingly, they are not generic methods and are applicable only for the supposed special cases. Besides, they sometimes utilize a reference signal that necessitates to use an auxiliary subsystem being completely dependent on the system [82, 81]. Thus, it is necessary to look for a general method which can estimate the real parameters of analog circuits using only the output of the system. Desired estimation

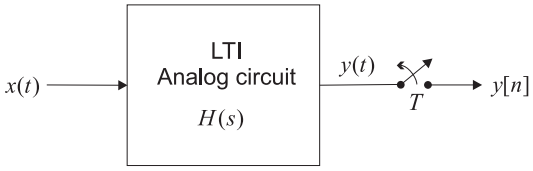

Figure 4.1. An arbitrary LTI analog circuit with transfer function $H(s)$. $y[n]$ represents the output after sampling.

method has to be independent of the type and the origins of errors. Then, one would be able to digitally compensate the analog imperfections of electronic circuits. It will be very useful particularly for mixed analog-digital circuits containing digital parts. Accordingly, calibration phase could be omitted in the fabrication process of electronic circuits. On the other hand, time-varying drifts (especially temperature drifts) would be possibly compensated in a real-time manner.

The aim of this chapter is to offer two methods for estimating the real parameters of transfer function of an analog circuit using the sampled output. The estimation algorithm has to be independent of the type and the source of analog imperfections. To formulate the problem, the unknown LTI analog system $H(s)$ is assumed according to the figure 4.1. Considering figure 4.1, it is supposed that the Nyquist sampling rate is at least used and that the sampled output $y[n]$ is the only available data. The objective is to estimate the real spectral parameters of the analog system (or the coefficients of $H(s)$) using the only available data $y[n]$. Regarding to the analog imperfections, the coefficients of numerator and denominator of $H(s)$ are the random variables which have the different distributions depending on the fabrication factors, the number and type of electronic elements and the circuit structure. The central (or expectation) values of these parameters are often known but the real values are subject to a random additive error (deviation from the typical values). Analog imperfections cause a change in the coefficients of $H(s)$ but have no effect on the order of the system $H(s)$. Accordingly, the real coefficients may be estimated in order to compensate the analog imperfections as the most direct way. An algorithm is then required to directly estimate the relative imperfections through the output samples. It is supposed to have K unknown parameters $\underline{\alpha} = [\alpha_1, \alpha_2, \ldots, \alpha_K]^T$ through which $H(s)$ is described. These parameters may be either the coefficients of $H(s)$ or any function of the coefficients such as cut-off frequency, resonance frequency and quality factor

for the first- and second-order analog circuits respectively. The transfer function of analog circuit may be described as follows:

$$H(s) = g(\underline{\alpha}, s) \tag{4.1}$$

Each element α_i of the vector $\underline{\alpha}$ is supposed to be randomly distributed around the known expected value $\alpha_{i_\circ}$ as follows:

$$\alpha_i = \alpha_{i_\circ} + \triangle\alpha_i = \alpha_{i_\circ}(1 + \delta_{\alpha_i}) \tag{4.2}$$

where δ_{α_i} describes the relative imperfection of α_i (or the relative deviation from the typical value $\alpha_{i_\circ}$) as follows:

$$\delta_{\alpha_i} = \frac{\triangle\alpha_i}{\alpha_{i_\circ}} \qquad i = 1, \ldots, K$$

where $\triangle\alpha_i$ is a random variable which represents the overall analog imperfections of α_i. The probability distribution of $\triangle\alpha_i$ is not necessarily Gaussian even in the case of Gaussian fabrication errors. It is desired to estimate unknown relative imperfections $\{\delta_{\alpha_1}, \delta_{\alpha_2}, \cdots, \delta_{\alpha_K}\}$ using only the output samples $y[n]$. In practice, the nominal values $\{\alpha_{1_\circ}, \alpha_{2_\circ}, \cdots, \alpha_{K_\circ}\}$ are a priori known, although this is not necessary (refer to the section 4.3). The structure of analog circuit (or simply the order of nominator and denominator of $H(s)$) is known since it is defined at the design phase. It is useful in the extraction of relative imperfections in the proposed blind estimation method (section 4.3). In this chapter, two methods are proposed and discussed for estimating the analog imperfections of LTI analog circuits. Second-Order Statistics (SOS) are used in section 4.2 to provide a mathematical model for analog imperfections. This mathematical model is presented in 4.2.1. Then, the performance of this SOS model is studied in 4.2.2. In section 4.2, Higher-Order Statistics (HOS) are used for estimating analog imperfections. General constraints of HOS methods are discussed in 4.3.1. Then, Super-Exponential Algorithm (SEA) is reviewed and used for the blind estimation of analog imperfections in 4.3.2 and 4.3.2. Finally, the results are summarized and the feasibility of the proposed estimation algorithms for the case of HFB-based A/D converters is discussed in section 4.4.

4.2 Second-order statistics method

4.2.1 Mathematical model of realization errors

In this section, a model is proposed for the blind estimation of analog imperfections. The proposed model is totally general and is applicable to every LTI circuit. Figure 4.1 is considered. Using the linear approximation of Taylor development, the transfer function $H(s)$ may be simplified. Assuming that the relative imperfections (δ_{α_i}) are very small ($\mid \delta_{\alpha_i} \mid \ll 1$), $H(s)$ may be approximated as follows:

$$\begin{aligned} H(s) &\cong g(\underline{\alpha}_\circ, s) + \sum_{i=1}^{K} \delta_{\alpha_i} \cdot (\alpha_i \frac{\partial g(\underline{\alpha}, s)}{\partial \alpha_i})\Big|_{\underline{\alpha}=\underline{\alpha}_\circ} \\ &= H_\circ(s) + \sum_{i=1}^{K} \delta_{\alpha_i} \cdot H_i(s) \end{aligned} \tag{4.3}$$

where $H_\circ(s)$ represents the transfer function of analog circuit when there is no imperfection and $H_i(s)$ is defined as follows:

$$H_i(s) = \alpha_i \frac{\partial g(\underline{\alpha}, s)}{\partial \alpha_i}\Big|_{\underline{\alpha}=\underline{\alpha}_\circ} \qquad i = 1, 2, \ldots, K \tag{4.4}$$

$H_i(s)$ does not have necessarily the same order as $H_\circ(s)$. Depending on the factors influencing on the distribution function of coefficients, $H_i(s)$ may have a different order in reference to the order of $H_\circ(s)$. Equally, the following relationship may be established in the time domain:

$$h(t) \cong h_\circ(t) + \sum_{i=1}^{K} \delta_{\alpha_i} \cdot h_i(t) \tag{4.5}$$

where each $h_i(t)$ is the impulse response associated with the respective transfer function $H_i(s)$. According to (4.4), $h_i(t)$ depends neither on analog imperfections nor on input-output signals.

To estimate the relative imperfection using only the output samples $y[n]$, it is required to have some assumptions about the input type. In the deterministic case, there would be no general solution, and the estimation may be realized by the methods depending on the type of deterministic signal. Supposing to have a

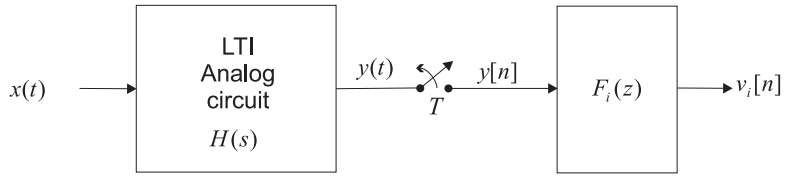

Figure 4.2. An LTI analog circuit with transfer function of $H(s)$ to which another auxiliary FIR filter of $F_i(z)$ has been applied.

stochastic input signal (not deterministic), the type of input distribution may be exploited like the blind estimation techniques. If the input signal is independent and identically-distributed (i.i.d.), the following equality holds [83]:

$$\sigma_y^2 = \sigma_x^2 \int (h(t))^2 dt \tag{4.6}$$

where σ_x^2 and σ_y^2 are the input and output variances respectively. Supposing that the filter $H(s)$ is band-limited and using sufficiently high sampling rate, (4.6) may be approximated in the discrete-time domain as follows:

$$\sigma_y^2 \cong \sigma_x^2 \sum_n (h[n])^2 \tag{4.7}$$

where $h[n]$ is obtained by sampling $h(t)$ with the sampling period T. Invoking (4.5) and (4.7), the following relationship is obtained:

$$\frac{\sigma_y^2}{\sigma_x^2} \cong \sum_n h_\circ[n]^2 + 2\delta_{\alpha_1} \sum_n h_1[n].h_\circ[n] + \ldots + 2\delta_{\alpha_K} \sum_n h_K[n].h_\circ[n] \tag{4.8}$$

where the relative imperfections δ_{α_i} and the input variance σ_x^2 are unknown. K additional equations are required to find the unknown relative imperfections. For this purpose, we propose to choose K auxiliary FIR filters which are applied separately to the system output $y[n]$ [84]. For instance, figure 4.2 shows this process after applying i^{th} auxiliary FIR filter $f_i[n]$. Then, (4.8) may be established for each new output signal $v_i[n]$ versus the original input $x(t)$ because the convolution of two filters $h[n]$ and $f_i[n]$ provides an LTI filter as well. Applying (4.8) to this new

configuration, the following relationship yields:

$$\frac{\sigma_{v_i}^2}{\sigma_x^2} \cong \sum_n s_{\circ i}[n]^2 + 2\delta_{\alpha_1} \sum_n s_{1i}[n].s_{\circ i}[n] + \cdots + 2\delta_{\alpha_K} \sum_n s_{Ki}[n].s_{\circ i}[n] \qquad (4.9)$$

where $s_{ji}[n]$ is an intermediate impulse response defined as following:

$$s_{ji}[n] = h_j[n] \star f_i[n] \qquad j \in \{\circ, 1, 2, \cdots, K\}$$

that $\star$ represents the convolution operation. Some choices of auxiliary FIR filters have been tried in the simulations. An FIR filter $f[n]$ approximating the inverse of typical transfer function $H_\circ(s)$ shows a good performance when $K = 1$ as shown in the next section 4.2.2 [84]. For $K > 1$, it is proposed to have a quasi-orthogonality in the frequency domain. This means that K mutually orthogonal FIR filters must be chosen. For example, k^{th} FIR filter $f_k[n]$ is a filter with a passing band of $[(k-1)\frac{\pi}{T}, k\frac{\pi}{T}]$ where T is the sampling period and $1 \leq k \leq K$. Considering (4.9) and (4.8), $K + 1$ equations may be obtained as following:

$$\begin{cases} C_{\circ\circ}\delta_{\alpha_1} + \cdots + C_{\circ K}\delta_{\alpha_K} + (\sigma_y^2)\frac{1}{\sigma_x^2} = d_\circ \\ C_{11}\delta_{\alpha_1} + \cdots + C_{1K}\delta_{\alpha_K} + (\sigma_{v_1}^2)\frac{1}{\sigma_x^2} = d_1 \\ \qquad\qquad \vdots\ \vdots\ \vdots \\ C_{K1}\delta_{\alpha_1} + \cdots + C_{KK}\delta_{\alpha_K} + (\sigma_{v_K}^2)\frac{1}{\sigma_x^2} = d_K \end{cases} \qquad (4.10)$$

where the $(K + 1)$ unknown parameters are $\{\delta_{\alpha_1}, \delta_{\alpha_2}, \ldots, \delta_{\alpha_K}, \frac{1}{\sigma_x^2}\}$. All the coefficients C_{ij} and d_i are independent of the input and imperfections. Invoking (4.10) and using Crammer method, each unknown relative imperfection δ_{α_i} is found as follows:

$$\delta_{\alpha_i} = \frac{b_\circ \sigma_y^2 + \sum_{k=1}^K b_k \sigma_{v_k}^2}{a_\circ \sigma_y^2 + \sum_{k=1}^K a_k \sigma_{v_k}^2} \qquad (4.11)$$

where $\mathbf{b}^{(i)} = [b_\circ, \cdots, b_K, a_\circ, \cdots, a_K]$ represent the coefficients vector of the model associated with δ_{α_i}. To provide the coefficients, some known imperfections are applied to the system and the coefficients are then approximated using the Least Squares (LS) method. In other words, N known relative imperfections are selected and the system is simulated using a white noise at the input. For having an overde-

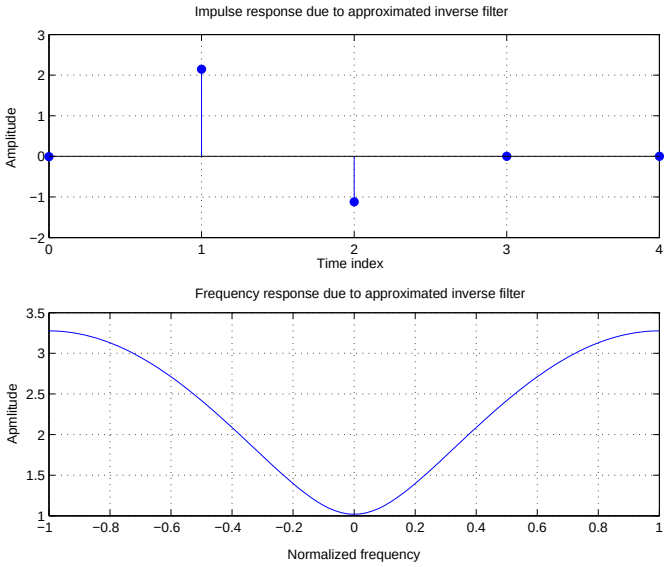

Figure 4.3. Impulse response (above) and frequency spectrum (below) due to the estimated inverse filter of an RC circuit.

termined problem, N is considered much larger than K ($N \gg K$). Therefore, the optimum vector of coefficients $\mathbf{b}_{opt}^{(i)}$ associated with the relative imperfection δ_{α_i} may be approximated as follows:

$$\mathbf{b}_{opt}^{(i)} = \arg \min_{\mathbf{b}^{(i)}} \|\delta_{\alpha_i}^m(\mathbf{b}^{(i)}) - \delta_{\alpha_i}^r\|^2 \tag{4.12}$$

that $\delta_{\alpha_i}^m$ and $\delta_{\alpha_i}^r$ represent the model and real values of the relative imperfection δ_{α_i}. This model can be separately established for each unknown imperfection ($\delta_{\alpha_i},\ 1 \leq i \leq K$).

4.2.2 Estimation of realization errors of the analog circuits using SOS-based model

The algorithm described in the previous section has been applied to several first- and second-order circuits. RC and RLC circuits are selected like the ones used in the HFB structures of chapter 3. The performance of estimation due to the model has been found dependent on the number of relative imperfections present in the system. Therefore, the results of simulations are discussed according to the number of unknown variables.

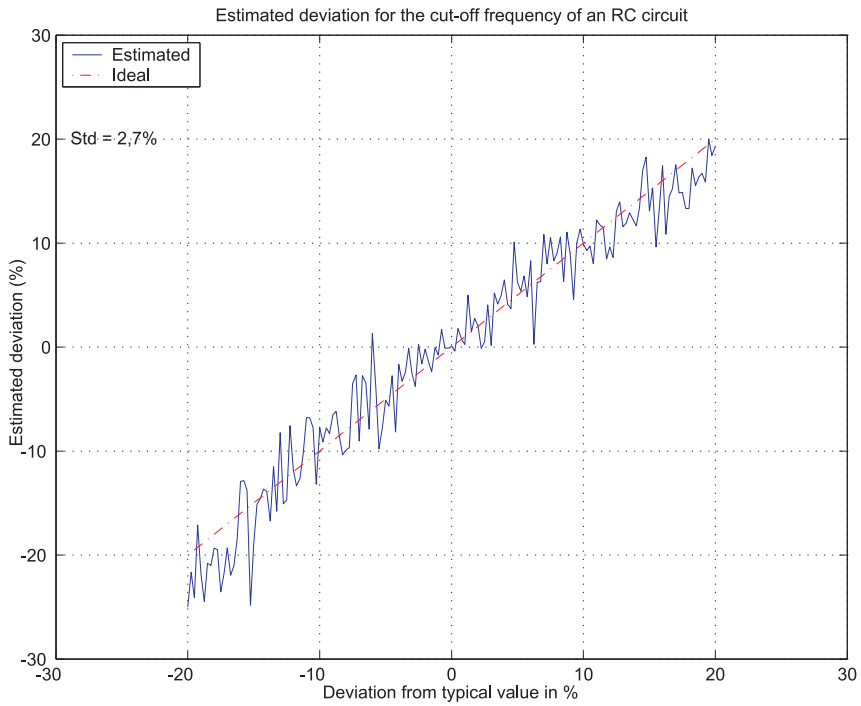

Figure 4.4. Estimated deviation (solid) from typical value of cut-off frequency versus real values for an RC circuit. The dashed line represents the ideal response.

◯ Unique unknown parameter

An analog circuit independent of its order may include only one unknown variable. If only one parameter is affected by analog imperfections and is unknown, then just one auxiliary filter will be required. An approximative inverse FIR filter with three non-zero coefficients has been used for the RC and RLC circuits. The impulse and frequency responses of that auxiliary FIR filter have been shown in figure 4.3. This FIR filter was obtained by blind equalization technique applied to an RC circuit [85]. The model is implemented for an RC circuit with the imperfections considered through its cut-off frequency. The estimation has been implemented for the imperfection range of ±20%. Figure 4.4 shows the estimated deviation from typical values versus the real values in this case. The average precision of this estimation is ±2.7% (ratio of the standard deviation of the estimation errors on real values in percent). Figure 4.5 shows the result of the estimation associated with a second-order RLC circuit. In this case, the resonance frequency is subject to the analog imperfections. The estimation is again considered for a range of

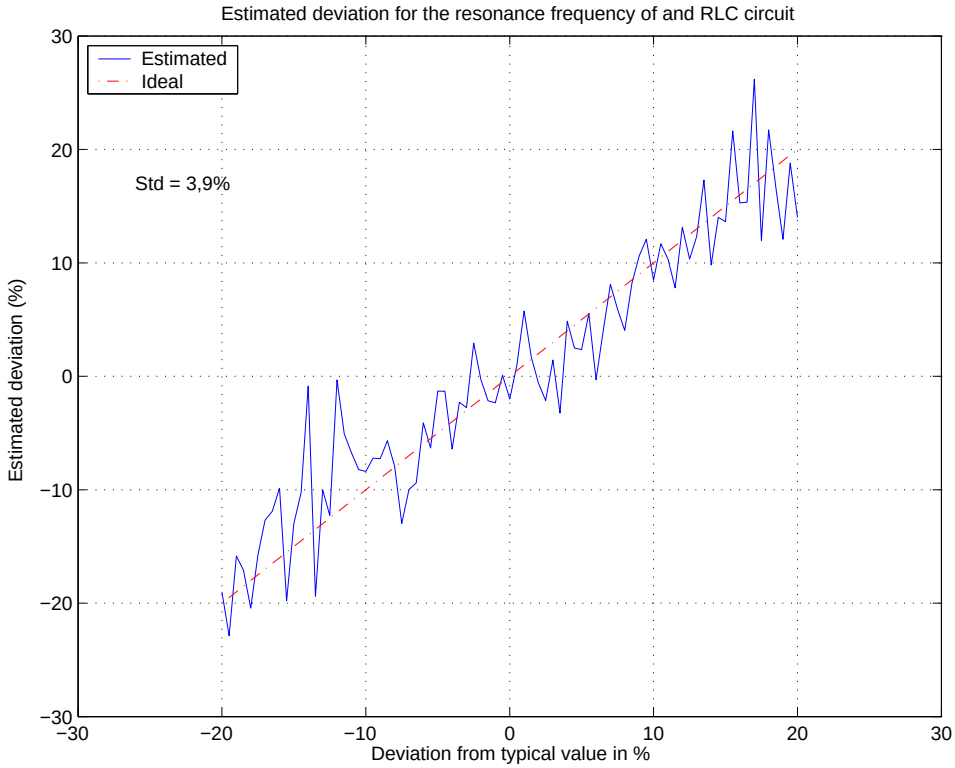

Figure 4.5. Estimated deviation (solid) from typical value of resonance frequency versus real values for an RLC circuit. The dashed line represents the ideal response.

±20%. The same auxiliary filter has been again used. There is a standard deviation of ±3.9% for the errors of this estimation. It is seen that the performance of estimation degrades in the case of second-order circuit.

◯ Two unknown parameters

This method has been used in the case of two unknown variables, considering an RC circuit including analog imperfections applied to its DC-gain and cut-off frequency. The estimation is implemented for the imperfections in the range of ±20%. Figure 4.6 demonstrates the result of the estimation. The values of standard deviation for the estimation errors are ±2.1% and ±4.6% associated to the parameters of DC-gain and cut-off frequency respectively. Considering a shorter range of estimation, the performance is improved.

The proposed homographic model (4.11) is useful when the input $x(t)$ is white (i.i.d.). It is applicable for both Gaussian and non-Gaussian signals since only SOS

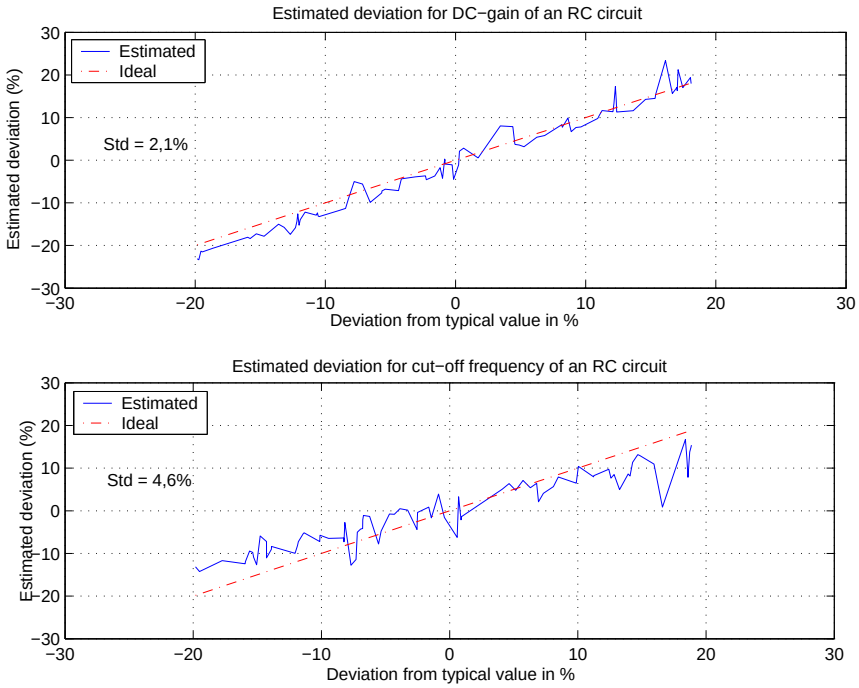

Figure 4.6. Estimated deviation (solid) from typical value versus real values for DC-gain (above) and cut-off frequency (below) of an RC circuit. The dashed lines represent the ideal responses.

parameters are used. The performance of estimation is not so acceptable for applications such as HFB structures which need a very high precision (see chapter 3). Larger the number of unknown coefficients of $H(s)$, worse is the performance of this SOS model for estimating analog imperfections. This is originated from the correlations between different coefficients of $H(s)$. For example, both resonance frequency and quality factor of an RLC circuit would vary even if only the resistor R includes imperfections and the inductance L and the capacitor C have no imperfection. The other reason for the low performance of this model is related to the approximation error involved in (4.7). The approximation error of (4.7) depends on the sampling period T. If T tends to zero, this approximation error will be zero. Figure 4.7 exhibits the effects of approximation in the discrete-time domain by (4.7) as well as the linearization procedure.

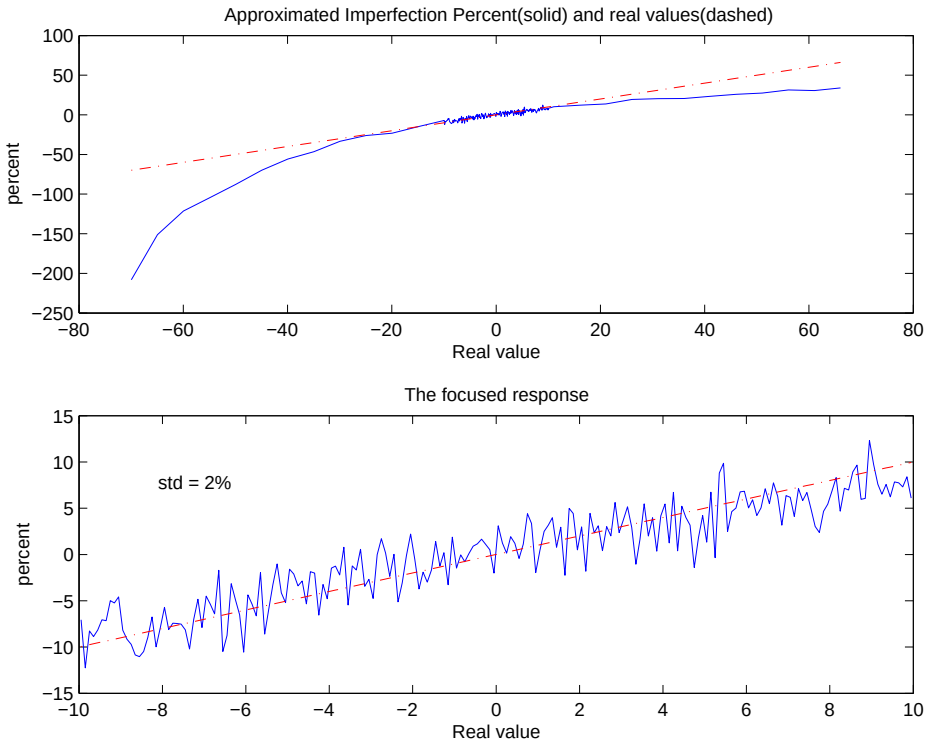

Figure 4.7. The curve (in solid) represents the result of the estimation and the one in dashed illustrate the real values of the imperfection percent. Below is a focus of the result in the range of linearization. This is due to a first-order analog circuit with the unity gain and the linearization is realized in the limit of $\pm 10\%$ imperfections.

4.3 Higher-order statistics method

4.3.1 General constraints

Blind deconvolution or equalization is referred to the case where the input of an unknown LTI system is desired to be reconstructed using only the output signal. The equalization is mostly implemented using Higher-Order Statistics (HOS) techniques [83]. Regarding to the properties of HOS, cumulants and polyspectra are blind to any Gaussian process because all cumulants of the order higher than two are equal to zero for a Gaussian process [83]. Accordingly, the input would be supposed to be a non-Gaussian i.i.d. process for implementing the blind equalization. An equalization technique looks adaptively for the inverse filter of unknown system. This inverse filter is often considered as an FIR filter called equalizer filter

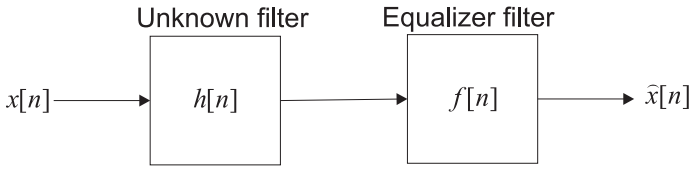

Figure 4.8. Blind equalization system. Equalizer filter f_n is an FIR filter with length L. $\widehat{x}[n]$ approximates the unknown input signal $x[n]$ in this system.

(see figure 4.8).

To realize blind deconvolution techniques, an objective or contrast function is generally considered (refer to appendix D). Equalization is realized through optimizing the equalizer filter $f[n]$ so that the criterion function is maximized (or minimized for Constant Modulus Algorithm (CMA) criterion) [83]. Contrast functions are some specific functions in terms of the cumulants due to $y[n]$ and $\widehat{x}[n]$ (refer to appendix D). The third order cumulants are null for the signals with symmetric distributions [83]. Therefore, fourth-order cumulant of $\widehat{x}[n]$ is chosen to be non-zero for the symmetric distributions. The analog input has been considered with a uniform distribution in the simulations. Super-Exponential Algorithm (SEA) proposed by Shalvi and Weinstein has been used in order to have a rapid convergence [86]. This algorithm provides an iterative procedure for updating the coefficients of equalizer filter. Before implementing the updating algorithm, it is required to calculate the vector of input/output cross cumulant (fourth-order cumulant) $\mathbf{d}$ and the output covariance matrix $\mathbf{R}$ (refer to appendix D). The current value of the equalizer filter $\mathbf{f} = [f_0, f_1, \cdots, f_{L-1}]^T$ is used to compute the next updated equalizer. L is the length of the equalizer filter $\mathbf{f}$. Using cumulant operation cum$(\cdot)$, the i^{th} element d_i of the vector $\mathbf{d}$ $(L \times 1)$ is obtained as follows:

$$d_i = \text{cum}(\hat{x}_n, \hat{x}_n, \hat{x}_n, y_{n-i}) \quad 0 \leq i \leq L-1 \tag{4.13}$$

Each element R_{ij} of the covariance matrix $\mathbf{R}$ $(L \times L)$ is calculated as following:

$$R_{ij} = \frac{\text{cum}(y_{n-i}, y_{n-j})}{\sigma_x^2} \tag{4.14}$$

where σ_x^2 stands for the variance of unknown input. If σ_x^2 is not a priori known, it can be substituted with any positive real number in (4.14). In this case, there would exist an ambiguity on the amplitude (refer to appendix D). In other words, the exact inverse filter is scaled to the estimated inverse filter $f[n]$. Now, the iterative algorithm of SEA for obtaining the updated equalizer $\mathbf{f}_{new}$ is implemented as follows [86]:

$$\begin{aligned} \mathbf{V} &= \mathbf{R}^{-1}\mathbf{d} \\ \mathbf{f}_{new} &= \frac{1}{\sqrt{\mathbf{V}^H\mathbf{R}\mathbf{V}}}\mathbf{V} \end{aligned} \tag{4.15}$$

where $(\cdot)^H$ denotes transpose-conjugate operation and $\mathbf{V}$ $(L \times 1)$ represents an intermediate vector. The old value of equalizer vector is implicitly incorporated in (4.15) through taking part in the calculation of $\mathbf{d}$ and $\mathbf{R}$. The covariance matrix $\mathbf{R}$ is positive-definite (existence of inverse matrix) and there is only one converging point which is associated with the inverse filter [83]. However, this algorithm may in practice converge to false results (spurious local maxima) for the reasons such as inappropriate length of equalizer L, insufficient number of data utilized in the cumulant calculation, nonlinearities of the system and then some initializations of the equalizer [83]. Initialization problem can be handled in the estimation of analog imperfections because the nominal analog system is a priori known. Hence, the related typical equalizer may be used as the initial value of equalizer.

4.3.2 Estimation procedure for analog circuits

Figure 4.9 shows the implementation through which analog imperfections may be estimated by blind equalization. Equalizer filter $F(z)$ is supposed to be an FIR filter with length L. For estimating the imperfections of analog circuit, the procedure is realized in two phases. Firstly, blind equalization method (SEA procedure) is applied to the system as explained in the preceding section. It provides an FIR filter $f[n]$ which approximates the inverse filter associated with the analog circuit. At the second phase, the real coefficients of $H(s)$ are estimated. The order of nominator and denominator of $H(s)$ is supposed to be known. Then, the equalizer $F(z)$ would tend to $\frac{1}{H(s)}$. The coefficients of $H(s)$ may be found through minimizing the

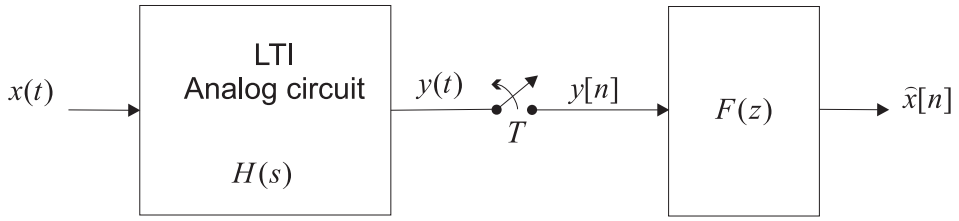

Figure 4.9. An LTI analog circuit with transfer function of $H(s)$ to which the equalizer $F(z)$ has been applied.

error expression which follows:

$$H_{opt}(s) = \arg \quad \min_{H(s)} \ \| \frac{1}{H(s)} - F(e^{j\omega}) \|_{s=j\frac{\omega}{T}} \quad w \in \rho \tag{4.16}$$

where T is the sampling period utilized in the first phase and ρ is the frequency band of interest. Depending on the transfer function of the analog system, ρ is appropriately selected so that the contribution of the unknown parameter is highlighted. For example, it can be concentrated about the nominal resonance frequency for an RLC circuit. The real coefficients of $H(s)$ and evidently the respective deviations from nominal values are obtained from $H_{opt}(s)$.

4.3.3 Simulations for estimating the analog imperfections

◯ First-order circuit

The algorithm that was explained in the previous section is now applied to several first- and second-order analog circuits. Firstly, a first-order RC circuit is considered. There are two parameters describing the transfer function of a general RC circuit: DC-gain g (gain at the zero frequency) and cut-off frequency ω_c. Respective transfer function can be described as follows:

$$H(s) = \frac{g\omega_c}{s + \omega_c} \tag{4.17}$$

For estimating the DC-gain g (scale factor), it is required to know a priori the variance of the analog input (refer to 4.3.1). The first stage (blind equalization) has been realized 1000 times for each deviation from nominal values using an FIR equalizer ($L = 9$). The algorithm has converged to the spurious local maxima

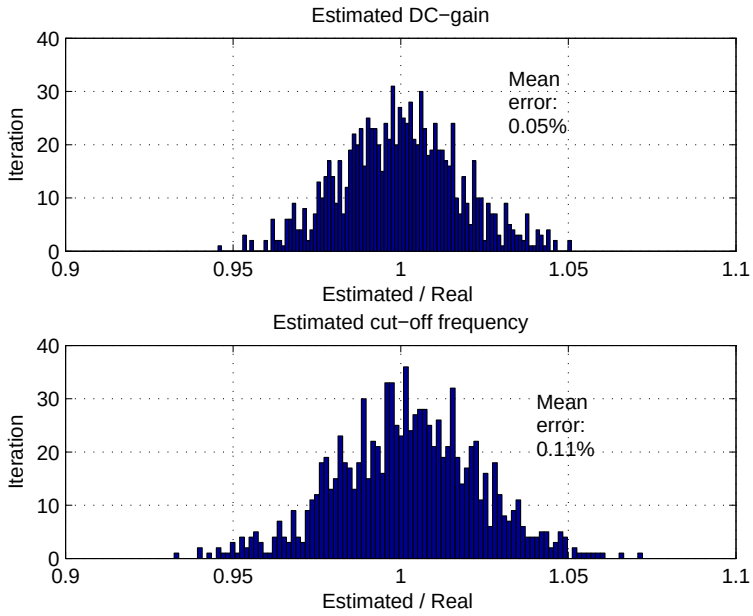

Figure 4.10. Histogram due to the ratio of estimated to real values after 1000 sample paths of noise for an RC circuit. The real deviation from the nominal values are 20% and 10% for the cut-off frequency and the DC-gain respectively.

(false results) in 5% of the times when the initial equalizer is a dirac impulse (all coefficients are zero except the middle one). Using an initial equalizer associated with nominal RC circuit (no deviation from nominal values) at the initialization procedure of blind equalization, the algorithm always converges to the global maximum. Figure 4.10 shows the histogram of the results for the realization of the algorithm supposing an RC circuit having 20% and 10% deviations from nominal cut-off frequency and DC-gain respectively. This histogram is in terms of the ratio of the estimated to real parameter values. The histogram illustrates the distribution of the results due to 1000 sample paths of the noise. The average values of the results estimate the unknown deviations from nominal values (for DC-gain and cut-off frequency) with an error of 0.05% and 0.11% respectively.

This simulation was implemented for different deviations from nominal values as well. The average estimation errors are shown in figure 4.11. The mean estimation error is always less than 0.25% for 1000 sample paths of noise. Using larger repetition number in the simulation, the mean values will better approximate the deviation from nominal values.

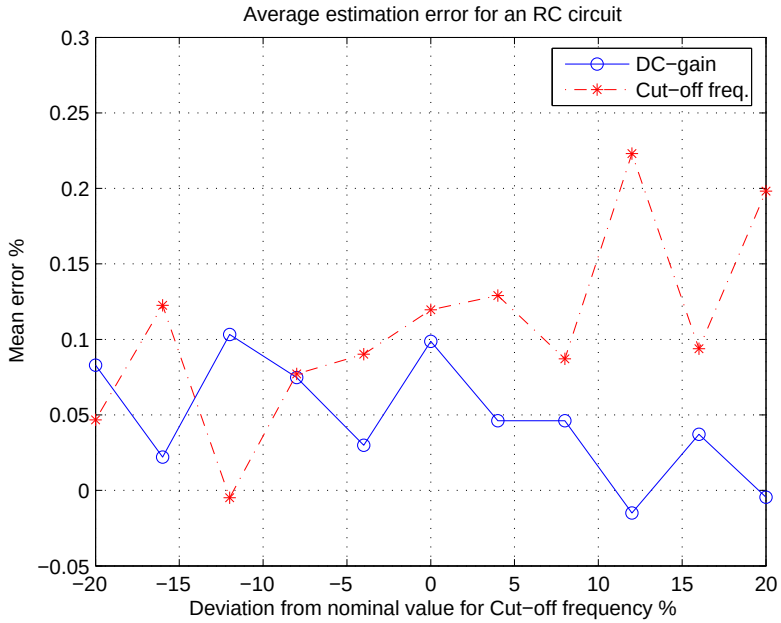

Figure 4.11. Average errors of the estimation due to the DC-gain (solid) and the cut-off frequency (dashed) versus the real values of the deviation from nominal cut-off frequency for the general RC circuits.

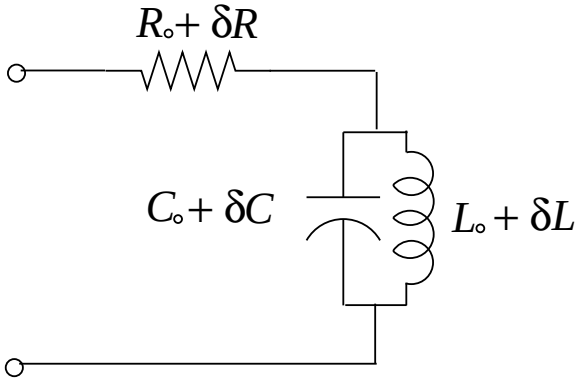

Figure 4.12. The arbitrary RLC circuit used in the simulations. $\{R_\circ, L_\circ, C_\circ\}$ are the design values to which the unknown realization errors $\{\delta R, \delta L, \delta C\}$ are applied.

◯ Second-order circuit

The algorithm is implemented for an RLC circuit as well (refer to figure 4.12). Related transfer function is described as following:

$$H(s) = \frac{\frac{\omega_r}{Q} s}{s^2 + \frac{\omega_r}{Q} s + \omega_r^2} \tag{4.18}$$

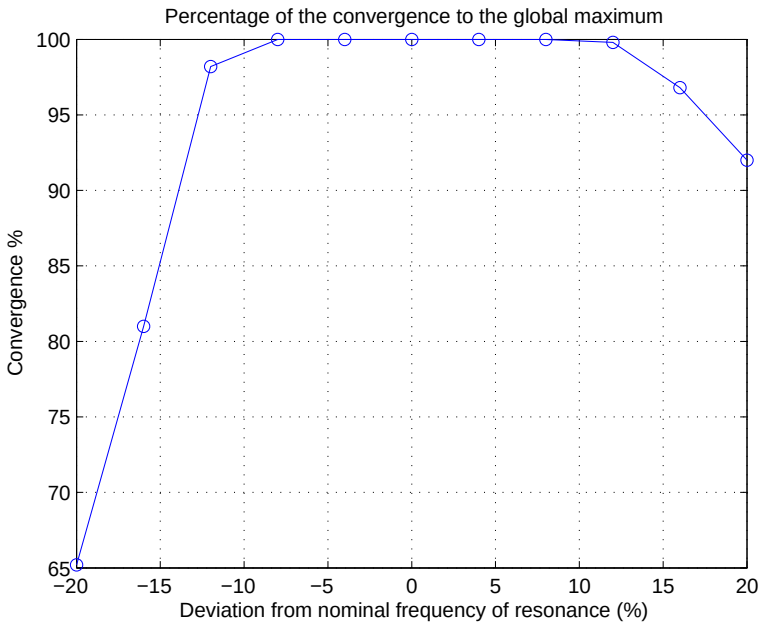

Figure 4.13. The percentage of convergence to the global maximum. Horizontal axis shows the percentage of deviation from the nominal frequency of resonance. Deviation from nominal quality factor is fixed (10%) and the algorithm is initialized by nominal values.

Deviations from nominal values for the quality factor (Q) and the resonance frequency (ω_r) are supposed to be the unknown parameters. There is no need for the variance of input at the algorithm in the RLC case because the unknown parameters are independent of any scaling factor. Using a random initialization, the algorithm of blind equalization (first phase) converges to the spurious local maxima in 35% of times. Using the nominal equalizer (related to the circuit with no deviations from nominal values) in the initialization of algorithm, the rate of convergence to spurious local maxima changes. The percentage of convergence to the global maximum in terms of deviations from nominal frequency of resonance is shown in figure 4.13. However, converging to spurious local maxima causes no problem in practice even with random initialization because the incorrect equalizers are conveniently detected and put aside. Figure 4.14 illustrates the histogram of the results when the deviations from the nominal frequency of resonance and quality factor are supposed 20% and 10% respectively. The algorithm is repeated 500 times using an equalizer with the length $L = 41$. The average error of es-

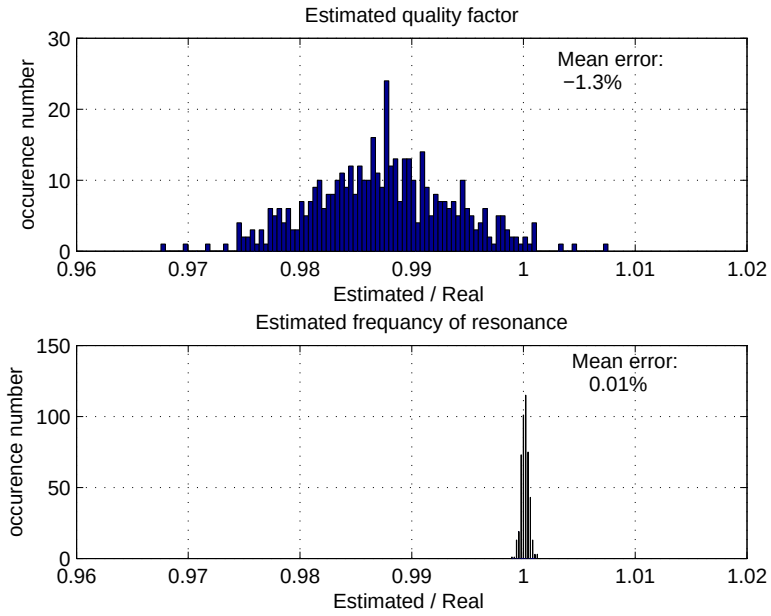

Figure 4.14. Histogram due to the ratio of estimated to real values after 500 sample paths of noise for an RLC circuit. The real deviation from the nominal values are 20% and 10% for the resonance frequency and the quality factor respectively.

timation are 0.01% and -1.3% for the frequency of resonance and quality factor respectively. Figure 4.15 shows the mean errors due to the several implementation of the algorithm supposing different deviations from the nominal values. The simulations show that this algorithm (first phase) is very sensitive to the sampling period. In fact, the larger the sampling frequency, the longer equalizer is required for compensating the lower levels of the spectrum amplitude at the frequency extremes (the frequencies near to $\pm\frac{\pi}{T}$). This is approved through analysis of the distribution of the mean errors particularly in figure 4.15. In the RLC case, the presence of a zero situated on the origin ($\omega = 0$) increases the rate of convergence to spurious local maxima since the algorithm tries to compensate this zero (infinite gain for real equalizer at zero frequency). In practice, there is a resistance in series with inductance that removes the associated zero in the spectrum. The bias appeared in the estimation of the quality factor (see figure 4.14) is due to this zero as well. The bias value depends on the sampling frequency used as well as to the frequency interval (ρ) through which the estimation is optimized.

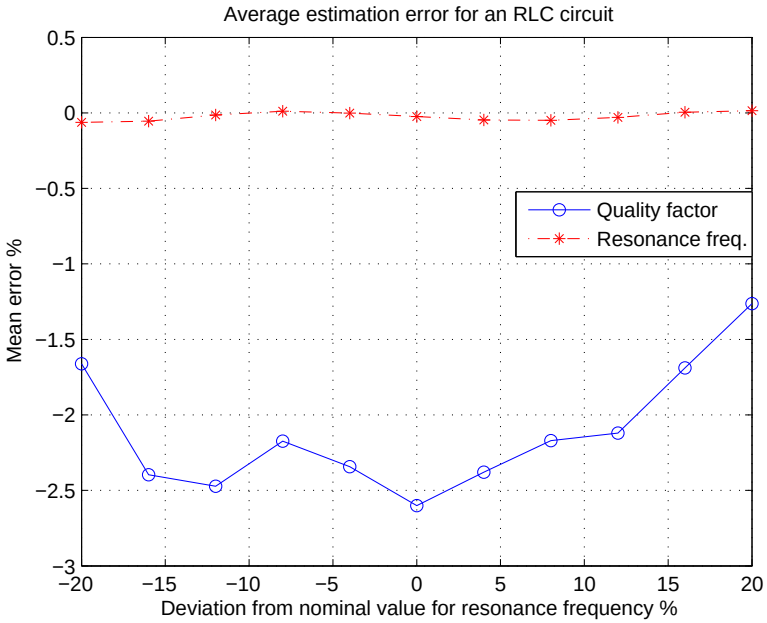

Figure 4.15. Average errors of the estimation due to the quality factor (solid) and the resonance frequency (dashed) versus the real values of the deviation from nominal resonance frequency for the RLC circuits.

4.4 Summary and discussion

The estimation of analog circuit imperfections involved in analog or mixed analog-digital circuits is studied and carried out in this chapter. Digital estimation of analog imperfections is much more attractive than analog techniques such as calibration and laser trimming. Moreover, the time-varying imperfections such as temperature drifts may only be compensated by digital techniques for some applications such as HFB-based A/D converters. For compensating the realization errors of analog circuits, two techniques have been proposed and discussed in this chapter. Firstly, a SOS-based model of analog imperfections has been proposed for estimating the relative imperfections. It appears more useful when the transfer function of LTI circuit includes only one erroneous coefficient. The performance of estimation of this model is limited to several percents. Then, blind equalization methods have been offered as a good candidate for estimating analog imperfections. SEA algorithm has been used in the simulations exploiting its rapid convergence properties. In this case, the precision of estimation of the analog imperfections is

better (about 0.2%) than SOS model. However, SEA algorithm uses HOS parameters. Then, it is useful only for non-Gaussian input signals. Besides, it needs the structure of unknown LTI circuit (or the order of analog circuit). Computations burden is much more than SOS model as well.

Both proposed SOS model and HOS blind equalization technique have been considered in the cases where the sampling rate is equal to or more than the Nyquist rate. This constraint is a necessary condition for using the algorithm of HOS blind equalization (SEA algorithm) [83] as well as the proposed SOS model. Therefore, both the estimation methods proposed in this chapter are not applicable to the classical HFB-based A/D converters which include essentially an undersampling process at each branch (refer to the section 5.1). In return, the HFB structures have a multi-channel architecture that may be exploited in the estimation procedure. Both the techniques proposed in this chapter have not used the mutual information of multi-channel HFB structure. Blind equalization techniques have been also proposed for Multiple-Input Multiple-Output LTI systems in terms of Blind Source Separation (BSS) methods [87]. Nevertheless, they are not applicable for the classical HFB structures. This issue is discussed and studied in the next chapter.

Chapter 5

New structures for hybrid filter bank A/D converters

Whenever you find you are on the side of the majority, it is time to pause and reflect.
- Mark Twain

5.1 Introduction

HFB-based A/D converters exhibit a large sensitivity to the analog imperfections of analysis filter bank as shown in the chapter 3 (refer to the section 3.3). On the other hand, the analog circuits (analysis filter bank of HFB) are always subject to the analog imperfections originating from the fabrication phase or versatile factors such as temperature drifts (refer to 3.3). Thus, for practically using the HFB structure in A/D conversion, it is necessary to somehow compensate or eliminate the high sensitivity of HFB to realization errors. As a suitable choice, it seems reasonable to use the digital part of HFB structure for handling the above-mentioned high sensitivity to the realization errors. Both the analog imperfections and analog input signal are unknown in the HFB architecture. Thus, the relative realization errors would have to be corrected in a blind way.
Two SOS- and HOS-based techniques were used for estimating the analog imperfections in the preceding chapter 4. The HOS-based methods generally lead to a more

accurate estimation than the SOS-based ones as it is seen in chapter 4 [88]. Then, the blind deconvolution methods are preferred to the SOS-based model in the HFB case (reminding that a high precision is needed). However, the proposed methods have been used for estimating the analog non-idealities (figure 4.1) provided that two conditions hold (refer to chapter 4). Firstly, the analog circuit should represent an LTI system. Secondly, the available digital output is supposed to be obtained from sampling at a rate higher or at least equal to the Nyquist frequency associated with the analog input. Now, the classical architecture of HFB-based A/D converter is considered (see figure 3.1). To estimate the realization errors of analysis filter bank, either the output of each branch ($x_k[n]$ $0 \leq k \leq M-1$) or the reconstructed signal $y[n]$ may be used. The mentioned blind methods cannot be applied to the outputs of branches ($x_k[n]$, $0 \leq k \leq M-1$) because the Nyquist rate does not hold (the output $x_k(t)$ of each analysis filter is undersampled at $\frac{1}{MT}$ which is M times less than the Nyquist frequency $\frac{1}{T}$). Considering the reconstructed output signal $y[n]$, the Nyquist rate is maintained. It was mentioned that the output $y[n]$ would be a shifted version of original input if the PR condition holds (refer to the section 3.2.1) as follows:

$$y[n] = x(t)\Big|_{t=nT-n_dT}$$

In the PR case, the output $y[n]$ can then be obtained from the original input $x(t)$ by sampling (at $\frac{1}{T}$) the output of an LTI system (a pure delay $H_{eq}(s) = e^{-s(n_dT)}$) to which $x(t)$ has been applied (n_d stands for the delay considered in the reconstruction). However, it is evident that the PR condition cannot practically hold according to two reasons: the restrictions of digital synthesis filters and analog imperfections of analysis filters bank. If PR condition does not hold, the output $y[n]$ may be related to the input by one distortion $T_0(e^{j\omega})$ and $M-1$ aliasing functions $T_m(e^{j\omega})$ as following (refer to the relations (3.1) and (3.2)):

$$Y(e^{j\omega}) = \underbrace{\frac{1}{T}T_0(e^{j\omega})\widetilde{X}(j\frac{\omega}{T})}_{\text{distortion term}} + \underbrace{\frac{1}{T}\sum_{m=1}^{M-1} T_m(e^{j\omega})\widetilde{X}(j\frac{\omega}{T} - j\frac{2\pi}{MT}m)}_{\text{aliasing terms}} \qquad (5.1)$$

Although, the distortion term can be modeled by an analog LTI system (followed by sampling at $\frac{1}{T}$), but each aliasing term is associated with a pure non-LTI system considering the frequency shifting in the input signal $\widetilde{X}(j\frac{\omega}{T} - j\frac{2\pi}{MT}m)$ (equal to a multiplication in the time domain as $x(t)e^{-j\frac{2\pi}{MT}mt}$). Accordingly, the global HFB system may be modeled in practice by a non-LTI system followed by sampling at the Nyquist rate $\frac{1}{T}$. Considering the above-mentioned conditions, the proposed SOS- and HOS-based methods cannot in practice be applied to the output $y[n]$ of classical HFB architecture either because it represents a non-LTI system. It is reminded that this is again originated from the undersampling process $M > 1$. If no undersampling is considered (i.e. $M = 1$), the aliasing terms disappear according to (5.1). Finally, it can be concluded that the proposed blind techniques are not applicable to the conventional HFB-based A/D converters, though quantization process and word-length effects have been neglected.
To overcome this obstacle, new HFB structures are proposed in this chapter for the A/D conversion purpose. A new HFB architecture would be useful if it holds one or both of the following properties:

1. Less sensitive to the realization errors of analysis filter bank compared to the classical HFB.

2. The relationship between the related input and output is LTI and includes no decimation.

The first property may be looked for through a rearrangement of the equations associated with the PR condition. For this purpose, we have proposed the two-stage HFB-based ADC using a modification in the PR equations. Invoking the second strategy, new HFB structures would be obtained to which the compensation techniques may be applied for decreasing the associated sensitivity to the realization errors. In the next section 5.2, modifying the classical HFB structure, two-stage HFB architecture is obtained. Then, the performance and sensitivity of two-stage HFB are discussed. The section 5.3 deals with the new HFB architectures providing an LTI relationship and without any decimation between the related input and output. For this purpose, a different arrangement of the analog input samples is interpreted as the new input signal so that a Multiple-Input Multiple-Output (MIMO) architecture is obtained. We have proposed two possible MIMO HFB

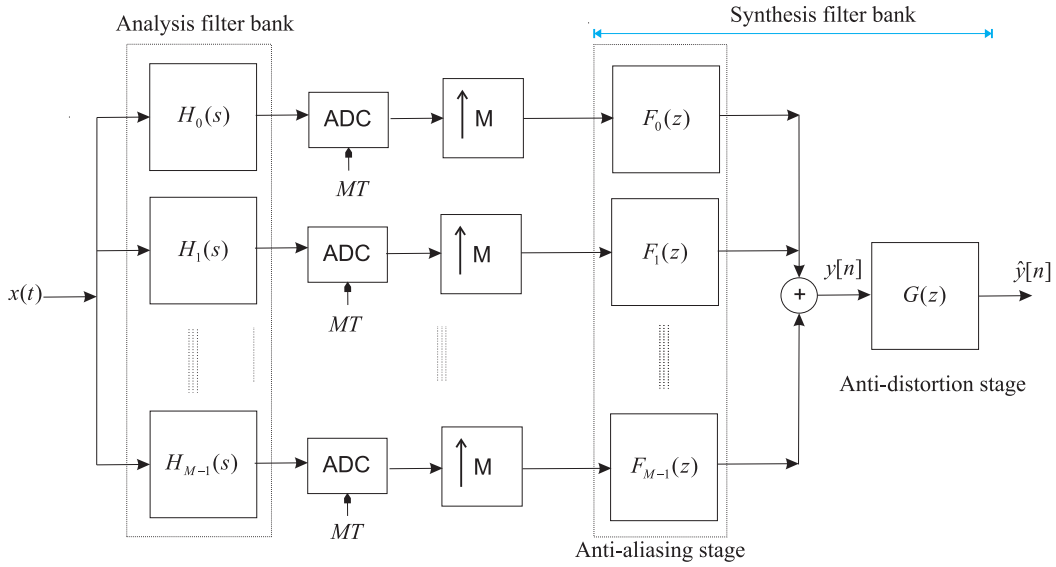

Figure 5.1. Two-stage architecture for the HFB-based A/D conversion. The synthesis procedure is implemented in two stages by: Anti-aliasing filter bank $F(z)$ and then anti-distortion filter $G(z)$.

architectures in the section 5.3. These new architectures are studied in terms of performance and sensitivity in the subsections 5.3.3.1 and 5.3.4.2.

5.2 Two-stage HFB A/D converter

5.2.1 Architecture and frequency-domain analysis

Considering two strategies explained in the previous section 5.1, the main idea is here to look for a possible new architecture which may lead to a better performance as well as less sensitivity to the realization errors. Invoking the original HFB architecture (see figure 3.1) and the PR equations (3.3), it is possible to classify the PR equations of an M-channel HFB at each arbitrary frequency into two categories: one distortion-related equation and $M-1$ aliasing-related equations. Therefore, the synthesis part may be designed in two stages. Firstly, the aliasing interferences are eliminated considering only the aliasing-related equations. At the second stage, distortion effects are compensated. Figure 5.1 better illustrates this idea. The effects of quantization are neglected like the chapter 3. Figure 5.2 shows the relative HFB structure without the quantization process. To obtain a

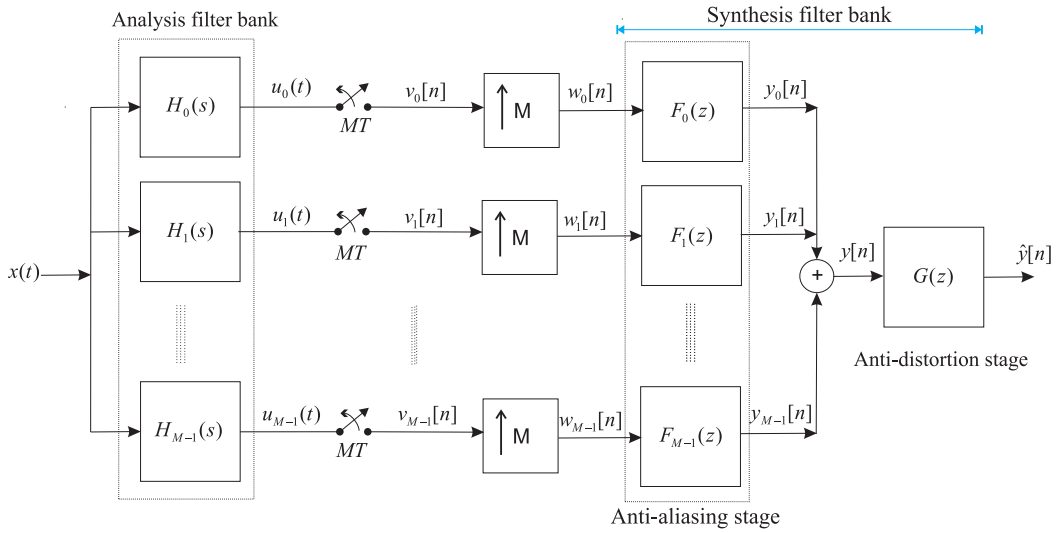

Figure 5.2. The model of two-stage HFB-based A/D converter neglecting quantization process. The A/D converters have been substituted by simple samplers.

spectral representation for the output in the frequency domain, the input signal is assumed to be band-limited to $[-\frac{\pi}{T}, \frac{\pi}{T}]$. T is the global sampling period which holds the Nyquist sampling criterion for the original input $x(t)$. To better formulate the frequency representation of output, two intermediate variables are defined as follows. $\widetilde{H}_i(j\Omega)$ represents the periodic extension of the analysis filter $H_i(j\Omega)$ considering only the frequency interval $[-\frac{\pi}{T}, \frac{\pi}{T}]$. The input signal spectrum is null for the frequencies out of this band. $\widetilde{X}(j\Omega)$ represents similarly the periodic extension of the input signal with the period $\frac{2\pi}{T}$ (refer to the appendix A). Then, the spectral description of the output $y[n]$ of anti-aliasing stage for an M-branch architecture may be described as:

$$Y(e^{j\omega}) = \sum_{m=0}^{M-1} \widetilde{X}(j\frac{\omega}{T} - j\frac{2\pi}{MT}m) \cdot T_m(e^{j\omega}) \tag{5.2}$$

where $T_0(e^{j\omega})$ stands for the distortion function and $\{T_m(e^{j\omega}),\ 1 \leq m \leq M-1\}$ are the $(M-1)$ aliasing terms. These terms may be obtained as following (refer to the appendix A):

$$T_m(e^{j\omega}) = \frac{1}{M} \sum_{k=0}^{M-1} \widetilde{H}_k(j\frac{\omega}{T} - j\frac{2\pi}{MT}m) F_k(e^{j\omega}) \tag{5.3}$$

Considering the anti-distortion filter $G(z)$, the overall distortion and aliasing functions of two-stage structure may be described as follows:

$$\widehat{T}_m(e^{j\omega}) = T_m(e^{j\omega}).G(e^{j\omega}), \quad 0 \leq m \leq M-1 \tag{5.4}$$

To have a simple and convenient design, the synthesis filter bank may be realized by FIR digital filters. The design phase of synthesis filters is now a bit different from the one due to the classical HFB architecture. The synthesis part consisting of anti-aliasing and anti-distortion filters is designed in two stages. The aliasing terms are nullified through the anti-aliasing filter bank $\{F_i(z),\ i = 0, 1, ..., M-1\}$ at the first stage. For this purpose, neglecting the effects of anti-distortion filter $G(z)$, 5.2 is used. Thus, $M-1$ equations are obtained at an arbitrary frequency ω as follows:

$$T_m(e^{j\omega}) = 0 \qquad 1 \leq m \leq M-1 \tag{5.5}$$

The only difference with the PR equations (3.3) of classical HFB is that the distortion term $T_0(e^{j\omega})$ is not considered in (5.5). Invoking (5.5) and (5.3), there are M unknown values $\{F_i(e^{j\omega}),\ i = 0, 1, ..., M-1\}$ versus only $M-1$ equations. The solution of this problem is discussed in the next subsection 5.2.2.
At the second stage, the overall distortion function $\widehat{T}_0(e^{j\omega})$ is considered. To maintain the PR conditions, it is possible to have just a pure delay as the distortion function. Considering the anti-aliasing filters obtained in the first stage, following equation may be used for designing the anti-distortion filter $G(z)$:

$$\widehat{T}_0(e^{j\omega}) = Me^{-j\omega n_d} \tag{5.6}$$

where n_d represents the delay of reconstructed signal $\hat{y}[n]$ in comparison with the related input signal $y[n]$. Using (5.6), the anti-distortion FIR filter $G(z)$ may be designed. However, it will have some effects on the aliasing terms. In practice, $G(z)$ will not considerably deteriorate the aliasing terms since all aliasing functions are made sufficiently small (ideally null) by the preceding anti-aliasing filter bank. The simulations prove this issue (refer to the subsection 5.2.3). The product of each aliasing function by the input signal spectrum is an undesired signal appearing at the output of A/D converter. Then, the sum of the aliasing terms multiplied

by the input signal spectrum may be considered as an additive noise at the output of the A/D converter (refer to (5.2)). Accordingly, the aliasing functions can be considered as a limitation on the output resolution in terms of number of bits. Regarding the aliasing effects on the output precision, it is necessary to note that there are $(M-1)$ aliasing functions. The classical "6 dB/bit" law can be used to provide a rough idea of the precision at the output associated with the aliasing functions contribution [69].

5.2.2 Design of two-stage HFB using FIR synthesis filters

In the two-stage HFB architecture, the synthesis filters $\{F_i(z), i = 0, 1, \cdots, M-1\}$ are designed to eliminate only the aliasing terms. Besides, the anti-distortion filter $G(z)$ is accommodated to compensate the deviations of the distortion expression versus the constant function. To design anti-aliasing filter $F_i(z)$, the analysis matrix of chapter 3 may be used again (refer to section 3.2.2). FIR filters are used to realize conveniently the anti-aliasing filters. It is supposed to use L coefficients for each FIR anti-aliasing filter. N frequency points are selected so that N is much larger than L ($N \gg L$) to have a suitable interpolation (frequencies are spread out through the band of interest). Then, following relationship may be considered for designing the anti-aliasing filters:

$$(\mathcal{H}.\mathbb{A})\mathbf{f} = \mathbf{0} \tag{5.7}$$

The matrix $\mathcal{H}$ is just the same $\mathbb{H}$ used in (3.15) except the equations (the rows) relative to the distortion are omitted. Thus, it is a matrix with the dimension of $2(M-1)N \times 2MN$. There is a zero vector with the size of $2(M-1)N \times 1$ in the right side of the equality. To approximate the matrix equation (5.7), it is necessary to hold following criterion:

$$\mathbf{f}_\circ = \arg \quad \min_{\mathbf{f}} \|\mathcal{H}\mathbb{A}\mathbf{f}\| \tag{5.8}$$

$$\text{subject to} \quad \|\mathbf{f}\| = 1$$

where the normalization constraint $\|\mathbf{f}\| = 1$ is considered to avoid the evident solution ($\mathbf{f} = 0$) and any scaling ambiguity since the equalizer $\mathbf{f}$ contributes inversely

in the design of antialiasing filter (in (5.9)) to compensate any deviation of distortion function in reference to a pure delay of unity gain. According to the theory of the Singular Value Decomposition (SVD), the solution locates in the null space of the coefficient matrix $\mathcal{H}\mathbb{A}$ [71]. In other words, $\mathbf{f}_\circ$ is the singular vector of the coefficient matrix $\mathcal{H}\mathbb{A}$ associated with the least singular value. It is the optimum solution for (5.8).

To design the anti-distortion filter $G(z)$, two possibilities exist. It is possible to utilize a blind equalization method which will adapt to the specific realization of the analysis filters. In this case, the input has to be white and non-gaussian (refer to the appendix D). Using blind equalization technique, the anti-distortion filter would be adaptive. However, it can only adaptively compensate the distortion function. Aliasing terms would be additive noises. In this case, blind equalization cannot converge unless the aliasing interferences are considerably less than the distortion function (refer to the appendix D).

As the second way, it is possible to rearrange and solve the distortion equations directly. This method is valid for all the inputs in contrary to the blind method. The equations associated with the distortion may be summarized in the vectorial form as following:

$$(E.A_g)\mathbf{g} = \mathbf{c} \tag{5.9}$$

where the components are defined as follows:

$$\mathbf{g} = \begin{bmatrix} g[0] \\ g[1] \\ \\ \vdots \\ \\ g[L'-1] \end{bmatrix}_{L'\times 1} \qquad \mathbf{c} = \begin{bmatrix} Me^{-j\omega_1 n_d} \\ Me^{-j\omega_2 n_d} \\ \\ \vdots \\ \\ Me^{-j\omega_N n_d} \end{bmatrix}_{N\times 1}$$

$$E = \begin{bmatrix} \sum_{k=0}^{M-1} \widetilde{H}_k(j\frac{\omega_1}{T})F_k(e^{j\omega_1}) & & \\ & \ddots & \\ \mathbf{0} & & \mathbf{0} \\ & & \sum_{k=0}^{M-1} \widetilde{H}_k(j\frac{\omega_N}{T})F_k(e^{j\omega_N}) \end{bmatrix}_{N\times N}$$

and,

$$A_g = \begin{bmatrix} 1 & e^{-j\omega_1} & \cdots & e^{-j\omega_1(L'-1)} \\ & \vdots & \vdots & \\ 1 & e^{-j\omega_N} & \cdots & e^{-j\omega_N(L^{'}-1)} \end{bmatrix}_{N\times L'}$$

where the anti-distortion filter with the impulse response $\mathbf{g}[n]$ is supposed to be an FIR filter defined in the interval $0 \leq n \leq L' - 1$ with the length of L'.
Applying the LS optimization technique to (5.9), the anti-distortion FIR filter may be designed.

5.2.3 Implementation and performance of two-stage HFB structure

To observe the behavior of the two-stage HFB architecture, an 8-branch HFB structure has been considered. One of the analysis filters is a low-pass filter (RC circuit) and the other ones are the second-order RLC circuits with the same bandwidth $\frac{\pi}{8T}$ and distributed through the whole band of interest (like the one used in chapter 3 shown in figure 3.2). An oversampling ratio 6% is used in order to reach the acceptable levels of aliasing (refer to the section 3.2.4). The simulations are carried out for the classical HFB architecture as well as the two-stage HFB structure. Figure 5.3 demonstrates the aliasing and distortion functions versus normalized discrete-time frequencies associated to the conventional HFB structure. The synthesis filter bank includes FIR digital filters with 64 coefficients. All eight functions of aliasing and distortion are simultaneously illustrated. This simulation is accomplished for a two-stage HFB structure as well. 64 coefficients are similarly used for the FIR synthesis filters together with an oversampling ratio of 6%. Figure 5.4

shows the related aliasing and distortion terms of this two-stage HFB structure. Distortion functions for both the structures remain at an acceptable level (0 dB) with a standard deviation lower than $10^{-3}dB$. However, the performance of the aliasing functions are considerably different in the two structures. Comparing figures 5.3 and 5.4, one can obviously notice that the performance of the proposed two-stage HFB structure is much better than the classical one. This superiority of performance is observed for the FIR synthesis filters including 32 coefficients as well (refer to table 5.1). To better compare the performances of the classical structure with those of the proposed two-stage architecture, the first aliasing terms ($\widehat{T}_1(e^{j\omega})$) associated with the two structures are simultaneously shown. Figure 5.5 compares the first aliasing terms in the two-stage and classical structures assuming 32 coefficients for the FIR synthesis filters. Figure 5.6 illustrates this comparison when each of the FIR synthesis filters consists of 64 coefficients. According to 5.2, the product of the m^{th} aliasing function and $\widetilde{X}(j\frac{\omega}{T} - j\frac{2\pi}{MT}m)$ appears at the output

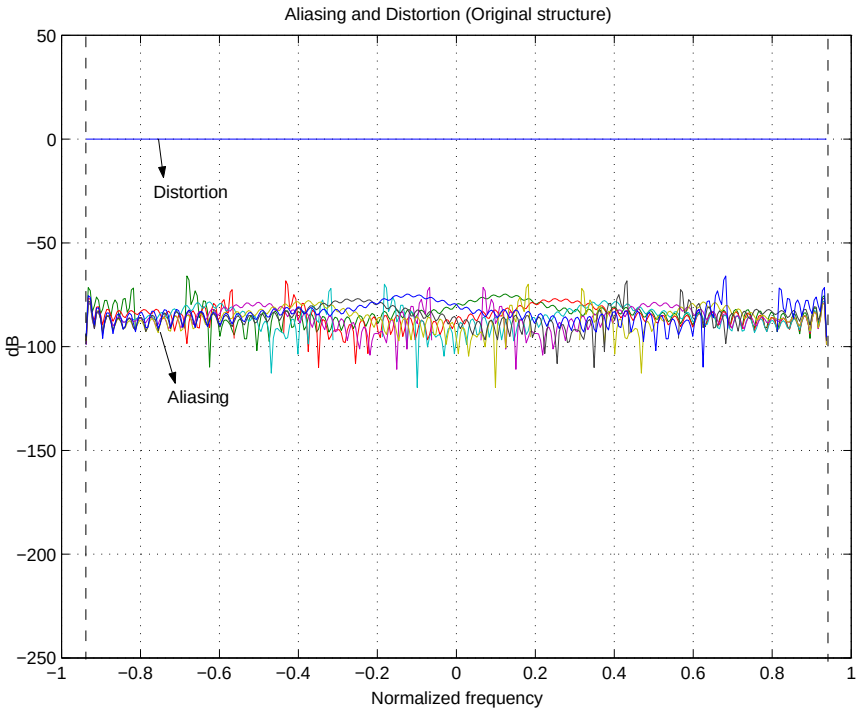

Figure 5.3. Distortion and aliasing functions (dB) versus normalized frequency due to the classical HFB structure of 8-channel. An oversampling ratio of 6% is used. Each synthesis filter consists of 64 coefficients.

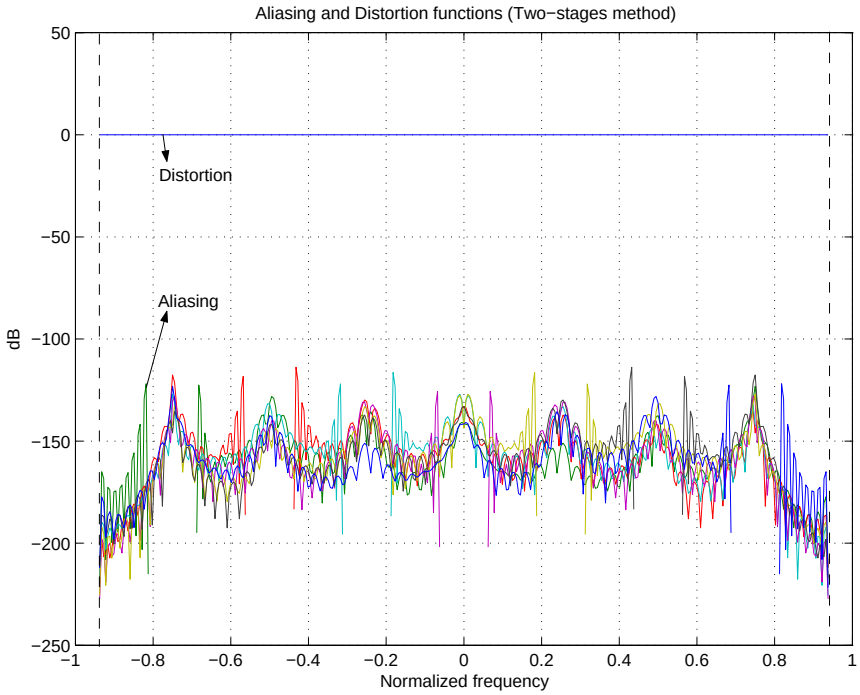

Figure 5.4. Distortion and aliasing functions (dB) versus normalized frequency due to an 8-channel two-stage HFB structure. An oversampling ratio of 6% is considered. 64 coefficients are used for each synthesis filter.

$(1 \leq m \leq (M-1))$. Thus, the narrow oversampling band for which the input spectrum is supposed null is shifted in the frequency domain. The shift value is $\frac{2\pi}{MT}m$ for the m^{th} aliasing term. A gap (6% of total bandwidth) may be seen in figures 5.5 and 5.6. It is due to the oversampling process (refer to the section 3.2.4).

Figures 5.5 and 5.6 show that there is an obviously better performance for

Table 5.1. Comparison of two-stage and classical HFB for $L = 32$

Method	Original	Two-stage
Mean aliasing (dB)	-49.1	-67.3
Max. aliasing (dB)	-37.5	-46.7
Precision (bits)	5	8

the two-stage HFB structure. Tables 5.1 and 5.2 list the maximum and average aliasing functions for these structures assuming different lengths for the synthesis

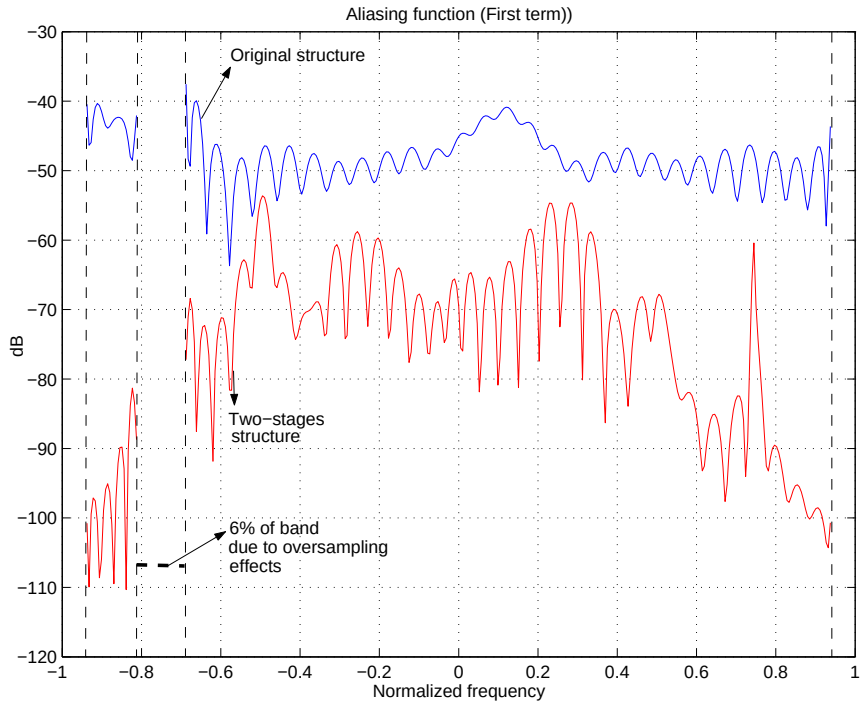

Figure 5.5. First aliasing functions ($\widehat{T}_1(e^{j\omega})$) versus normalized frequency due to the original structure (blue) and two-stage architecture (red) with FIR synthesis filters having 32 coefficients. An oversampling ratio of 6% has been used. The zero gap at the negative frequencies is due to the oversampling band which is shifted for every aliasing term.

Table 5.2. Comparison of two-stage and classical HFB for $L = 64$

Method	Original	Two-stage
Mean aliasing (dB)	-84.5	-148
Max. aliasing (dB)	-65.9	-113.9
Precision (bits)	11	22

FIR filters (32 and 64 coefficients). An oversampling ratio of 6% has been used for both cases. Both tables show that the performance of two-stage HFB is better than the classical one in terms of both the mean and maximum aliasing. However, it is reminded that the two-stage architecture uses an additional (anti-distortion) digital filter. The last row in the above-mentioned tables shows an approximated maximal achievable number of bits due to the aliasing effects. Since the quantiza-

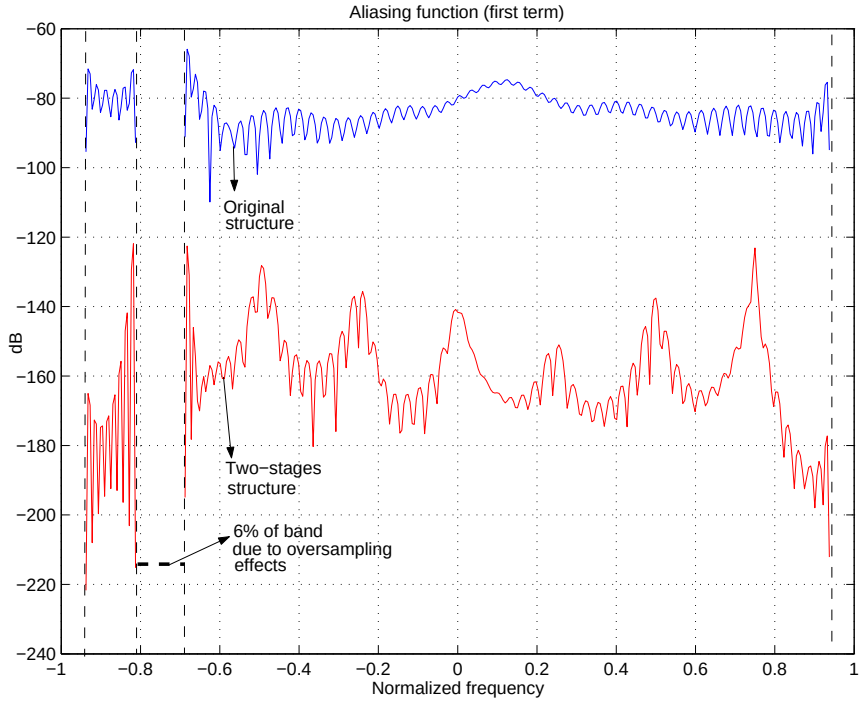

Figure 5.6. First aliasing functions ($\widehat{T}_1(e^{j\omega})$) versus normalized frequency due to the original structure (above) and two-stage architecture (below) when 64 coefficients are utilized for each FIR synthesis filter. The oversampling ratio of 6% has been utilized. The zero gap at the negative frequencies is due to oversampling which is shifted for every aliasing term.

tion process in each branch of the structure results in a lower output precision, the real output precision may practically be some bits lower than the ones mentioned in the tables.

5.2.4 Sensitivity to realization errors

Up to this point of the chapter 5, it has been supposed that the analog part of two-stage and classical HFB structures is perfect and without any analog imperfection. In this subsection, the influence of analog realization imperfections on the performance is studied. In the real world, the practical aliasing level is different from above-mentioned simulation values because the analysis filter bank (analog circuits) includes the imperfections associated with the fabrication phase or drifts such as temperature drift (refer to the section 3.3). In practice, only the design (or nominal) values of the analysis filters are known. The synthesis filter bank

is designed according to those values. So, the designed digital filter bank is not optimum for the actual analysis filter bank. To measure the sensitivity of HFB structure to realization errors, the relative deviation $S_{\mathbf{f}}$ of synthesis filter bank is used as described in the section 3.3. This measure would be almost independent from the length of FIR synthesis filters [74]. The electronic elements (R, C and L) of analysis filter bank are assumed to include Gaussian random deviations from their nominal values. The standard deviation of the error distribution is used as the parameter of deviation from typical (or design) values. Using an 8-branch HFB structure, the simulations have been carried out for 1000 trials of the Gaussian realization errors. The performance is studied versus the deviation from typical values. Figure 5.7 demonstrates $S_{\mathbf{f}}$ versus the deviation from typical values for the classical and two-stage HFB structures in logarithmic scale. It may be seen that the two-stage HFB structure is much more sensitive to the analog imperfections. Figure 5.8 shows the mean and maximum aliasing versus the deviations from typical values without oversampling process. Figure 5.9 shows the

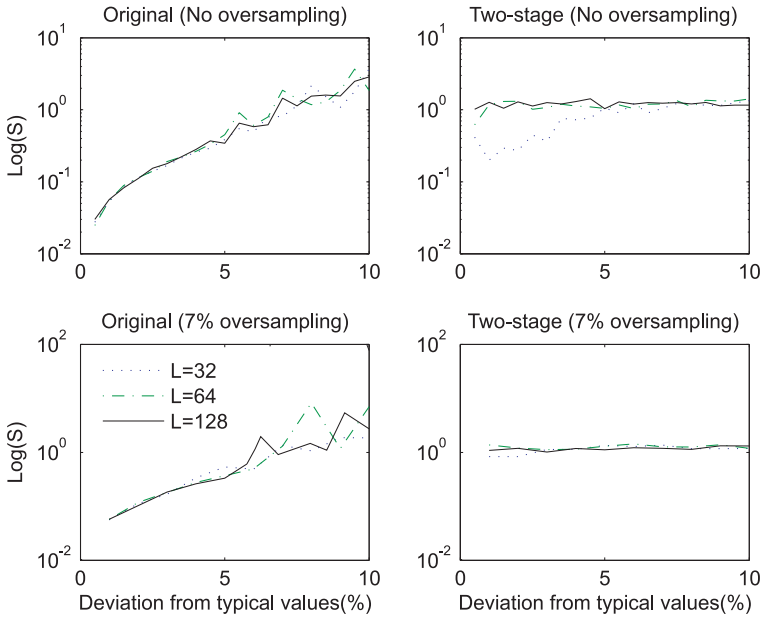

Figure 5.7. Sensitivity $S_{\mathbf{f}}$ (logarithmic) versus the deviation from typical values (%) for the case of no oversampling (above) and with oversampling 7% (below). The curves are related to the classical (left) and two-stage (right) structures. L represents the length of FIR synthesis filters.

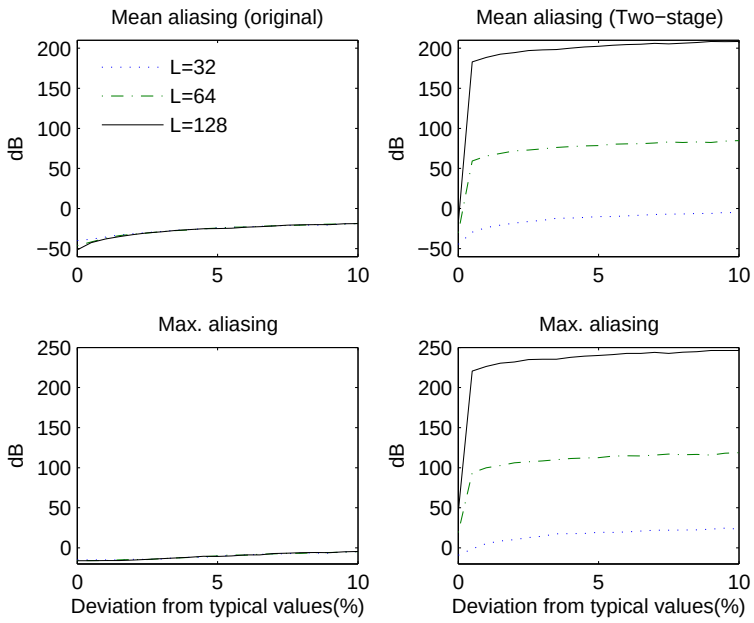

Figure 5.8. Mean (above) and maximum (below) aliasing functions in dB versus the deviation from typical values (%). The curves belong to the classical (left) and two-stage (right) structures and no oversampling has been used. L represents for the number of coefficients used for FIR synthesis filters.

same variables when the oversampling ratio is equal to 7%. It may be seen that the two-stage HFB is not useful without oversampling because the aliasing is so large. The classical HFB appears less sensitive to analog imperfections. However, the performance of the original HFB is not practically acceptable in the presence of realization errors (figure 5.9). Practically, the classical HFB is less sensitive to analog imperfections than the two-stage one. Nevertheless, it needs a compensation mechanism for being used in the architecture of wide-band A/D conversion. It may be seen that the performance is no longer acceptable when the electronic circuits of the analysis filter bank are subject to deviations from typical values higher than 1% (figure 5.9). Finally, two-stage HFB structure does not provide an architecture with less sensitivity, though it leads to a better performance than classical one in the absence of analog imperfections.

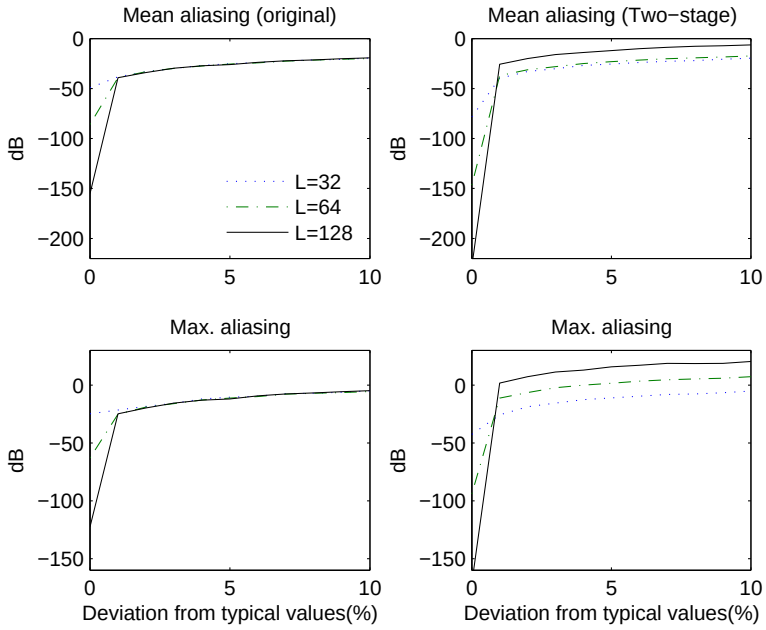

Figure 5.9. Mean (above) and maximum (below) aliasing functions in dB versus the deviation from typical values (%). The curves belong to the classical (left) and two-stage (right) structures and the oversampling ratio 7% has been used. L shows the length of FIR synthesis filters.

5.3 Multiple-Input Multiple-Output structures for HFB A/D converter

5.3.1 Necessity of MIMO HFB structures

As it was explained in the previous section, both two-stage and classical HFB structures show a large sensitivity to the realization errors so that a compensation method has to be considered for correcting these errors. The required compensation method would be a blind estimation technique since neither the input nor the exact transfer function of system are known. If the deviations from the nominal values are estimated for the analysis filters, the proper transfer functions of analysis filters would be available for being used in the design of synthesis filters. Blind equalization (deconvolution) reviewed in the chapter 4 cannot be exploited in the classical HFB case because of the undersampling process existing at each branch (refer to the section 5.1). To better explain, the undersampling process at

the rate $\frac{1}{MT}$ may mathematically be interpreted by two operations: a decimation process (1 out of M) preceded by the sampling procedure at the Nyquist rate $\frac{1}{T}$ (see figure 5.10). For using blind deconvolution techniques, it is essential first of all to have an LTI system relating the input and output signals (section 5.1). Besides, no decimation should exist between input-output so that no spectral overlapping occurs. The main objective of this section is to provide new architectures for HFB-based A/D converters so that the associated input and output relationship is LTI and no decimation is included between them. In practice, the signals $x_0[n]$, $x_1[n]$, ..., $x_{M-1}[n]$ are the only available signals for processing (see figure 3.1). Figure 5.11 illustrates the HFB-based A/D converter structure without the synthesis stage (see figure 3.1). This part of HFB is here called the *analysis part*. The analysis part includes apparently a decimation procedure at each branch between input and output. In this section, we try to model the analysis part without any modification so that an LTI relationship governs between the inputs and outputs of proposed model without any decimation between them. To complete the HFB structure of A/D conversion, the *synthesis part* would be later designed according to the proposed model of analysis part. Observing the analysis part (figure 5.11), it is proposed to define new virtual input signals so that the decimation process exists no longer between the new input signals and the outputs of analysis part $x_0[n]$, $x_1[n]$, ..., $x_{M-1}[n]$. It means to somehow eliminate the decimation procedure existing between input and output at each branch. It is evident that the decimation cannot be totally omitted (otherwise why we use HFB-based ADC?). Then, the only way would be to consider the input signal after the decimation

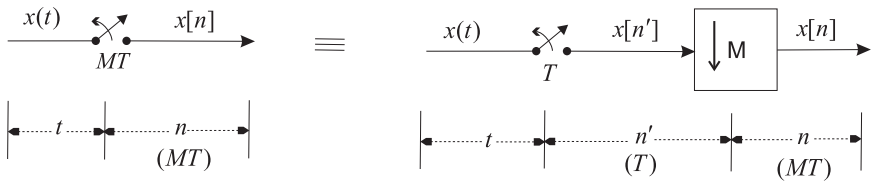

Figure 5.10. The sampling process at the rate $\frac{1}{MT}$ is equal to the cascade form of two processes. The sampling at the rate $\frac{1}{T}$ in series with the decimation procedure (1 out of M). n and n' are the discrete-time indices associated with the sampling rates $\frac{1}{MT}$ and $\frac{1}{T}$ respectively.

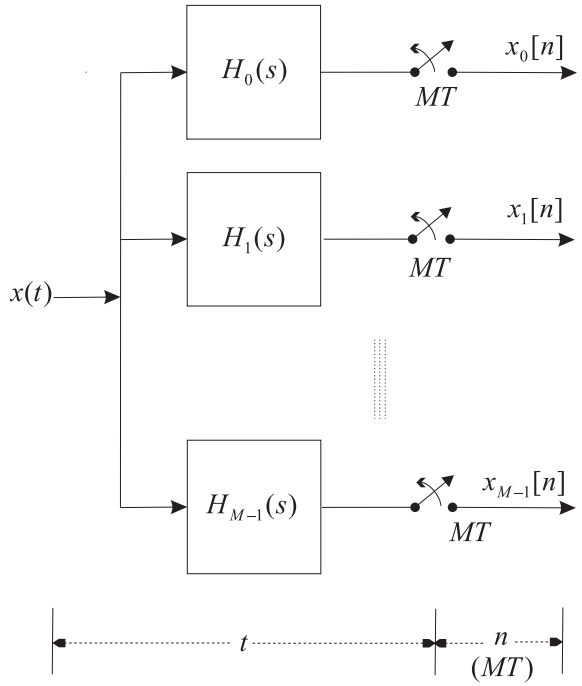

Figure 5.11. The *analysis part* of the HFB-based A/D converter. Quantization process has been neglected. The only available signals are $x_0[n]$, $x_1[n]$, ..., and $x_{M-1}[n]$.

operation. This idea would lead to a MIMO model for HFB structures since M inputs are defined associated with M decimation processes. This concept is exploited in the next subsections. We will offer two possible MIMO models for the HFB structures. To better figure out these new architectures, an interpretation of analysis part is presented in the next subsection 5.3.2 that is fully described in the discrete-time domain. Sections 5.3.3.1 and 5.3.4.2 provide two possible MIMO models for the analysis part which establish an LTI relationship between the related inputs and outputs. For convenience, both these MIMO models are described in the discrete-time domain using the discrete-time model of HFB extracted in the subsection 5.3.2.

Note that following notations are always respected in the coming sections of this chapter:

- *M: Number of branches in HFB structure*
- *n: Discrete-time index associated with the sampling rate $\frac{1}{MT}$*
- *n': Discrete-time index associated with the sampling rate $\frac{1}{T}$*

5.3.2 Discrete-time model of HFB A/D converter

For obtaining the LTI MIMO models of HFB structure, it is more convenient to have the analysis part fully described in the discrete-time domain. A discrete-time model of analysis part is obtained in this subsection. The analysis part has already been modeled in the discrete-time domain by Shu et al. to obtain a minmax criterion [59]. We propose here a totally different method for providing its discrete-time model. The analysis part of HFB shown in figure 5.11 may be rearranged using the concept of figure 5.10. Accordingly, the analysis part may be regarded as shown in figure 5.12. $x(t)$ is supposed to be the analog input and band-limited

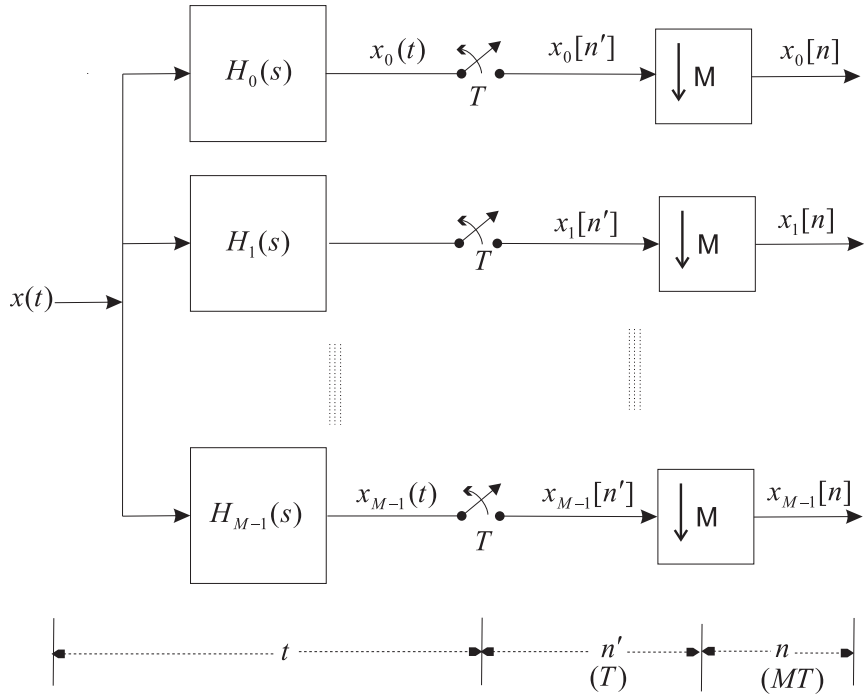

Figure 5.12. The *analysis part* of the HFB-based A/D converter shown in terms of the decimation procedure. The anti-aliasing filter has been neglected as the positive bandwidth σ of the analog input $x(t)$ holds the Nyquist criterion ($\frac{1}{T} \geq 2\sigma$).

to the Nyquist rate $\frac{1}{T}$. Then, the analog input $x(t)$ may be sampled without any spectral overlapping at the sampling rate $\frac{1}{T}$. According to the sampling theory, $x(t)$ can be represented in the discrete-time domain by $x[n']$ as following:

$$x[n'] = x(n'T), \qquad n' = \cdots, -2, -1, 0, 1, 2, 3, \cdots \tag{5.10}$$

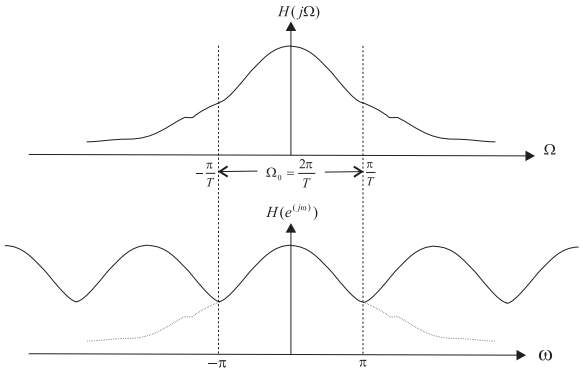

Figure 5.13. Analog filter $H(j\Omega)$ and its equivalent filter $H(e^{j\omega})$ in the discrete-time model.

where n' represents the time index. According to the figure 5.12, the output $x_k(t)$ of the filter $H_k(s)$ can be explained in the frequency-domain as follows:

$$X_k(j\Omega) = H_k(j\Omega)X(j\Omega) \qquad k = 0, 2, ..., M-1$$

Since $X(j\Omega)$ is a band-limited signal ($\frac{1}{T} \geq 2\sigma$), $X_k(j\Omega)$ will be band-limited as well. Considering this property, $H_k(j\Omega)$ can be substituted with another analog filter $H_k^{'}(j\Omega)$ as follows:

$$X_k(j\Omega) = H_k^{'}(j\Omega)X(j\Omega) \qquad k \in \{0, 2, ..., M-1\}$$

where $H_k^{'}(j\Omega)$ is defined as:

$$H_k^{'}(j\Omega) = \begin{cases} H_k(j\Omega) & \Omega \in [-\frac{\pi}{T}, +\frac{\pi}{T}] \\ \\ 0 & elsewhere \end{cases} \tag{5.11}$$

$H_k^{'}(j\Omega)$ would be useful for obtaining the equivalent filter for the analog analysis filters in the discrete-time domain. According to (5.11), $H_k^{'}(s)$ is evidently band-limited. Its impulse response $h_k^{'}(t)$ may be sampled without any spectral overlapping considering the sampling rate $\frac{1}{T}$. If the continuous-time impulse response $h_k^{'}(t)$ is sampled at the rate $\frac{1}{T}$, the discrete-time impulse response $h_k[n']$ is

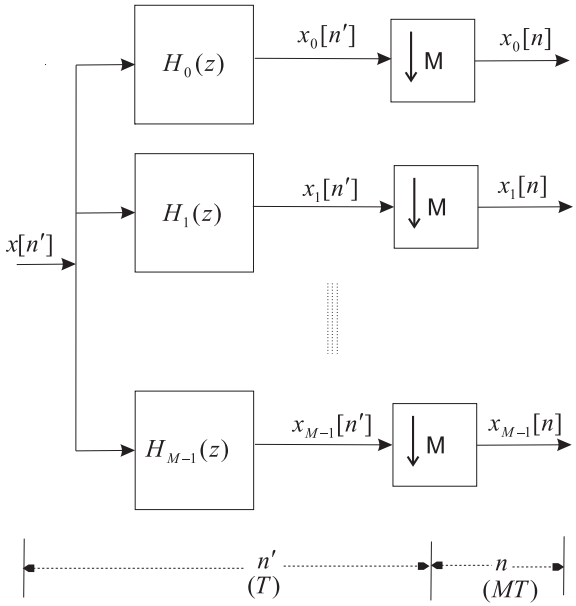

Figure 5.14. The discrete-time model for the *analysis part* of HFB-based A/D converter. The only available signals are $x_0[n]$, $x_1[n]$, ..., and $x_{M-1}[n]$. n' and n represent the discrete-time indices associated with the sampling rates $\frac{1}{T}$ and $\frac{1}{MT}$ respectively.

obtained as following:

$$h_k[n'] = h_k'(t)\Big|_{t=n'T} \qquad n' = \cdots, -2, -1, 0, 1, 2, 3, \cdots$$

This relationship can be described in the frequency-domain as follows:

$$H_k(e^{j\omega}) = \frac{1}{T}\sum_{m=-\infty}^{+\infty} H_k'(j\Omega - \frac{2\pi}{T}m)\Big|_{\Omega=\frac{\omega}{T}}$$

that ω and Ω stand for the discrete-time and continuous-time frequencies respectively. According to (5.11), the analog filter $H_k(j\Omega)$ of analysis part can be replaced by $H_k'(j\Omega)$. On the other hand, the filter $H_k'(j\Omega)$ may be represented by $H_k(e^{j\omega})$ in the discrete-time domain. The analog filter $H_k(j\Omega)$ may conclusively be substituted by $H_k(e^{j\omega})$ in the discrete-time domain. Figure 5.13 shows this equality for an exemplary analog filter. Therefore, the continuous-time components $x(t)$ and $H_k(j\Omega)$ of the analysis part may be represented in the discrete-time domain by $x[n']$ and $H_k(e^{j\omega})$ respectively. With this substitution, the samplers are eliminated and the discrete-time model of analysis part is obtained. This discrete-time model is shown in figure 5.14. Considering that model, the objective of HFB-based A/D conversion is to achieve the unknown signal $x[n']$.

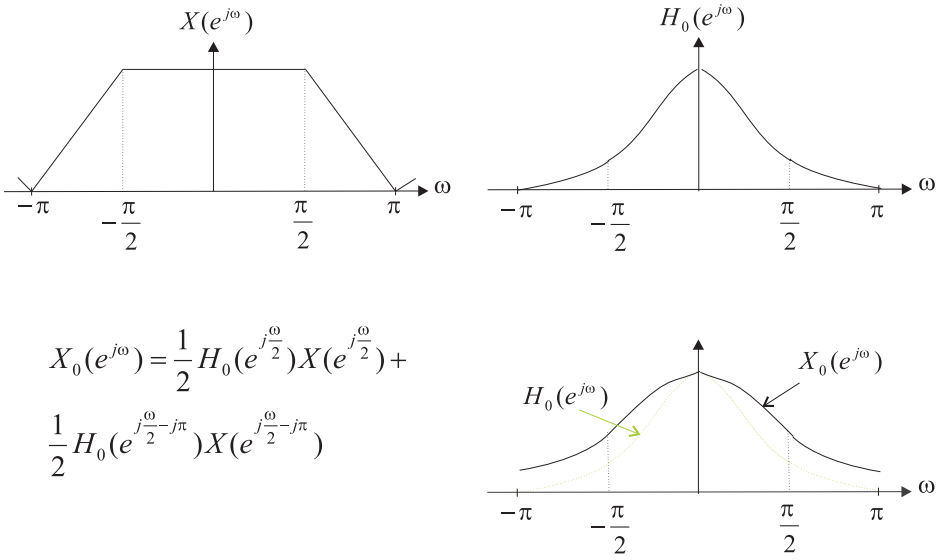

Figure 5.15. The output $X_0(e^{j\omega})$ of analysis part related to the first branch of a two-branch HFB that $X(e^{j\omega})$ and $H_0(z)$ are the frequency responses of the input and analysis filter respectively.

5.3.3 Subband Hybrid Filter Bank A/D Converter

5.3.3.1 Subband MIMO model of analysis part

• General illustration

In this part, the idea of subband MIMO model is simply demonstrated by general diagrams. The discrete-time model of analysis part associated with the HFB-based A/D converter is considered (figure 5.14). Firstly, we show how the output of each branch is mathematically related to the original input $x[n']$ with a non-LTI relation. For convenience, the analysis part of a two-branch HFB ($M = 2$) is considered. Without loss of generality, the frequency responses of the original input $X(e^{j\omega})$ and the analysis filter $H_0(e^{j\omega})$ are supposed to be as shown in figure 5.15. It is reminded that the DTFT of discrete-time signals are periodic with the period 2π. Then, the frequency axis is demonstrated between $[-\pi, \pi]$ (for a period). Figure 5.15 shows the output $x_0[n]$ of the branch associated with the analysis filter $H_0(z)$ in the frequency domain as well. According to figure 5.14, $x_0[n]$ may be

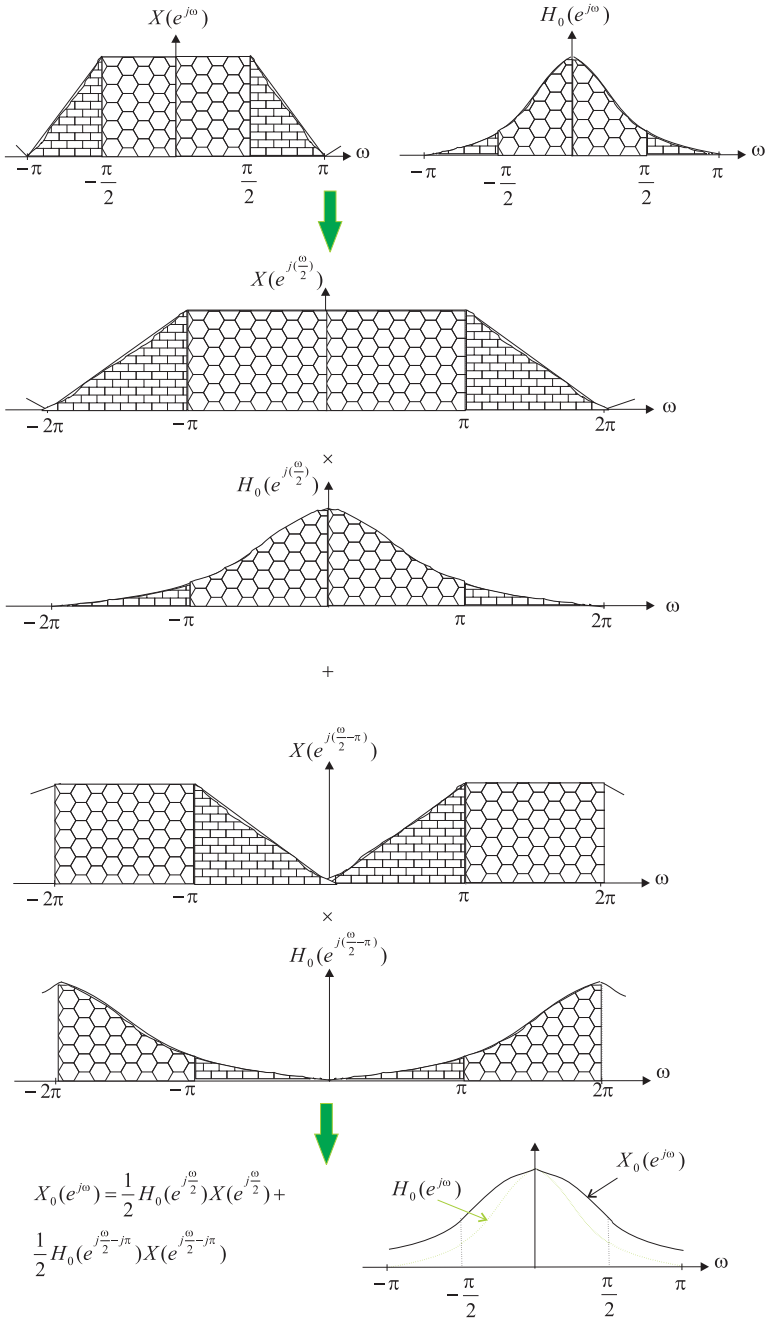

Figure 5.16. The detailed demonstration of the decimation after filtering. The input $X(e^{j\omega})$ passes an analysis filter $H_0(e^{j\omega})$ and then decimated by $M = 2$. The output $X_0(e^{j\omega})$ has an LTI relationship with the spectral parts shown in hexagons and bricks.

described for a two-branch HFB as follows:

$$x_0[n] = x[n'] \star h_0[n']\Big|_{n'=2n}$$

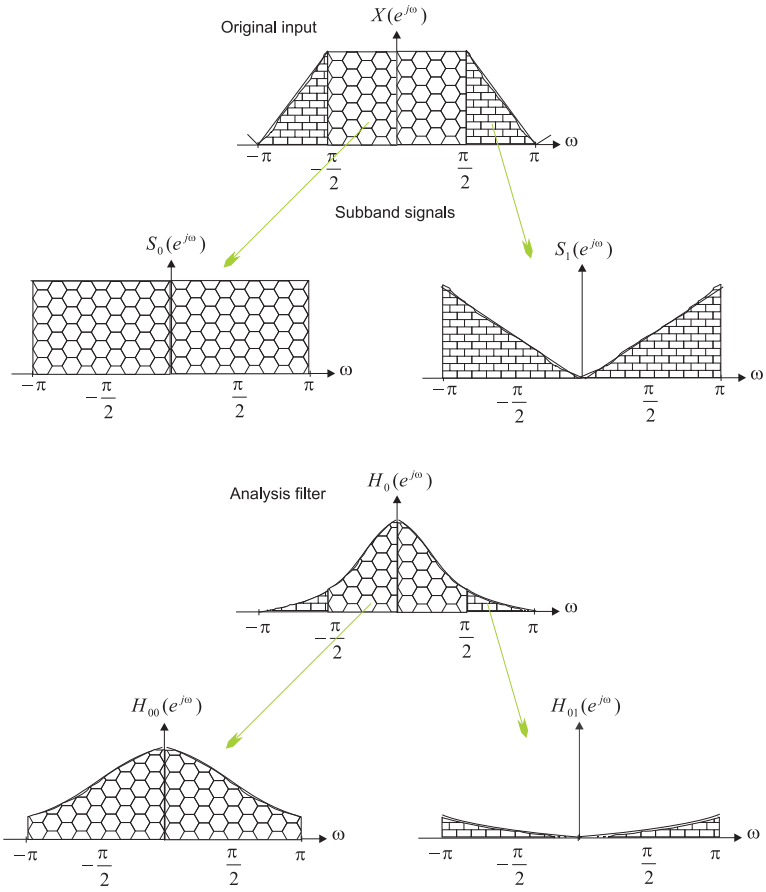

Figure 5.17. The extraction of subband signals from the original input $X(e^{j\omega})$ for a two-branch HFB structure. The subband signals $S_0(e^{j\omega})$ and $S_1(e^{j\omega})$ are obtained by decimating (one out of 2) from the narrow-band parts of the original input. The associated LTI filters $H_{00}(e^{j\omega})$ and $H_{01}(e^{j\omega})$ may be obtained similarly from the analysis filter $H_0(e^{j\omega})$.

where $h_0[n']$ is the discrete-time impulse-response function of $H_0(z)$ and $\star$ represents the convolution operation. The decimation appears by the substitution $n' = 2n$. This relationship may be demonstrated in the frequency domain as following:

$$X_0(e^{j\omega}) = \frac{1}{2}\left[X(e^{j\frac{\omega}{2}}).H_0(e^{j\frac{\omega}{2}}) + X(e^{j(\frac{\omega}{2}-\pi)}).H_0(e^{j(\frac{\omega}{2}-\pi)})\right] \tag{5.12}$$

The second term of above equality (5.12) includes a frequency shift which clearly corresponds to a non-LTI operation. However, this spectral overlapping cannot be conveniently discovered in the figure 5.15. To better observe the relationship 5.12, this equality is shown in figure 5.16. The spectrum has been divided into two parts $0 \leq |\omega| \leq \frac{\pi}{2}$ and $\frac{\pi}{2} \leq |\omega| \leq \pi$ shown in hexagonal and brick patterns respectively in this figure. It may be seen that these two spectral parts of the input $X(e^{j\omega})$

and analysis filter $H_0(e^{j\omega})$ are multiplied. Then, the spectral overlapping occurs only at the last point where these two products are added (see figure 5.16). The decimation procedure is represented by two operations in reference with these two narrow bands: spectral dilating, and addition. The frequency dilating causes no spectral overlapping on these two bands. If these two narrow-band components of the input signal are considered as the new input signals, there exist no spectral overlapping and the new inputs would have an LTI relationship with the output $X_0(e^{j\omega})$. Figure 5.17 shows schematically these new input signals. The new input signals $S_0(e^{j\omega})$ and $S_1(e^{j\omega})$ can be obtained from the narrow-band components of the original input $X(e^{j\omega})$ by decimation (refer to figure 5.17). We call these signals the *subband* components of the input $x[n']$. It may be seen that $X_0(e^{j\omega})$ is produced from the subband signals $S_0(e^{j\omega})$ and $S_1(e^{j\omega})$ as follows (figure 5.16):

$$X_0(e^{j\omega}) = S_0(e^{j\omega})H_{00}(e^{j\omega}) + S_1(e^{j\omega})H_{01}(e^{j\omega}) \tag{5.13}$$

According to (5.13), $X_0(e^{j\omega})$ is obtained from the subband signals $S_0(e^{j\omega})$ and $S_1(e^{j\omega})$ passing through two LTI filters $H_{00}(e^{j\omega})$ and $H_{01}(e^{j\omega})$. This may be generalized to the other branches. In general case (see figure 5.14), we can state that the outputs $x_0[n]$, $x_1[n]$, ..., and $x_{M-1}[n]$ of analysis part may be associated to M subband signals through an LTI relationship as there will exist M subband signals for an M-branch HFB structure. Considering the subband signals as the new input vector, an LTI model may be obtained for the analysis part. This model is mathematically discussed and provided in the next subsection.

• Mathematical description

The discrete-time model of analysis part associated with the HFB-based A/D converter is again considered (figure 5.14). For having an LTI system, it is required to relate the available signals $x_0[n]$, $x_1[n]$, ..., and $x_{M-1}[n]$ to the input $x[n']$ through an LTI relationship. It is evident that this relationship is non-LTI because of decimation procedure (supposing $M > 1$). Using the decimation procedure in the k^{th} branch, the following equation is obtained:

$$x_k[n] = h_k[n'] \star x[n']\Big|_{n'=Mn} \qquad k \in \{0, 1, ..., M-1\} \tag{5.14}$$

that $\star$ stands for the convolution operation. This relation can be equally established in the frequency domain as follows:

$$X_k(e^{j\omega}) = \frac{1}{M}\sum_{m=0}^{M-1} H_k(e^{(j\frac{\omega}{M}-j\frac{2\pi}{M}m)})X(e^{(j\frac{\omega}{M}-j\frac{2\pi}{M}m)}) \tag{5.15}$$

ω represents the Discrete-Time Fourier Transform (DTFT) frequency. The frequency representation of discrete-time signal is periodic with the period interval of 2π [69]. The spectral overlapping related to the decimation procedure is seen through the equation (5.15). According to the preceding subsection, we now propose to consider M discrete-time signals $s_0[n]$, $s_1[n]$, ..., and $s_{M-1}[n]$ called subband signals. Figure 5.18 shows how $s_k[n]$ may be extracted from the original input $x[n']$ in the frequency domain. The subband signals may be obtained from the frequency decomposition of the input signal $x[n']$ into M narrow-band signals followed by the decimation. This process may be interpreted in the frequency domain as follows (refer to figure 5.18). For $k = 0, 2, ...$, it is:

$$S_k(e^{j\omega}) = \begin{cases} \frac{1}{M}X(e^{j\frac{\omega}{M}+jk\frac{\pi}{M}}) & \omega \in [0,\pi] \\ \\ \frac{1}{M}X(e^{j\frac{\omega}{M}-jk\frac{\pi}{M}}) & \omega \in [-\pi,0] \end{cases} \tag{5.16}$$

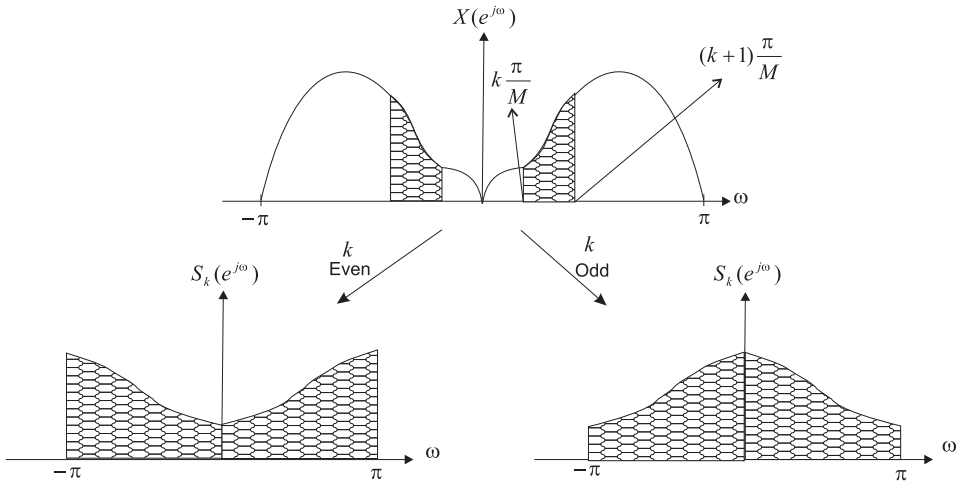

Figure 5.18. The schematic illustration for extracting each subband signal $S_k(e^{j\omega})$ $(0 \leq k \leq M-1)$ from the original signal $X(e^{j\omega})$.

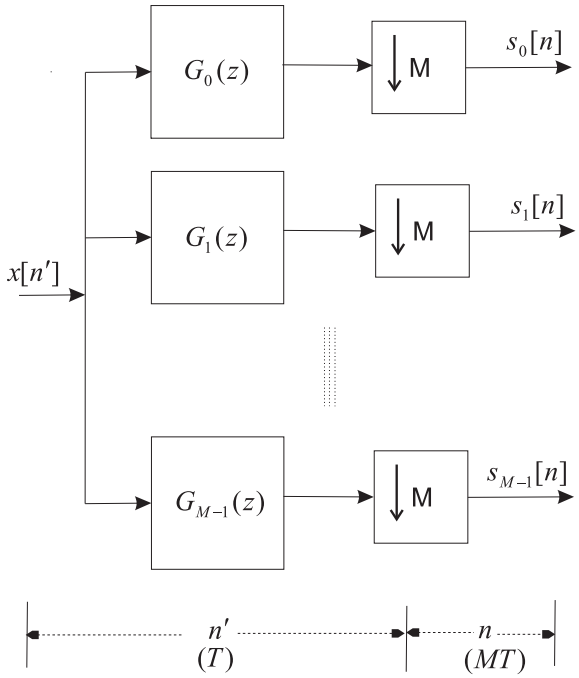

Figure 5.19. Each subband signals $s_k[n]$ is obtained from the original signal $x[n']$ by the decimation preceded with the subband filter $G_k(z)$.

and for $k = 1, 3, ...,$ it will be:

$$S_k(e^{j\omega}) = \begin{cases} \frac{1}{M} X(e^{j\frac{\omega}{M} - j(k+1)\frac{\pi}{M}}) & \omega \in [0, \pi] \\ \\ \frac{1}{M} X(e^{j\frac{\omega}{M} + j(k+1)\frac{\pi}{M}}) & \omega \in [-\pi, 0] \end{cases} \tag{5.17}$$

where $S_k(e^{j\omega})$ is the frequency representation of $s_k[n]$ for $0 \leq k \leq M-1$. These signals are like the subband signals used in the audio/speech processing and coding [72]. They can be obtained in the time-domain from the tandem of a subband filtering bank and a decimation procedure. Figure 5.19 illustrates schematically how the subband signals may be produced. For instance, the k^{th} subband signal $s_k[n]$ can be obtained as follows. Firstly, the original signal $x[n']$ is passed through the k^{th} subband filter $G_k(e^{j\omega})$. After filtering, the decimation procedure is carried out to eliminate the zero parts of the spectrum. The subband filter $G_k(e^{j\omega})$ is

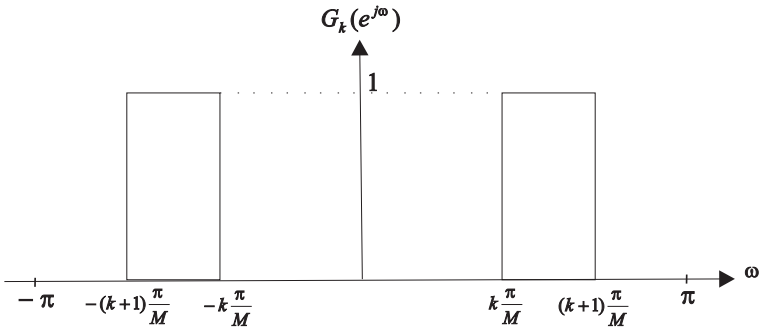

Figure 5.20. The frequency response of the subband filter $G_k(e^{j\omega})$. It is zero for all the frequencies $|\omega| \leq \pi$ except $k\frac{\pi}{M} \leq |\omega| < (k+1)\frac{\pi}{M}$.

defined as following (for $|\omega| \leq \pi$):

$$G_k(e^{j\omega}) = \begin{cases} 1 & k\frac{\pi}{M} \leq |\omega| < (k+1)\frac{\pi}{M} \\ \\ 0 & \text{elsewhere} \end{cases} \tag{5.18}$$

$G_k(e^{j\omega})$ has been shown in figure 5.20. There is no spectral overlapping or ambiguity due to the decimation procedure in the production of $s_0[n]$, $s_1[n]$, ..., and $s_{M-1}[n]$ because of the narrow-band nature of subband filters.
The available signals $x_0[n]$, $x_1[n]$, ..., and $x_{M-1}[n]$ (the outputs of analysis part) may be reconstructed in terms of these subband signals. According to 5.15 - 5.18, each available signal $x_k[n]$ may be produced by the subband signals as following:

$$X_k(e^{j\omega}) = \sum_{m=0}^{M-1} H_{km}(e^{j\omega}) S_k(e^{j\omega}) \tag{5.19}$$

The filters $H_{k0}(z)$, $H_{k1}(z)$, ..., and $H_{k(M-1)}(z)$ are extracted from the analysis filter $H_k(z)$ through a process similar to the production of subband signals (equations (5.16) and (5.17)). $H_{km}(e^{j\omega})$ is the $(k,m)^{th}$ element of analysis matrix $\mathbf{H}(z)$ which is described in the next paragraph. If m is even ($m = 0, 2, ...$), $H_{km}(e^{j\omega})$ is obtained as following:

$$H_{km}(e^{j\omega}) = \begin{cases} \frac{1}{M} H_k(e^{j\frac{\omega}{M} + jm\frac{\pi}{M}}) & \omega \in [0, \pi] \\ \\ \frac{1}{M} H_k(e^{j\frac{\omega}{M} - jm\frac{\pi}{M}}) & \omega \in [-\pi, 0] \end{cases} \tag{5.20}$$

and in the odd case ($m = 1, 3, ...$), it is:

$$H_{km}(e^{j\omega}) = \begin{cases} \frac{1}{M} H_k(e^{j\frac{\omega}{M} - j(m+1)\frac{\pi}{M}}) & \omega \in [0, \pi] \\ \\ \frac{1}{M} H_k(e^{j\frac{\omega}{M} + j(m+1)\frac{\pi}{M}}) & \omega \in [-\pi, 0] \end{cases} \tag{5.21}$$

At last, the available signals $x_0[n]$, $x_1[n]$, ..., and $x_{M-1}[n]$ can be described in terms of the subband signals $s_0[n]$, $s_1[n]$, ..., and $s_{M-1}[n]$ through an LTI relationship. It leads to:

$$\mathbf{x}[n] = \mathbf{H}[n] \star \mathbf{s}[n] \tag{5.22}$$

where:

$$\mathbf{x}[n] = \Big[x_0[n], x_1[n], ..., x_{M-1}[n]\Big]^T$$

$$\mathbf{s}[n] = \Big[s_0[n], s_1[n], ..., s_{M-1}[n]\Big]^T$$

and the analysis matrix $\mathbf{H}[n]$ is an $M \times M$ matrix of discrete-time filters. The $(i, j)^{th}$ element of $\mathbf{H}[n]$ is the impulse response $h_{ij}[n]$ of the subband analysis filter $H_{ij}(z)$ (refer to (5.20) and (5.21)) as follows:

$$\mathbf{H}[n] = \begin{bmatrix} h_{00}[n] & h_{01}[n] & ... & ... & h_{0(M-1)}[n] \\ & \vdots & \vdots & \vdots & \\ & \vdots & \vdots & \vdots & \\ h_{(M-1)0}[n] & h_{(M-1)1}[n] & ... & ... & h_{(M-1)(M-1)}[n] \end{bmatrix}$$

In the frequency domain, the convolution is substituted with the simple multiplication. The vectors $\mathbf{X}(e^{j\omega})$ and $\mathbf{S}(e^{j\omega})$ are supposed in the frequency domain as:

$$\mathbf{X}(e^{j\omega}) = \Big[X_0(e^{j\omega}), X_1(e^{j\omega}), ..., X_{M-1}(e^{j\omega})\Big]^T$$

$$\mathbf{S}(e^{j\omega}) = \Big[S_0(e^{j\omega}), S_1(e^{j\omega}), ..., S_{M-1}(e^{j\omega})\Big]^T$$

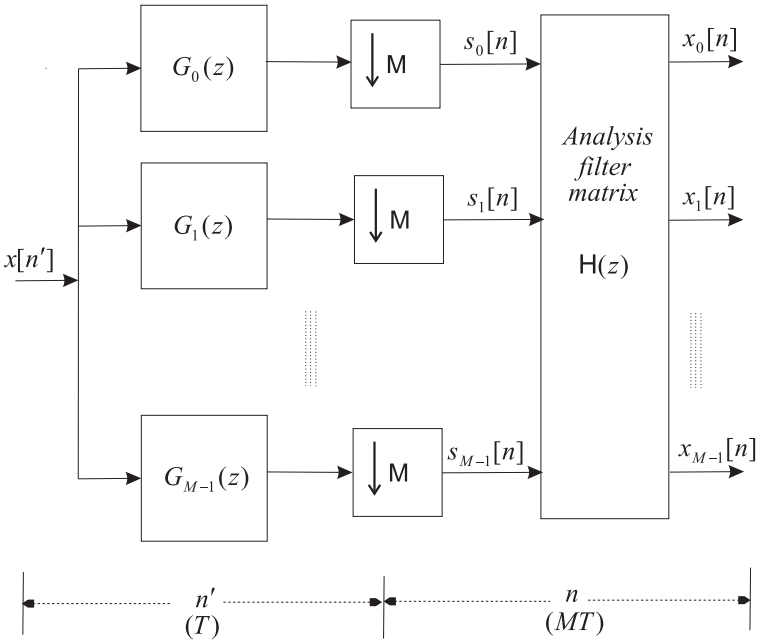

Figure 5.21. The subband MIMO model for the analysis part of HFB-based A/D converter. The inputs $s_0[n]$, $s_1[n]$, ..., and $s_{M-1}[n]$ are the subbands of the original input $x[n']$. $x_0[n]$, $x_1[n]$, ..., and $x_{M-1}[n]$ are the only available signals.

Then, (5.22) may be rewritten in the frequency domain as follows:

$$\mathbf{X}(e^{j\omega}) = \mathbf{H}(e^{j\omega})\mathbf{S}(e^{j\omega}) \tag{5.23}$$

where the analysis matrix $\mathbf{H}(e^{j\omega})$ is the $M \times M$ matrix of discrete-time filters in the frequency domain. Thus, the subband signals vector $\mathbf{s}[n]$ is related to the available signals vector $\mathbf{x}[n]$ through an LTI operation. Substituting the model of subband signals (figure 5.19) and using 5.22, the analysis part of HFB structure may be modeled in the discrete-time domain using a MIMO structure as shown in figure 5.21. Assuming the subband signals $\mathbf{s}[n]$ as the new inputs, an LTI system has been achieved. The decimation procedure exists no longer between input-output signals. It leads to an LTI MIMO system for which $\mathbf{s}[n]$ and $\mathbf{x}[n]$ are the input and output vectors respectively.

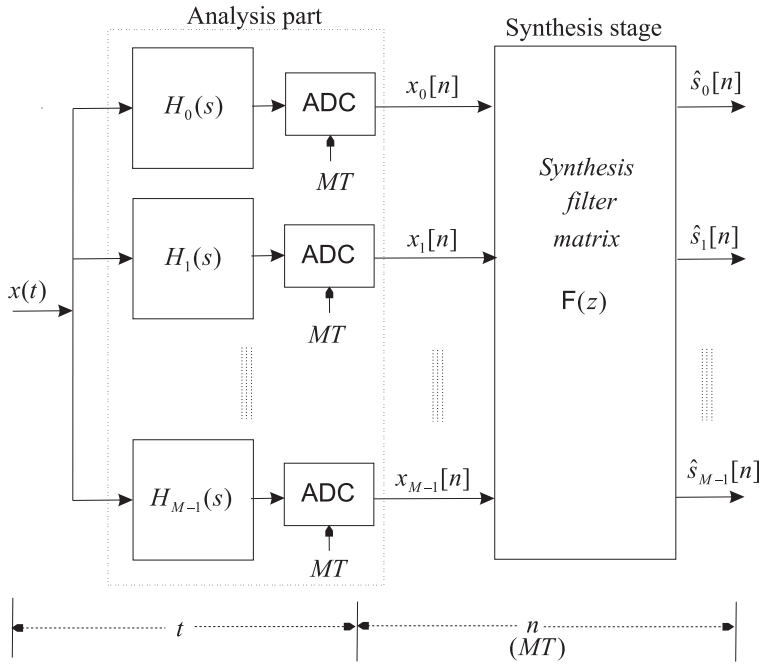

Figure 5.22. The subband architecture of HFB-based A/D converter for estimating the (narrow-band) subband components of the input signal. The outputs $\hat{s}_0[n]$, $\hat{s}_1[n]$, ..., and $\hat{s}_{M-1}[n]$ are the estimated subband signals.

5.3.3.2 Subband architecture for HFB-based A/D converter

Using the MIMO model of analysis part (figure 5.21), a new HFB-based A/D converter may be proposed. Figure 5.22 shows this subband architecture of HFB-based A/D converter. In fact, this architecture will perform simultaneously both A/D conversion and frequency demultiplexage (through decimation). Now, the unknown inputs $s_0[n]$, $s_1[n]$, ..., and $s_{M-1}[n]$ are reconstructed instead of the original input $x[n']$. The original input $x[n']$ can nevertheless be obtained from the subband signals as explained later in this subsection.

To implement this multiple-output HFB-based A/D conversion, an $M \times M$ matrix $\mathbf{F}(z)$ of FIR filters is required for the synthesis stage. In fact, the synthesis filters matrix would tend to the inverse of analysis filters matrix defined in (5.22). For obtaining the synthesis filters matrix $\mathbf{F}(e^{j\omega})$, the quantization noise of A/D converters is again neglected. Thus, a MIMO model may be found for the subband HFB-based A/D converter of figure 5.22. Integrating figures 5.21 and 5.22, the MIMO HFB A/D converter may be substituted by the model shown in figure 5.23.

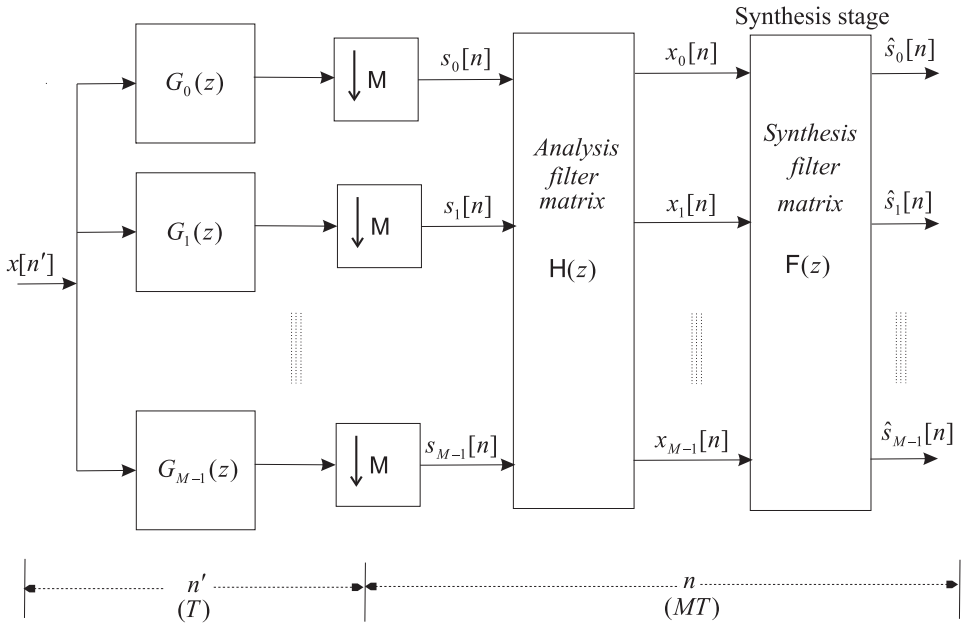

Figure 5.23. The model of subband MIMO HFB-based A/D converter in the discrete-time domain. The subband components of the input signal are estimated as the output signals.

Considering figure 5.23, PR equations will be:

$$\mathbf{F}(e^{j\omega}).\mathbf{H}(e^{j\omega}) = \mathbf{I}.e^{-j\omega n_d} \tag{5.24}$$

where $\mathbf{I}$ represents the identity matrix $(M \times M)$ and n_d stands for an arbitrary delay. n_d is considered for maintaining the causality.
Using the prefixed analysis filters, the equation (5.24) leads to the following solution of synthesis filters at each frequency ω:

$$\mathbf{F}(e^{j\omega}) = e^{-j\omega n_d}\mathbf{H}^{-1}(e^{j\omega}) \tag{5.25}$$

where the existence of the inverse matrix $\mathbf{H}^{-1}(e^{j\omega})$ has implicitly been supposed (refer to the section 3.2.2). This relation may be established for N frequency points (here equally spaced in the band of interest). Thus, the frequency response of each synthesis filter $F_{ij}(e^{j\omega})$ is achieved using (5.25). An FIR filter may be estimated for the $(i,j)^{th}$ element of synthesis filter matrix. Using FIR estimations of synthesis filters, some distortion and interferences may appear. The outputs may

be interpreted in terms of distortion and Inter-Channel Interference (ICI) terms. ICI terms are equivalent for the aliasing terms considered in the classical HFB structure (see chapter 3). Supposing that the solution of (5.25) is approximated by a matrix $\mathbf{F}(e^{j\omega})$ of FIR synthesis filters, $\mathbf{T}(e^{j\omega})$ is defined as following:

$$\mathbf{T}(e^{j\omega}) = \mathbf{F}(e^{j\omega})\mathbf{H}(e^{j\omega})$$

$\mathbf{T}(e^{j\omega})$ is a matrix containing distortion and ICI functions. It shows that the estimated value $\hat{s}_k[n]$ of k^{th} subband signal $s_k[n]$ may be developed in the frequency domain as:

$$\hat{S}_k(e^{j\omega}) = \underbrace{T_{k,k}(e^{j\omega})S_k(e^{j\omega})}_{\text{distortion term}} + \underbrace{\sum_{m=0,m\neq k}^{M-1} T_{k,m}(e^{j\omega})S_m(e^{j\omega})}_{\text{ICI terms}} \tag{5.26}$$

The k^{th} diagonal element $T_{(k+1)(k+1)}(e^{j\omega})$ of $\mathbf{T}(e^{j\omega})$ describes the distortion function related to the subband signal $S_k(e^{j\omega})$. The other $M-1$ elements of k^{th} row of $\mathbf{T}(e^{j\omega})$ represent the relative ICI terms. $e^{-j\omega n_d}$ is the ideal value of the distortion function and the ICI elements are desired to be ideally null. The proposed subband HFB architecture for A/D conversion has particular characteristics. The properties of subband HFB may be summarized as following:

1. $x_0[n]$, $x_1[n]$, ..., and $x_{M-1}[n]$ are the only available and known signals. The desired unknown signals for the A/D conversion are the subband signals $s_0[n]$, $s_1[n]$, ..., and $s_{M-1}[n]$ in the subband HFB structure. However, the original input $x[n']$ can be reconstructed through the output vector as shown in figure 5.24. It requires an extra computational load. For reconstructing the original input, it is better to use the TDM architecture described in the section 5.3.4 which provides directly the reconstructed original input without any extra computation. Then, the suband architecture would be useful if it is desired to obtain the subband components of input.

2. The computations are implemented in parallel for subband HFB structure. All digital computations are then carried out on the signals associated with the sampling period MT for the subband HFB.

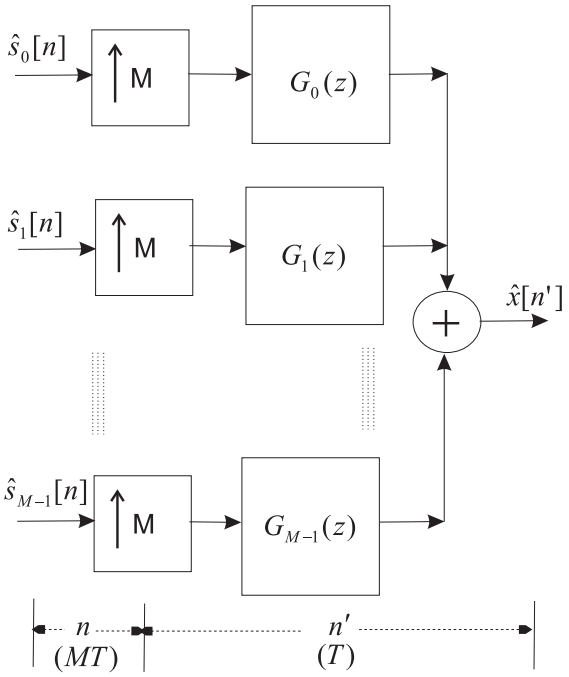

Figure 5.24. The original signal $x[n']$ may be reconstructed from the subband signals. $G_k(z)$ represents the k^{th} subband filter explained by (5.18) and $\widehat{x}[n']$ stands for the reconstructed original input.

3. Knowing the analysis filters, the matrix of analysis filters may be calculated and hence, the subband architecture may be implemented using (5.25). The subband architecture uses the same hardware as the classical HFB but differs in the digital part.

4. A subband HFB-based A/D converter may be very interesting for the applications such as software radio and intelligent Frequency Division Multiple Access (FDMA). The subband HFB A/D converter may be considered as an FDMA receiver which implements the A/D conversion and frequency demultiplexage simultaneously (software radio).

5. There is not any condition for using the proposed subband architecture except the total Nyquist criterion is respected ($\frac{1}{T} \geq 2\sigma$).

6. As the subband architecture of HFB-based A/D converter provides a MIMO LTI system between the inputs and outputs, the multichannel blind deconvolution techniques might be exploited for compensating the analog imperfections of analysis filter bank as well as the other techniques such as automatic noise cancelation in contrary to the classical HFB (refer to the section 5.1).

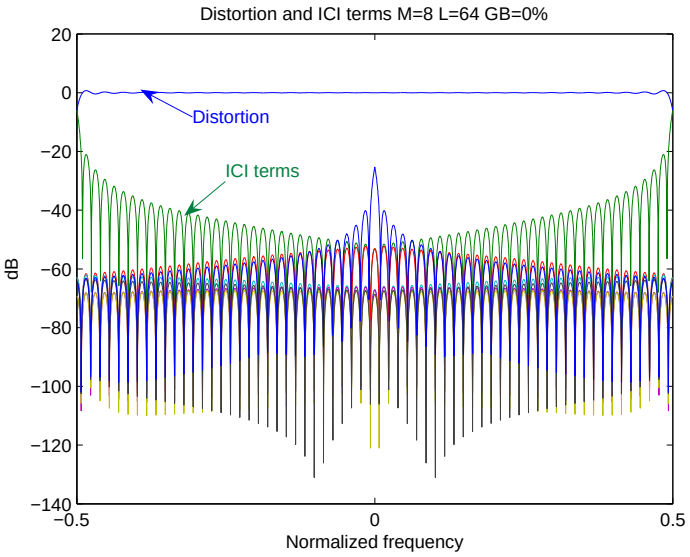

Figure 5.25. Distortion and ICI functions due to 4^{th} subband signal $x_3[n]$ in the case where no guard band is used. The synthesis part uses FIR filters with 64 coefficients ($GB = 0$).

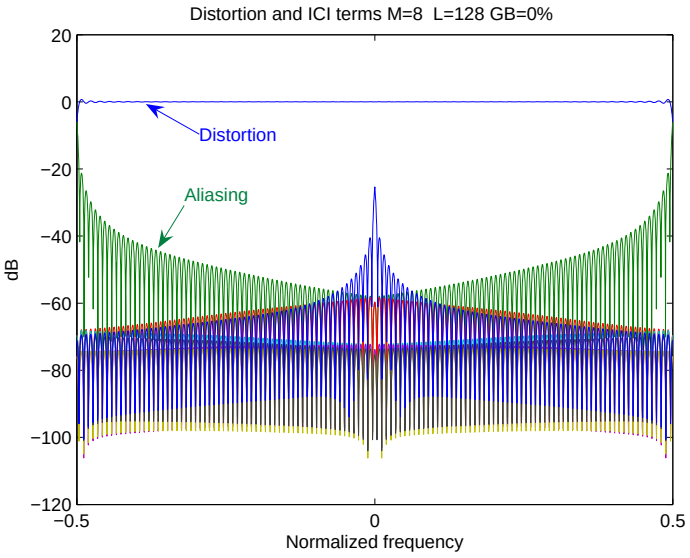

Figure 5.26. Distortion and ICI functions (in dB) due to 4^{th} subband signal $x_3[n]$ versus the normalized frequency. Each FIR synthesis filter consists of 128 coefficients. The whole spectrum has been considered for useful signal (no guard band).

5.3.3.3 Performance of Subband HFB architecture

◯ Simulations in the frequency domain

The subband architecture is simulated for an 8-channel HFB structure using the same analysis filter bank mentioned in chapter 3. Figure 5.25 shows the distortion and ICI functions related to the subband signal $s_3[n]$. Each FIR synthesis filter has been assumed to include 64 coefficients. The distortion and ICI averages

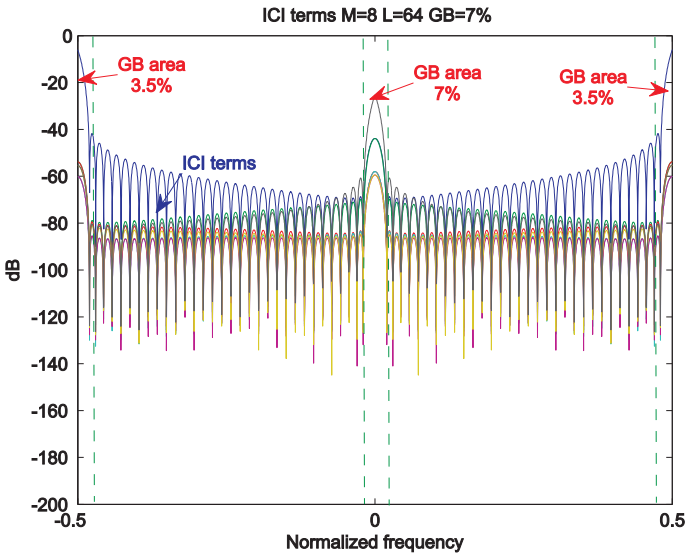

Figure 5.27. The ICI functions due to the 4^{th} subband component (subband HFB structure) versus normalized frequency. Each FIR synthesis filter includes 64 coefficients and a GB ratio of 7% has been used.

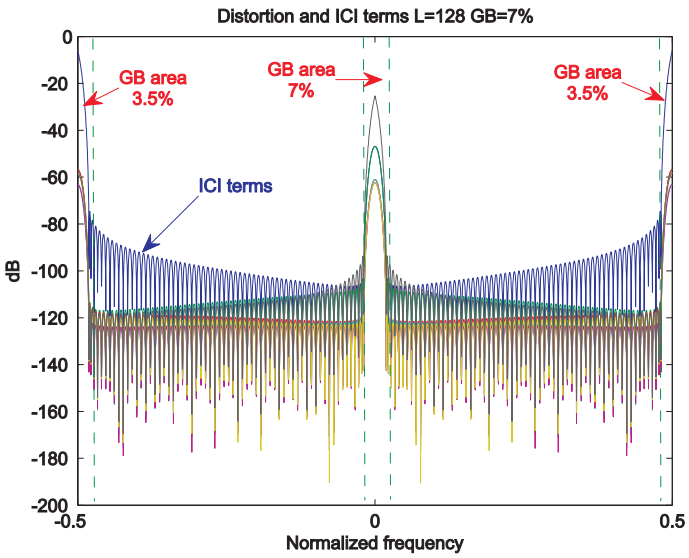

Figure 5.28. The ICI functions related to the 4^{th} subband component (subband HFB structure) versus normalized frequency. The length of each FIR synthesis filter is considered 128 coefficients. 7% of each subband spectrum is used as guard band.

are -0.04 dB and -60 dB respectively. The performance is not so acceptable for practical applications (reminding that the quantization noise would be added as well). The poor performance is related to the limited capabilities of FIR synthesis filters. In fact, there is only one group of synthesis filters leading to no ICI terms. These ideal synthesis filters are obtained from inverting the analysis matrix (refer to 5.25). The FIR digital filters (with a limited number of coefficients such as 64

Table 5.3. The ICI and distortion averages of an eight-branch subband HFB structures considering $L = 32$, 64 and 128 coefficients.

Eight-branch Subband HFB structure (in dB)				
Guard band	0%		7%	
L	ICI mean	Distortion	ICI mean	Distortion
32	-51	-0.15	-63	-7E-3
64	-60	-0.04	-81	4.3E-4
128	-67	-0.02	-118	2.2E-5

coefficients) cannot exactly approximate those ideal synthesis filters. The approximation degrades at the frequency borders for each subband signal as shown in figure 5.25 (around $w = 0$ and $w = \pi$). The ICI and distortion of this eight-branch subband HFB is shown in figure 5.26 in the case where each FIR synthesis filter consists of 128 coefficients. The associated ICI average is -67 dB. To improve the performance of subband HFB structures, we propose to consider some percents of each subband spectrum as Guard Band (GB) since an incompatibility appears in the PR equations at low and high frequencies. Thus, the proposed guard band permits to eliminate the PR equations associated with the frequency borders. This proposed guard band would cover low (around $w = 0$) and high (around $w = \pi$) frequencies at the spectrum of each subband. Applying a small GB ratio, the results are largely improved. Figures 5.27 and 5.28 illustrate the distortion and ICI terms when 7% of each subband is regarded as guard band for $L = 64$ and $L = 128$ respectively. L stands for the number of coefficients used by each FIR synthesis filter. It may be seen that the performance in terms of ICI and distortion mean values have largely improved. Table 5.3 lists the ICI and distortion averages in dB for the subband HFB structures in the cases where no guard band and a guard band ratio of 7% are used. The variable L shows the number of coefficients of FIR synthesis filters in this table. The ICI and distortion averages have not been here compared with the aliasing and distortion terms of classical HFB because they do not cover the same spectrum. In return, their performances are compared in terms of output resolution resulted from the temporal simulations in the next subsection.

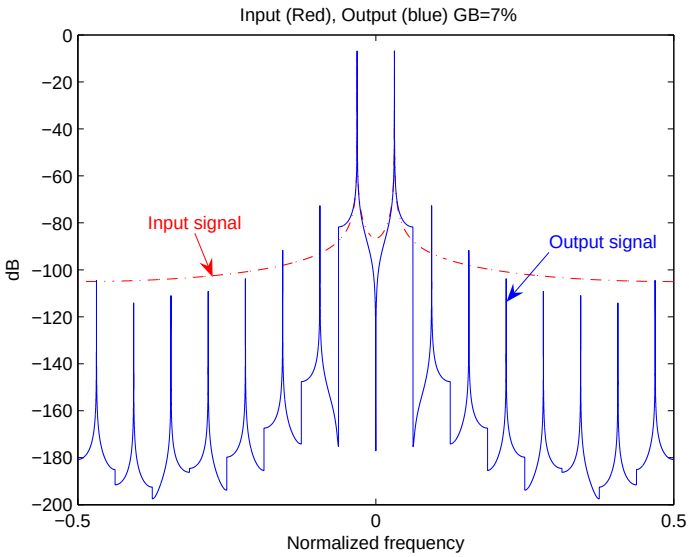

Figure 5.29. The input and output spectra (in dB) versus normalized frequencies for a subband HFB-based ADC using FIR synthesis filters with 64 coefficients and a GB ratio 7%. Analog input is a sinusoidal signal at the middle of the first subband spectrum. All subband output are null except the first one in which the input signal is considered.

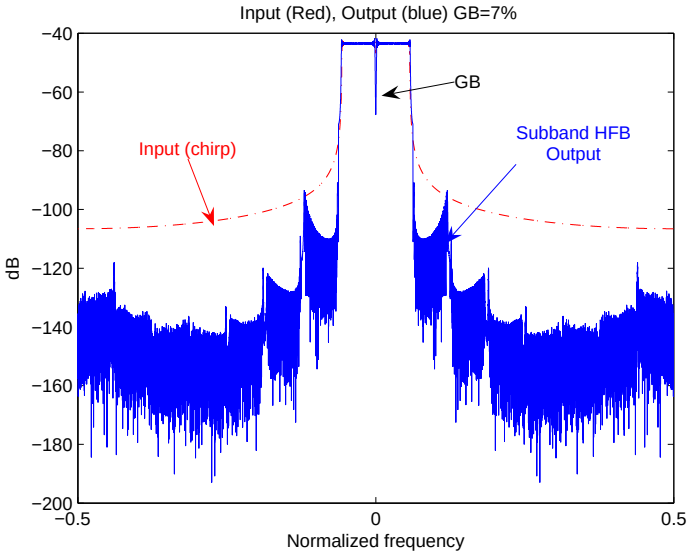

Figure 5.30. The input and output spectra (in dB) versus normalized frequencies for a subband HFB structure using FIR synthesis filters of 64 coefficients and a GB ratio of 7%. The analog input is a chirp signal sweeping the spectrum of first subband. All subband outputs are null except the first one which includes the input chirp.

◯ Simulations in the time domain

• Resolution

The classical and subband HFB structures have been simulated in the time domain to compare directly the output resolutions. For comparing with the output signal of classical HFB, the reconstruction process (figure 5.24) has been applied to the output vector of subband HFB architecture. The results of simulations

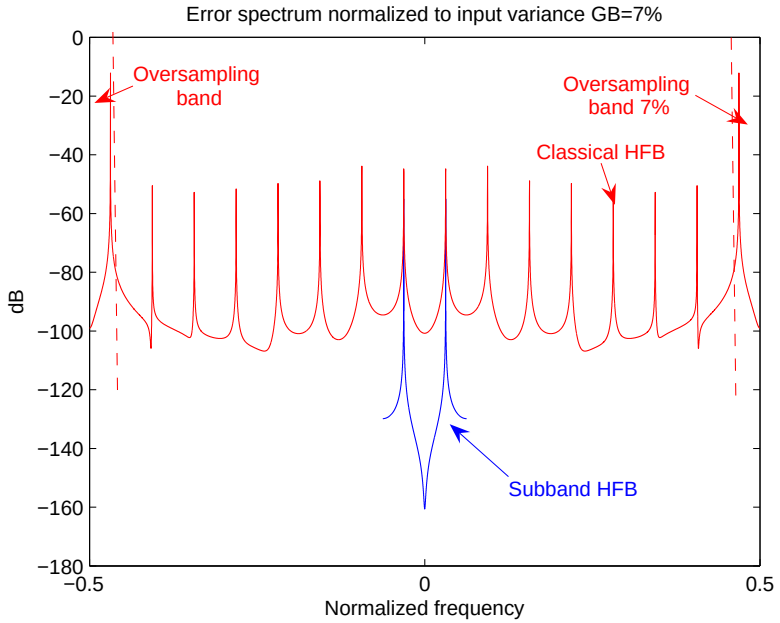

Figure 5.31. The error spectra (normalized to the input variance) (in dB) versus normalized frequencies for the subband (blue) and classical (red) HFB structures. FIR synthesis filters include 64 coefficients and a the same GB and oversampling ratio of 7% is used. Analog input is a sinusoidal signal at the middle of the first subband spectrum. All subband outputs are null except the first one in which the input signal is considered.

are discussed and compared regarding the output resolution, sensitivity to analog imperfections and computation load. The same set of analysis filters used in the preceding subsection have been considered in this part as well. Different input signals such as sinusoidal and chirp signals are applied for evaluating the respective performance. Considering a sinusoidal signal at the frequency $0.5\frac{\pi}{8T}$ (in the middle of the first subband), the Discrete-Time Fourier Transform (DTFT) of the output and input signals is shown in figure 5.29. It may be seen that all subband outputs are null except the output of the first subband $\widehat{s}_0[n]$ which is directly corresponding to the original input. Figure 5.30 shows the spectra of input and output for the subband HFB in the case where a chirp signal is considered as input. All the subband outputs are zero else the one related to the first subband in conformity with the input chirp. It may be seen that no signal component appears at the GB spectral area unless the original input includes a component at the GB area. This issue will be highlighted in the following remarks. To better study the performance, the error signal is compared for both the subband and classical

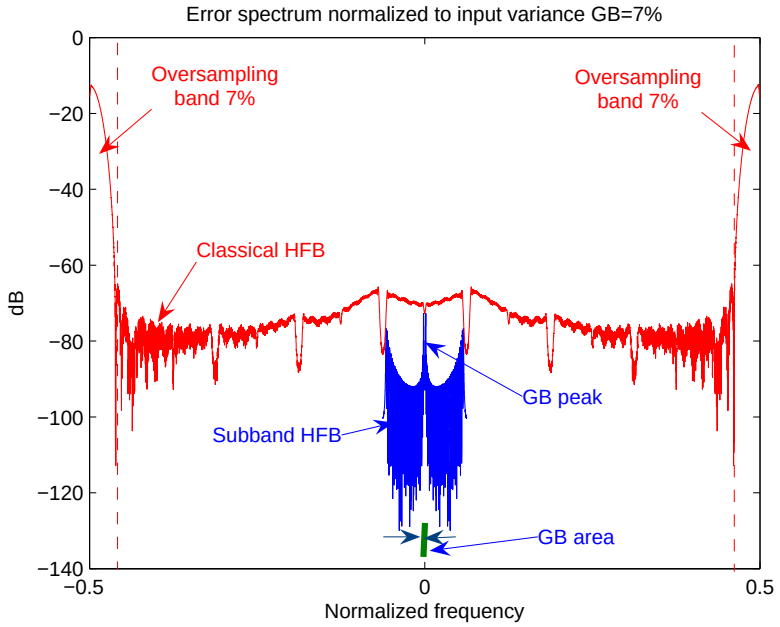

Figure 5.32. The error spectra (normalized to the input variance) (in dB) versus normalized frequencies for the subband (blue) and classical (red) HFB structures considering FIR synthesis filters with 64 coefficients and the same oversampling and GB ratio of 7% for the classical and subband HFBs respectively. Analog input is a chirp sweeping the first subband spectrum. All subband outputs are null except the first one in which the input signal is considered.

architectures considering the same input signals. Regarding the above-mentioned sinusoidal signal, the error spectrum is illustrated in the figure 5.31. In the subband HFB case, the error appears only in the first subband spectrum and the other subband signals may be assumed null according to figure 5.30. Figure 5.32 shows the error spectra for the classical and subband architectures considering a chirp sweeping the first subband spectrum as the input signal. The error spectrum covers again only the first subband spectrum for the subband HFB since it was mentioned that all subband outputs are null except the first subband $\hat{s}_0[n]$ in the case of subband HFB (see 5.30). According to figures 5.31 and 5.32, the error signal of the classical HFB not only covers the whole spectrum, but also always is non-zero in the oversampling spectral area. In other words, it may be interpreted that the error related to one input subband appears at the other $M-1$ subbands on the output of M-channel classical HFB-based ADC. Thus, a digital filter is always necessary to omit the output components at the oversampling area (here

$|\Omega| \geq 0.93\pi$) for the classical HFB. Otherwise, the output resolution of classical HFB-based ADC is so much low. In the subband HFB case, this post-filtering procedure for filtering out the GB spectral area is not required unless the original input spectrum covers the GB parts. The output resolutions of both (subband and classical) HFB structures are listed in table 5.4 considering the FIR synthesis filters with 64 and 128 coefficients. The resolution due to the conventional HFB is related to the case where post-filtering has been applied. It may be seen that subband HFB-based ADC provides a better resolution than the classical structure supposing FIR synthesis filters of the same order.

Table 5.4. Resolution of HFB-based ADC assuming the chirp and sinusoidal signals as input. Having FIR synthesis filters with 64 coefficients, the same oversampling and GB ratios of 7% are used for the classical and subband HFBs respectively.

Output resolution (in bits)		
HFB architecture	Input signal	
	Sinusoidal	Chirp
Classical HFB	9.9	9.6
Subband HFB	10.5	10.1

• Sensitivity analysis

Each electronic element is often associated with a nominal value plus a deviation or realization error. To study the sensitivity to the realization errors, the subband and classical HFB structures have been simulated considering Gaussian-distributed realization errors for the electronic elements of analysis filter bank. The HFB structures are supposed to include eight branches with the same analysis filter bank used in the preceding sections. The simulations have been repeated for 1000 trials of random mutually-independent realization errors. Firstly, an analog input is considered including one sinusoidal signal located at the middle of first subband ($0.5\frac{\pi}{8T}$). Figure 5.33 shows the average resolution of both (subband and classical) HFB structures versus STandard Deviation (STD) of error distribution considering 64 coefficients for each FIR synthesis filter. The resolutions have been shown in the presence or without Post-Filtering (PF) procedure. As it was mentioned in the preceding subsection, PF process filters out the signal component at the oversampling and GB spectral areas for the classical and subband HFBs

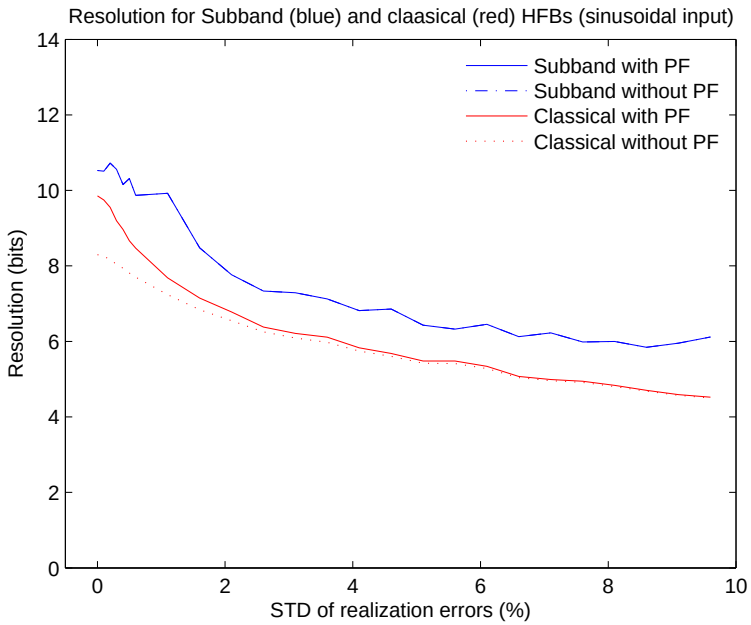

Figure 5.33. The resolution (in bits) of the classical and subband HFB-based ADC versus STD of realization errors for a sinusoidal input signal. Gaussian errors have been applied to the electronic elements constituting the analysis filter bank. Each FIR synthesis filter includes 64 coefficients and both the oversampling and GB ratios are 7%.

respectively. It is seen that the subband HFB exhibits a less sensitivity to the realization errors than the classical HFB for this sinusoidal input. The simulations have been reestablished for a chirp input signal sweeping the first subband spectrum as well. Figure 5.34 demonstrates the output resolutions versus the STD of error distribution for the classical and subband HFBs.

• **Computational complexity**

The classical HFB-based A/D converter consists of M FIR synthesis filters, but the subband architecture needs M^2 ones (compare figures 2.6 and 5.22). For an FIR filter with L coefficients, L multiplying operations and delay components are effectively necessary. Then, for implementing the synthesis stage, the subband architecture will need M^2L multiplications to be compared with ML ones in the classical case. However, the subband HFB structure provides M output samples compared with only one output sample of the classical HFB. Therefore, the computational complexity per each output sample is equivalent for both HFB structures. To thoroughly compare the computational complexity, the design phase has to be

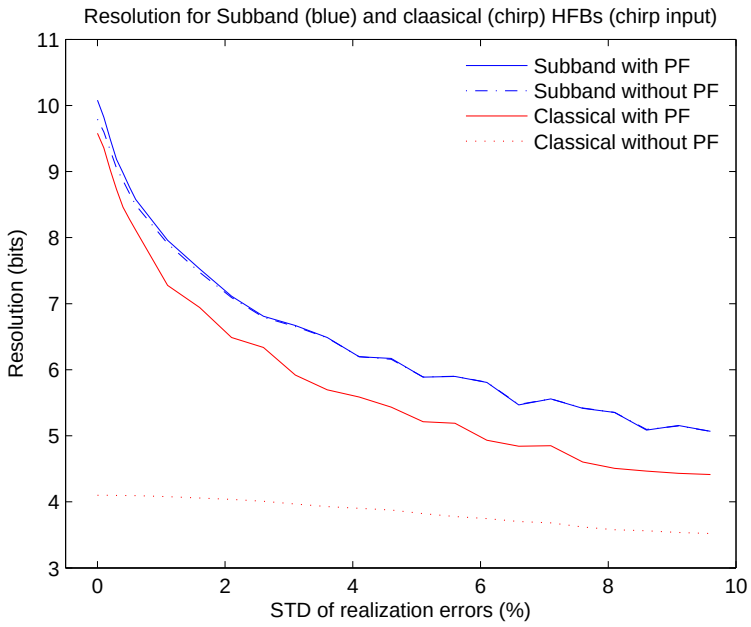

Figure 5.34. The resolution (in bits) of the classical and subband HFB-based ADC versus STD of realization errors considering a chirp input signal. Gaussian errors have been applied to the electronic elements constituting the analysis filter bank. Each FIR synthesis filter includes 64 coefficients and both the oversampling and GB ratios are 7%.

considered as well. In the design phase, FIR synthesis filters are obtained. Assuming N frequency points for designing the synthesis filters, conventional HFB structure would require the inversion of an $MN \times MN$ matrix (refer to the chapter 3). The subband HFB needs the inversion operation of N matrices of $M \times M$ (refer to the previous section). In practice, N must be much larger than M ($N >> M$) to have an acceptable interpolation. Thus, the design phase of classical HFB architecture is obviously much more complex than the subband one. The complexity of the design phase is particularly important when an adaptive method would be applied to estimate the real analysis filter bank for compensating realization errors. For example, the design phase of synthesis filters should be regularly repeated to compensate the variations due to temperature drifts. Accordingly, the subband HFB-based ADC may be preferred to the conventional structure when realization errors are regularly compensated. However, there would be a computational overload if the original analog signal $x(t)$ is required. The original signal may be reconstructed from the estimated subband signals in this case.

5.3.4 Time-Division Multiplexing architecture for HFB-based ADC

Before beginning this subsection, it is necessary to remind that the signals $s_0[n]$, $s_1[n]$, ..., *and* $s_{M-1}[n]$ *and the analysis filters matrix* $\mathbf{H}[n]$ *used here are totally different from the ones mentioned in the previous subsection (subband HFB). This notation is here repeated to avoid complexity.*

5.3.4.1 MIMO Time-Division Multiplexing model of analysis part

In the previous section 5.3.3, a MIMO model was obtained for analysis part which led to a MIMO architecture for the HFB-based A/D converter. From another point of view, Single-Input Multiple Output (SIMO) model of analysis part (figure 5.11) includes a non-LTI operation because the associated discrete-time signals are related to two timing periods: T and MT. This phenomenon is originated from the decimation procedure (a pure time-variant operation) in the HFB structure that provides a switch between two timing periods. For eliminating the time-variant decimation operation, a MIMO model would be a good candidate. In this section, a new MIMO model is obtained without using the concept of subband filters. Again, the discrete-time model of analysis part (figure 5.14) is considered. To have a MIMO model without the concept of subband filtering, the input signal $x[n']$ is taken on parallel in the time-domain. An $M \times 1$ vector of signals $s_0[n]$, $s_1[n]$, ..., and $s_{M-1}[n]$ is defined as following:

$$\mathbf{s}[n] = \begin{bmatrix} s_0[n] \\ s_1[n] \\ \vdots \\ s_{M-1}[n] \end{bmatrix} = \begin{bmatrix} x[n'] \\ x[n'-1] \\ \vdots \\ x[n'-(M-1)] \end{bmatrix}_{n'=nM} \tag{5.27}$$

These signals may be called Time-Division Multiplexing (TDM) signals. The relationship (5.27) is better shown by figure 5.35 using polyphase structure [89, 90]. The TDM signals defined in (5.27) can be interpreted in the frequency domain as well. For instance, the Fourier transform $S_k(e^{j\omega})$ of k^{th} TDM signal $s_k[n]$ would

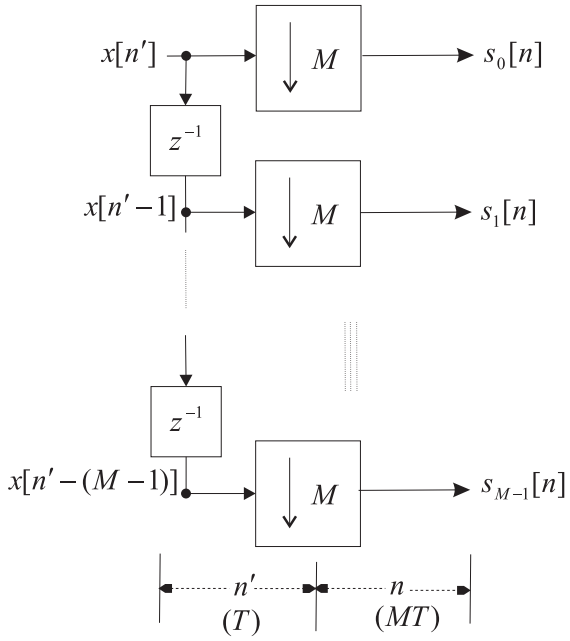

Figure 5.35. The polyphase structure showing the relation between the new-defined decimated input signals $s_0[n]$, $s_1[n]$, ..., and $s_{M-1}[n]$ and the original input signal $x[n']$.

be:

$$S_k(e^{j\omega}) = \frac{1}{M} e^{-j\frac{\omega}{M}k} \sum_{m=0}^{M-1} e^{j\frac{2\pi}{M}km} X(e^{j\frac{\omega}{M} - j\frac{2\pi}{M}m}) \tag{5.28}$$

According to (5.27), no signal or information is lost if TDM signals are considered. In fact, the input signal $x[n']$ is decomposed into M parallel signals $s_0[n]$, $s_1[n]$, ..., and $s_{M-1}[n]$ (a simple serial to parallel operation). Besides, using new decimated TDM signals, the discrete-time index n is associated with the time period of MT. Now, it is necessary to find a description for the outputs $\mathbf{x}[n]$= $[x_0[n]$, $x_1[n]$, ..., $x_{M-1}[n]]^T$ of analysis part in terms of the new-defined TDM input vector $\mathbf{s}[n]$. Invoking the equation (5.14), following relationship is obtained ($k \in \{0, 1, ..., M-1\}$):

$$x_k[n] = \sum_{m=-\infty}^{\infty} h_k[m]x[n'-m]\Big|_{n'=Mn} \tag{5.29}$$

It shows a convolution operation followed by the decimation procedure ($n' = Mn$). The integer m can be decomposed as follows:

$$m = lM + r \quad l \in \mathbb{Z},\ r \in \{0, 1, 2, ..., M-1\}$$

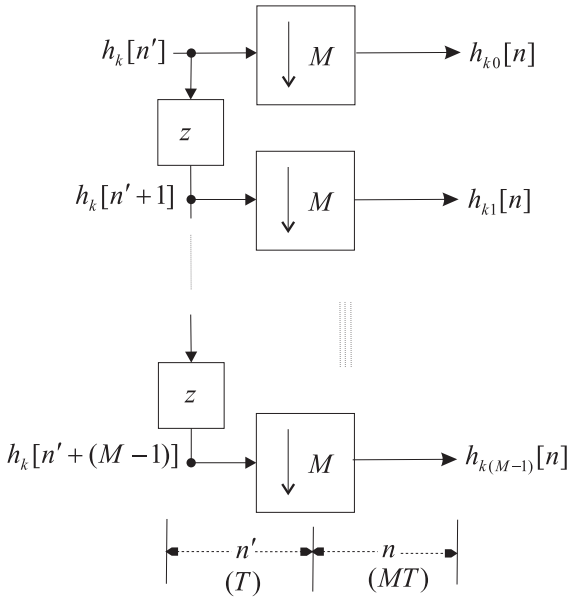

Figure 5.36. The generating model for the elements $h_{k0}[n]$, $h_{k1}[n]$, ..., and $h_{k(M-1)}[n]$ of the analysis filters matrix $\mathbf{H}[n]$. This filters are associated with the analysis filter $H_k(e^{j\omega})$ due to the k^{th} branch of HFB structure.

that $\mathbb{Z}$ represents the set of integers. Accordingly, (5.29) can be rewritten as follows:

$$\begin{aligned} x_k[n] &= \sum_{r=0}^{M-1} \sum_{l} h_k[Ml+r].x[Mn-lM-r] \\ &= \sum_{r=0}^{M-1} \sum_{l} h_k[Ml+r].x[M(n-l)-r] \end{aligned} \tag{5.30}$$

To better reformulate (5.30), M intermediate digital filters $h_{kj}[n]$ $(0 \leq j \leq M-1)$ are defined in terms of the analysis filter $h_k[n']$ as follows:

$$h_{kj}[n] = h_k[Mn+j] \qquad 0 \leq j \leq M-1 \tag{5.31}$$

Now, using (5.31) and (5.30), the relationship (5.29) may be rewritten as:

$$\begin{aligned} x_k[n] &= \sum_{r=0}^{M-1} \sum_{l} h_{kr}[l].s_r[n-l] \\ &= \sum_{r=0}^{M-1} h_{kr}[n] \star s_r[n] \end{aligned} \tag{5.32}$$

where $\star$ represents the convolution operation. Then, above relationship provides a LTI relationship between the available signals $x_0[n]$, $x_1[n]$, ..., and $x_{M-1}[n]$ (the outputs of analysis part) and the TDM input signals $s_0[n]$, $s_1[n]$, ..., and $s_{M-1}[n]$. Each digital filter $h_{kj}[n]$ is extracted from the analysis filter $h_k[n']$ according to (5.31). Figure 5.36 illustrates schematically how digital filters $h_{kj}[n]$ $(0 \leq j \leq M-1)$ are produced from the analysis filter $h_k[n']$. The presence of prediction operators z^{+1} may be incorrectly interpreted that these digital filters are not causal and nor realizable. However, the following lemma 5.3.1 shows that the digital filters $h_{k0}[n]$, $h_{k1}[n]$, ..., and $h_{k(M-1)}[n]$ are causal and stable provided that $h_k[n']$ is causal and stable.

Lemma 5.3.1. *$f[n']$ is supposed to be a causal and stable discrete-time filter. If the filters $f_0[n]$, $f_1[n]$, ..., and $f_{M-1}[n]$ $(M > 1)$ are defined as following:*

$$f_r[n] = f[n' + r]\Big|_{n'=Mn} \qquad r \in \{0, 1, 2, ..., M-1\}$$

Then, all M digital filters of $f_0[n]$, $f_1[n]$, ..., and $f_{M-1}[n]$ are stable and causal as well.

Proof. Firstly, the causality is demonstrated. $f[n']$ is causal, then:

$$f[n'] = 0 \qquad for\ n' < 0$$

According to the assumptions, $f_r[n]$ is:

$$f_r[n] = f[Mn + r] \qquad 0 \leq r \leq M-1$$

For the integers $n \leq -1$, it may be shown that:

$$n \leq -1 \ \Rightarrow \ Mn + r \leq -M + r < 0 \Longrightarrow f_r[n] = 0$$

Therefore, $f_r[n]$ is a causal discrete-time filter for $0 \leq r \leq M-1$.
Secondly, the stability of $f[n']$ (BIBO definition) provides that:

$$\sum_{n'=-\infty}^{\infty} \Big| f[n'] \Big| < L < \infty$$

According to the assumptions, we have:

$$\sum_{n'=-\infty}^{\infty} \left| f[n'] \right| = \sum_{r=0}^{M-1} \sum_{n=-\infty}^{\infty} \left| f[Mn+r] \right|$$

Thus:

$$\sum_{r=0}^{M-1} \sum_{n=-\infty}^{\infty} \left| f_r[n] \right| < L$$

As each term $\sum_{n=-\infty}^{\infty} \left| f_r[n] \right|$ for $0 \leq r \leq M-1$ is positive, then it is found that:

$$\sum_{n=-\infty}^{\infty} \left| f_r[n] \right| < L \qquad r \in \{0, 1, ..., M-1\}$$

and implies that $f_r[n]$ is a stable discrete-time filter as long as $0 \leq r \leq M-1$. □

Thus, in the case of HFB-based A/D converters, all these digital filters are realizable because the analysis filters are realistic (causal and stable). In the frequency domain, the digital filter $h_{kr}[n]$ may be described as follows (for $0 \leq k \leq M-1$ and $0 \leq r \leq M-1$):

$$H_{kr}(e^{j\omega}) = \frac{1}{M} e^{j\frac{\omega}{M}r} \sum_{m=0}^{M-1} e^{-j\frac{2\pi}{M}rm} H_k(e^{j\frac{\omega}{M} - j\frac{2\pi}{M}m}) \tag{5.33}$$

Therefore, using equation (5.32) for $0 \leq k \leq M-1$, it can be shown in the matrix format that:

$$\mathbf{x}[n] = \mathbf{H}[n] \star \mathbf{s}[n] \tag{5.34}$$

where the vector $\mathbf{x}[n]$ and the matrix $\mathbf{H}[n]$ are:

$$\mathbf{x}[n] = \Big[x_0[n], x_1[n], ..., x_{M-1}[n] \Big]^T$$

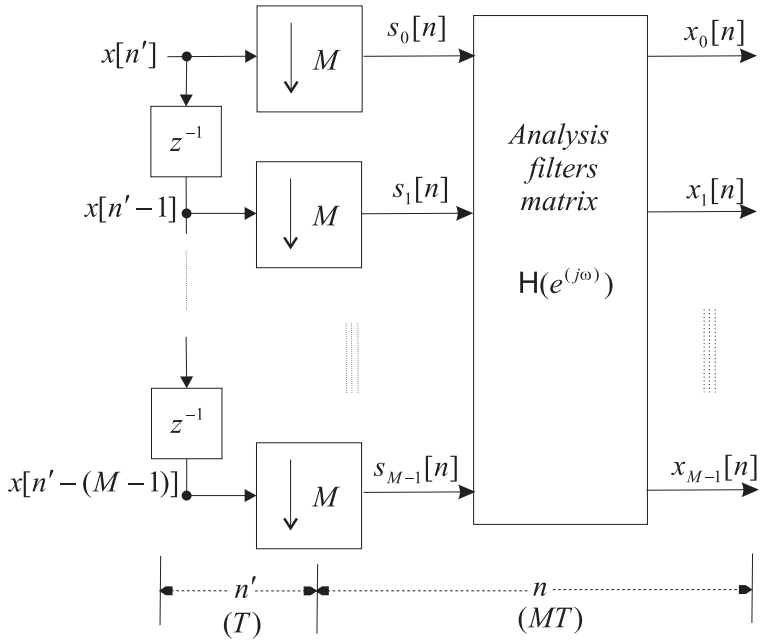

Figure 5.37. Model of analysis part of the HFB-based ADC on the basis of TDM inputs.

$$\mathbf{H}[n] = \begin{bmatrix} h_{00}[n] & h_{01}[n] & \dots & \dots & h_{0(M-1)}[n] \\ & \vdots & & \vdots & \vdots \\ & \vdots & & \vdots & \vdots \\ h_{(M-1)0}[n] & h_{(M-1)1}[n] & \dots & \dots & h_{(M-1)(M-1)}[n] \end{bmatrix}$$

$\mathbf{H}[n]$ represents an $M \times M$ matrix whose elements are the impulse response of discrete-time filters. This LTI MIMO model can be shown in the frequency domain as follows:

$$\mathbf{X}(e^{j\omega}) = \mathbf{H}(e^{j\omega})\mathbf{S}(e^{j\omega}) \tag{5.35}$$

Accordingly, an LTI MIMO model is obtained for the analysis part of HFB structure using the available $\mathbf{x}[n]$ and TDM $\mathbf{s}[n]$ signals as the output and input respectively. This linear model has been illustrated in figure 5.37. It is necessary to remind that above MIMO TDM model is totally different from the one obtained in the previous subsection 5.3.3.1 (the subband HFB). The subband model is extracted in terms of subband components of the input signal $x[n']$, but above MIMO TDM model is on the basis of time-division signal components. The ma-

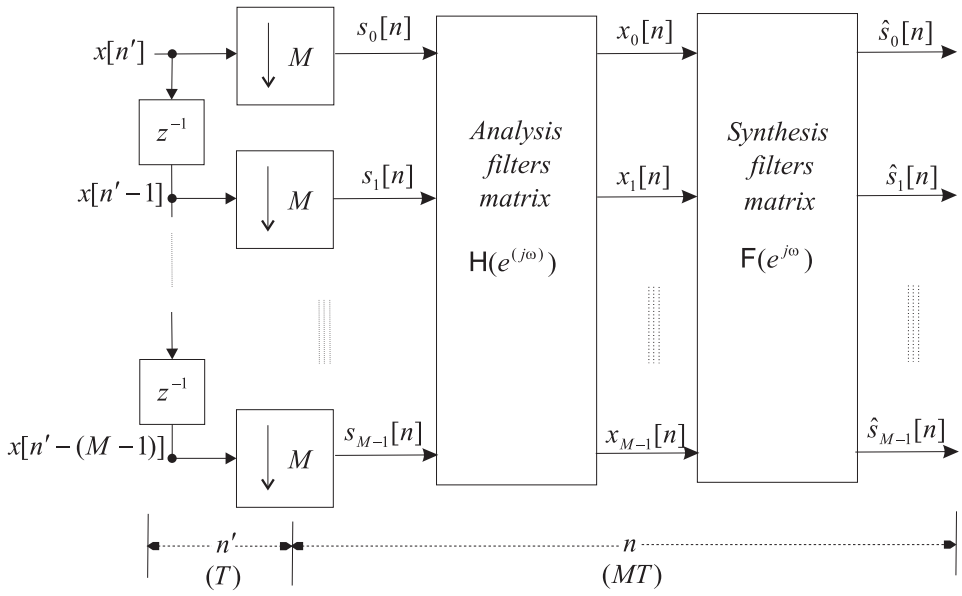

Figure 5.38. The model of TDM HFB-based A/D converter using the concept of TDM signals $s_0[n]$, $s_1[n]$, ..., and $s_{M-1}[n]$. The signals $x_0[n]$, $x_1[n]$, ..., and $x_{M-1}[n]$ are the only available signals. The synthesis filters matrix $\mathbf{F}[n]$ approximate the inverse of analysis filter matrix $\mathbf{H}[n]$ multiplied by a delay term.

trix of $\mathbf{H}[n]$ in two MIMO models are then totally different, although there is some mathematical relationship between them. The synthesis filters of the HFB-based A/D converter realized for these two MIMO models are different as well.

5.3.4.2 TDM architecture for HFB-based A/D converter

Considering the MIMO TDM model of analysis part (figure 5.37), a new multiple-output configuration for the HFB-based A/D converter may be obtained. The block-diagram of TDM HFB-based A/D converter would be exactly as the same one proposed for the subband HFB-based A/D converter (figure 5.22). However, the synthesis filters matrix $\mathbf{F}(e^{j\omega})$ is different in two MIMO HFB structures which leads only to a software difference. Thus, figure 5.22 can also be regarded schematically as the architecture of TDM HFB-based A/D converter. Substituting the TDM model of analysis part, the model of TDM HFB-based A/D converter may be obtained as shown in figure 5.38 neglecting the quantization noise. The computations of synthesis filters matrix are performed regarding to this model. For obtaining the synthesis filters matrix of FIR filters, the relationships (5.24) and (5.25)

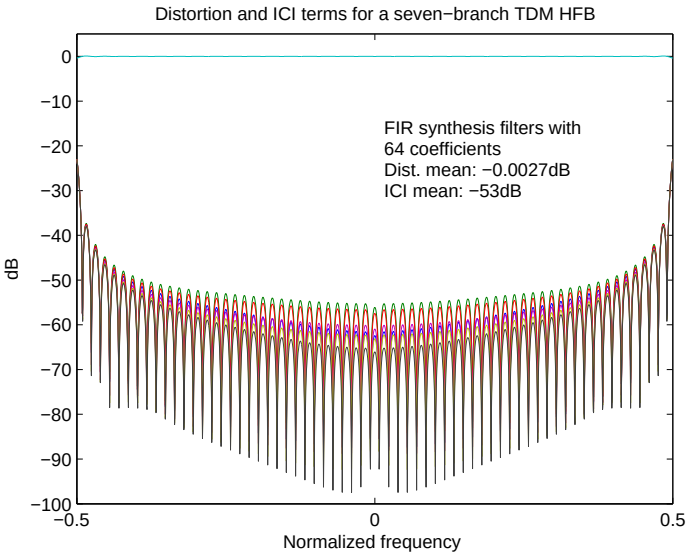

Figure 5.39. Distortion and ICI terms of fourth TDM component $s_3[n]$ in dB versus normalized frequency for a seven-branch HFB. The FIR synthesis filters consist of 64 coefficients.

may again be used. However, the elements of analysis filters matrix $\mathbf{H}(e^{j\omega})$ would be provided by (5.33). Moreover, the TDM signals are estimated in this case. TDM HFB architecture appears more interesting than the subband one since the original signal $x[n']$ may be conveniently reconstructed from the TDM signals $\mathbf{s}[n]$ by (5.27) (only an operation of parallel to serial). There are many applications such as satellite and Global System for Mobile (GSM) communications where TDM concept is used [91, 92]. The TDM HFB-based A/D converter may seem very interesting for these applications so that the concepts of software radio and intelligent spectrum sharing would be simply realizable.

The characteristics of proposed TDM HFB-based A/D converter may be summarized as follows:

1. The only available signals are $x_0[n]$, $x_1[n]$, ..., and $x_{M-1}[n]$ like the former subband architecture. However, the input signal $x[n']$ (or the analog input $x(t)$ after sampling at $\frac{1}{T}$) is directly obtained in this case without any extra computation.

2. Using above TDM model, M samples of the input signal $x[n']$ are achieved in parallel and at the same time in contrary to the classical HFB architecture where only one sample of $x[n']$ is obtained after each synthesis-filtering process.

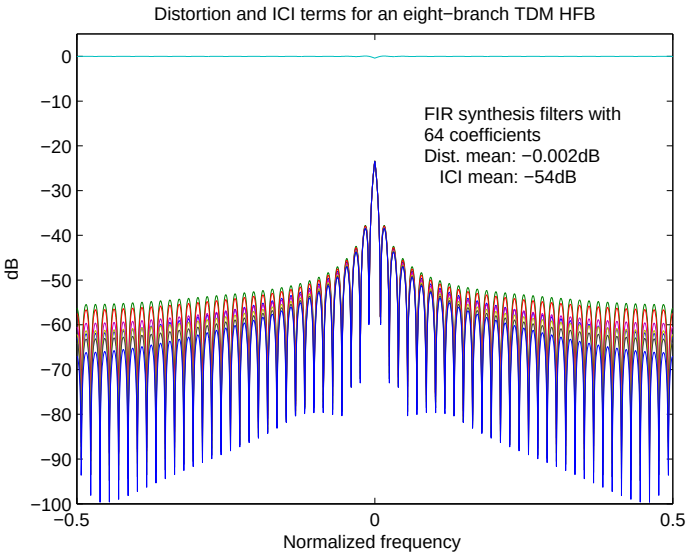

Figure 5.40. Distortion and ICI terms of fourth TDM component $s_3[n]$ in dB versus normalized frequency for an eight-branch HFB. The FIR synthesis filters include 64 coefficients.

3. There is no longer a need for upsamplers (zero-padding). All digital computations are associated with the sampling period MT like the subband HFB.

4. A Time-Division Multiple-Access (TDMA) A/D converter can be implemented using this structure. This may be very interesting for the applications such as the mobile (GSM) and satellite communications [93]. An intelligent spectrum managing would conveniently be possible in this case.

5. There is no condition for using the proposed TDM HFB architecture else the global sampling Nyquist criterion.

6. There is no decimation process between the input-output in the TDM architecture of HFB-based A/D converter. Then, multichannel blind deconvolution or automatic noise canceling techniques may be exploited to compensate the analog imperfections. This capability does not exist for the classical HFB.

5.3.4.3 Performance of TDM HFB architecture

The TDM architecture of HFB-based ADC is simulated considering the same analysis filter bank of previous sections which are simply-realizable. An RC and $(M-1)$ RLC circuits are used in the analysis filer bank for an M-channel HFB structure. The simulations are carried out in both frequency and time domains.

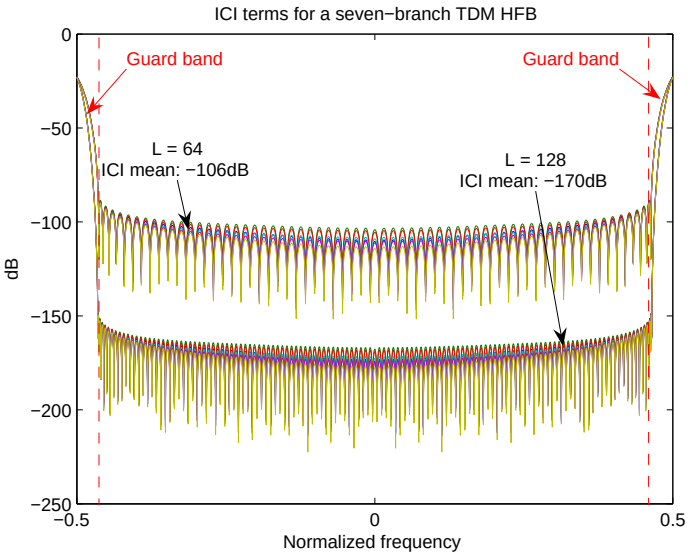

Figure 5.41. ICI terms of fourth TDM component $s_3[n]$ in dB versus normalized frequency for a seven-branch HFB. The FIR synthesis filters include 64 and 128 coefficients.

• Frequency domain

Firstly, the proposed TDM structure is simulated in the frequency domain. Supposing the seven- and eight-branch HFB structures ($M = 7,\ 8$), the distortion and ICI terms related to the TDM signal $s_3[n]$ are shown in figures 5.40 and 5.39 respectively. Considering the figures 5.40 and 5.39, it may be seen that the ICI terms degrade around the frequencies of zero and $\pm\pi$ for the even and odd number of branches respectively. This phenomenon has been observed for the various number M of branches. This poor performance of TDM HFB at low and high frequencies for an even or odd number of branches respectively may be described in terms of the condition number of related equations matrix. Referring to figure 5.45, it may be seen that the condition number is larger at low and high frequencies for the eight- and seven-branch TDM HFB structures. To improve the performance of TDM architecture, a Guard Band (GB) may be used at low or high frequencies depending on the number of branches. If the number M of branches is odd, a percentage of the spectrum related to each TDM signal is allocated to the GB at the high frequencies. It means each TDM signal would be considered at the spectrum interval $[-(1-\alpha)\pi, (1-\alpha)\pi]$ where α represents the ratio of GB to the whole spectrum 2π. In the even case, the GB is accommodated near the low frequencies. In other words, each TDM signal would include no information at the frequency

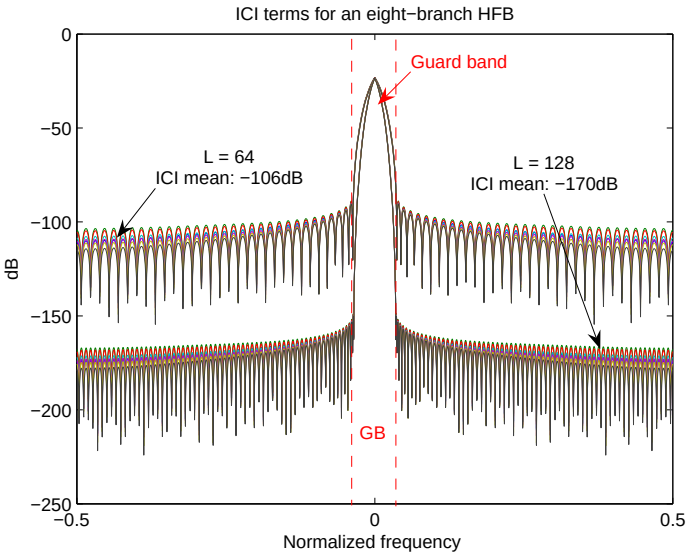

Figure 5.42. ICI terms of fourth TDM component $s_3[n]$ in dB versus normalized frequency for an eight-branch HFB. The FIR synthesis filters include 64 and 128 coefficients.

interval $[-\alpha\pi, \alpha\pi]$ if α stands again for the ratio of GB to the whole spectrum 2π. Figure 5.41 exhibits the ICI terms related to the TDM signal $s_3[n]$ of a seven-branch HFB considering a GB ratio of 7%. The FIR synthesis filters have 128 and 64 coefficients. This process has been carried out in the case of eight-branch HFB $M = 8$ considering a GB ratio of 7% as well. The related ICI terms are shown in figure 5.42. To better show the performance improvement by using GB, table 5.5 provides the distortion and ICI mean values for the seven- and eight-branch TDM HFB structures considering 64 and 128 coefficients at each FIR synthesis filter. The performance has apparently improved by using a GB ratio of 7%.

• **Time domain**

The behavior of TDM HFB structures are simulated in time-domain in this section. The eight-branch TDM HFB architecture of the previous subsection has been simulated and various signals are applied at the input. The outputs follow the input signals with a delay. It is necessary to remind that the delay would be Mn_dT in the TDM HFB case where M, n_d and T represent the number of branches, the delay considered at each branch and Nyquist sampling period respectively. It is M times larger than the delay n_dT of the classical HFB architecture. This difference is associated with the different time indices used in the reconstruction equations. In fact, the reconstruction equation (3.6) is established in reference to the decimated

Table 5.5. The ICI and distortion averages for the seven- and eight-branch TDM HFB structures considering $L = 64$ and $L = 128$.

Seven-branch TDM HFB (in *dB*)				
Guard band	0		7%	
L	ICI mean	Distortion	ICI mean	Distortion
64	-53.5	-0.0027	-106	-3.5E-10
128	-58.8	-0.0013	-169	2.1E-10
Eight-branch TDM HFB (in *dB*)				
Guard band	0		7%	
L	ICI mean	Distortion	ICI mean	Distortion
64	-54.1	-0.0023	-106	2.2E-7
128	-59.4	-0.0012	-170	2.5E-10

digital signals with the sampling period MT in the case of TDM HFB structure. For conveniently observing the performance, the spectrum of error signal is shown in figures 5.43 and 5.44. Figure 5.43 shows the error spectrum when the input is a sinusoidal signal at the frequency $\omega_\circ = \frac{0.5\pi}{8T}$. For this sinusoidal input, no signal appears at the guard bands of eight TDM components. A parallel to serial operation has been applied to the TDM outputs of TDM HFB architecture. It enables us to reconstruct the original input signal through the TDM components. To better compare the performances, the spectrum of error signal is demonstrated for both classical and TDM HFB structures in this figure. An oversampling ratio 7% has been considered for the classical HFB. Similarly, a GB ratio of 7% has been assumed in the design of synthesis filters for the TDM HFB. It may be seen that the TDM HFB exhibits clearly a better performance than the classical HFB for this sinusoidal input. An important signal appear at the oversampling spectral area for the classical HFB so that a post-filtering is necessary to omit this part of output signal. For example, Signal-to-Noise Ratio (SNR) at the output of classical HFB structure remains at $49dB$ without the post-filtering. If the oversampling spectral area is filtered out, the output SNR would be $73dB$ for the classical HFB. In return, no signal appears at the guard bands of TDM HFB structure for this sinusoidal input signal. The TDM HFB provides a SNR of $123dB$ in this case which is $50dB$ better than the classical architecture.

Then, two important aspects may be noted in this case. Firstly, the classical HFB

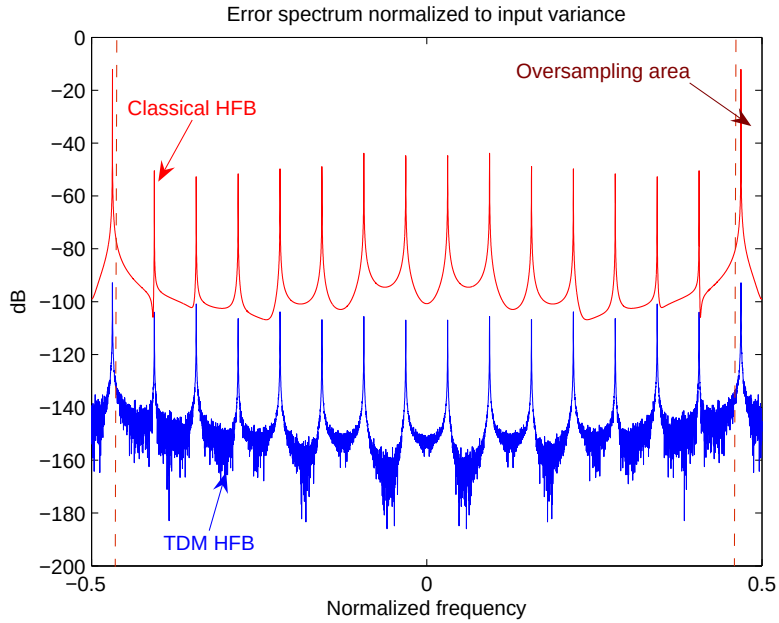

Figure 5.43. The error spectrum associated with the TDM (blue) and classical (red) HFB structures. Both structures consist of eight branches and use 64 coefficients for the FIR synthesis filters.

structure needs a post-filtering process to filter out the oversampling spectral area even no input signal is present at the oversampling spectral band. The TDM HFB does not need any post-filtering if the analog input does contain no signal at the guard bands. Secondly, the TDM HFB provides a much higher SNR than the classical one for this sinusoidal input. Figure 5.44 provides a comparison between the TDM and classical HFBs supposing a chirp input signal. The input chirp sweeps the spectrum at the interval $[0, \frac{\pi}{T}(1-\alpha)]$ that α is supposed to be the oversampling ratio of 7% ($\alpha = 0.07$). As figure 5.44 shows, the oversampling area has not been filtered out for the classical HFB neither the GB peaks due to the TDM HFB. Neglecting the oversampling and GB spectral regions, the classical and TDM architectures provide the output SNR of $63dB$ and $91dB$ respectively. However, the output of the classical HFB has to be filtered to the frequency interval $[-(1-\alpha)\pi, (1-\alpha)\pi]$. The output of each branch of the TDM HFB is to be post-filtered with the same filter. Thus, the TDM HFB would need M digital filtering process applied to the outputs of M branches. Finally, the simulations in time domain exhibit that the TDM HFB architecture may lead to a better perfor-

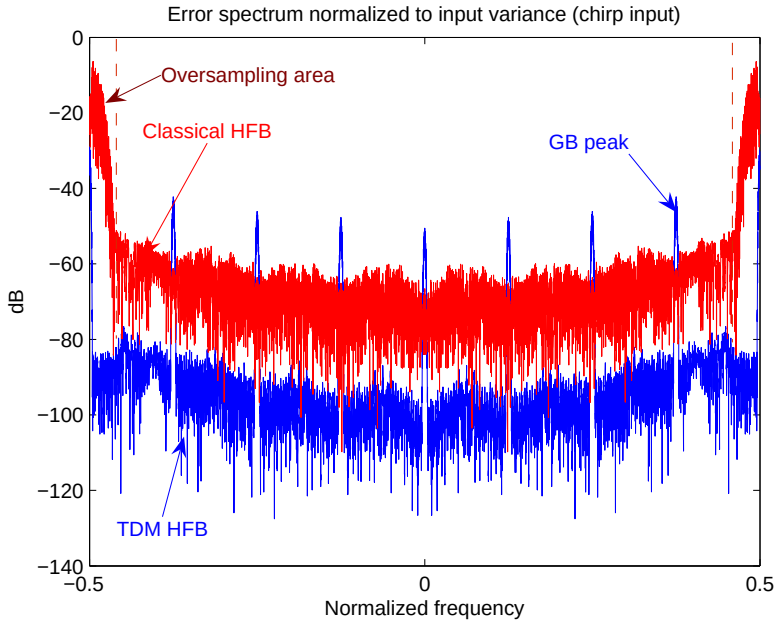

Figure 5.44. The error spectrum associated with the TDM (blue) and classical (red) HFB structures. Both structures include eight branches and use 64 coefficients for the FIR synthesis filters.

mance than the classical one in the absence of realization errors with respect to the ICI (versus aliasing in the classical case) interference terms.

• Computational complexity

Like the subband HFB architecture, M^2 digital filters construct the synthesis filter bank of the TDM HFB structure compared to M digital filters required in the classical architecture. The TDM HFB provides M output samples at each time instant (refer to figure 5.38). At each cycle, an output sample $\widehat{x}[n']$ is obtained through the classical HFB architecture, but M output samples $\{\widehat{x}_0[n], ..., \widehat{x}_{M-1}[n]\}$ are provided by the TDM one. For comparing the number of multiplications at each cycle, the results of the section 5.3.3.3 may be reused since the structure of TDM HFB includes a matrix of M^2 digital filters like to the subband HFB. Then, the TDM HFB affects M^2L multiplications at each cycle where L represents the length of each FIR synthesis filter. The classical HFB needs ML multiplications at each cycle. However, considering the number of output samples obtained from each architecture, both the classical and TDM HFBs make ML multiplications

per output sample. The TDM HFB may seem more interesting than subband one from this point of view, because no digital calculation is required to reconstruct the original input signal $x[n']$ from the TDM output components but only a parallel to serial operation. A comprehensive comparison between these various HFB architectures is presented in the section 5.4.

5.3.4.4 Sensitivity of TDM HFB architecture

It was mentioned in the previous sections that the TDM HFB architecture includes M^2 digital filters in the synthesis stage. The classical HFB would have only M digital synthesis filters. Then, the relative sensitivity S_f of synthesis filter $f[n]$ (section 3.3) may not be a good candidate for comparing the sensitivity of these structures. However, the condition number of analysis matrix may be considered as a suitable measure for showing the sensitivity to the analog imperfections as it was described in section 3.3. Figure 5.45 shows the condition number of analysis matrices versus the normalized frequency for the eight- and seven-branch TDM structures. It is reminded that there is an $M \times M$ analysis matrix associated with each frequency point in the TDM case (refer to section 5.3.4.2). Observing

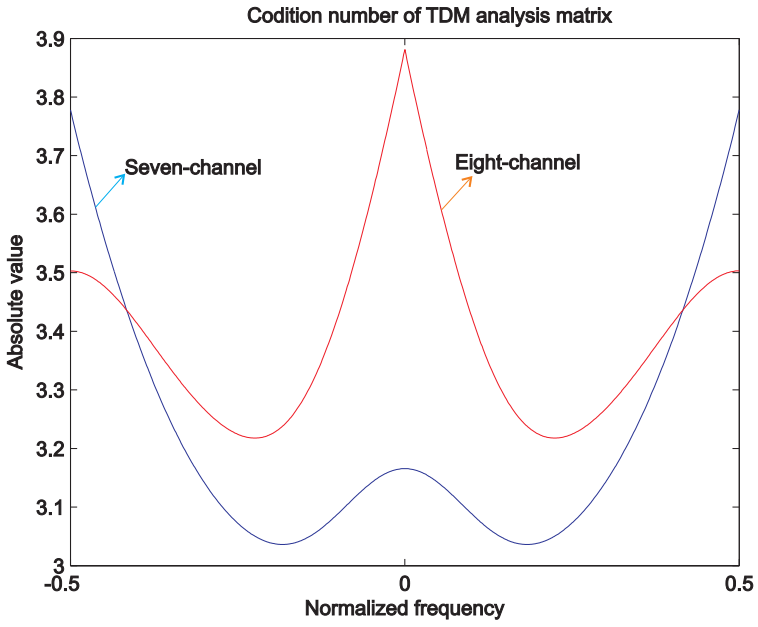

Figure 5.45. The condition number of analysis matrices versus normalized frequency for seven- and eight-branch TDM HFBs are shown in blue and red respectively.

figure 5.45, it is firstly found that the average value of condition number for the TDM HFB is so smaller than the condition number associated with the classical HFB (refer to section 3.2.4 and figure 3.12). It was mentioned that the sensitivity of the solution (here the synthesis filters) to the deviations of the analysis matrix coefficients (or the realization errors in this case) is proportional with the square of related condition number (section 3.3.2.1). Then, the TDM HFB would be less sensitive to the realization errors than the classical one. On the other hand, the sensitivity of the classical HFB architecture increases largely with the oversampling ratio because of the exponential growth of the related condition number (see figure 3.12). In the TDM case, the guard band (equivalent factor for the oversampling band) has no effect on the condition number because it causes no modification in the coefficients analysis matrix. Considering the guard bands, just the respective equations of perfect reconstruction are neglected to avoid the non-conformity of these equations. The figure 5.45 conforms also with the definition of guard bands for the even and odd number of branches (M) (section 5.3.4.3). It is seen that the condition number is larger at either high frequencies or lower frequencies for odd and even number M of branches respectively.

To better study the sensitivity to the realization errors, the output resolutions may directly be compared in time domain supposing different values of analog imperfections. For this purpose, both the classical and HFB structures are simulated in the time domain. The same eight-branch HFB architectures used in the previous section are considered. Both the oversampling and GB ratios are considered 7% for the classical and TDM HFBs respectively. To observe the effects of realization errors, all electronic elements (R, C and L) included in the analysis filter bank are considered with a Gaussian profile. The standard deviation of Gaussian distribution is employed for representing the analog imperfections. Sweeping the analog imperfections at the interval $[0, 10\%]$, the simulations are repeated for 1000 trials of each value of realization error. Each trial of realization errors is mutually-independent versus the other trials. The output resolution of HFB structures are used for comparison. Firstly, the input is assumed to be a sinusoidal signal at the frequency $\omega_\circ = \frac{0.5\pi}{8T}$. Figure 5.46 shows the output resolution (in bits) of the classical and TDM HFBs versus the realization errors. If Post-Filtering (PF) is applied for eliminating the oversampling and GB spectral areas in the classical and TDM

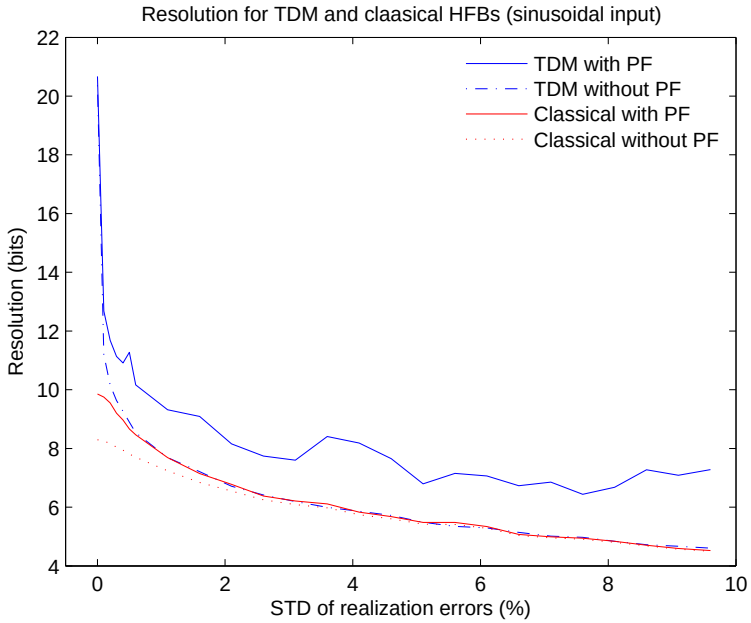

Figure 5.46. The output resolution of the classical (in red) and TDM (in blue) HFB architectures versus the relative realization errors. A sinusoidal signal has been applied to the input and Post-Filtering (PF) is considered for eliminating the oversampling and GB areas for the classical and TDM cases respectively.

cases respectively, the TDM HFB architecture is associated with a performance of 3 bits better than the one related to the classical HFB in the presence of realization errors. It means that the TDM HFB is less sensitive than the classical one to the realization errors in the case of sinusoidal input. In other words, the SNR at the output of this eight-branch TDM HFB is about $20dB$ better than the one related to the classical HFB. If GB spectral areas are not filtered out in the TDM HFB, it leads to the same resolution that a classical HFB may provide with eliminating the oversampling band. This shows that the TDM HFB architecture may provide at worst case (meaning without PF) the same performance that the classical one. To have a comparison in the whole spectrum, a chirp input sweeping the frequency interval $[0, \frac{\pi}{T}(1-\alpha)]$ is applied to both the TDM and classical structures. α stands for the oversampling ratio of 7% ($\alpha = 0.07$). Like to the sinusoidal case, a similar procedure is applied to obtain the sensitivity to the realization errors. Figure 5.47 illustrates the output resolution of TDM and classical HFBs versus the STandard Deviation (STD) of realization errors. For the chirp input signal, the TDM HFB

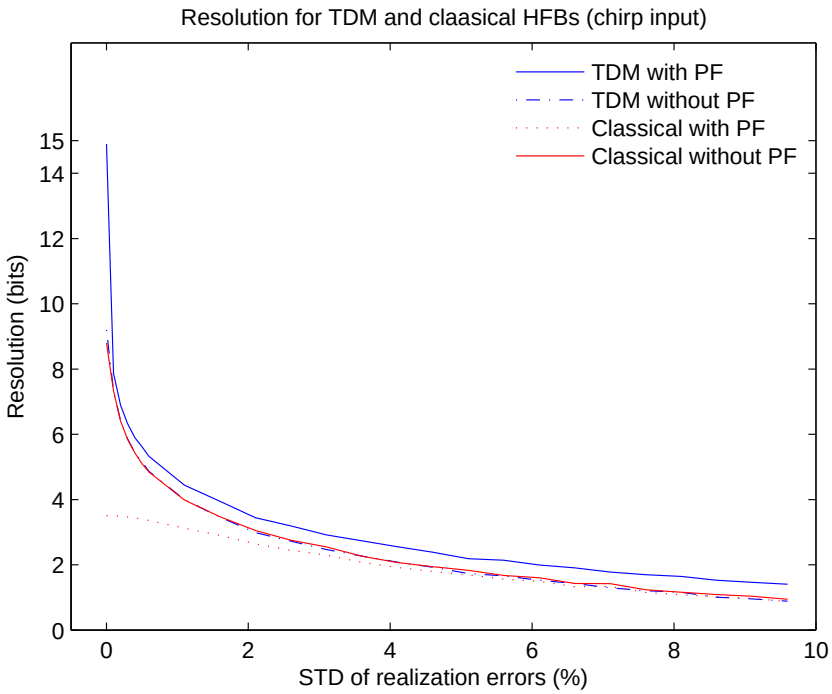

Figure 5.47. The output resolution of the classical (in red) and TDM (in blue) HFB architectures versus the relative realization errors. A chirp signal is considered as the input and Post-Filtering (PF) is considered for eliminating the oversampling and GB spectra for the classical and TDM HFBs respectively.

architecture exhibits a better performance of about 1 bit in the presence of analog imperfections than the classical HFB. It is reminded that the performance of TDM HFB is much better than the one related to the classical HFB in the absence of realization errors (refer to the figure 5.47 at the STD of errors equal to zero). Another interesting result may be deducted from these two simulations. According to figures 5.46 and 5.47, the TDM HFB may provide a performance approximately equal to the classical HFB even if no Post-Filtering (PF) is considered to eliminate the GB spectral areas. However, if the oversampling spectral area is not post-filtered out in the classical HFB, the performance degrades so much.

5.4 Summary and discussion

In this chapter, several new HFB architectures have been offered for realizing the HFB-based A/D conversion. It is shown that a blind method such as the blind

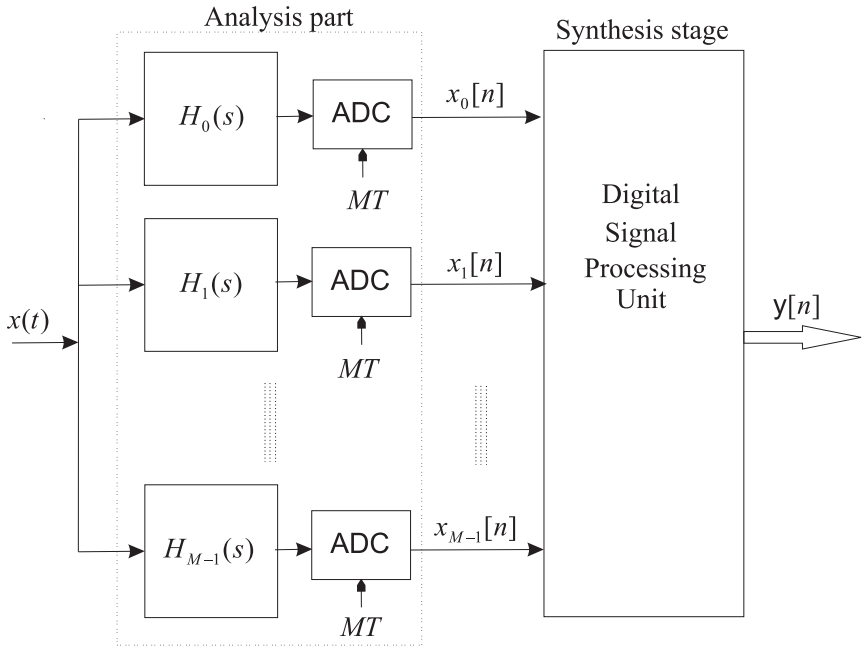

Figure 5.48. The general architecture for HFB-based ADC. The output $\mathbf{y}[n]$ may include either one or a vector of sequences depending on the type of architecture. The synthesis stage may also consist of either a vector or a matrix of digital filters.

deconvolution techniques is necessary to estimate the realization errors of the analog analysis filter bank, since the classical HFB is much sensitive to these analog imperfections. On the other hand, the mentioned blind methods cannot directly be applied to the classical HFB A/D converters because of undersampling process existing at each branch between the input and output. The proposition of new HFB architectures has concentrated on two objectives. Firstly, a new HFB architecture may result in a less sensitivity to the realization errors than the classical HFB. The second aim is to provide an LTI relationship between the input and output of new HFB architecture without any undersampling so that a blind deconvolution technique may be applicable to estimate or compensate the realization errors (refer to section 5.1).

The four types of (classical, two-stage, subband and TDM) HFB architectures have the same analysis part. But, the difference is in the digital part which constitutes the synthesis stage. In other words, a general diagram of an HFB-based ADC may be considered independent of its architecture type as shown in figure 5.48. The synthesis stage of the general HFB-based ADC may represent either a matrix or

Table 5.6. The comparison of all four types of HFB architectures in reference to the applicability of a blind estimation technique to correct the analog imperfections.

Applicability of estimation techniques to the outputs				
Technique	The type of M-branch HFB Architecture			
	Classical	Two-stage(a)	Subband	TDM
Decorrelation technique	No	No	Yes	Yes
Blind deconvolution	No	No	Yes	Yes
(a) Anti-aliasing filter bank is regarded.				

a vector of FIR digital filters for the subband , TDM or classical and two-stage architectures respectively. Anyway, they are different only in the digital signal processing unit (software) and then realizable on the same hardware platform. This may be very attractive for realizing the ideas such as the Software-Defined Radio (SDR) systems for which all the manipulations including frequency management would be implemented in the digital part. Finally, the general HFB-based A/D converter may be a good candidate for implementing the SDR systems as well as the future telecommunication services.

However, the four different types of HFB architectures may be compared in reference to various parameters. Table 5.6 compares the four (classical, two-stage, subband and TDM) HFB architectures in terms of the possibility to exploit the blind techniques for estimating or possibly compensate the realization errors. The TDM and subband HFB structures are the only ones which provide an LTI relationship without any decimation between the related inputs and outputs. The HFB architectures are different only in the synthesis stage as it was mentioned. The various parameters of synthesis stages are compared for the proposed HFB architectures versus the classical one in table 5.7. The two-stage exhibit much more sensitivity to realization errors than the classical one. On the other hand, it cannot provide a minimum acceptable performance when no oversampling process is used. Accordingly, the classical HFB is in practice preferred to the two-stage HFB architecture. The other proposed TDM and subband HFBs exhibit a group of interesting characteristics. Although a subband or TDM M-branch HFB structure includes M^2 FIR synthesis filters compared to the M ones required for the classical HFB, but the computations per each output sample are the same for

Table 5.7. The comparison of all four types of HFB architectures in terms of the parameters of synthesis stage.

Comparison of HFB architectures in terms of synthesis stage characteristics				
Parameter	The type of M-branch HFB Architecture			
	Classical	Two-stage	Subband	TDM
Number of filters	*M*	*M+1*	*MxM*	*MxM*
Number of multiplications/output sample	*ML*	*ML+La*	*ML*	*ML*
Analysis matrix size	*MNxMN*	*MNxMN*	*MxM*	*MxM*
Constraint for design	oversampling band	oversampling band	guard band	guard band
Zero-padding	needed	needed	not needed	not needed
Delay length	*L/2*	*L/2 + La/2*	*ML/2*	*ML/2*
Model for designing FIR filters	SISO	SISO	MIMO	MIMO
Output-Input relation	non-LTI	non-LTI	LTI	LTI

M: Number of HFB branches
N: Number of frequency points used in the design phase
L: Length of synthesis filters
La: Length of anti-distortion digital filter

Table 5.8. The comparison of the classical, subband and TDM HFB architectures in terms of output resolution (in bits) considering a sinusoidal input located at the middle of first subband.

Output resolution (in bits) for a sinusoidal input			
Realization errors (%)	The type of 8-branch HFB Architecture		
	Classical	Subband	TDM
0%	9.9	10.5	21
1%	8	10	9.8
5%	5.8	7	8

all of them. This is originated from MIMO architecture of TDM and subband HFBs. On the other hand, the design phase for the classical HFB is associated with inverting a huge analysis matrix particularly for large number of branches. In practice, the TDM and subband HFB architectures are much more compatible than the classical HFB with increasing the number M of branches. Finally, the synthesis stage of subband and TDM HFBs provide M output samples at each cycle. The output of TDM HFB may directly provide the original input signal. Nevertheless, the original input can be reconstructed from the outputs of subband structure through a reconstruction stage (figure 5.24). The outputs of subband HFB are corresponding to the subband components of the original input which

Table 5.9. The comparison of the HFB architectures in reference to the output resolutions supposing a chirp input signal sweeping the first subband.

Output resolution (in bits) for a chirp input			
Realization errors (%)	The type of 8-branch HFB Architecture		
	Classical	Subband	TDM
0%	9.6	10.1	17
1%	7.2	8.0	8.6
5%	5.3	6.1	6.6

may be interesting in the FDMA systems. The TDM and subband HFBs not only are interesting regarding to their possibility to use blind estimation techniques, but also exhibit a better performance compared to the classical HFB. Tables 5.8 and 5.9 list the output resolutions considering a sinusoidal and a chirp input signal respectively. The sensitivity of TDM and subband HFBs also appears to be less than the one related to the classical HFB in this case.

Finally, it may be seen that the high sensitivity of HFB architectures necessitates to consider a compensation mechanism to provide an acceptable output resolution in the presence of realization errors of analog part of the system (analysis part) (see figure 5.48).

Chapter 6

Conclusion

Each problem that I solved became a rule which served afterwards to solve other problems.
- Rene Descartes

6.1 Brief survey on the results

This thesis deals with the HFB-based A/D converters. As the practical implementation of HFB-based ADCs generally encounters the important obstacle of high sensitivity to the realization errors, efforts have been made in this thesis to more profoundly study this problem and to propose a group of possible solutions. To exclusively focus on the main problem, namely the sensitivity of the classical HFB structures to the realization errors, the quantization noise has been neglected in this thesis report unless the opposite is indicated. Considering he constraints of high frequency electronic circuits, simply-realizable first- and second-order analog filters have been used in the analysis filter bank. For convenience, the synthesis filters are implemented by FIR digital filters as well. To better analyze the HFB architecture, the design phase has been formulated in the matrix form. The origins of high sensitivity to the realization errors have been shown to associate with the related analysis matrix. It has been shown that the oversampling process causes a large increase in the sensitivity, although it provides a better performance in the absence of analog imperfections. It is also shown that there is always an optimal

oversampling ratio depending on the number of branches and analysis filter bank. The optimum value for an eight-channel HFB using first- and second-order analysis filters is about 7%.

The optimization technique of TLS has been used as a candidate for reducing the sensitivity of LS solution. TLS led to no improvement because the design of FIR synthesis filters of HFB structures is a non-zero residual problem. It has been shown that the classical HFB architecture with practical FIR synthesis filters may not implement the real A/D converters unless a compensation technique is considered to reduce or eliminate the high sensitivity to the analog imperfections. To aim at an HFB architecture compensated in reference to the analog imperfections, the capability of estimation methods have been reviewed in estimating the realization errors of general analog circuits. For estimating the realization errors of analog circuits, two techniques have been proposed and discussed. Firstly, a SOS-based model of analog imperfections has been proposed for estimating the relative imperfections. It appears more useful when the transfer function of LTI circuit includes only one erroneous coefficient. Blind equalization methods have been tried for estimating analog imperfections as the second way. SEA algorithm has been used in the simulations because of its suitable convergence properties. Since the SEA algorithm uses HOS parameters, it is useful only for non-Gaussian signals. Besides, it needs a priori the structure of unknown LTI circuit (or the order of analog circuit). Computations burden is much more than SOS model as well. However, the SEA algorithm provides a better precision of estimation than the proposed SOS-based model. These two estimation techniques are acceptable in the cases where the Nyquist criterion holds. Both the proposed estimation methods can not directly be applied to the HFB-based A/D converters because of time-varying characteristics existing at each branch of HFB.

Then, several new (two-stage, subband and TDM) HFB architectures have been offered for realizing the HFB-based A/D conversion to result either in less sensitivity to the realization errors or in an LTI relationship between the input and output. The only difference of the four (classical, two-stage, subband and TDM) HFB structures is in the digital part which constitutes the related synthesis stage. This could be very interesting for the applications such as Software-Defined Radio (SDR) systems to include a digital manipulation of the spectrum. The two-stage

HFB architecture provides a better performance than the classical HFB in the absence of realization errors (considering an additional anti-distortion filter). Nevertheless, the two-stage HFB is much more sensitive to the realization errors of analysis filter bank than the classical HFB architecture. Besides, a blind method can be applied only to the anti-distortion stage. Therefore, the two-stage HFB-based A/D converters are not practically preferable in reference to the classical ones. The TDM and subband HFB structures not only are less sensitive to the realization errors than the classical one, but also provide an LTI relationship between the inputs and outputs. Then, a blind method such as blind deconvolution technique may be applied to TDM and subband HFBs. It results in a capability to estimate the analog imperfections and hence to correct them. Some possible HFB architectures in which the analog imperfections may be estimated and compensated are discussed in the next section 6.2.

6.2 Perspectives

The high sensitivity of HFB architecture to analog imperfections appears as an important challenge in the realization of HFB-based ADC. This problem may be handled by two groups of solutions: indirect and direct correction. The direct methods are only applicable for MIMO architectures such as the subband and TDM HFBs which provide an LTI relationship between the outputs and inputs. Applying a blind equalization or decorrelation method to the output vector, the corrected input samples are directly obtained. For indirect correction, an estimation algorithm may be used to obtain the realization errors or the real transfer functions associated with the analysis filter bank. Having the real spectral parameters of analysis filter bank, the design phase of FIR synthesis filters can be again established to correct the previous synthesis stage. Thus, a new (compensated) synthesis filter bank would be available for using in the HFB architecture. Invoking the mentioned methods, some compensated HFB architectures are proposed in this section. On the other hand, two types of algorithms may be used to correct the HFB architectures: Automatic Noise Canceling (ANC) algorithms and blind deconvolution methods. The ANC algorithms are a type of decorrelation methods [70]. The blind deconvolution methods may be classified for two types

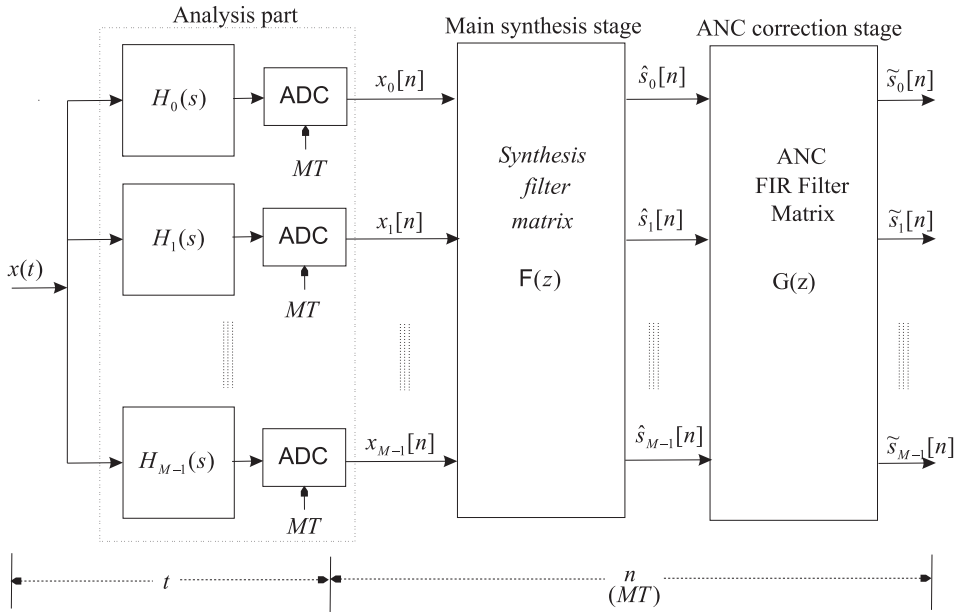

Figure 6.1. The HFB ADC compensated by ANC algorithm to correct the analog imperfections. The synthesis stage may be either the TDM or subband architecture. The ANC correction stage $G(z)$ is adaptively adjusted by the related outputs.

of LTI systems: Single-Input Single-Output (SISO) and Multiple-Input Multiple-Output (MIMO). The case of SISO has been used in chapter 4. A short survey on the deconvolution techniques for SISO LTI systems may be found in appendix D. However, for the HFB architectures, the blind deconvolution of MIMO LTI systems is applicable because of MIMO structures of the TDM and subband HFBs. The MIMO blind deconvolution belongs to the Blind Source Separation (BSS) techniques associated with the convolutive mixtures [87].

• Direct compensation of analog imperfections

Using ANC algorithm, the original input samples may directly be estimated. Then, it does not require to estimate the real analysis filter bank. The compensation procedure is intrinsically integrated in the ANC algorithm. This method is applicable only to the TDM or subband HFB architectures. The prerequisite condition for using an ANC algorithm is that the vector of input sequences are mutually uncorrelated. In the TDM HFB case, it means that the original analog input is a second-order white process. Figure 6.1 shows the HFB-based ADC architecture compensated by ANC algorithm. The inputs $\{\widehat{s}_0[n], \widehat{s}_1[n], ..., \widehat{s}_{M-1}[n]\}$ of ANC

procedure may be the TDM or subband components of the original input $x(t)$ depending on the TDM or subband synthesis stage respectively. The ANC filter matrix $G(z)$ is an $M \times M$ matrix of FIR filters whose diagonal elements are identity ($\delta(n - n_d)$). $G(z)$ is adaptively modified according to the output signals $\{\widetilde{s}_0[n], ..., \widetilde{s}_{M-1}[n]\}$. Figure 6.2 demonstrates schematically the structure of ANC filter matrix. The TDM or subband components of input have to be uncorrelated

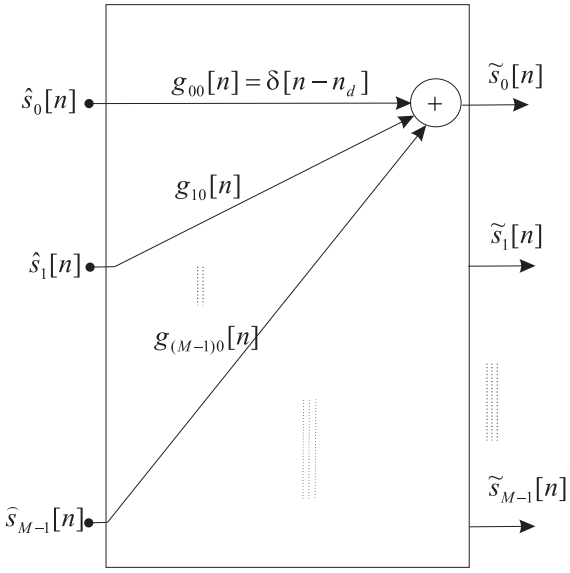

Figure 6.2. The general structure of ANC algorithm where $g_{ij}[n]$ is an FIR filter representing the $(i, j)^{th}$ element of ANC filter matrix $G(z)$ and is adaptively modified.

depending on the type of HFB architecture. The ANC algorithm can even improve the output resolution in the absence of any realization errors because the ICI terms appear as noise signals at each branch.

The proposed HFB structure may lead to a simple two-branch ADC as shown in figure 6.3. It is associated with a simplified TDM architecture when $M = 2$. This two-branch ADC uses only one analog filter and the other analysis filter has been supposed to be an all-pass (unity) filter for more convenience. Accordingly, one TDM component $s_0[n]$ is available without any ICI interferences. To obtain the second TDM component $s_1[n]$, the simplified synthesis filter matrix including only two digital filters $F_{10}(z)$ and $F_{11}(z)$ are used. At last, to reject the residual interferences of first TDM component in the estimated second TDM component $\widehat{s}_1[n]$, an ANC stage is used including only one adaptive FIR digital filter $G_1(z)$. According to the ANC algorithm, $G_1(z)$ would be adaptively adjusted by the related output so that the contribution of first TDM component $s_0[n]$ in the second output $\widetilde{s}_1[n]$

is minimized. The final output resolution would depend on the performance of

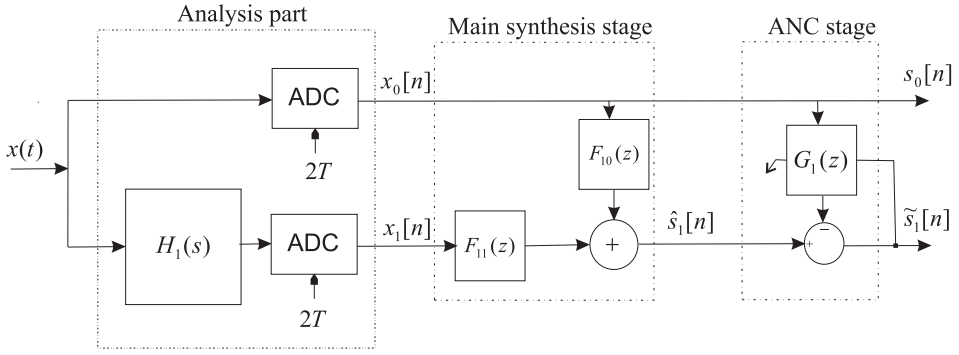

Figure 6.3. A simplified two-branch HFB-based ADC architecture based on the TDM architecture to which the ANC algorithm is applied. The HFB structure includes only one analog filter $H_1(s)$ and one ANC FIR digital filter $G_1(z)$.

ANC algorithm. It depends on many factors such as the length of ANC FIR filter and performance of adaptive noise canceling algorithm.

The estimation of input signals may alternatively be realized by a BSS algorithm as well. In fact, an ANC algorithm may be assumed as a special case of BSS methods. Figure 6.1 may be considered as the general structure of HFB-based ADC compensated by the BSS techniques if the ANC FIR filter matrix $G(z)$ is substituted with a BSS FIR filter matrix. In the BSS case, an FIR filter matrix is again used but the adaptive correction algorithm is a BSS technique. The BSS techniques often employ Higher-Order Statistics (HOS). For this purpose, the original input is generally assumed to be a non-Gaussian white signal.

• Compensation by estimating the real analysis filter bank

There is another possibility to use the aforementioned ANC and BSS techniques for estimating the real transfer functions of analysis filter bank. This idea is schematically demonstrated in the figure 6.4. The diagram shows a feedback path for correcting the synthesis filters. In this method, all types of HFB architectures may be accommodated in the main synthesis stage. The output $y[n]$ may be one or a vector of signal sequences according to the main synthesis architecture. The estimation block may provide the real spectral parameters of analysis filter bank which are useful to correct the analog imperfections.

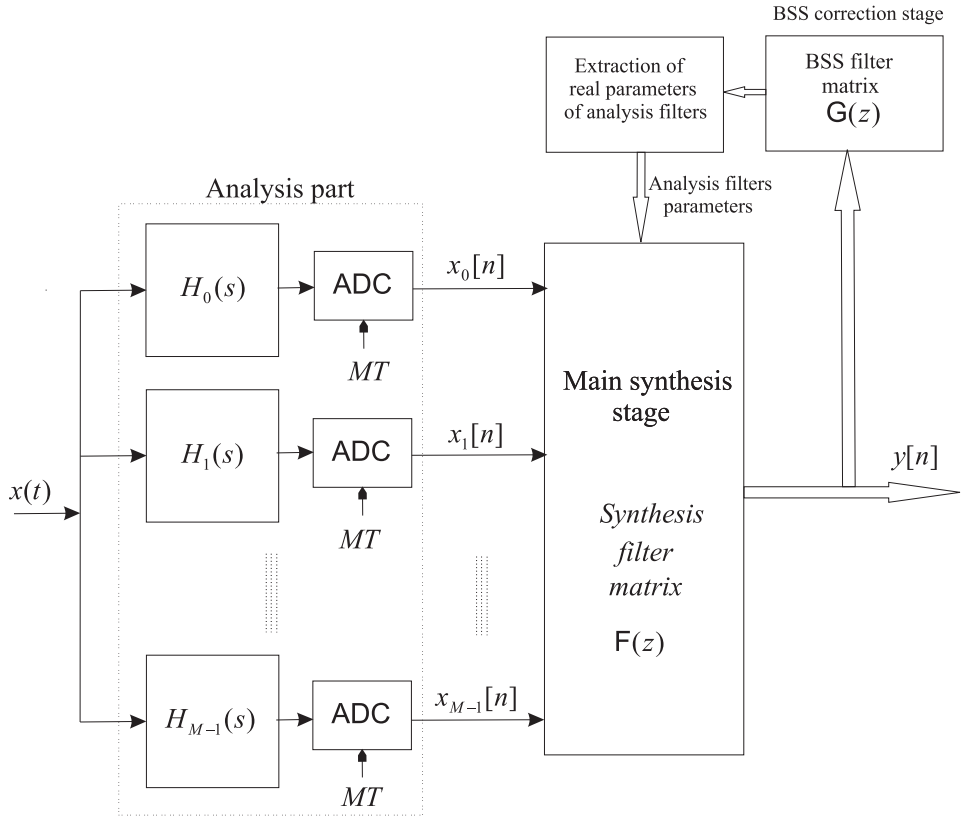

Figure 6.4. The HFB-based ADC architecture with a compensation block. A blind technique used to estimate the real analysis filter bank. Applying the estimated analysis filter bank, the synthesis filter bank is corrected.

Appendix A

Frequency representation of HFB-based A/D converters

A.1 Introduction

Perfect Reconstruction (PR) equations and their extensions are traditionally used for designing the HFB-based A/D converters. Hence, the comprehension of PR equations and their conditions would be very essential in order to either reduce the computational complexity or prevent from more round-off or calculation errors appearing through the exhaustive computations of HFB implementation such as matrix inversion. Accordingly, we present a new formulation of PR equations and its conditions in this appendix. Then, the symmetry of PR equations is discussed and we show that only one out of M parts of the whole spectrum is required to be considered for the design phase of the M-branch HFB structure.

A.2 Frequency Analysis of maximally-decimated Hybrid Filter Bank ADC

The main focus is on the structures of HFB-based A/D converters in this section (see figure 2.6). The quantization noise of A/D converters is neglected to highlight the interference and distortion terms appearing through the HFB architectures. The PR equations provide a relationship between the output and input of HFB

so that both the analysis and synthesis filter banks are incorporated. Then, one of the analysis or synthesis filter banks may be designed having a priori the other one provided that the PR equations are available.

Neglecting the nonlinear effects of A/D converter such as quantization noise and the effects of sample-and-hold circuits at each channel, an HFB ADC may be simplified as illustrated in figure A.1 (refer to chapter 3). Observing the Nyquist criterion for global system, the analog input $x(t)$ is supposed to be limited in the frequency domain between $[-\frac{\pi}{T}, \frac{\pi}{T}]$ where T represents the global sampling period so that $\Omega_\circ = \frac{2\pi}{T}$ stands for the Nyquist sampling rate.

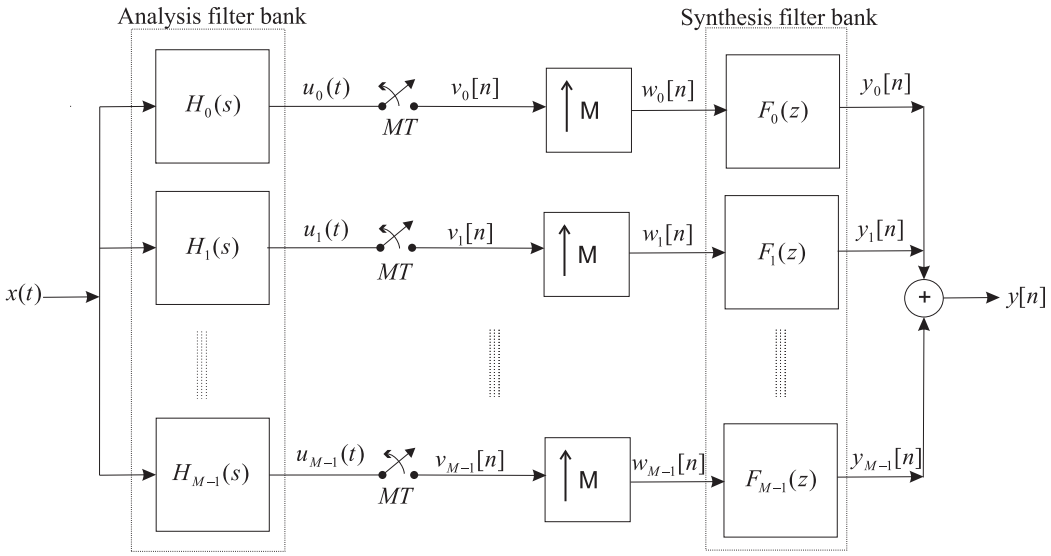

Figure A.1. Simplified HFB-based A/D converter considering the maximally-decimated architecture. Neglecting the Quantization process, each A/D converter has been substituted by a simple sampler at $\frac{1}{MT}$.

According to the structure of figure A.1, the input signal $x(t)$ after being filtered and sampled can be represented as following:

$$U_k(j\Omega) = X(j\Omega) \cdot H_k(j\Omega) \qquad k = 0, 1, \ldots, M-1 \tag{A.1}$$

$$V_k(e^{j\omega}) = \frac{1}{MT} \sum_{p=-\infty}^{+\infty} U_k(j\frac{\omega}{MT} - j\frac{2\pi}{MT}p) \tag{A.2}$$

that $U_k(j\Omega)$ and $V_k(e^{j\omega})$ stand for the spectral representation of $u(t)$ and $v[n]$ respectively. It is worth to point out that the input signal $X(j\Omega)$ is modulated by

an LTI system ($H_k(j\Omega)$) at each branch, and then down-sampled at $\frac{1}{MT}$. The following spectral description may be obtained considering the interpolator operation (up-sampling):

$$W_k(e^{j\omega}) = V_k(e^{jM\omega}) = \frac{1}{MT}\sum_{p=-\infty}^{+\infty} U_k(j\frac{\omega}{T} - j\frac{2\pi}{MT}p) \tag{A.3}$$

and then we can conclude as follows:

$$Y_k(e^{j\omega}) = F_k(e^{j\omega}) \cdot W_k(e^{j\omega}) \tag{A.4}$$

$$Y(e^{j\omega}) = \sum_{k=0}^{M-1} Y_k(e^{j\omega}) \tag{A.5}$$

Substituting and integrating all preceding relationships in equation A.5, we can finally state that:

$$Y(e^{j\omega}) = \frac{1}{MT}\sum_{p=-\infty}^{+\infty} X(j\frac{\omega}{T} - j\frac{2\pi}{MT}p) \cdot \sum_{k=0}^{M-1} H_k(j\frac{\omega}{T} - j\frac{2\pi}{MT}p) \cdot F_k(e^{j\omega}) \tag{A.6}$$

Using *lemma 1* (at the end of appendix A), we can rewrite above relationship as following:

$$Y(e^{j\omega}) = \frac{1}{MT}\sum_{m=0}^{M-1} \widetilde{X}(j\frac{\omega}{T} - j\frac{2\pi}{MT}m) \cdot \sum_{k=0}^{M-1} \widetilde{H}_k(j\frac{\omega}{T} - j\frac{2\pi}{MT}m) \cdot F_k(e^{j\omega}) \tag{A.7}$$

where $\widetilde{X}(j\Omega)$ and $\widetilde{H}_k(j\Omega)$ are periodic extensions of $X(j\Omega)$ and $H_k^{'}(j\Omega)$ with the period of $\Omega_\circ = \frac{2\pi}{T}$. There is no aliasing term through mentioned periodic extensions leading to $\widetilde{X}$ and $\widetilde{H}_k$ because the Nyquist rate is $\Omega_\circ$. $H_k^{'}(j\Omega)$ is formed by the part of $H_k(j\Omega)$ described between $[-\frac{\Omega_\circ}{2}, +\frac{\Omega_\circ}{2}]$ as below:

$$H_k^{'}(j\Omega) = \begin{cases} H_k(j\Omega) & \Omega \in [-\frac{\Omega_\circ}{2}, +\frac{\Omega_\circ}{2}] \\ \\ 0 & \text{elsewhere} \end{cases} \tag{A.8}$$

Figure 5.13 shows the periodic extension for an exemplary analog filter. To define

the distortion and aliasing functions, we had better rewrite equation A.7 as follows:

$$Y(e^{j\omega}) = \underbrace{\widetilde{X}(j\frac{\omega}{T}) \cdot T_{\circ}(e^{j\omega})}_{\text{distortion part}} + \underbrace{\sum_{m=1}^{M-1} \widetilde{X}(j\frac{\omega}{T} - j\frac{2\pi}{MT}m) \cdot T_m(e^{j\omega})}_{\text{aliasing part}} \tag{A.9}$$

Integrating with the equation A.7, the following definition may be obtained for the distortion $T_{\circ}(e^{j\omega})$ and aliasing $T_m(e^{j\omega})$ functions:

$$\begin{cases} T_{\circ}(e^{j\omega}) = \frac{1}{MT}\sum_{k=0}^{M-1} F_k(e^{j\omega}) \cdot \widetilde{H}_k(j\frac{\omega}{T}) \\ \\ T_m(e^{j\omega}) = \frac{1}{MT}\sum_{k=0}^{M-1} F_k(e^{j\omega}) \cdot \widetilde{H}_k(j\frac{\omega}{T} - j\frac{2\pi}{MT}m) \\ \qquad\qquad\qquad\qquad\qquad\qquad\qquad\qquad\qquad\qquad m = 1,\ldots,M\text{-}1 \end{cases} \tag{A.10}$$

A.3 Perfect Reconstruction for Hybrid Filter Bank

We now observe PR conditions and criteria to facilitate the filter design procedure employed in the implementation phase. To have a PR filter bank, the following set of equations are sufficient to hold:

$$\begin{cases} T_{\circ}(e^{j\omega}) = e^{-j\omega n_d} \\ \\ T_m(e^{j\omega}) = 0 \qquad \text{m=1,}\ldots\text{,M-1} \end{cases} \tag{A.11}$$

where n_d stands for an arbitrary integer (or real number in global view) that minimizes the error of above equalities. To follow readily, the conditions may be explained in vector/matrix form. So:

$$F(\omega) = \left[\begin{array}{cccc} F_0(e^{j\omega}) & F_1(e^{j\omega}) & \cdots & F_{M-1}(e^{j\omega}) \end{array} \right]^T_{M\times 1} \tag{A.12}$$

$$H(\omega) = \left[\begin{array}{cccc} \widetilde{H}_0(j\frac{\omega}{T}) & \widetilde{H}_1(j\frac{\omega}{T}) & \cdots & \widetilde{H}_{M-1}(j\frac{\omega}{T}) \end{array} \right]_{1\times M} \tag{A.13}$$

$$A(\omega) = \begin{bmatrix} H(\omega) \\ H(\omega - \frac{2\pi}{M}) \\ \\ \vdots \\ \\ H(\omega - \frac{2\pi(M-1)}{M}) \end{bmatrix}_{M \times M} \tag{A.14}$$

Therefore, A is a matrix of $M \times M$ which is computed at every arbitrary discrete time frequency $\omega \in \mathbb{R}$. PR criteria are now possible to be described as following.

$$A \cdot F = B \tag{A.15}$$

$$B = \begin{bmatrix} e^{-j\omega n_d} & 0 & \cdots & 0 \end{bmatrix}^T \tag{A.16}$$

B is a fixed vector of the dimension $M \times 1$. Above matrix equation A.15 may hold in any arbitrary frequency $\omega \in \mathbb{R}$. The analysis matrix A has a very useful property. Brown has shown that there is a close relationship between the columns of the inverse matrix A^{-1} of A (if existing) [33] so that:

$$\begin{cases} e^{j\omega_p n_d} \cdot F(\omega_p) = (p+1)^{th} \text{ column of } A^{-1}(\omega) \\ \\ \omega_p \ = \ \omega - \frac{2\pi}{M} p \qquad\qquad \text{p = 0,. . . ,M-1} \end{cases} \tag{A.17}$$

This property may be exploited in design phase of synthesis filters. Accordingly, we can conclude following issues which may be very advantageous in the implementation of HFB architecture:

- *Overlap of analysis filters*
  Based upon the previous section, there is no criterion or condition assumed by the analysis or synthesis filter banks for holding the PR equation except the existence of inverse of the analysis matrix at every frequency. Thus, analysis filters are not required to be in contiguous frequency bands. For example, an analog filter of unity ($H_k(j\Omega) = 1$) may be used or even the analysis filters can overlap. This is useful for the practical realization of analysis filter bank.

- *computational efficiency*
  According to A.17, it is not necessary to spread out the frequency points throughout the whole spectrum $\pm\pi$ for the design phase. It is enough to suppose the frequency samples at a narrow band of $\frac{2\pi}{M}$ for example $[-\pi, -\pi + \frac{2\pi}{M}]$. The rest of spectrum is covered by the columns of inverse matrix (A^{-1}). This characteristic provides efficiency in computation.

Lemma 1: A function $Y(\omega)$ of ω is supposed as follows:

$$Y(\omega) = \sum_{p=-\infty}^{+\infty} X(\omega - \frac{\Omega_\circ}{M} p) \tag{A.18}$$

where M is an integer $(M \geq 1)$. If the periodic extension $\widetilde{X}(\omega)$ of $X(\omega)$ with the period $\Omega_\circ$ is defined as $\widetilde{X}(\omega) = \sum_{k=-\infty}^{+\infty} X(\omega - \Omega_\circ k)$ then, the above equality may be described using only M terms as following:

$$Y(\omega) = \sum_{m=0}^{M-1} \widetilde{X}(\omega - \frac{\Omega_\circ}{M} m) \tag{A.19}$$

Proof: Using a new counter variable as $p = k + mM$, in which $0 \leq m \leq M-1$ and $k = 0, \pm 1, \pm 2, \ldots$, we can rewrite the equality A.18 as follows:

$$\begin{aligned} Y(\omega) &= \sum_{m=0}^{M-1} \sum_{k=-\infty}^{+\infty} X(\omega - \frac{\Omega_\circ}{M}(m + kM)) \\ &= \sum_{m=0}^{M-1} \sum_{k=-\infty}^{+\infty} X(\omega - \frac{\Omega_\circ}{M} m - \Omega_\circ k) \\ &= \sum_{m=0}^{M-1} \widetilde{X}(\omega - \frac{\Omega_\circ}{M} m) \end{aligned} \tag{A.20}$$

Thus, the relationship A.19 is apparently obtained.

Appendix B

Performance of LS optimization method in the presence of errors in variables

The sensitivity of Least Squares (LS)optimization method to the errors of coefficients is presented in this appendix [74]. To generally discuss about the sensitivity of an over-determined problem, the following one-dimensional optimization problem is considered:

$$\Lambda.\mathbf{f} = b \tag{B.1}$$

where $\mathbf{f}$ and b are the unknown parameters and known fixed-value vectors $(n \times 1)$ respectively. The matrix of coefficients Λ is an $m \times n$ matrix such that $m > n$ to have an over-determined problem. The parameters $\mathbf{f}$ and all the coefficients of b and Λ are assumed to be real-valued for convenience. The aim of optimization is to look for an optimal parameters vector $\mathbf{f}$ so that a presumed criterion is minimized (or maximized regarding to the type of criterion). Using LS method, this criterion is a 2-norm error as follows:

$$\mathbf{f}_{LS} = \arg \min_{\mathbf{f}} \|\Lambda.\mathbf{f} - b\|_2 \tag{B.2}$$

It is supposed that $\Lambda_\circ$ and $b_\circ$ represent the coefficients when there is no perturbation (or without any errors in variables). The LS solution for the unperturbed

problem is:

$$\mathbf{f}_\circ = (\Lambda_\circ^T \Lambda_\circ)^{-1} \Lambda_\circ^T . b_\circ \tag{B.3}$$

$$\mathbf{r}_\circ = \|\Lambda_\circ . \mathbf{f}_\circ - b_\circ\|_2$$

where $\mathbf{r}_\circ$ is called the residual of the solution. If this value is null, it is called a zero-residual problem. Otherwise, it is a non-zero residual problem [74]. The residual is possible to be described through the angle $\theta_\circ$ as follows:

$$\begin{aligned} \sin\theta_\circ &= \frac{\|\Lambda_\circ . \mathbf{f}_\circ - b_\circ\|}{\|b_\circ\|} \\ &= \frac{\mathbf{r}_\circ}{\|b_\circ\|} \end{aligned} \tag{B.4}$$

where $\|\cdot\|$ stands for the 2-norm value. Now, it is supposed that the real coefficients Λ and b include some perturbations (or imperfections). Then, they may be described in terms of unperturbed coefficients $\Lambda_\circ$ and $b_\circ$ as follows:

$$\Lambda = \Lambda_\circ + \Delta\Lambda$$

$$b = b_\circ + \Delta b$$

$\Delta\Lambda$ and Δb represent the matrix and vector of errors respectively. The condition number $\kappa(\Lambda)$ of the coefficient matrix Λ is defined as follows:

$$\begin{aligned} \kappa(\Lambda) &= \|\Lambda\| . \|\Lambda^\dagger\| \\ &= \frac{\sigma_1}{\sigma_r} \end{aligned} \tag{B.5}$$

where $\Lambda^\dagger$ is the respective pseudo-inverse matrix. σ_1 and σ_r stand for the largest and the least non-zero singular values associated to the coefficient matrix Λ. The rank of Λ is r ($r \leq n$). The rank of Λ and $\Lambda_\circ$ are supposed to be equal and to remain unchanged. It means that the errors do not change the rank number of the coefficient matrix. The sensitivity may be interpreted in terms of different measures. It is here described in terms of the unknown vector $\mathbf{f}$. Then, the sensitivity $S_\mathbf{f}$ is considered as the relative modification of the solution vector which

occurs because of the errors in the coefficients vector and matrix as follows:

$$S_{\mathbf{f}} = \frac{\|\Delta \mathbf{f}\|}{\|\mathbf{f}_\circ\|} = \frac{\|\mathbf{f} - \mathbf{f}_\circ\|}{\|\mathbf{f}_\circ\|} \tag{B.6}$$

where $\mathbf{f}$ and $\mathbf{f}_\circ$ are the solutions of perturbed and unperturbed cases respectively according to the same optimization technique. The errors are often unknown. An inequality containing the upper limit of sensitivity would be useful for interpreting the effects of errors. The coefficient matrix is supposed to be full column rank so that there is no zero singular value or equally $n = r$. Following discussion is related to this case. Otherwise, some modifications would be necessary.
There are always three terms contributing in the sensitivity value: the residual component, the component due to $\Delta\Lambda$, and the component related to Δb. Following theorem describes the sensitivity limit for the LS solution. It is evident that the limit is quite different for various optimization methods.

Theorem B.0.1. Upper bound on the absolute error in the LS solution
Considering above-mentioned over-determined problem B.1, if the constants ε and μ are supposed so that following relationships always hold:

$$\|\Delta\Lambda\| \leq \varepsilon\sigma_1 \quad \textit{and} \quad \|\Delta b\| \leq \varepsilon\|b_\circ\|$$

$$\mu = \varepsilon.\kappa(\Lambda_\circ) = \varepsilon\frac{\sigma_1}{\sigma_n} < 1$$

then, following inequality may be established for the LS solution:

$$\|\Delta \mathbf{f}\| \leq \frac{\varepsilon}{\sigma_n}\Big[\frac{\sigma_1 \mathbf{r}_\circ}{\sigma_n(1-\mu^2)} + \frac{\sigma_1\|\mathbf{f}_\circ\|}{1-\mu} + \frac{\|b_\circ\|}{1-\mu}\Big] \tag{B.7}$$

where three terms are associated with the residual component, $\Delta\Lambda$ and Δb respectively [74].

If the problem is non-zero residual, the residual component is generally dominant. In this case, the absolute error due to the errors would approximately be proportional to the square of the condition number related to the coefficient matrix. Otherwise, it is directly proportional to the condition number. The worst case for the non-zero residual problem occurs when the following criterion comes

true:

$$\Lambda\Lambda^T \mathbf{r}_\circ \parallel \Lambda \upsilon_n \tag{B.8}$$

where υ_n is the n^{th} right singular vector of the matrix Λ. In this case, the residual component will exactly contribute in the inequality.
In the zero-residual case, the bound will change to the following form:

$$\|\Delta\mathbf{f}\| \leq \frac{\varepsilon}{\sigma_n} \frac{\sigma_1 \|\mathbf{f}_\circ\| + \|b_\circ\|}{1-\mu} \tag{B.9}$$

The bound introduced by theorem B.0.1 may be rewritten for the description of relative errors of the solution. To better demonstrate the contribution of condition number, a parameter is defined as follows:

$$F(\mathbf{f}) = \frac{\|\Lambda.\mathbf{f}\|}{\|\mathbf{f}\|} \tag{B.10}$$

This parameter $F(\mathbf{f})$ is always between the least and the largest singular values of the coefficient matrix Λ. Using this parameter, the bound of the theorem B.0.1 can be described as following:

$$\frac{\|\Delta\mathbf{f}\|}{\|\mathbf{f}_\circ\|} \leq \varepsilon \Big[\frac{\sigma_1}{\sigma_n} \frac{F(\mathbf{f}_\circ)}{\sigma_n} \frac{\tan\theta_\circ}{1-\mu^2} + \frac{\sigma_1}{\sigma_n} \frac{1}{1-\mu} + \frac{F(\mathbf{f}_\circ)}{\sigma_n} \frac{1}{\cos\theta_\circ} \frac{1}{1-\mu} \Big] \tag{B.11}$$

There are again three components which contribute in the bound definition. The residual component is again proportional to the square of the condition number but the middle term (or the contribution of imperfections of the coefficient matrix) is directly proportional to the condition number. In the case of zero-residual problems, Total Least Squares (TLS) optimization technique is less sensitive than the LS method [74]. The TLS method minimizes the 2-norm of the matrix $[\Delta\Lambda; \Delta b]$. In return, the LS solution is associated with the minimum of the error vector Δb or with the Frobenius norm of residual vector. However, TLS and LS solutions tend to each other when the coefficient matrix Λ is very far from the rank deficiency. TLS and LS solutions are nearly equal if one of the following conditions is held:

- The set of equations $\Lambda.\mathbf{f} = b$ is only slightly incompatible. This is the case where the least singular value σ'_{n+1} of the matrix $[\Lambda; b]$ is sufficiently small.

- The Frobenius norm $\|b\|_F$ is small, i.e., TLS solution becomes very close to the LS solution.
- $\sigma_n >> \sigma_{n+1}^{'}$.
- The coefficient vector b is close to the largest singular vector of Λ.

In fact, all above items represent the same criterion. To have another interpretation, the Singular Value Decomposition (SVD) components may be used. Following equality reveals the SVD development associated with the coefficient matrix Λ:

$$\Lambda = U\Sigma V^T \tag{B.12}$$

where Σ is an $m \times n$ diagonal matrix including the singular values of Λ [71]. According to the SVD analysis, the Frobenius norm of the singular values variations $\Delta\Sigma$ is always less or equal to the Frobenius norm of the errors matrix $[\Delta\Lambda; \Delta b]$ as follows:

$$\|\Delta\Sigma\|_F \leq \|[\Delta\Lambda; \Delta b]\|_F \tag{B.13}$$

This can equally reveal that the absolute change in a singular value is not larger than the absolute change of the total matrix $[\Delta\Lambda; \Delta b]$ as following:

$$|\sigma_i^{'} - \sigma_i^{'\circ}| \leq \|[\Delta\Lambda; \Delta b]\|_2 \quad for\ i = 1, 2, \cdots, n+1 \tag{B.14}$$

The above inequality may be used to have a raw measure for the modification of solution when the coefficient matrix Λ and vector b are perturbed by errors.♠

Appendix C

Total Least Squares optimization method

The term Total Least Squares (TLS) appeared in 1980 [94], although this optimization method had been introduced using the SVD in 1970 by Golub [95, 96]. The main principle of the TLS problem is here formulated using the SVD. One important application of TLS problems is to estimate the unknown parameters associated with the errors-in-variables model. The model of errors-in-variables may be described as following. It is assumed that a process may be modeled by m linear equations as following:

$$\Lambda_\circ \mathbf{f} = \mathbf{b}_\circ$$

where $\mathbf{f}$ represents the vector $(n \times 1)$ of n unknown parameters. $\Lambda_\circ$ and $\mathbf{b}_\circ$ stand for the $m \times n$ matrix of data and the $m \times 1$ vector of measurement respectively. In practice, $\Lambda_\circ$ and $\mathbf{b}_\circ$ are not available but their erroneous forms (Λ and $\mathbf{b}$) as following:

$$\Lambda = \Lambda_\circ + \Delta\Lambda \qquad \mathbf{b} = \mathbf{b}_\circ + \Delta\mathbf{b}$$

that $\Delta\Lambda$ and $\Delta\mathbf{b}$ represent the measurement errors. The basic problem of TLS seeks to:

$$\underset{\left[\widehat{\Lambda};\widehat{\mathbf{b}}\right] \in\ \mathcal{R}^{m\times(n+1)}}{\text{mininmize}} \quad \left\| [\Lambda; \mathbf{b}] - \left[\widehat{\Lambda}; \widehat{\mathbf{b}}\right] \right\|_F \tag{C.1}$$

$$\text{subject to} \quad \widehat{\mathbf{b}} \ \in \ R(\widehat{\Lambda}) \tag{C.2}$$

where $\|.\|_F$ represents the Frobenius norm of matrix. The above criterion leads to the optimum $\left[\widehat{\Lambda}_{opt}; \widehat{\mathbf{b}}_{opt}\right]$ which minimizes the relation C.1. The TLS solution $\mathbf{f}_{TLS}$ of parameters will be any vector satisfying:

$$\widehat{\Lambda}_{opt}.\mathbf{f}_{TLS} = \widehat{\mathbf{b}}_{opt} \tag{C.3}$$

The TLS solution is equivalent to the LS one in the specific case. For this purpose, let us assume that $\Lambda_\circ$ has full-rank and all rows of errors matrix $\left[\Delta\Lambda; \Delta\mathbf{b}\right]$ are i.i.d. with zero mean and covariance matrix $\sigma_v^2\mathbf{I}$. Then it may be proved that the TLS solution $\mathbf{f}_{TLS}$ of $\Lambda\mathbf{f} \approx \mathbf{b}$ estimates the *true* parameter values (the LS solution $\mathbf{f}_{LS}$), given by $\Lambda^\dagger\mathbf{b}$ ($\Lambda^\dagger$ represents the pseudo-inverse of Λ). In other words, $\mathbf{f}_{TLS}$ converges to $\mathbf{f}_{LS}$ as m tends to infinity. Whatever is the distribution of errors, this property of TLS is valid.

• **Basic TLS solution**

The decomposition of SVD may be used for solving the TLS problems [74]. The basic TLS problem $\Lambda\mathbf{f} \approx \mathbf{b}$ may equally be described as following:

$$\left[\Lambda; \mathbf{b}\right]\left[\mathbf{f}^{\,T}; -1\right]^T \approx 0$$

Let the SVD of $\left[\Lambda; \mathbf{b}\right]$ be as follows:

$$\left[\Lambda; \mathbf{b}\right] = U\Sigma V^T \tag{C.4}$$

where Σ is an $m \times (n+1)$ diagonal matrix including the singular values:

$$\Sigma = \mathrm{diag}(\sigma_1, \sigma_2, ..., \sigma_{n+1})$$

If the $(n+1)^{th}$ singular value σ_{n+1} is non-zero ($\sigma_{n+1} \neq 0$), the coefficient matrix $\left[\Lambda; \mathbf{b}\right]$ is of rank $n+1$. Thus, the set of equations C.4 is incompatible. To obtain a solution, the rank of coefficient matrix must be reduced to n. It is shown that the best TLS approximation $\left[\Lambda_{opt}; \mathbf{b}_{opt}\right]$ of the coefficient matrix, which minimizes the deviations in variances, is given by:

$$\left[\Lambda_{opt}; \mathbf{b}_{opt}\right] = U\Sigma_{opt}V^T \tag{C.5}$$

where Σ_{opt} is the same diagonal matrix Σ except the $(n+1)^{th}$ singular value is put zero as following:

$$\Sigma_{opt} = \text{diag}(\sigma_1, \sigma_2, ..., \sigma_n, 0)$$

Then, for obtaining the TLS solution vector $\mathbf{f}_{TLS}$, it is sufficient to solve the compatible set of equations C.3. According to the SVD theory, it is clear that its solution is given by the only right singular vector $\mathbf{v}_{n+1}$ (i.e., the last column of V). The TLS solution $\mathbf{f}_{TLS}$ is then obtained by scaling v_{n+1} so that its last component is -1 as following:

$$\left[\mathbf{f}_{TLS}^{T}\ , -1\right]^{T} = \frac{-1}{V_{(n+1),(n+1)}}\mathbf{v}_{n+1} \tag{C.6}$$

If $V_{(n+1),(n+1)} \neq 0$, then the TLS solution vector $\mathbf{f}_{TLS}$ is obtained according to above relation C.6. If the TLS solution exists, it may be described as follows:

$$\mathbf{f}_{TLS} = \left(\Lambda^T\Lambda - \sigma_{n+1}\mathbf{I}\right)^{-1}\Lambda^T\mathbf{b} \tag{C.7}$$

It may be interesting to compare the TLS solution with the LS one $\mathbf{f}_{LS}$:

$$\mathbf{f}_{LS} = \left(\Lambda^T\Lambda\right)^{-1}\Lambda^T\mathbf{b} \tag{C.8}$$

The LS and TLS solutions would be the same if the $(n+1)^{th}$ singular value σ_{n+1} of coefficient matrix is null.

Appendix D

Blind deconvolution techniques

D.1 Introduction

There have been historically two challenging concepts of inverse problems concerning LTI systems. An LTI system may represent any linear convolution operation appeared in either the concrete physical systems such as LTI telecommunication channels and earth's reflectivity impulse response due to earthquakes or the virtually concepts like the convolutional coding. These two concepts are different according to the desired unknowns: the estimation of the input and the identification of the LTI system. Both of them are supposed to use only the system response or output. Masssey et. al. published a pioneering work in this regard in 1968 [97, 98]. They tried to formulate the necessary and sufficient conditions for the existence of a feed-forward inverse for a linear sequential circuit concerning the concepts of convolutional codes [99].

Depending on the desired unknown parameter, it is called either system identification or deconvolution. The system identification (or equally the channel estimation in telecommunication) is referred to when one wants to find the system impulse response but blind deconvolution (channel equalization) is mostly considered while the input signal of unknown system or channel is desired to be somehow reconstructed. However, both are very closely related [100]. The system identification and deconvolution are utilized in so many fields. The first applications were concerning with the inverse convolutional codes and communication channel equalization [97, 100]. During recent years, there exist a wide group of applicability in

many diverse fields e.g. sonar, radar, plasma physics, biomedicine, seismic data processing, image reconstruction, harmonic retrieval, time-delay estimation, adaptive filtering, noise cancelation, array processing, cellular telecommunication and ultrasonic Non-Destructive Evaluation (NDE). It has mostly been implemented using Higher-Order Statistics (HOS) [101]. It has been shown that HOS-based methods exhibit a better performance even in the cases that Second-Order Statistics (SOS)-based algorithms like Linear Prediction Error(LPE) method is applicable [86].

The idea of deconvolution or equalization is simply to compensate the non-ideal characteristics of a system or channel by additional filtering and dates back to the use of loading coils to improve the characteristics of telephone cables for voice transmission [102]. Then,classical deconvolution is concerned with the task of recovering an excitation signal, given the response of a known time-variant linear operator to that excitation [103]. The deconvolution or equalization (being more common in telecommunication texts) is classified depending on some features. Equalization may be called non-blind, semi-blind or blind. Non-blind and semi-blind equalizers are referred to respectively when the impulse response of system is known or a training signal (or pilot) is transmitted. Blind equalizers nevertheless reconstruct the input signal using only the output or received signal. When both the system impulse response and the response or output are observable (non-blind case), the equalizer approximates the inverse of known distortion system or channel. As an example, classical equalizers of telephone channels were designed to recover the voice signals using an approximation of the telephone cable lines [100, 99].

The rapidly-rising need for higher speed data transmission to furnish computer communications through widespread network of voice band-width channels faced with some difficulties like channel variations. The needing adaptive equalizers realized in the MODulator-DEModulator(MODEM) stages employed some training signals and were adapted to varying channels through a semi-blind manner [104, 105]. The adaptive semi-blind equalizers were still inefficient and at times unrealizable in order to overcome the problem of new computer networks. Fast startup equalization was not possible and it was to be held by control unit of a computer network regarding to the initial training period that was necessary in the adaptive equalizers. Furthermore, the multipoint networks had some problems

in retraining the tributary receivers because of extensive changes in channel characteristics or simply because a tributary was not powered on during initial network synchronization. To realize large or heavily loaded multipoint systems having increasing data throughput and a simple network monitoring, Godard proposed a blind equalization method or " Self-Recovering equalizer", in 1980 [106]. Through a blind equalizer, there is no longer a need to the training sequences and every data terminal or tributary in the network would be capable to achieve complete adaptation without a need to the cooperation of the control station and therefore without disrupting normal data transmission to other terminals.

The blind deconvolution was later developed in telecommunication fields through pioneering works of Sato in [105], Benveniste et. al. in 1980 [107] and Shalvi and Weinstein in 1990 [108]. However, this concept had been already proposed and realized in the research of seismic studies by Wiggins (1978) and Donoho (1981) [109]. All of the blind equalization techniques have utilized the HOS methods either implicitly (like Godard and Sato works) or explicitly like Shalvi and Weinstein one [88]. The deconvolution or equalization includes either Maximum Likelihood(ML) methods, Second-Order Cyclostationary Statistics (SOCS) (i.e. cyclic correction-based methods, or HOS-based methods ($>= 3$)). The ML methods derive the optimum equalizer according to a presumed probability density function (pdf) of signals while the SOCS and HOS-based methods obtain the blind equalizers using the SOCS or HOS characteristics of the signals respectively. Higher-Order Moments or cumulants are mostly exploited in blind equalization techniques whereas blind channel estimation or system identification methods commonly use Higher-Order Spectra[101].

According to the characteristics of the input signal and the channel or system properties, the blind equalization methods may be classified as well. HOS-based methods are not useful when the input process is Gaussian. If a random process is Gaussian, all its cumulants with the order higher than 2 are zero. If the unknown channel or system is stable and causal (minimum-phase or maximum-phase) and the input is white noise (i.i.d. random process), classical linear prediction error methods (LPE) can be used for equalization. In this case, the solution is not optimal unless the input is Gaussian. For non-Gaussian case, available adaptive estimations can be used but they would be asymptotically minimax for causal ARMA

processes. When the system is neither minimum-phase nor maximum-phase, the methods generally use HOS moments or cumulants. Second-order moments are actually unable to distinguish the phase ambiguities. Shalvi and Weinstein proposed the Super-Exponential Algorithm (SEA) for blind deconvolution in 1993 [86]. The SEA includes a very fast converging iterative algorithm using HOS cumulants for blind equalization in a batch processing sense. This method nevertheless suffers from divergence problem in some special cases. Hybrid SEA proposed by Chi et. al. handles this problem [88].

The equalization or deconvolution methods are also possible to be classified according to the type of equalizer filters utilized. Classical equalizers consist of only a feed-forward tapped delay line (non-recursive) that are in fact equivalent to a real FIR filter. However, it may cause some problems in the realization and also needs heavy calculations if the length of required equalizer (the order of FIR filter) is very large. Truncation of very large FIR equalizers may produce an intolerable level of errors. Using some output feedback lines in equalizer design or the recursive equalizers, there is no longer a need for very long FIR equalizers. The larger, the length of impulse response of unknown system, its equalizer would correspond to a lower order [100]. However, both recursive and nonrecursive equalizers may be realized either online or in the batch processing mode.

D.2 Higher-Order Statistics and Cumulants

D.2.1 Introduction

Higher-Order Statistics (HOS) have been used in the system identification and equalization as long as a half century. The motivations behind the use of HOS in signal processing are indispensable. The HOS-based techniques for identifying or equalizing non-minimum phase systems are at times the only techniques being capable in this regard [110]. Many algorithms of signal processing exploit HOS-based methods either implicitly or explicitly. Indeed second-order moments or SOS-based methods are unable to distinguish between the systems with the same spectral density functions but with different phases [111]. Hence, they are limited to deal with minimum-phase (or equally maximum-phase) systems. In other words SOS-based

methods are limited to stable and causal LTI systems. Furthermore, SOS-based methods are optimal only in the cases where the input signal is Gaussian. It has been shown that HOS-based techniques show a better performance even in the case of minimum-phase LTI systems than SOS-based methods such as LPE [86]. The concepts of cumulant extrema in HOS are often used in blind deconvolution or equalization of LTI systems, whereas the methods of HOS spectra are mostly utilized for channel estimation or system identification [103, 110]. These two categories are nevertheless related to each other [110]. In this appendix, the principal focus is on the blind deconvolution techniques. Before dealing with the equalization algorithms, a brief summary of the concepts used in HOS such as cumulants are presented. The signals are assumed for convenience to be real-valued.

D.2.2 Moments

A stationary stochastic process or random time-series is supposed to be generated by a sequence of independent or dependent samples of a generating random variable X. This generating random variable is defined by a probability density function (pdf) $p_{_X}(x)$. The probability density function associated with a discrete- or continuous-time random variable can uniquely be described in terms of a set of discrete parameters called moments. The n^{th}-order moment of the random variable X is specified by:

$$m_{_X}(n) = E(X^n) = \int_{-\infty}^{+\infty} x^n f_{_X}(x)dx \qquad n = 1, 2, \ldots \tag{D.1}$$

If n^{th} order moment is finite, then all its moments of the order smaller than n exist as well. First-order moment is called the mean value of a random variable X (shown by $m_{_X}$).

D.2.3 Central Moments

Central moments interpret that how a random variable is distributed about its mean value. The n^{th}-order central moment of X is formally defined as:

$$\mu_{_X}(n) = E[(X - m_{_X})^n] = \int_{-\infty}^{+\infty} (x - m_{_X})^n f_{_X}(x)dx \qquad n = 1, 2, \ldots \tag{D.2}$$

The first-order central moment is evidently null. The second-order central moment is always referred to as the variance of random variable as following:

$$\sigma_X^2 = \mu_X(2) \tag{D.3}$$

Variance implicates the average dispersion of the random variable around its mean value. The third-order central moment is typically referred as a determination of "skewness" of the probability density function of a random variable around the mean value. The fourth-order central moment is one of the important statistical values that it often says how much flatness or "Kurtosis" is involved in the probability density function. "Kurtosis" is a Latin word standing for the shoulder and it is also a statistical parameter closely related to fourth-order central moment. The kurtosis is nevertheless different from the fourth-order central moment [103]. It is evident that central moments are zero for any random process which is realized by a symmetric generating random variable.

D.2.4 Moment Generating functions

It was mentioned that a random variable can uniquely and completely be determined in terms of its moments. In fact, this philosophy originates from the definition of Fourier Transform (FT). The Fourier transform of a probability density function is called the moment generating function of the associated random variable (with the sole difference of using the negative frequency index). It can readily be shown that the moments actually correspond to the coefficients in the Taylor development of the Fourier transform. The analysis and synthesis relationships are as following:

$$\begin{cases} \Phi_X(\omega) = E(e^{j\omega x}) = \int_{-\infty}^{+\infty} e^{j\omega x} f_X(x) dx \\ \\ f_X(x) = \frac{1}{2\pi} \int_{-\infty}^{+\infty} \Phi_X(\omega) e^{-j\omega x} d\omega \end{cases} \tag{D.4}$$

The moment generating function always exist because the probability density function is a non-negative real-valued function with a total integral of unity. According to the properties of probability density functions, the moment generating function

will always hold the under-below relationships:

$$\Phi_X(0) = 1$$

$$|\Phi_X(\omega)| \leq 1 \qquad \text{for all } \omega \in \mathcal{R}$$

$$\Phi_X^*(\omega) = \Phi_X(-\omega)$$

If one expands the moment generating function in terms of its Mclaurent-Taylor series, there will obviously be found a close correspondence between the moments and this expansion as follows:

$$\begin{aligned} \frac{d^k \Phi_X(\omega)}{d\omega^k}|_{\omega=0} &= (-j)^k . E(X^k) \\ &= (-j)^k . m_X(k) \qquad k = 1, 2, \ldots \end{aligned} \tag{D.5}$$

In other words, the moment generating function could also be described as following:

$$\Phi_X(\omega) = \sum_{k=0}^{n} \frac{1}{k!} E(X^k)(j\omega)^k + r_n(\omega) \tag{D.6}$$

The remainder function $r_n(\omega)$ is so that $\frac{r_n(\omega)}{\omega^n}$ tends to zero in the limit as ω approaches zero. Some properties of the moment generating function are very important through the signal processing perspective as follows:

$$Y = aX \iff \Phi_Y(\omega) = \Phi_X(a\omega)$$

$$Y = X + a \iff \Phi_Y(\omega) = e^{j\omega a}\Phi_X(\omega)$$

$$Y = X_1 + X_2 \iff \Phi_Y(\omega) = \Phi_{X_1}(\omega).\Phi_{X_2}(\omega)$$

where it is assumed that a is a scalar value and X_1 and X_2 are two independent random variables.

D.2.5 Cumulants

The natural logarithm of probability values always implicates the amount of information existing in the related sequence. This concept is also useful in the utilization of moment generating functions. The natural logarithm of the moment generating function is commonly referred to as the cumulant generating function.

$$\begin{aligned} \Psi_X(\omega) &= \ln[\Phi_X(\omega)] \\ &= \ln[E\{e^{j\omega}\}] \end{aligned} \tag{D.7}$$

According to the properties of the moment generating function, the cumulant generating function holds apparently following properties:

$$Y = aX \iff \Psi_Y(\omega) = \Psi_X(a\omega)$$

$$Y = X + a \iff \Psi_Y(\omega) = e^{j\omega a} + \Psi_X(\omega)$$

$$Y = X_1 + X_2 \iff \Psi_Y(\omega) = \Psi_{X_1}(\omega) + \Psi_{X_2}(\omega)$$

where a is a scalar value and X_1 and X_2 are two independent random variables. The k^{th}-order cumulant of a random variable may be described as:

$$C_X(k) = (-j)^k \left. \frac{d^k \Psi_X(\omega)}{d\omega^k} \right|_{\omega=0} \tag{D.8}$$

It can readily be shown that a real random variable corresponds to the real-valued cumulants. Moreover, the cumulant generating function can be defined in terms of the cumulants as follows:

$$\Psi_X(\omega) = \sum_{k=1}^{n} \frac{1}{k!} C_X(k)(j\omega)^k + r_n(\omega) \tag{D.9}$$

If n^{th}-order moment exists, there will exist a finite value for n^{th}-order cumulant as well. One can describe the cumulants as the functions of the associated mean and central moments of desired random variable. There are hereunder for instance

some exemplary relationships[103]:

$$C(1) = m_X$$

$$C(2) = \mu(2) = \sigma_X^2$$

$$C(3) = \mu(3)$$

$$C(4) = \mu(4) - 3\mu(2)^2$$

$$C(5) = \mu(5) - 10\mu(3)\mu(2)$$

$$C(6) = \mu(6) - 15\mu(4)\mu(2) - 10\mu(3)^2 + 20\mu(2)^3$$

$$C(7) = \mu(7) - 21\mu(5)\mu(2) - 35\mu(4)\mu(3) + 210\mu(3)\mu(2)^2$$

$$C(8) = \mu(8) - 28\mu(6)\mu(2) - 56\mu(5)\mu(3) - 35\mu(4)^2 +$$
$$420\mu(4)\mu(2)^2 + 560\mu(3)^2\mu(2) - 630\mu(2)^4$$

where for the purpose of simplicity, the subscript of X has been omitted. It is necessary to remind that for the stochastic processes having a Gaussian generating random variable, all cumulants of the order higher than 2 are null.

Theorem D.2.1. The linear combinations of independent random variables
let a random variable Y be a linear combination of M independent random variables $\{X_1, X_2, \ldots, X_M\}$ as:

$$Y = \sum_{i=1}^{M} a_i X_i$$

where all a_i are scalar values. Then, the following relationships always hold:

$$\phi_Y(\omega) = \prod_{k=1}^{M} \phi_{X_k} a_k(\omega) \tag{D.10}$$

$$\begin{cases} \Psi_Y(\omega) = \sum_{k=1}^{M} \Psi_{X_k}(a_k\omega) \\ \\ C_Y(n) = \sum_{k=1}^{M} a_k^n C_{X_k}(n) \end{cases} \tag{D.11}$$

where $C_Y(n)$ is the n^{th}-order cumulant.
The proof can be found in [103].

Lemma D.2.2. *Let $\{h_n\}$ be the unit impulse response of an LTI system.The time-series $\{X_n\}$ as the input of this system is supposed to be a white noise (samples of an i.i.d. random process) and moreover, the p^{th}-order cumulant related to the input $\{X_n\}$ is assumed to be finite. Then, we will have following relationship for the response time-series $\{Y_n\}$:*

$$C_Y(p) = C_X(p) \sum_k (h_k)^p \tag{D.12}$$

Proof. The proof may readily be obtained using above-mentioned theorem D.2.1. □

D.2.6 Normalized Cumulants

Using above definitions D.12, the cumulants depend on the magnitude of the random variable. For making the cumulants invariant to the scalar multipliers, a normalization operation is necessary as well. Accordingly, the normalized cumulant with order (p, q) associated with the random variable $\{X_n\}$ may be defined as follows:

$$K_X(p, q) = \frac{C_X(p)}{|C_X(q)|^{\frac{p}{q}}} \tag{D.13}$$

where it is necessarily assumed that the cumulant $C_X(q)$ is non-zero. Using the normalized cumulants D.13, we can readily show that:

$$Y = aX \iff K_Y(p, q) = K_X(p, q)$$

where a is a scalar parameter. The different values of (p, q) have been tried and proposed in blind deconvolution. For instance, in the case where no noise is present, it has been proposed to use the pairs $(p = 3,\ q = 2)$ or $(p = 4,\ q = 2)$. In the presence of an additive gaussian noise, the pair $(p = 6,\ q = 4)$ is offered or others the case $q = 2$ has been proposed as well [103]. More discussions will be presented through the next subsections. Considering the normalized cumulants, following

lemma is used in the related blind equalization techniques.

Lemma D.2.3. *Holding the same conditions that the ones of lemma D.2.2, we can rewrite the result in terms of normalized cumulants as following:*

$$K_Y(p,q) = \frac{\sum_k (h_k)^p}{\left|\sum_k (h_k)^q\right|^{\frac{p}{q}}} K_X(p,q) \tag{D.14}$$

According to above lemma, we can easily deduct the following remarks.

- *The sign of normalized cumulants for both the excitation and response processes is the same provided that p is an even integer.*
- *The normalized cumulants of outputs of two LTI systems associated with the unit-impulse responses of $\{h_n\}$ and $\{ah_n\}$ are the same for any non-zero scalar value as long as the excitation processes are the same.*

D.2.7 Extension to Complex-Valued Data

Throughout the preceding sections, it has been supposed that the signal and the impulse response of the system and equalizer are real-valued. This is not condition but for convenience. A brief overview for the complex valued case is hereunder presented. Let $\mathbf{X}$=$\{x_1[n],\ x_2[n],\ \ldots,\ x_M[n]\}$ be a set of complex-valued random processes. The joint characteristic function or joint moment generating function can be defined as follows:

$$\begin{aligned} \Phi_{\mathbf{X}}(\omega) &= E\{e^{j\omega^T \mathbf{X}}\} \\ &= E\{e^{j\sum_{i=1}^{M} \omega_i x_i}\} \end{aligned} \tag{D.15}$$

Like to the preceding section and the definition of the cumulant generating function for real-valued data, it can readily be extended to the complex case. Therefore, we will have following relationship standing for joint cumulant generating function:

$$\begin{aligned} \Psi_{\mathbf{X}}(\omega) &= \ln[\Phi_{\mathbf{X}}(\omega)] \\ &= \ln[E\{e^{j\omega^T \mathbf{X}}\}] \end{aligned} \tag{D.16}$$

Hence, it is possible to have the joint cumulant of m arbitrary signals $\{x_{k_1}[n]$, $x_{k_2}[n]$, ..., $x_{k_m}[n]\}$ belonging to the above-mentioned set of M random signals as follows:

$$\mathrm{cum}(x_{k_1}[n], x_{k_2}[n], \ldots, x_{k_m}[n]) = (-j)^m \quad \frac{\partial^m ln\Psi_{\mathbf{X}}(\omega)}{\partial\omega_{k_1} \ldots \partial\omega_{k_m}}|_{\omega=0} \tag{D.17}$$

It is also possible to simplify this definition and to describe the joint cumulants in terms of the moments. Supposing that $x_1[n]$, $x_2[n]$, ... are zero-mean random signals, the joint cumulants in terms of moments may be described as follows:

$$\mathrm{cum}(x_1[n], x_2[n]) = E\{x_1 x_2\}$$

$$\mathrm{cum}(x_1[n], x_2[n], x_3[n]) = E\{x_1 x_2 x_3\}$$

$$\begin{aligned}\mathrm{cum}(x_1[n], x_2[n], x_3[n], x_4[n]) = {} & E\{x_1 x_2 x_3 x_4\} - E\{x_1 x_2\}E\{x_3 x_4\} \\ & -E\{x_1 x_3\}E\{x_2 x_4\} - E\{x_1 x_4\}E\{x_2 x_3\}\end{aligned}$$

For more convenience in the practical applications, it may simply be noted as:

$$\mathrm{cum}(\underbrace{x[n], x[n], \ldots, x[n]}_{\text{p terms}}; \ldots) = \mathrm{cum}(x : p; \ldots)$$

where,

$$C_x(p) = \mathrm{cum}(x : p)$$

$$C_x(p, q) = \mathrm{cum}(x : p \ ; \ x^* : q)$$

that $\mathrm{cum}(x : p)$ and $\mathrm{cum}(x : p \ ; \ x^* : q)$ are called p^{th}- and $(p, q)^{th}$-order cumulants respectively. It is evident that for real-valued signal $x[n]$, we have $C_x(p + q) = C_x(p, q)$. All the properties already explained in the real-value case are still generally valid. For instance, following properties hold [112]:

- *Linearity:* $\mathrm{cum}(\sum_i a_i x_i; \ldots) = \sum_i a_i \mathrm{cum}(x_i; \ldots)$.
- *Independent Signals:* If the set of random signals $\{x_1[n]$, $x_2[n]$, ..., $x_M[n]\}$ can be divided into two or more subgroups being mutually-independent subsets, then their joint cumulant equals null provided that they all include zero-mean generating random variable .

- *Gaussian Signals:* If M arbitrary jointly-gaussian processes are considered, the associated joint cumulant is zero provided that $M > 2$ even if the signals are non-zero mean.

- *Variance:* For any complex-valued random process $x[n]$, we can consider following equalities where $Var(x)$ and m_x are the variance and mean values of the process $x[n]$ respectively.

$$C_x(1,1) = Var(x)$$

$$C_x(1) = m_x$$

- *White noise:* For a complex-valued white random process (i.i.d. sequence) $x[n]$ the following equality always holds:

$$\begin{aligned} &\text{cum}(x[n-k_1];\ldots;x[n-k_p];x^*[n-m_1];\ldots;x^*[n-m_q]) = \\ &\qquad \begin{cases} C_x(p,q) & \text{if } k_1 = \ldots = k_p = m_1 = \ldots = m_q \\ 0, & \text{otherwise} \end{cases} \end{aligned} \tag{D.18}$$

The lemma explained in the real-valued signal case are also possible to be generalized and considered in the complex case.

Lemma D.2.4.
Let $\{h_n\}$ be the unit impulse response of an LTI system.The complex time series $\{x_n\}$, the input of the system is supposed to be a white noise (samples of an i.i.d. random process) and moreover, the $(p,q)^{th}$-order cumulant due to the input $\{x_n\}$ is assumed to be finite. Then, we will have following relationship for the response time series $\{y_n\}$.

$$C_y(p,q) = C_x(p,q) \sum_n [(h_n)^p (h_n^*)^q] \tag{D.19}$$

The proof may readily be achieved through above-mentioned properties [83].

Theorem D.2.5. The linear combinations of independent random variables
It is supposed that $\{h_n\}$ is the unit impulse response of an LTI system, with an excitation of i.i.d. random sequence (white noise) $\{x_n\}$. The associated system

response $\{y_n\}$ *is a stationary random process. The* $(p,q)^{th}$*-order cumulant related to the input* $\{x_n\}$ *is supposed to be finite and non-zero, and* p *and* q *are some arbitrary non-negative integers so that* $p+q>2$*. If* $C_x(1,1)=C_y(1,1)>0$*, then following inequality always holds:*

$$|C_y(p,q)| \leq |C_x(p,q)| \tag{D.20}$$

where the equality holds if and only if $\{h_n\}$ *is a shifted and scaled version of unit-impulse sequence* $\alpha\delta(n-n_d)$*.*

D.2.8 Empirical Cumulants

In practice, the exact cumalants are unknown and therefore they can only be approximated because it is possible neither to have the random process during the whole time axis nor to use the infinite samples in the computations. Thus, sample cumulants which are approximated by a finite duration of random processes will approximate its real and unknown measures. Supposing a finite length N of the signal sequence, the samples $\{x[n]|\ n=1,2,\ldots,N\}$ are available. It is desired to approximate the relevant statistical parameters like the moments and the cumulants. For convenience, we suppose again that the sequence samples are all real-valued.

Standard central moments due to this sequence can be approximated as follows:

$$\widehat{\mu}_x(p)=\frac{1}{N}\sum_{n=1}^{N}[x[n]-\widehat{m}_x]^p \tag{D.21}$$

$$\widehat{m}_x=\frac{1}{N}\sum_{n=1}^{N}x[n]$$

To approximate sample cumulants for an arbitrary sequence $\{x[n]|n=1,2,\ldots,N\}$, it is enough to use D.21 along with the relationships presented in the preceding subsections. For instance, integrating mentioned relationships, it is possible to approximate 6^{th}-order sample cumulant as follows:

$$\widehat{C}_x(6)=\widehat{\mu}_x(6)-15\widehat{\mu}_x(2)-10\widehat{\mu}_x(3)^2+30\widehat{\mu}_x(2)^3$$

Empirical cumulants and moments are an approximation of the associated real values. Using these approximated parameters through the techniques of equalization, the problems of convergence and incorrect extremum will appear. As a result, the number N of data samples used will play an important role in the algorithms which are going to be explained in the next sections.

D.3 Blind Deconvolution

D.3.1 SISO blind deconvolution

Blind deconvolution or equalization of Single-Input Single-Output (SISO) systems is a signal processing procedure to restore the source signal $\{X_n\}$ from the received signal $\{Y_n\}$ given by (refer to figure D.1):

$$y[n] = y_s[n] + w[n]$$

$$y_s[n] = h[n] * x[n]$$

$y_s[n]$ is the noise free signal distorted by the unknown LTI SISO system $h[n]$ and $w[n]$ is supposed to be an additive noise. It is desired to possibly reconstruct the pure input $x[n]$ through utilization of the only available signal $y[n]$.

This problem has been handled during recent years using HOS in which $x[n]$ is

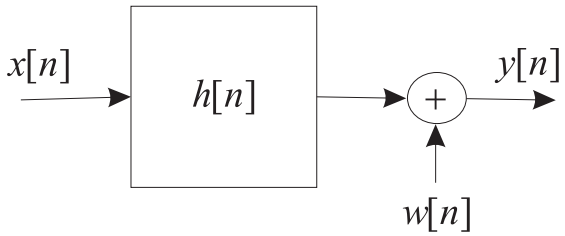

Figure D.1. The SISO model of a telecommunication channel.

assumed to be any non-Gaussian random process and $w[n]$ is preferably a Gaussian noise being independent of the input. Regarding to the properties of HOS, cumulants or polyspectra are blind to any Gaussian process because all cumulants of the order higher than 2 are equal to zero for a Gaussian process. In this case, SOS-based techniques are mostly exploited. On the other hand, SOS-based methods

(autocorrelation and power spectrum density) are unable to distinguish uniquely the poles of an LTI system $h[n]$ (if it is non-minimum phase). Therefore, the SOS-based methods such as LPE filter can be only applied when the unknown systems is minimum-phase (or equally maximum phase). Furthermore, their performance is highly sensitive to additive noise since autocorrelation of the received signal $y[n]$ equals the sum of its counterpart for both the noise free $y_s[n]$ and the additive noise. Supposing a white additive noise, following equation is mostly regarded in this regard.

$$|Y(e^{j\omega})|^2 = |H(e^{j\omega})|^2.|X(e^{j\omega})|^2 + \sigma_w^2 \tag{D.22}$$

Accordingly, HOS-based methods are a suitable candidate for equalizing unknown non-minimum phase LTI systems as well as a better performance is anticipated in the minimum-phase case. All HOS-based equalization methods are almost common in the following conditions as a prerequisite for achieving the inverse system in the equalizer.

CS1: Unknown LTI system is stable ($\sum_n |h[n]| < \infty$) and $H(z)$ has no zero on the unit circle $|z| = 1$.

CS2: The source signal is supposed to be a non-Gaussian and white (i.i.d) random process.

CS3: The source signal and the additive noise are independent.

CS4: The noise is a Gaussian white or colored random process.

However, Gamboa and Gassiat have recently proposed a mathematical analysis for the blind deconvolution in the case where the input may be a colored signal [111]. Furthermore, the suitably-chosen channel encoding schemes have been offered for non-white source signals [88].

Equalizer is a specially-chosen filter or transfer function so that applying to the response of unknown system, the result approximates the unknown input as well as possible. If assumed a linear feed-forward equalizer (a linear tapped-delay line or precisely an FIR filter), we will have the following relationship:

$$\begin{aligned} \widehat{x}[n] &= f[n] * y[n] \\ &= \widehat{x}_s[n] + \widehat{x}_N[n] \end{aligned} \tag{D.23}$$

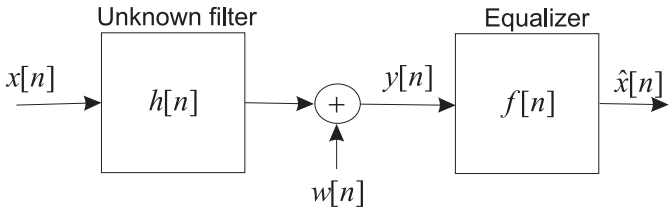

Figure D.2. The equalization setup for a SISO telecommunication channel.

where $\widehat{x}_s[n]$ and $\widehat{x}_N[n]$ are the signal and noise components in the equalized output. It is also possible to consider the whole block as an LTI system through which it is desired to have an output which approximates the input as close as possible. The overall system of equalization procedure may be described as:

$$s[n] = h[n] * f[n]$$

where $s[n]$ represents the overall system consisting of unknown LTI system and the equalization filter unit-impulse responses. Accordingly, the problem of SISO blind deconvolution is equivalent to the problem of finding the coefficients of the equalizer $f[n]$ such that the signal component $\hat{x}_s[n]$ approximates the source signal $x[n]$ as close as possible (up to a scale factor and a time delay) while maintaining the lowest increase in the power of noise component $\hat{x}_N[n]$. For evaluating the performance of equalizer, it is enough to view how close the overall system $s[n]$ is to $\alpha\delta[n - n_d]$. A commonly-used measure for this purpose is Inter-Symbol Interference (ISI) defined as:

$$\text{ISI} = \frac{\sum_n |s[n]|^2 - s_{max}^2}{s_{max}^2} \tag{D.24}$$

$$s_{max} = \max \quad |s[n]|$$

Another common parameter for measuring the equalization performance is the Maximum Distortion(MD) defined as follows:

$$\text{MD} = \frac{\sum_n |s[n]| - s_{max}}{s_{max}} \tag{D.25}$$

where $\{s_n\}$ stands again for the overall system unit-impulse response (unknown system in tandem with equalizer).
Clearly MD and ISI are zero if $\{s_n\}$ equals a shifted and scaled version of unit impulse function $\alpha\delta[n - n_d]$. A small value of MD or ISI indicates the proximity to the desired solution[86].
To equalize an unknown LTI system, the proposed methods use commonly a criterion which is to be either maximized or minimized for the optimum desired equalizer. The algorithms are all iterative but differ from two points of view. Firstly, they are categorized according to the specific criterion or the contrast function which provides an extremum (maximum or minimum) for the optimum equalizer filter. Secondly, they differ through the iterative algorithm of updating the equalizer coefficients for achieving the extremum vector of the criterion. The gradient methods including the steepest descent algorithm or stochastic gradient procedure are mostly used in this regard. The initialization of equalizer for iteratively optimizing is so important. The initial filter used for the equalizer plays a major role in the convergence and the correctness of the result. All these aspects are hereunder briefly studied considering different methods of blind equalization. In addition to the iterative algorithms, a non-iterative analysis has been presented by Benveniste et. al. [107]. They have proved and used the following theorem as the basis for the equalization problem.

Theorem D.3.1. *Considering an LTI system $\{h_n\}$ to which an excitation $\{x_n\}$ being a sequence of i.i.d. random variables with non-Gaussian distribution of ν is applied as its input. ν is supposed to be symmetric and with a finite variance. The output associated to the system $\{h_n\}$ is applied to a feed-forward equalizer having at least two non-zero coefficients. If the distribution of equalized output (random variable) is still ν, then the overall system equals to $\alpha\delta(n - n_d)$.*

D.3.1.1 The Criteria

According to the theorem D.2.5, a group of universal deconvolution criteria may be achieved which are either constrained or unconstrained. Meanwhile, the first criteria proposed in the telecommunication areas were extracted heuristically though they are really the special cases of cumulant-based extrema later offered. Some

important and principal criteria are hereunder listed:

- *Godard Criterion:* Godard proposed a new approach for blind equalization in QAM system. It was later shown that his criterion is actually equal to the cumulant-based criteria. He heuristically looked for cost functions being independent of the output phase so that it can be optimized without any carrier information. He proposed to minimize the "dispersion function" of order p as follows:

$$\begin{aligned} &\text{minimize} \quad E[(|\hat{x}[n]|^p - R_p)^2] \\ &\text{subject to: } R_p = \frac{E[|x[n]|^{2p}]}{E[|x[n]|^p]} \end{aligned} \tag{D.26}$$

  The constant R_p is used to control the gain of equalizer so that to achieve a perfect equalization. If R_p is replaced with any desired positive value, there will be only an ambiguity in the amplitude. If $p = 2$, this algorithm (Godard-2) is also called the Constant Modulus Algorithm (CMA) which is widely used. However, this criterion works only for the sub-Gaussian signals. In other words, it works only when the kurtosis of the input is negative. Godard dispersion function has widely been treated and used in the case of $p = 2$.

- *Maximum Response Cumulant:* This is the earliest and the most straight criterion which one can extract using theorem D.2.5. To equalize closely the original white input sequence, it is enough that the overall system $\{s_n\}$ approximates $\alpha\delta[n - n_d]$. There will always exist an ambiguity in the amplitude (α) and a delay (n_d) because they can not be discovered through the cumulant measure. Thereby, it is possible to use the following constrained criterion for the equalization:

$$\begin{aligned} &\text{maximize} \quad |C_{\hat{x}}(p, q)| \\ &\text{subject to: } C_x(1, 1) = C_{\hat{x}}(1, 1) \end{aligned} \tag{D.27}$$

  where p and q are two positive integers so that $p + q > 2$.
  As discussed in the preceding sections, different values for the pair of (p, q) have been proposed such as $(4, 2)$ and $(6, 2)$. This criterion may be simplified

as follows for the case of real-valued data as following:

$$\text{maximize} \quad |C_{\hat{x}}(p)| \tag{D.28}$$

$$\text{subject to: } \sigma_x^2 = \sigma_{\hat{x}}^2$$

where p is a positive integer so that $p > 2$.

- *Benevniste criterion:* Benveniste has offered a modification for the above-mentioned maximum cumulant criterion which is useful for the digital signals in the applications such as telecommunication. Assuming that the real and imaginary components of the input complex sequence are independent, the following criterion may be used:

$$\text{maximize} \quad |C_{\hat{x}_r}(p)| \tag{D.29}$$

$$\text{subject to: } \sigma_x^2 = \sigma_{\hat{x}}^2$$

or equally

$$\text{maximize} \quad |C_{\hat{x}_{im}}(p)| \tag{D.30}$$

$$\text{subject to: } \sigma_x^2 = \sigma_{\hat{x}}^2$$

where $\hat{x}_r$ and $\hat{x}_{im}$ are real and imaginary parts of the equalized output respectively.

- *Normalized Cumulant Criterion:* As it is just seen, cumulant-based criteria offered are all constrained. One way for having an unconstrained criterion is to exploit the normalized cumulants. Therefore, following family of normalized cumulant criteria are possible to be considered.

$$\text{maximize} \quad \frac{|C_{\hat{x}}(p,q)|}{(C_{\hat{x}}(1,1))^{\frac{p+q}{2}}} \tag{D.31}$$

that for real-valued signals, this criterion can be considered as follows:

$$\text{maximize} \quad \frac{|C_{\hat{x}}(p)|}{(C_{\hat{x}}(2))^{\frac{p}{2}}} \tag{D.32}$$

This contrast function was firstly proposed by Donoho (considering $p = 2$) and Wiggins.

- *Unconstrained Cumulant criterion:* Another method for changing the original cumulant-based criterion into an unconstrained counterpart, is to add a penalty term as follows:

$$\text{maximize} \quad \{|C_{\hat{x}}(p,q)| + g(C_{\hat{x}}(1,1))\} \tag{D.33}$$

where $g : [0, \infty) \longrightarrow \mathbb{R}^1$ is a piece-wise continuous real-valued function. To have only an maximum for above-mentioned criterion, this function has to maintain some properties [83].As an interesting result, it has been shown that Godard-2 or CMA algorithm can be achieved through a specially-chosen $g(.)$ as follows:

$$\text{maximize} \quad \{|C_{\hat{x}}(2,2)| - 2\sigma^2 + 2k\sigma + k^2\} \tag{D.34}$$

$$\sigma = C_{\hat{x}}(1,1)$$

Supposing k equal to R_p of the Godard-2 algorithm, both algorithms would be the same.

D.3.1.2 The Iterative Updating

In the preceding subsection, an overview was presented about the criteria or contrast functions which consist of an extremum at the optimum equalizer. To find the optimum equalizer filter, it is necessary to somehow look for the extremal points of the criteria. The conventional and mostly common approach is to use the gradient vector in the iterative updating procedure. A tapped-delay line equalizer (or an FIR filter) with length of $L = L_2 - L_1 + 1$ is considered so that:

$$\mathbf{f} = \{f[n] \;\; | \;\; L_1 \leq n \leq L_2\}$$

For convenience, the constraint of the criteria (the equality of the variances) may hold by the following relationship:

$$C_x(1,1) = C_{\hat{x}}(1,1) \quad \Longleftrightarrow \quad \|s_n\| = \sum_n |s_n|^2 = 1 \tag{D.35}$$

Thus, the iterative update of stochastic gradient method for finding maximum of a criterion can be described as follows:

$$\mathbf{s}^{'} = \mathbf{s} + \delta \frac{\partial \Psi}{\partial \mathbf{s}} \tag{D.36}$$

$$\mathbf{s}^{"} = \frac{1}{\|\mathbf{s}^{'}\|}\mathbf{s}^{'}$$

that the vector $\mathbf{s}$ represents the total impulse response $s[n]$ in the vectorial form $\mathbf{s}$=$[\cdots,\ s[-1], s[0],\ s[1],\ \cdots]^T$. The vector $\mathbf{s}^{"}$ stands for the updated impulse response after applying the iterative algorithm. It is reminded that all criteria have been described in terms of the total system consisting of the unknown filter h_n in tandem with the equalizer filter f_n ($s[n] = h[n] * f[n]$). Accordingly, the true direction of the gradient vector toward the extremum has been defined in terms of $s[n]$. The total system impulse response is evidently unknown since h_n is not available. Furthermore, the iterative algorithm is defined in terms of equalizer coefficients. Then, this updating algorithm can approximately be realized by following iterative procedure [83]:

$$\mathbf{f}^{'} = \mathbf{f} + \delta(\mathbf{H}^{\mathbf{H}}\mathbf{H})^{-1}\frac{\partial \Psi}{\partial \mathbf{f}} \tag{D.37}$$

$$\mathbf{f}^{"} = \frac{1}{\sqrt{\mathbf{f}^{'H}\mathbf{H}^{\mathbf{H}}\mathbf{H}\mathbf{f}^{'}}}\mathbf{f}^{'}$$

where $\mathbf{f}$ and the operator $(.)^H$ stand for the impulse-response of equalizer and the conjugate-transpose operation respectively. The step size of the gradient algorithm is illustrated by δ as well. The matrix $\mathbf{H}$ is defined as below:

$$\mathbf{H} = \{H_{ij} \ \mid \ H_{ij} = h_{i-j},\ L_1 \leq j \leq L_2\}$$

Shalvi and Weinstein have offered another algorithm which converges in a very fast rate to the desired equalizer regardless of the initialization point. They called this algorithm as Super-Exponential Algorithm (SEA). This algorithm updates the equalizer coefficients according to the following iterative procedure:

$$\mathbf{f}^{'} = \mathbf{R}^{-1}\mathbf{d} \tag{D.38}$$

$$\mathbf{f}^{"} = \frac{1}{\sqrt{\mathbf{f}'^{H}\mathbf{R}\mathbf{f}'}}\mathbf{f}'$$

where $\mathbf{R} = \mathbf{H}^{\mathbf{H}}\mathbf{H}$ is a matrix with the dimension $L \times L$ and $\mathbf{d}$ is a vector of $L \times 1$ defined as following:

$$d_n = \text{cum}(\hat{x} : p; \hat{x}^* : q-1; y^*_{t-n}) \tag{D.39}$$

The integers p and q stand for the order of the cumulant used in the chosen criterion (or the $(p,q)^{th}$ order cumulant). It is evident that all these algorithms are not realizable unless the matrix $\mathbf{R}$ is available. This matrix may be calculated through the following relationship:

$$R_{nm} = \frac{\text{cum}(y^*_{t-n}; y_{t-m})}{C_x(1,1)} \tag{D.40}$$

It is interesting to note that $\mathbf{R}^{-1}$ is equal to the identity matrix if a whitening operation is placed as a prefilter before the equalizer stage. In other words, it corresponds to the spectral whitening operation which had firstly been suggested by Benveniste et. al.

Therefore, the only prerequisite information about the input is its variance. Nevertheless, the variance value may be replaced by the sample variance of equalized output or any desired positive real number. There certainly exist an ambiguity in the amplitude in this case.

D.3.2 MIMO blind deconvolution

It is supposed that there are K different input signals $\{x_1[n],\ x_2[n],\ \ldots,\ x_K[n]\}$ which simultaneously pass through a Multiple-Input Multiple-Output (MIMO) LTI system and produce M output sequences $\{y_1[n],\ y_2[n],\ \ldots,\ y_K[n]\}$ in the presence of independent additive noises. The associated model for a typical MIMO telecommunication channel is illustrated in figure D.3. For convenience, the signals are illustrated in vectorial form as below:

$$X[n] = [x_1[n], x_2[n], \ldots, x_K[n]]^T$$
$$Y[n] = [y_1[n], y_2[n], \ldots, y_M[n]]^T$$
$$W[n] = [w_1[n], w_2[n], \ldots, w_M[n]]^T$$

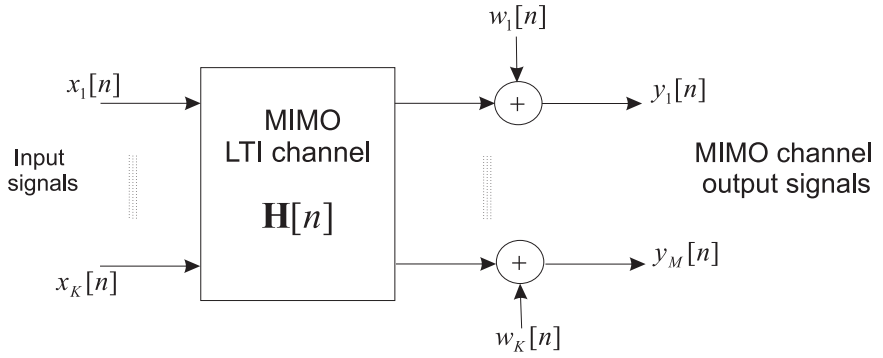

Figure D.3. The linear MIMO model of a telecommunication channel.

where $X[n]$, $Y[n]$ and $W[n]$ are the input, output and noise vectors associated with the MIMO LTI model of the telecommunication channel respectively. Then, we will have following equations governing on the channel model:

$$\begin{aligned} Y[n] &= Y_s[n] + W[n] \\ Y_s[n] &= \mathbf{H}[n] * X[n] \end{aligned} \tag{D.41}$$

$Y_s[n]$ is the noise-free output of the system which is distorted by $M \times K$ MIMO LTI system represented by the matrix $\mathbf{H}[n]$. Using D.41, it may readily be discovered that there exist not only ISI components but also Multiple Access Interference (MAI) components at the output vector because each element of $Y_s[n]$ is a mixture of all the source signals $\{x_k[n],\ k = 1, 2, \ldots, K\}$. Accordingly, blind equalization of the MIMO system $\mathbf{H}[n]$ (figure D.4) is a problem in which both the ISI and MAI contributions have to be eliminated. In other words, it is to recover the source signals $X[n]$ with only the output signals $Y[n]$. This type of problem is met in many applications such as DS/CDMA systems, multiple-antenna systems, fractionally spaced equalization in signal antenna, time delay estimation through multiple sensors, and seismic signal processing. In the past decade, blind equalization of MIMO channels using HOS-based methods has been extensively reported. The following conditions are often assumed through all those applications:

- $M1$: The $M \times K$ LTI MIMO system is stable.
- $M2$: Each of the K inputs is a zero-mean non-Gaussian i.i.d. stochastic process and they are all mutually independent.

- $M3$: The noise $W[n]$ is a zero-mean Gaussian vector random process.
- $M4$: The input signal and the additive noises are statistically independent.

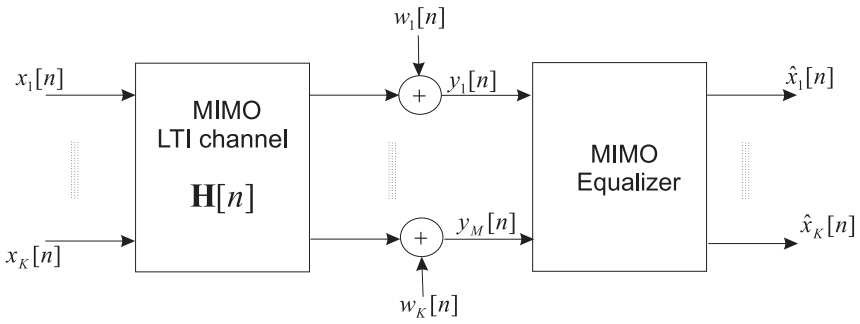

Figure D.4. The general model of a MIMO telecommunication channel with the related equalizer.

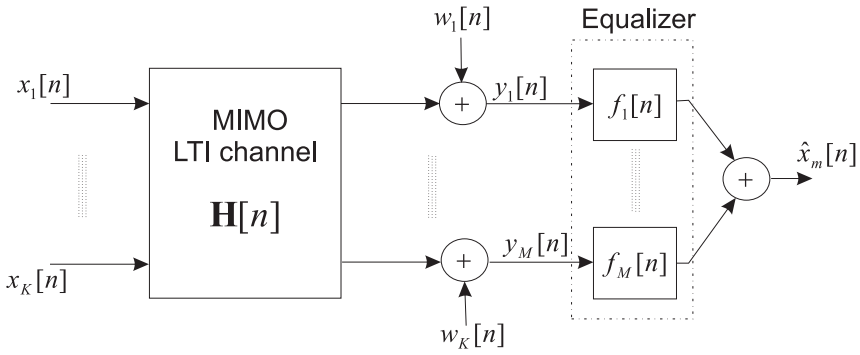

Figure D.5. The model of a MIMO telecommunication channel along with an equalizer. This equalizer can equalize only one input signal $x_m[n]$ at each realization $m \in \{1, 2, \ldots, K\}$.

The extension of $MIMO$ blind equalization method to the case of temporally-colored inputs is also possible. Using the equalization part, it is desired to reconstruct the input signals by using only the output of MIMO system $\{y_k[n],\ k = 1, 2, \ldots, M\}$. There are two possibilities for realizing the equalizer. Using an MIMO equalizer, it may be possible to calculate simultaneously all of the output signals (see figure D.4). The related equalizer would include a matrix of digital filters. In this case, the computations will be very heavy and it may even be practically impossible. Another option is to utilize a simpler equalizer as shown in figure D.5. In this method, it is possible to calculate each time only one of the

inputs. However, the K input signals may be estimated through the Multistage Successive Cancelation procedure (MSC). Using the MSC procedure, one would face with the essential problem of error propagation. The error will be propagated in the signal estimation from a stage to the next stage in this case. the algorithm for MSC procedure is described in figure D.6. This problem has been discussed in terms of MIMO Blind Source Separation (BSS) as well. It concerns with the non-stantaneous or convolutive source mixtures.

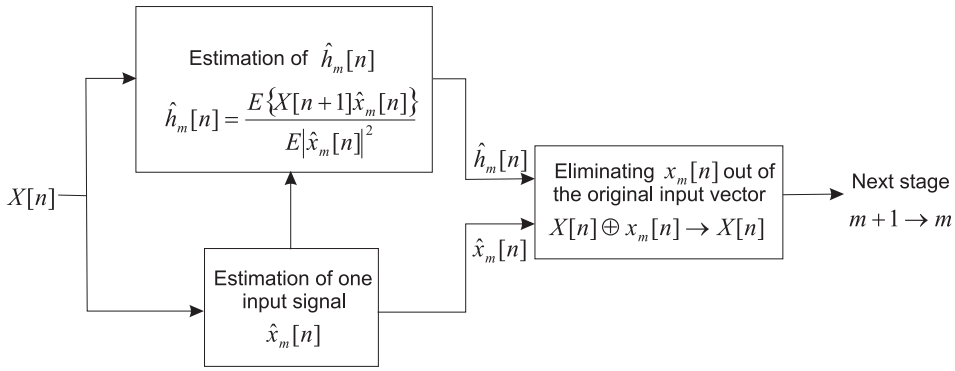

Figure D.6. The MSC Algorithm.

Bibliography

[1] Schreier, R. and G. Temes (2004) *Understanding Delta-Sigma data converters*, Wiley-IEEE Press, USA.

[2] Tuttlebee, W. and R. Manor (1999) "Software radio technology: a european perspective," *IEEE Communications Magazine*, pp. 118–123.

[3] Franca, J., A. Petraglia, and S. K. Mitra (1997) "Multirate Analog-Digital systems for signal processing and conversion," *Proceedings of the IEEE*, **85**(2), pp. 242–262.

[4] Velazquez, S. R., T. Q. Nguyen, and S. Broadstone (1998) "Design of Hybrid Filter Banks for Analog/Digital conversion," *IEEE Transactions On Signal Processing*, **46**(4), pp. 956–967.

[5] Asemani, D. and J. Oksman (2006) "Influences of oversampling and analog imperfections on hybrid filter bank A/D converters," in *49th IEEE International Midwest Symposium on Circuits and Systems*, San Juan (Puerto Rico).

[6] Sanada, Y. and M. Ikehara (2001) "Digital compensation scheme for coefficient errors of complex filter bank parallel A/D converter in low-IF receivers," in *Proceedings of IEEE 55th Vehicular Technology Conference*, vol. 4, pp. 1680–1684.

[7] Pinheiro1, M., P. Batalheiro, A. Petraglia, and M. Petraglia (2001) "Improving the near-perfect hybrid filter bank performance in the presence of realization errors," in *Proceedings of IEEE International Conference on Acoustics, Speech and Signal Processing*, vol. 2, Salt Lake City, USA, pp. 1069–1072.

[8] Zhao, S., C. Shen, X. Su, and Y. Yao (2003) "A parallel ADC structure for software radio receiver," in *Proceedings of Conference on Convergent Technologies for Asia-Pacific Region*, vol. 3, Beijing, China, pp. 1025 – 1027.

[9] Velazquez, S. R. (1997) *Hybrid Filter Banks for Analog/Digital Conversion*, Ph.D. thesis, Massachusetts Institute of Technology, USA.

[10] Lowenborg, P. (2001) *analysis and synthesis of asymmetric filter banks with applications to analog to digital conversion*, Ph.D. thesis, Linkopings university, Linkopings , Sweden.

[11] Asemani, D. and J. Oksman (2005) "Two-stage synthesis filters for hybrid filter banks A/D converters," in *Proceedings of IEEE Workshop on Signal Processing Systems (SiPS)*, Athens , Greece, pp. 133–136.

[12] Shannon, C. E. (1949) "Communications in the presence of noise," in *Proceedings of IRE*, vol. 37, pp. 10–21.

[13] Nyquist, H. (1928) "Certain topics in telegraph transmission theory," *AIEE Transactions*, **47**(4), pp. 617–644.

[14] Folkesson, K. (2004) *ADC modeling from a System Perspective and Design of RF-Sampling Radio Receivers*, Ph.D. thesis, Linkoping university, Linkoping, Sweden.

[15] Abidi, A. A. (1993) "Trends in high performance data conversion," in *Proceedings of International Symposium on VLSI Technology, Systems, and Applications*, pp. 329–330.

[16] Stewar, R. W. (1995) "An Overview of Sigma Delta ADCs and DAC Devices," in *Proceedings of IEE Colloquium on Oversampling and Sigma-Delta Strategies for DSP*, London, UK, pp. 1–9.

[17] Bourdopoulos, G. I. and et. al. (2003) *Delta-sigma Modulators modeling, design and applications*, Imperial college press, London, UK.

[18] Murmann, B. and B. E. Boser (2004) *Digitally assisted pipeline ADCs*, Kluwer academic publishers, London, UK.

[19] Petraglia, A. and S. K. Mitra (1992) "High-speed A/D conversion incorporating a QMF bank," *IEEE Transactions on Instrumentation and Measurement*, **41**(4), pp. 427–431.

[20] Mitola, J. (1983) "Software Radios Survey, Critical Evaluation and Future Directions," *IEEE AES Systems Magazine*, pp. 25–36.

[21] Romdhane, M. B. and P. Loumeau (2004) "Analog to digital conversion specifications for ultra wide band reception," in *Proceedings of IEEE International Symposium on Signal Processing and Information Technology*, pp. 157– 160.

[22] Weidong, L. and Y. Yan (1998) "Software Radio: Technology and Implementation," in *Proceedings of International Conference on Communication Technology ICCT'98*, Beijing, China, pp. 1–5.

[23] Mitola, J. and G. Q. Maguire (1999) "Cognitive radio: making software radios more personal," *IEEE personal communications*, **41**(aug.), pp. 13–18.

[24] Kraemer, B. (2003) "Data conversion considerations for software radios," in *Proceedings of IEEE* 5^{th} *Symposium on Spread Spectrum Techniques and Applications*, vol. 2, pp. 546–550.

[25] Mitola, J. (1992) "Software radios - survey, critical evaluation and future directions," in *Proceedings of National Telesystems Conference*, pp. 13/15 – 13/23.

[26] ——— (1999) "Software Radio Architecture: A Mathematical Perspective," *IEEE journal on selected areas in communications*, **17**(4), pp. 514–538.

[27] Vasseaux, T., B. Huyart, P. Loumeau, and J. Naviner (1999) "A track/hold-mixer for direct-conversion by subsampling," in *Proceedings of IEEE International Symposium on Circuits and Systems*, vol. 4, pp. 584–587.

[28] Black, W. C. and A. A. Hogges (1980) "Time interleaved converter arrays," in *Proceedings of IEEE international Solid-state circuits conference.*

[29] ——— (1980) "Time interleaved converter arrays," *IEEE Journal of Solid-state Circuits*, **SC-15**(6), pp. 1022–1029.

[30] Kurosawa, N., H. Kobayashi, and et. al. (2001) "Time interleaved converter arrays," *IEEE Transactions on Circuits and Systems-I: Fundamental Theory and Applications*, **46**(3), pp. 261–271.

[31] Fogel, L. J. (1955) "A note on the sampling theorem," *IRE Tram. Inform Theory*, **IT-1**, pp. 47–48.

[32] Papoulis, A. (1977) "Generalized Sampling Expansion," *IEEE Transaction On Circuits and Systems*, **CAS-24**(11).

[33] Brown, J. (1981) "Multi-channel sampling of low pass signals," *IEEE Transaction On Circuits and Systems*, **CAS-28**(2), pp. 101–106.

[34] ——— (1989) "Generalized sampling and the reconstruction problem for maximally decimated filter banks," in *proceedings of IEEE International Conference on Acoustics, Speech and Signal Processing*, vol. 2, pp. 1195–1198.

[35] Vaidyanathan, P. and V. Liu (1988) "Classical Sampling Theorems in the context of multirate and polyphase Digital Filter Banks structures," *IEEE Transactions On Acoustics, Speech and Signal Processing*, **36**(9), pp. 1480–1495.

[36] Seidner, D. and M. Feder (1999) "Generalized sampling and the reconstruction problem for maximally decimated filter banks," in *proceedings of IEEE International Conference on Acoustics, Speech and Signal Processing*, vol. 3, pp. 1637–1640.

[37] Petraglia, A. and S. K. Mitra (1990) "High Speed A/D conversion using QMF banks," in *Proceedings of IEEE International Symposium on Circuits and Systems*, pp. 2297–2800.

[38] Petraglia, A., F. Maloberti, and S. K. Mitra (1991) "QMF-Based A/D converters: Overview and new results," in *Proceedings of International Conference on A/D and D/A Conversion*, pp. 112–117.

[39] Franca, J. E., S. K. Mitra, and A. Petraglia (1993) "Recent Developments and future trends of multirate Analog-Digital systems," in *Proceedings of IEEE International Symposium on Circuits and Systems*, pp. 1042–1045.

[40] Desgreys, P., A. Tauvel, and P. Loumeau (2002) "SC and SI techniques performances faced with technological advances (in CMOS)," in *Proceedings of IEEE International conference on Electronics, Circuits and Systems*, vol. 1, pp. 53–56.

[41] Velazquez, S. R., T. Q. Nguyen, S. R. Broadstone, and J. K. Roberge (1994) "A hybrid filter bank approach to analog-to-digital conversion," in *Proceedings of the IEEE-SP International Symposium on Time-Frequency and Time-Scale Analysis*, pp. 116–119.

[42] ——— (1994) "High-performance advanced filter bank analog-to-digital converter for universal RF receivers," in *Proceedings of the IEEE-SP International Symposium on Time-Frequency and Time-Scale Analysis*, pp. 229–232.

[43] Oliaei, O. (1998) "High-Speed A/D and D/A converters using Hybrid Filter Banks," in *Proceedings of IEEE International Conference on Electronics, circuits and Systems*, Geneva , Switzerland, pp. 143–146.

[44] Lowenborg, P., H. Johansson, and L. Wanhammar (2003) "Two-channel digital and hybrid Analog/Digital multirate filter banks with very low-complexity analysis or synthesis filters," *IEEE Transactions on circuits and Systems*, **50**(7), pp. 355–367.

[45] ——— (2000) "A class of two-channel approximately perfect reconstruction hybrid analog/digital filter banks," in *Proceedings of IEEE International Symposium on Circuits and Systems*, Geneva, Switzerland.

[46] ——— (1999) "A class of two-channel hybrid analog/digital filter banks," in *Proceedings of IEEE Midwest Symposium on Circuits and Systems*, New Mexico, USA.

[47] ——— (1999) "On the frequency response of M-channel mixed analog and digitall maximally decimated filter banks," in *Proceedings of European conference on Circuits Theory and Design*, Stresa, Italy.

[48] ——— (2001) "A survey on filter bank A/D converters," in *Proceedings of Swedish System-on-Chip Conference*, pp. 133–136.

[49] Lelandais-Perrault, C. (2006) *Systèmes de numérisation hautes performances- étude des solutions à bancs de filtres hybrides - Extension des fonctionnalités* -, Ph.D. thesis, Paris university, Orsay, France.

[50] Petrescu, T. (2006) *Systèmes de numérisation hautes performances- étude des solutions à bancs de filtres hybrides*, Ph.D. thesis, Paris university, Orsay, France.

[51] Lowenborg, P., H. Johansson, and L. Wanhammar (2000) "A class of two-channel IIR/FIR filter banks," in *Proceedings of European Signal Processing conference.*

[52] ——— (2000) "A two-channel hybrid analog and IIR digital filter bank approximating perfect magnitude reconstruction," in *Proceedings of IEEE Nordic Signal Processing Symposium*, Kolmerden, Sweden.

[53] Lelandais-Perrault, C., D. Silion, T. Petrescu, and D. Poulton (2005) "Hybrid filter bank A/D converters using IIR synthesis filters," in *IEEE Midwest Symposium on Circuits and Systems.*

[54] Petrescu, T., J. Oksman, and P. Duhamel (2005) "Synthesis of hybrid filter banks by global frequency domain least squares solving," in *Proceedings of IEEE International Symposium on Circuits And Systems.*

[55] Petrescu, T. and J. Oksman (2003) "Synthesis of hybrid filter banks for A/D conversion with implementation constraints-optimized frequency response approach-," in *Proceedings of IEEE Midwest Symposium for Circuits and Systems.*

[56] Petrescu, T., C. Lelandais-Perrault, and J. Oksman (2004) "Synthesis of hybrid filter banks for A/D conversion with implementation constraints-mixed distortion/aliasing optimization," in *Proceedings of IEEE International Symposium on Circuits And Systems*, vol. 2, pp. 997–1000.

[57] Collette, J. and M. Barre (2006) "On simulations about the precision of non-uniform hybrid filter bank analog/digital converters," in *IEEE International Conference on Acoustics, Speech and Signal Processing*, Toulouse, France.

[58] Lelandais-Perrault, C., D. Poulton, and J. Oksman (2005) "Bandpass hybrid filter bank A/D converters with software-controlled bandwidth and resolution," in *IEEE European Conference on Circuits Theory and Design*, vol. I, pp. 51–54.

[59] Shu, H., T. Chen, and B. Francis (1997) "Minimax Design of Hybrid Multirate Filter Banks," *IEEE Transactions on circuits and Systems-II: analog and digital signal processing*, **44**(2), pp. 120–128.

[60] ——— (2004) "Minmax design of hybrid multirate filter banks," in *Proceedings of IEEE International Symposium on circuits And Systems*, vol. 2, pp. 324–327.

[61] Lookabaugh, T., M. Perkins, and C. Cadwell (1989) "Analysis/synthesis systems in the presence of quantization," in *Proceedings of IEEE International Conference on Acoustics, Speech and Signal Processing*, vol. 2, Glasgow, UK, pp. 1341–1344.

[62] Lowenborg, P. and H. Johansson (2004) "Quantization noise in filter bank analog-to-digital converters," in *Proceedings of IEEE International Symposium on Circuits And Systems*, vol. 2, pp. 601–604.

[63] ——— (2001) "Analysis of gain and time skew errors in filter bank based A/D converters," in *Proceedings of IEEE International Symposium on circuits And Systems*, Dayton, Ohio.

[64] Petrescu, T. and J. Oksman (2006) "Sensitivity of hybrid filter banks A/D converters to analog realization errors and finite word length," in *Proceedings of IEEE International Conference on Acoustics, Speech and Signal Processing*, Toulouse, France.

[65] Elbornsson, J. (2001) "Blind Equalization of Static Nonlinearities in SA-ADC," in *Proceedings of CCSSE'01*, Linkopings university, Sweden.

[66] Guilloud, F., B. Boutillon, and J. L. Danger (2001) "Étude d'un algorithme itératif de repliement spectral lors d'une conversion A/N parrallèle," in *5ème Journée Nationale du Réseau Doctoral de Microélectronique*, Grenoble, France.

[67] Camarero, D., J. F. Naviner, and P. Loumeau (2004) "Digital background and blind calibration for clock skew error in time-interleaved Analog-to-Digital converters," in *Proceedings of* 17^{th} *Symposium on Integrated Circuits and Systems Design*, pp. 228–232.

[68] Lelandais-Perrault, C., D. Poulton, and J. Oksman (2003) "Synthesis of hybrid filter banks for A/D conversion with implementation constraints-Direct Approach-," in *IEEE Midwest Symposium on Circuits and Systems*.

[69] Oppenheim, A. and R. Schafer (1989) *Discrete-time signal processing*, Prentice Hall, Englewood Cliffs , NJ., USA.

[70] Widrow, B., J. Glover, and et al. (1975) "Adaptive Noise Cancelling: Principles and Applications," *Proceedings of the IEEE*, **63**(12), pp. 1692–1717.

[71] Mitra, S. (2001) *Digital Signal Processing: a computer-based approach*, McGraw-Hill, USA.

[72] Vetterli, M. and J. Kovcevic (1995) *Wavelets and Subband Coding*, Prentice Hall, Englewood Cliffs , NJ., USA.

[73] Wang, Y. and A. Abidi (1990) "CMOS active filter design at very high frequencies," *IEEE journal of solid-state circuits*, **25**(6), pp. 1562–1574.

[74] Huffel, S. V. and J. Vanderwalle (1991) *The total Least Squares Problem: Computational Aspects and Analysis*, SIAM, USA.

[75] De Groen, P. (1996) "An introduction to total least squares," *Nieuw Archief voor Wiskunde*, **14**(12), pp. 237–253.

[76] Mastronardi, N., P. Lemmerling, and S. Van Huffel (2001) "The structured total least squares problem," *Contemporary Mathematics*, **280-1**(12), pp. 157–176.

[77] Valaee, s. and P. Kabal (1994) "Wide-band array processing using Total Least-Squares transformations," in *Proceedings of seventh Workshop on Statistical Signal and Array Processing*, Quebec, Canada, pp. 133–136.

[78] Guo, H. and R. A. Renaut (2001) "A Regularized Total Least Squares Algorithm," in *Proceedings of the Third International workshop on TLS and Errors-in-Variables Modeling*, Leuven, Belgium, pp. 57–66.

[79] Baker, D. W. and E. A. Herr (1965) "Parasitic effects in microelectronic circuits," *IEEE Transactions on electron devices*, pp. 161–167.

[80] Gray, P. and R. Meyer (1984) *Analysis and Design of Analog integrated circuits*, Wiley, New York, USA.

[81] Sun, T., A. Wiesbauer, and G. Temes (1998) "Adaptive compensation of analog circuit imperfections for cascaded delta-sigma ADCs," in *Proceedings of IEEE International Conference on Circuits and Systems*, vol. 1, pp. 405–407.

[82] Jut, P., K. Suyama, P. Ferguson, and L. W. (1995) "A highly linear switched capacitor DAC for multi bit sigma-delta D/A applications," in *Proceedings of IEEE International Conference on Circuits and Systems*, vol. 1, pp. 9–12.

[83] Haykin, S. (ed.) (2000) *Unsupervised adaptive filtering volume II: Blind Deconvolution*, John Wiley and sons, USA.

[84] Asemani, D., J. Oksman, and D. Poulton (2006) "Modeling the imperfections of analog circuits using second order statistics," in *Proceedings of International Symposium on Communications, Control and Signal Processing (ISCCSP)*, Marrakech (Morocco).

[85] ——— (2006) "Digital estimation of analog imperfections using blind equalization," in *Proceedings of the 14th European Signal Processing Conference*, Florence (Italy).

[86] Shalvi, O. and E. Weinstein (1993) "Super-Exponential Methods for Blind Deconvolution," *IEEE Transactions on Information Theory*, **39**(2), pp. 504–519.

[87] Haykin, S. (ed.) (2000) *Unsupervised adaptive filtering volume I: Blind source separation*, John Wiley and sons, USA.

[88] Chi, C. Y., C. Y. Chen, C. H. Chen, and C. C. Feng (2003) "Batch Processing Algorithms for Blind Equalization Using Higher-Order Statistics," *IEEE Signal Processing Magazine*, pp. 25–49.

[89] Vaidyanathan, P. P. (1993) *Multirate Systems and Filter Banks*, Prentice Hall, Engle-wood Clifs , USA.

[90] Vaidyanathan, P. P. and V. C. Liu (1998) "Classical sampling theorems in the context of multirate and polyphase digital filter bank structures," *IEEE Transactions on Acoustics, Speech and Signal Processing*, **36**(9), pp. 1480–1495.

[91] Pappaport, T. (2001) *Wireless Communications: Principles and Practice*, Prentice Hall, Engle-wood Clifs , USA.

[92] Agrange, X., P. Godlewski, and S. Tabbane (2000) *Réseaux GSM-DCS*, Hermes Science, Paris, France.

[93] Walke, B. H. (2002) *Mobile Radio Networks*, John Wiley, USA.

[94] Golub, G. and C. Van Loan (1980) "An analysis of the Total Least Squares problem," *Siam J. Numer. Anal.*, **17**, pp. 883–893.

[95] Golub, G. and C. Reinsch (1970) "Singular value decomposition and least squares solutions," *Numer. Math.*, **14**, pp. 403–420.

[96] Golub, G. (1973) "Some modified matrix eigen value problems," *Siam Rev.*, **15**, pp. 318–344.

[97] Massey, J. L. and M. K. Sain (1968) "Inverse of Linear Sequential Circuits," *IEEE Transactions on Computers*, **C-17**(4), pp. 330–337.

[98] Yuan, F. M. (1975) "Minimal Dimension Inverses of Linear Sequential Circuits," *IEEE Transactions on Automatic Control*, **AC-20**(1), pp. 42–52.

[99] Yuan, S. P. (1970) "A note on Inversion of Linear Systems," *IEEE Transactions on Automatic Control*, (August), pp. 492–493.

[100] Newhall, E., S. Qureshi, and C. F. Simone (1971) "Technique for Finding Approximate Inverse Systems and its Application to Equalization," *IEEE Transactions on Communication Technology*, **Com-19**(6), pp. 1116–1127.

[101] Mendel, J. M. (1991) "Tutorial on higher-Order Statistics(Spectra) in Signal Processing and system Theory: Theoretical Results and Some Applications," *Proceedings of the IEEE*, **79**(3), pp. 278–305.

[102] Quershi, S. (1982) "Adaptive Equalization," *IEEE Communications Magazine*, (March), pp. 9–16.

[103] Cadzow, J. (1996) "Blind Deconvolution via Cumulant Extrema," *IEEE Signal Processing Magazine*, (May), pp. 24–42.

[104] Giltin, R. D. and J. E. Mazo (1973) "Comparison of Some Cost functions for Automatic Equalization," *IEEE Transactions on communications*, pp. 233–237.

[105] Sato, Y. (1973) "A Method of Self-Recovering Equalization for Multilevel Amplitude-Modulation Systems," *IEEE Transactions on communications*, pp. 679–682.

[106] Godard, D. N. (1980) "Self-Recovering Equalization and Carrier Tracking in Two-Dimensional Data Communication Systems," *IEEE Transactions on communications*, pp. 1867–1875.

[107] Benveniste, A., M. Goursat, and G. Ruget (1980) "Robust Identification of a Non-minimum Phase System: Blind Adjustment of a Linear Equalizer in Data Communications," *IEEE Transactions on Automatic Control*, **AC-25**(3), pp. 385–399.

[108] Shalvi, O. and E. Weinstein (1990) "New Criteria for Blind Deconvolution of Non-minimum Phase Systems(Channels)," *IEEE Transactions on Information Theory*, **36**(2), pp. 312–321.

[109] Tugnait, J. K. (1992) "Comments on 'New Criteria for Blind Deconvolution of Non-minimum Phase Systems(Channels)," *IEEE Transactions on Information Theory*, **38**(1), pp. 210–213.

[110] Nikias, C. L. and J. M. Mendel (1993) "Signal Processing with Higher-Order Spectra," *IEEE Signal Processing Magazine*, pp. 10–36.

[111] Gamboa, F. and E. Gassiat (1996) "Blind Deconvolution of Discrete Linear Systems," *The Annuals of Statistics*, **24**(5), pp. 1964–1981.

[112] Kay, S. M. (1993) *Fundamentals of Statistical Signal Processing, Estimation Theory*, Prentice Hall, USA.